To the Graduate Council:

I am submitting herewith a dissertation written by Jeffrey B. Connelly entitled "Structural Development, Strain History, and Timing of Deformation in the Eastern Great Smoky Mountains." I have examined the final copy of this dissertation for form and content and recommend that it be accepted in partial fulfillment of the requirements for the degree of Doctor of Philosophy, with a major in Geology.

Dr. Robert D. Hatcher, Jr., Major Professor

We have read this dissertation
and recommend its acceptance:

Bill Dunne

Steven G. Driese

Eric Drumm

Accepted for the Council:

Associate Vice Chancellor
and the Dean of the Graduate School

STRUCTURAL DEVELOPMENT, STRAIN HISTORY, AND TIMING OF DEFORMATION IN THE EASTERN GREAT SMOKY MOUNTAINS

A Dissertation

Presented for the

Doctor of Philosophy

Degree

The University of Tennessee, Knoxville

Jeffrey B. Connelly

May, 1993

DEDICATION

This dissertation is dedicated to my wife, Kelly, for her patience and understanding, and for the encouragement she provided throughout my graduate career.

ACKNOWLEDGMENTS

I would like to thank Dr. Nicholas Woodward for suggesting this project, and for his guidance and encouragement throughout its completion. I am also grateful to Dr. Robert Hatcher for serving as my major professor. His advice and insight into the geology of this area were invaluable. Dr. William Dunne is also thanked for his help throughout much of the dissertation. His advice concerning the strain analysis portion of this project was particularly valuable. I would also like to thank my other committee members, Dr. Steven Driese and Dr. Eric Drumm, for their comments and suggestions at the final stages of this dissertation. Dr. R. David Dallmeyer at the University of Georgia is thanked for allowing access to his geochronology laboratory and for his help in interpreting the $^{40}Ar/^{39}Ar$ results. I would also like to thank all the fellow graduate students at the University of Tennessee who made my time spent in Knoxville very enjoyable. Finally, I would like to thank my parents for providing me with unlimited educational opportunities. Financial support from the Great Smoky Mountains Conservation Association, the University of Tennessee, the Geological Society of America, and Sigma Xi is also greatly appreciated.

ABSTRACT

The present investigation reveals that the Greenbrier and Dunn Creek thrust sheets preserve well-formed ramp-related folds within the Great Smoky Mountains area. The Greenbrier thrust sheet preserves a ramp anticline at klippes of the Greenbrier thrust sheet in the eastern Great Smoky Mountains that can be traced discontinuously to the western Great Smoky Mountains where this anticline has been modified by later displacement along the Rabbit Creek fault. A ramp-related fold is also preserved in the main Greenbrier thrust sheet. The main Greenbrier fault was subsequently folded by an underlying ramp anticline within the Dunn Creek thrust sheet. These earliest thrust systems have therefore been reconstructed based on foreland models of ramps and flats. The thrust faults form a folded imbricate fan structure with lower hanging-wall ramp anticlines folding higher thrust sheets. The foreland-style thrust system was internally deformed later in the Taconic during emplacement of a thrust sheet now floored by the Miller Cove fault. The Taconic package of imbricated Ocoee strata was emplaced onto the Valley and Ridge during the Alleghanian orogeny by the late Miller Cove and Great Smoky thrust systems. Faults in these late systems occupied various parts of the early ductile thrust zones, and almost certainly excised significant lower parts of the three early thrust sheets.

Internal strain within sandstones of the Miller Cove, Dunn Creek, and Greenbrier thrust sheets was also investigated. The three-dimensional finite strain geometry was determined for 69 samples using the R_f/ϕ and normalized Fry methods. Microstructural observations indicate that strains were accommodated by those deformation mechanisms typical of low grade metamorphic conditions including dislocation flow (undulatory extinction, deformation lamellae, deformation bands, patchy extinction, serrated grain boundaries), pressure solution (stylolites, sutured grain boundaries, overgrowths), and brittle fracturing (microfractures, fluid inclusion planes). Finite strains recorded within the

sandstones are low and generally increase toward the hinterland (to the south). Mean X/Z strain ratios determined by the R_f/ϕ method for the Miller Cove, Dunn Creek, and Greenbrier thrust sheets are 1.29, 1.32, and 1.42, respectively. X/Z ratios determined using the Fry method are typically 5 to 20 percent higher. Principal strain axes within all thrust sheets exhibit subhorizontal strike-parallel X axes, subhorizontal transport-parallel Y axes, and steeply northwest plunging Z axes. Within hanging-wall ramp portions of the Dunn Creek thrust sheet, however, most X axes are parallel to transport and Y axes are parallel to strike. Two models were evaluated by strain factorization in an attempt to produce a sequence of strain events compatible with the finite strains observed in the two structural domains (hanging-wall flat and hanging-wall ramp). The first model involves compaction, layer-parallel shortening/extension, and simple shear. The second model is identical to the first with the exception of the addition of 90 degree rigid-body rotation following compaction to simulate samples from the hanging-wall ramp portions of the Dunn Creek thrust sheet. A sequence of strain events modeled by strain factorization, including 20 percent compaction, layer-parallel shortening of 5 percent, and thrust-parallel simple shear of 0.1, can produce the measured finite strains in the hanging-wall flat areas. The finite strains within the hanging-wall ramp portion of the Dunn Creek thrust sheet, however, require a different strain sequence, including 20 percent compaction by volume loss, 90 degree rigid body rotation following compaction, 20 to 30 percent horizontal extension, and a simple shear. The failure of a single model to account for observed finite strains in the two subdomains may be explained by: 1) Incorrectly assuming a single homogeneous strain across both subdomains; 2) The absence of compaction strains, although this would require another model to explain finite strains in the first subdomain; 3) Samples from the hanging-wall ramp area may yield unreliable results because of their fine-grained and matrix-rich compositions; or 4) The simplicity of the strain model, which assumes vertical bedding in the hanging-wall ramp where the average dip is 48 degrees

and beds are overturned.

The importance of Ordovician tectonothermal activity in the western Blue Ridge of the southern Appalachians has been questioned by recent reports of Late Devonian-earliest Mississippian fossils within regionally metamorphosed rocks. In addition, metamorphism of fossiliferous Early Devonian rocks within the Talladega belt and suggested stratigraphic correlations with rocks of the Murphy belt suggest only post-Silurian metamorphism. The recent reports are contrary to most previous geochronology that suggests Ordovician metamorphism, as well as stratigraphic evidence indicating a Late Proterozoic age for most western Blue Ridge protoliths. To evaluate these contradictory results, eleven whole-rock samples (chlorite to garnet zones) and three muscovite concentrates (staurolite and kyanite zones) from the eastern Great Smoky Mountains of the western Blue Ridge were analyzed with $^{40}Ar/^{39}Ar$ techniques. Most chlorite-grade samples record plateau and intermediate temperature ages of 440 to 460 Ma. Illite crystallinity characteristics indicate that these samples attained metamorphic conditions sufficient for complete rejuvenation of whole-rock systems. Most biotite- and garnet-grade whole-rock samples yield plateau and intermediate temperature ages of 340 to 350 Ma. Muscovite samples record plateau ages of 360 to 380 Ma. It is unlikely that whole-rock samples collected several kilometers apart could have experienced contrasting cooling histories resulting in 100 Ma differences in apparent age. Therefore, the $^{40}Ar/^{39}Ar$ results most likely indicate a polymetamorphic history in which a 440 to 460 Ma (Middle to Late Ordovician) event was overprinted by a 360 to 380 Ma (Middle to Late Devonian) event. This interpretation is consistent with metamorphic textures observed in the western Blue Ridge.

TABLE OF CONTENTS

PART		PAGE
1.	**INTRODUCTION**	1
2.	**TACONIAN FORELAND-STYLE THRUST SYSTEM IN THE GREAT SMOKY MOUNTAINS, TENNESSEE**	7
	INTRODUCTION	8
	GEOLOGIC SETTING	8
	Alleghanian Structures	11
	Pre-Alleghanian Structures	14
	TACONIAN THRUST FAULT GEOMETRIES	16
	Thrust Sheet Restoration	21
	DISCUSSION	21
	REFERENCES CITED	22
3.	**TECTONIC EVOLUTION OF THE GREAT SMOKY MOUNTAINS**	24
	INTRODUCTION	25
	REGIONAL GEOLOGY	28
	Stratigraphy	28
	Structural Geology	30
	Cleavage	31
	FAULT SYSTEMS	34
	Gatlinburg Fault	34
	Great Smoky Fault	35
	Miller Cove Fault	36
	Early Miller Cove Fault	39
	Dunn Creek-Line Springs-Rabbit Creek Fault System	39

Greenbrier Fault 41

Superimposed Imbricate Faulting 43

THRUST SEQUENCES 45

IMPLICATIONS FOR THRUST SHEET RESTORATION 52

SUMMARY 52

REFERENCES CITED 54

4. STRAIN VARIATIONS AND STRAIN FACTORIZATION WITHIN AN EARLY PALEOZOIC THRUST SYSTEM, EASTERN GREAT SMOKY MOUNTAIN FOOTHILLS, TENNESSEE 58

INTRODUCTION 59

SAMPLE DESCRIPTION 62

Microstructures 65

FINITE STRAIN ANALYSIS 73

Methods 73

Results 77

DISCUSSION 97

Strain Factorization 102

CONCLUSIONS 117

REFERENCES CITED 118

APPENDIX 120

5. POLYMETAMORPHIC EVOLUTION OF THE WESTERN BLUE RIDGE PROVINCE: EVIDENCE FROM $^{40}Ar/^{39}Ar$ WHOLE-ROCK SLATE/PHYLLITE AGES 124

INTRODUCTION 125

REGIONAL GEOLOGIC SETTING 127

ORDOVICIAN TECTONISM IN THE SOUTHERN APPALACHIANS 133

Evidence For Ordovician Tectonic Activity in the Southern Appalachians 134

Evidence Precluding Ordovician Tectonic Activity in the Southern Appalachians 137

GEOLOGY OF THE STUDY AREA 143

Stratigraphy 143

Fault Systems 143

Folds 145

Metamorphism 147

ANALYTICAL METHODS 148

Illite Crystallinity 149

$^{40}Ar/^{39}Ar$ Analyses 149

RESULTS 152

Illite Crystallinity 152

$^{40}Ar/^{39}Ar$ 152

COMPARISON WITH PREVIOUS GEOCHRONOLOGY 169

INTERPRETATION 170

TECTONIC IMPLICATIONS 172

REFERENCES CITED 174

VITA 186

LIST OF TABLES

TABLE **PAGE**

PART 4. STRAIN VARIATIONS AND STRAIN FACTORIZATION WITHINAN EARLY PALEOZOIC THRUST SYSTEM, EASTERN GREAT SMOKY MOUNTAINS FOOTHILLS, TENNESSEE

4.1. Matrices multiplied for the two models evaluated in this study; γ = shear strain, S = stretch, Δ = dilation. 105

PART 5. POLYMETAMORPHIC EVOLUTION OF THE WESTERN BLUERIDGE PROVINCE: EVIDENCE FROM $^{40}Ar/^{39}Ar$ WHOLE ROCK SLATE/PHYLLITE AND MUSCOVITE AGES

5.1. Location coordinates of dated samples. 148

5.2. Quartz-normalized illite crystallinity determined on bulk <2μm size fractions at the locations sampled for $^{40}Ar/^{39}Ar$ dating in the chlorite zone of the eastern Great Smoky Mountains, western Blue Ridge. 153

5.3. $^{40}Ar/^{39}Ar$ analytical data for incremental heating experiments on whole-rock slate/phyllite samples from the western Blue Ridge, Tennessee-North Carolina. 154

5.4. $^{40}Ar/^{39}Ar$ analytical data for incremental heating experiments on muscovite concentrates from the western Blue Ridge, Tennessee-North Carolina. 165

LIST OF FIGURES

FIGURE PAGE

PART 1. INTRODUCTION

1.1. Geologic map of the Great Smoky Monutains area showing locations of study areas in subsequent dissertation parts..... 4

PART 2. TACONIAN FORELAND-STYLE THRUST SYSTEM IN THE GREAT SMOKY MOUNTAINS, TENNESSEE

2.1. Geologic map of eastern Great Smoky Mountains..... 9

2.2. Cleavage trends and metamorphic isograds superimposed on regional geologic map.....12

2.3. Cross section through A-A' of Figure 2.1. 17

PART 3. TECTONIC EVOLUTION OF THE GREAT SMOKY MOUNTAINS

3.1. Regional map of the Great Smoky Mountains area. 26

3.2. Stratigraphic units of the Ocoee Supergroup. 29

3.3. Cleavage form lines and metamorphic isograds from the eastern Great Smoky Mountains (northeast corner of Figure 3.1). 32

3.4. Outline maps of the Miller Cove, Dunn Creek, and Greenbrier thrust sheets. 37

3.5. Cross section across the eastern Great Smoky Mountains through Webb Mountain. 46

3.6. Cross section across Cove Mountain in the central Great Smoky Mountains. 49

3.7. Cross section across Cades Cove in the western Great Smoky Mountains. ... 50

3.8. Schematic restored Ocoee basin prior to Ordovician deformation based on Figure 3.5. 53

PART 4. STRAIN VARIATIONS AND STRAIN FACTORIZATION WITHIN AN EARLY PALEOZOIC THRUST SYSTEM, EASTERN GREAT SMOKY MOUNTAINS FOOTHILLS, TENNESSEE

4.1. Geologic map of the eastern Great Smoky Mountains. 60

4.2. Geologic map of the eastern Great Smoky Mountains foothills area showing locations of samples used for strain analysis. 63

4.3. Photomicrographs of microstructures from the Miller Cove thrust sheet (Walden Creek Group). 66

4.4. Photomicrographs of microstructures from the Dunn Creek thrust sheet (Snowbird Group). 70

4.5. Photomicrographs of microstructures from the Greenbrier thrust sheet (Great Smoky Group). 74

4.6. Flinn plot of Fry and R_f/ϕ strain data separated by thrust sheet. 78

4.7. Comparison of Fry X/Z strain magnitudes and R_f/ϕ X/Z strain magnitudes separated by thrust sheet. 80

4.8. X/Y axial ratios as determined by the Fry method. 83

4.9. Cross sections through the study area with X/Z ellipses as determined by the Fry method shown. 84

4.10. Trend and plunge of principal strain axes for each sample as determined by the R_f/ϕ method. 87

4.11. Trend and plunge of principal strain axes for each sample as determined by the Fry method. 90

4.12. Equal-area lower hemisphere stereonets depicting orientations of principal strain axes as determined by the R_f/ϕ method ($X \geq Y \geq Z$). 93

4.13. Equal-area lower hemisphere stereonets depicting orientations of principal strain axes as determined by the Fry method ($X \geq Y \geq Z$). 95

4.14. Equal-area lower hemisphere stereonets depicting orientations of rotated principal strain axes as determined by the R_f/ϕ method ($X \geq Y \geq Z$). 98

4.15. Equal-area lower hemisphere stereonets depicting orientations of rotated principal strain axes as determined by the Fry method ($X \geq Y \geq Z$). 100

4.16. Conceptual model of strain events used for strain factorization. 103

4.17. Plot of strain ratio (R) in the profile direction (X/Z or Y/Z) against the angle between the longer axis of the ellipse in the profile direction (X or Y axis) and the shear direction. 106

4.18. Plot of strain ratio (R) in the profile direction (X/Z or Y/Z) against the angle between the longer axis of the ellipse in the profile direction (X or Y axis) and the shear direction for various values of compaction. 109

4.19. Plot of strain ratio (R) in the profile direction (X/Z or Y/Z) against the angle between the longer axis of the ellipse in the profile direction (X or Y axis) and the shear direction for different values of horizontal compaction (to simulate vertical compaction and 90 degree rigid body rotation). 113

PART 5. POLYMETAMORPHIC EVOLUTION OF THE WESTERN BLUE RIDGE PROVINCE: EVIDENCE FROM $^{40}Ar/^{39}Ar$ WHOLE ROCK SLATE/PHYLLITE AND MUSCOVITE AGES

5.1. Regional tectonic map of the southern Appalachian orogen. 128

5.2. Generalized geologic map of the southern Appalachian western Blue Ridge in the vicinity of the study area showing approximate positions of metamorphic isograds and locations and results of previous geochronologic studies. 131

5.3. Geologic map of the eastern Great Smoky Mountains area showing sample localities and metamorphic isograds. 139

5.4. Comparison of illite crystallinity based on the contrasting methods of Kubler (1967) and Teichmüller and others (1979). 150

5.5. $^{40}Ar/^{39}Ar$ apparent age and apparent K/Ca spectra of whole-rock analysis of slate/phyllite samples from the chlorite zone, Miller Cove and Dunn Creek thrust sheets. 160

5.6. $^{40}Ar/^{39}Ar$ apparent age and apparent K/Ca spectra of whole-rock analysis of slate/phyllite samples from the biotite and garnet zones, Dunn Creek and Greenbrier thrust sheets. 162

5.7. $^{40}Ar/^{39}Ar$ apparent age spectra of muscovite concentrates fron the staurolite and kyanite zones, Greenbrier thrust sheet. 167

PART 1

INTRODUCTION

The Great Smoky Mountains area comprises one of the best mapped large areas in the western Blue Ridge (Hamilton, 1961; Hadley and Goldsmith, 1963; King, 1964; Neuman and Nelson, 1965), and many important regional structural and stratigraphic relations are preserved here. The type localities for most rock units of the Ocoee Supergroup, the dominant stratigraphic unit in the western Blue Ridge, occur in the this area (King and others, 1958), and the most unambiguous evidence for premetamorphic faulting in the southern Appalachians, the Greenbrier fault, can be clearly identified here (Hadley and Goldsmith, 1963; King, 1964), despite questions of its presence elsewhere. In addition, recent questions concerning the age of the Ocoee Supergroup have arisen based on the report of Late Devonian-earliest Mississippian fossils from the Great Smoky Mountains and adjacent areas from what were believed to be Late Proterozoic rocks (Unrug and Unrug, 1990; Unrug and others, 1991). The eastern Great Smoky Mountains, the primary area of interest of this study, is structurally unique in the western Blue Ridge because large premetamorphic folds are present that are noncoaxial with later structures and are therefore easily identified. Although these early structures may be present elsewhere in the western Blue Ridge, parallelism with later structures and/or more extensive later deformation and metamorphism makes the early structures difficult to uniquely identify.

Despite the abundance of detailed mapping and the regional structural importance of the Great Smoky Mountains area, few structural reconstructions, mesofabric or strain analysis studies have been conducted here. The principal goal of this study is to provide additional constraints on the tectonic development of the Great Smoky Mountains area. Several approaches are taken including examining the thrust fault geometries of this area in light of foreland models of deformation to allow for more accurate structural reconstructions. Also, the sequence and kinematics of thrust sheet emplacement is

examined using finite strain and mesofabric analysis. In order to address the problem of timing of deformation, as well as providing constraints on the age of the Ocoee Supergroup, $^{40}Ar/^{39}Ar$ geochronologic methods are employed. The results of these methods will be used to demonstrate: (1) foreland-style thrust geometries may be used effectively to unravel the tectonic history of an external portion of an orogenic core; (2) factorization of three-dimensional finite strain can provide insight into the strain history of a polydeformed thrust faulted area; (3) $^{40}Ar/^{39}Ar$ geochronology of very low to medium grade regionally metamorphosed rocks may be used to constrain the timing of metamorphism, recognize polymetamorphism, and provide constraints on the age of the affected western Blue Ridge lithologies.

This dissertation is written in the form of individual papers and is a compilation of a number of different but related studies from the Great Smoky Mountains region. The locations of each of the study areas is presented in Figure 1.1. The four sections that follow are versions of four separate manuscripts that have already been published (Part 2, Connelly and Woodward, 1992; Part 3, Woodward and others, 1991; Part 4, Connelly and Dallmeyer, 1993) or are in preparation (Part 5). Because these sections were written as separate manuscripts about different aspects of the geology of the Great Smoky Mountains area, there is some repetition of material, although this has been kept to a minimum by removing the regional geology and local geology for some sections and by referring to text and figures from earlier sections. This dissertation need not be read from beginning to end in the order presented, as individual sections largely stand alone with the exception of some material about the regional and local geology. Part 2 of this dissertation concerns the structural geometries observed in the eastern Great Smoky Mountains. Part 3 extends this discussion of structural geometries to the entire Great Smoky Mountains region. A study of the strain history of the eastern Great Smoky Mountains foothills is

Figure 1.1. Geologic map of the Great Smoky Mountains area showing locations of study areas in subsequent dissertation parts. (modified from King and others, 1968; Hadley and Nelson, 1971, Walters, 1988, and Keller, 1980). ACS=Alum Cave syncline; BR=Big Ridge; CA=Cartertown anticline; CC=Cades Cove; CCA=Copeland Creek anticline; CGF=Colan Ground fault; CM=Cove Mountain; CRF=Chestnut Ridge fault; DCF=Dunn Creek fault; FBR=French Broad River; G=Gatlinburg; GAF=Gatlinburg fault; GBF=Greenbrier fault; GSF=Great Smoky fault; HF=Hayesville fault; LPR=Little Pigeon River; LSF=Line Springs fault; LTR=Little Tennessee River; MCF=Miller Cove fault; OF=Oconaluftee fault; PBF=Parsons Branch fault; PFF=Pigeon Forge fault; RCF=Rabbit Creek fault; RK=Roundtop klippe; TC=Tuckaleechee Cove; WC=Wear Cove; WM=Webb Mountain.

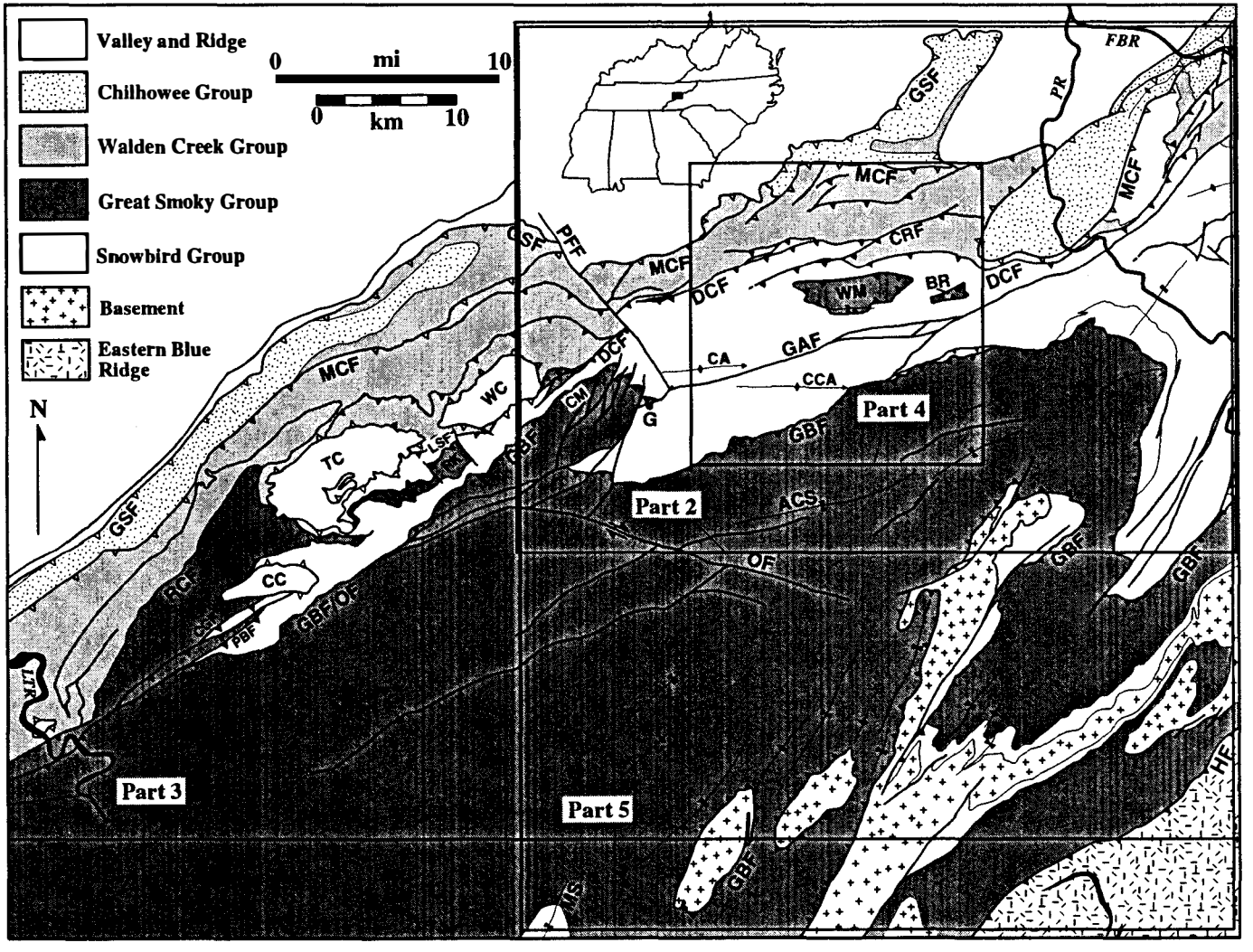
Valley and Ridge
Chilhowee Group
Walden Creek Group
Great Smoky Group
Snowbird Group
Basement
Eastern Blue Ridge
N
0 mi 10
0 km 10
Part 2
Part 3
Part 4
Part 5
GSF
MCF
PFF
DCF
CRF
WM
BR
GAF
CA
CCA
G
CM
WC
TC
LSF
GBF
ACS
OF
CC
RCF
PBF
GBF/OF
LTR
FBR
PR
HF

presented in Part 4. Part 5 addresses the problem of timing of deformation in the western Blue Ridge and the age of the Ocoee Supergroup using $^{40}Ar/^{39}Ar$ geochronology.

REFERENCES CITED

Connelly, J. B., and Woodward, N. B., 1992, Taconian foreland-style thrust system in the Great Smoky Mountains, Tennessee: Geology, v. 20, p. 177-180.

Connelly, J. B., and Dallmeyer, R. D., 1993, Polymetamorphic evolution of the western Blue Ridge province: Evidence from whole-rock slate/phyllite and muscovite ages: American Journal of Science, v. 293, p. 322-359.

Hadley, J. B., and Goldsmith, R., 1963, Geology of the eastern Great Smoky Mountains, North Carolina and Tennessee: U.S. Geological Survey Professional Paper 349-B, 118 p.

Hamilton, W. B., 1961, Geology of the Richardson Cove and Jones Cove quadrangles, Tennessee: U.S. Geological Survey Professional Paper 349-A, 55 p.

King, P. B., 1964, Geology of the central Great Smoky Mountains, Tennessee: U.S. Geological Survey Professional Paper 349-C, 148 p.

King, P. B., Hadley, J. B., Neuman, R. B., and Hamilton, W. B., 1958, Stratigraphy of the Ocoee Series, Great Smoky Mountains, Tennessee and North Carolina: Geological Society of America Bulletin, v. 69, p. 947-967.

Neuman, R. B., and Nelson, W. H., 1965, Geology of the western part of the Great Smoky Mountains, Tennessee: U. S. Geological Survey Professional Paper 349-D, 81 p.

Unrug, R., and Unrug, S., 1990, Paleontological evidence of Paleozoic age for the Walden Creek Group, Ocoee Supergroup, Tennessee: Geology, v. 18, p. 1041-1045.

Unrug, R., Unrug, S., and Palmes, S. L., 1991, Carbonate rocks of the Walden Creek Group in the Little Tennessee River valley: modes of occurrence, age, and significance for the basin evolution of the Ocoee Supergroup, *in* Kish, S. A., ed., Studies of Precambrian and Paleozoic stratigraphy in the western Blue Ridge: Carolina Geological Society Field Trip Guidebook, p. 27-37.

Woodward, N. B., Connelly, J. B., Walters, R. R., and Lewis, J. C., 1991, Tectonic evolution of the Great Smoky Mountains, *in* Kish, S. A., ed., Studies of Precambrian and Paleozoic Straigraphy in the western Blue Ridge: Carolina Geological Society Field Trip Guidebook, p. 57-68.

PART 2

TACONIAN FORELAND-STYLE THRUST SYSTEM IN THE GREAT SMOKY MOUNTAINS, TENNESSEE

INTRODUCTION

Intense Taconian and later metamorphism in the southern Appalachians has obscured the deformation effects of Ordovician orogenesis. The Great Smoky Mountains foothills, however, are only mildly metamorphosed, and many early structures are well preserved, offering an opportunity to successfully detect the style of this earlier event.

Structural styles within the western Blue Ridge province of the southern Appalachians have been described as characteristic of an orogenic hinterland rather than foreland, because the rocks are metamorphosed, faults have ductile fabrics, and deformation is polyphase. Within the Great Smoky Mountains, metamorphism and cleavage development postdate two major thrust fault systems. The purpose of this paper is to document the fundamental structural geometry of these early thrust systems. The faults of these premetamorphic thrust sheets will be shown to have ramp-flat thrust geometries characteristic of foreland-style fold-thrust belts.

GEOLOGIC SETTING

The study area is part of the western Blue Ridge province of the southern Appalachians and is in the eastern foothills of the Great Smoky Mountains (Fig. 2.1). The dominant stratigraphic unit in the western Blue Ridge is the Late Proterozoic Ocoee Supergroup, a 12-15-km-thick sequence of rift-related mainly terrigenous clastic metasedimentary rocks (e.g., King and others, 1958; Rast and Kohles, 1986). Three major lithologic sequences comprise the Ocoee Supergroup. These include the Snowbird Group, the Great Smoky Group, and the Walden Creek Group (King and others, 1958).

Figure 2.1. Geologic map of eastern Great Smoky Mountains. ACS=Alum Cave syncline; BR=Big Ridge; CA=Cartertown anticline; CCA=Copeland Creek anticline; CRF=Chestnut Ridge fault; CTA=Cataloochee anticlinorium; DCF=Dunn Creek fault; FCO=footwall cutoff; GAF=Gatlinburg fault; GBF=Greenbrier fault; GSF=Great Smoky fault; MCF=Miller Cove fault; PFF=Pigeon Forge fault; RA=Ravensford anticline; WM=Webb Mountain; WS=Waterville syncline; Cross section A-A' shown in Figure 2.3 (modified from King and others, 1968; Keller, 1980).

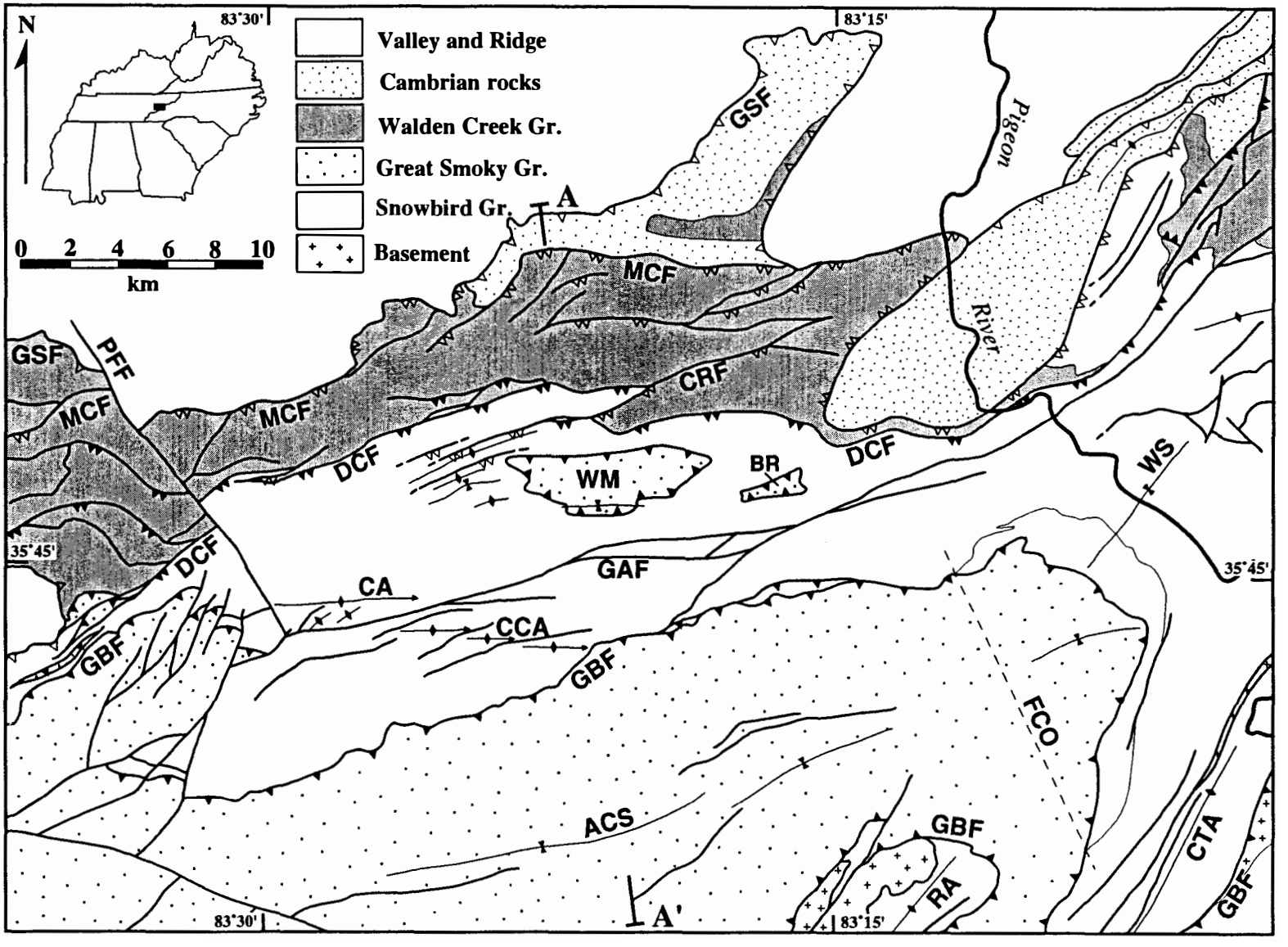
N
83°30'
Valley and Ridge
Cambrian rocks
Walden Creek Gr.
Great Smoky Gr.
Snowbird Gr.
Basement
0 2 4 6 8 10
km
A
A'
GSF
PFF
MCF
DCF
CRF
WM
BR
WS
Pigeon
River
GAF
CA
CCA
GBF
ACS
FCO
RA
CTA
83°15'
35°45'

Stratigraphic relations between these groups are uncertain in places because many rock units are in fault contact and vary considerably in thickness and lithology.

At least two major deformational events have affected the Great Smoky Mountains Foothills and resulted in five distinct fault systems. Three fault systems, the Great Smoky, Gatlinburg, and Miller Cove, are postmetamorphic and are probably Alleghanian. The Greenbrier and Dunn Creek fault systems are premetamorphic and are believed to be early Paleozoic structures. An additional early Paleozoic thrust sheet, now floored by the Miller Cove fault, was emplaced during regional cleavage development. Early Paleozoic structures are distinguished from late Paleozoic structures on the basis of their relations to regional cleavage and metamorphic isograds, and on the ductile nature of the early fault fabrics. Predominantly brittle fabrics are characteristic of the Alleghanian faults in this area.

Progressive Barrovian-type metamorphism affected rocks of the Great Smoky Mountains and increases from the sub-chlorite grade in the foothills to kyanite grade to the southeast (Hamilton, 1961; Hadley and Goldsmith, 1963) (Fig. 2.2). Recent $^{40}Ar / ^{39}Ar$ geochronologic results from the chlorite metamorphic zone of the study area, where cooling effects are minimal, indicate metamorphic cooling ages that range from ~460 to 420 Ma suggesting an Ordovician (Taconian) age of metamorphism (Connelly and Dallmeyer, 1991).

Alleghanian Structures

The Great Smoky fault is a major Alleghanian thrust fault and is part of the Blue Ridge-Piedmont fault system with between 350 to 500 km of inferred Alleghanian displacement (Hatcher, 1989). Seismic reflection data (e.g., Cook and others, 1979; Harris and others, 1981; Çoruh and others, 1987) document that over much of its areal extent, the Great Smoky thrust sheet is less than 5 to 7 km thick. Autochthonous basement

Figure 2.2. Cleavage trends and metamorphic isograds superimposed on regional geologic map (based on King, 1964; Hamilton, 1961; Hadley and Goldsmith, 1963; and Keller, 1980).

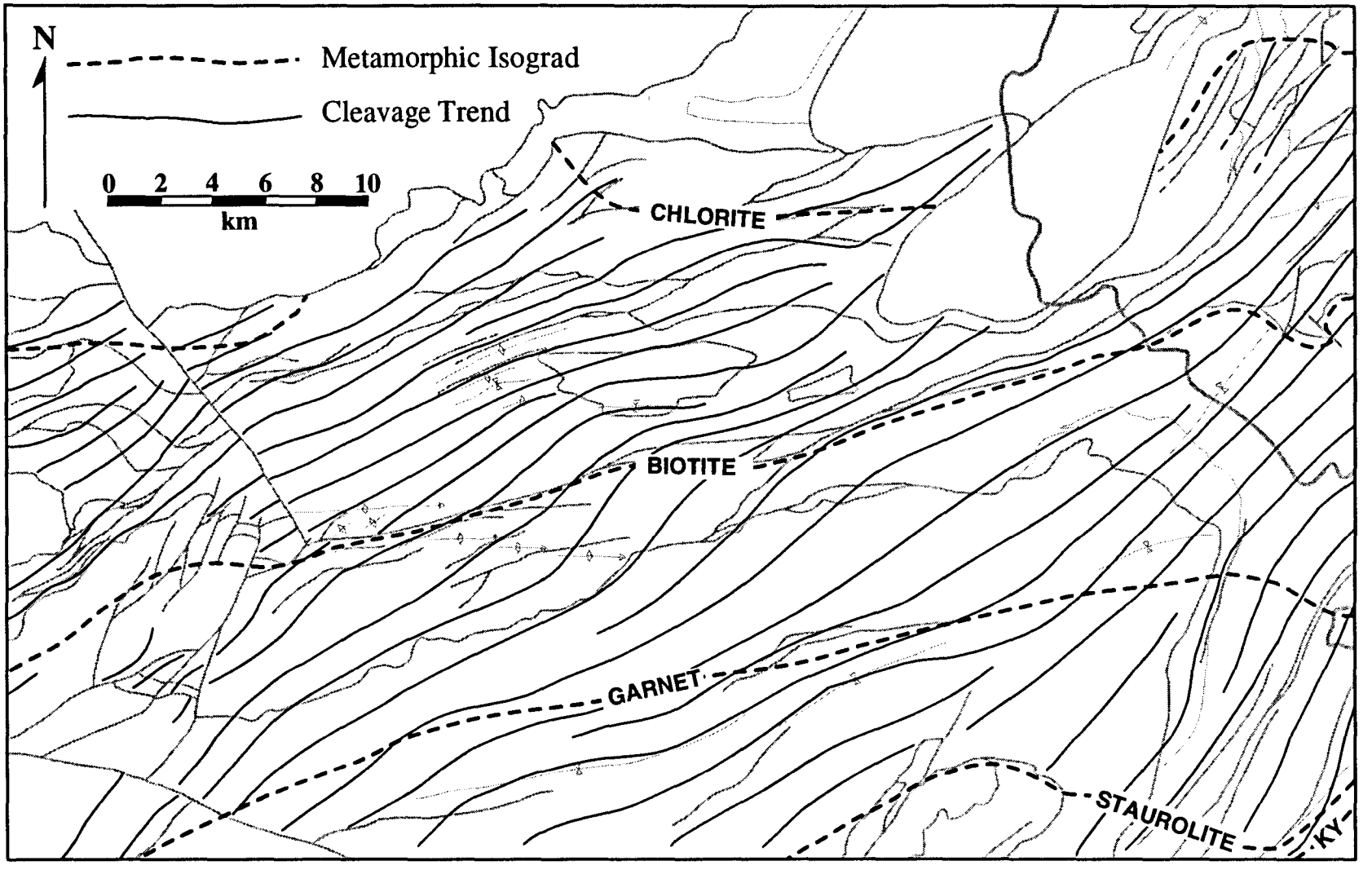
N
Metamorphic Isograd
Cleavage Trend
0 2 4 6 8 10
km
CHLORITE
BIOTITE
GARNET
STAUROLITE
KY

is separated from this thrust sheet by another 1 to 5 km of duplicated (duplexed) lower Paleozoic rocks with or without Proterozoic sedimentary rocks or basement. Windows through the thrust sheet suggest folding of the fault after emplacement. Other Alleghanian deformation within the Great Smoky thrust sheet in the study area is minor.

The Alleghanian Miller Cove fault separates cleaved and metamorphosed Ocoee strata from less cleaved and metamorphosed upper Ocoee, Chilhowee, and younger strata (Costello, 1984; Hatcher and others, 1989). The branch line between the Great Smoky and Miller Cove faults is at depth southwest of the Pigeon Forge fault, but is eroded northeast of this fault (Fig. 2.1). Thus, the Miller Cove fault is locally the frontal Blue Ridge fault.

The younger Gatlinburg and related faults are a primarily east-northeast trending system of brittle high-angle faults (Fig. 2.1). Both dip-slip and strike-slip motion occurred, although dip-slip predominates in the study area. Maximum displacement is about 2000 m (King, 1964).

Pre-Alleghanian Structures

The Greenbrier fault is a folded low-angle thrust that separates the Great Smoky Group from the underlying Snowbird Group in most areas (Fig. 2.1). Because the Greenbrier fault does not offset metamorphic isograds or affect regional cleavage, it is considered premetamorphic (Hadley and Goldsmith, 1963) and therefore Taconian.

North of the main outcrop belt of the Greenbrier thrust sheet, rocks very similar to Great Smoky Group types overlie Snowbird Group rocks at Webb Mountain and Big Ridge (Fig. 2.1). Hamilton (1961) left these rocks unclassified because of uncertain contact relations. Sharp truncation of structures along the northern contact indicates a fault, although along the southern contact, beds are parallel and were interpreted by Hamilton (1961) as stratigraphic. Connelly and others (1989) documented that the southern contact is faulted as well because of the presence of mylonites at this contact. The

unclassified formations at Webb Mountain and Big Ridge are therefore interpreted as Great Smoky Group equivalents and klippes of the Greenbrier fault.

A major structural feature within the Greenbrier thrust sheet is the Alum Cave Syncline (Hadley and Goldsmith, 1963) (Fig. 2.1). The northern limb of this fold dips 20° to 35° to the south with bedding concordant to the fault, whereas the southern limb is vertical to overturned with bedding truncated at a high angle by the fault. In contrast, the fault is parallel to or at a low angle to bedding in the footwall. The change in bedding-fault geometry across the Greenbrier fault indicates that the Alum cave syncline is rootless above the fault.

The other major premetamorphic fault, the Dunn Creek thrust fault, separates Snowbird Group rocks in the hanging wall from Walden Creek Group rocks in the footwall (Fig. 2.1). A premetamorphic age for the Dunn Creek fault is based on truncation of the fault by later synmetamorphic thrust faults (Connelly and others, 1989) and lack of offset of the chlorite isograd (Fig. 2.2) (Keller, 1980).

Major early folds within the Dunn Creek thrust sheet include the east-west trending Cartertown and Copeland Creek anticlines (Fig. 2.1). The folds are slightly offset by late high-angle faults. These anticlines have an angular to box geometry with steep to overturned northern limbs, a flat crest, and more gently dipping southern limbs. These folds are transected by later Taconian northeast-trending cleavage (Hamilton, 1961) (Fig. 2.2), and are therefore premetamorphic like the Dunn Creek fault.

Within the Miller Cove and Dunn Creek thrust sheets, a second generation of folding has been recognized that trends east-northeast. These structures are best observed northwest of Webb Mountain, where northwest-vergent map scale folds, commonly associated with ductile thrust faults, are present (Fig. 2.1). One of these ductile thrusts, the Chestnut Ridge fault, clearly truncates the premetamorphic Dunn Creek fault (Fig. 2.1). Within the Miller Cove thrust sheet, cleavage is axial planar to folds (e.g., Witherspoon, 1981; Sack, 1988) and commonly is parallel to the ductile thrust faults as well (Fig. 2.2). Within the Dunn Creek thrust sheet, cleavage transects most east-trending

folds but is axial planar to northeast-trending second-generation folds (Fig. 2.2). Interference between early east-trending folds and second-generation east-northeast-trending folds occurs throughout the Dunn Creek thrust sheet and results in steeply plunging second-generation folds with axial planar cleavage.

The ductile faults within the Miller Cove and parts of the Dunn Creek thrust sheets are associated with the folds and Taconian cleavage in these sheets. We infer that a Taconian detachment from which these ductile faults have splayed must therefore have underlain these thrust sheets. The Miller Cove fault is the present base of these Taconian thrust sheets, but it has brittle fault fabrics and is locally the frontal Blue Ridge fault, indicating an Alleghanian age. We believe that the present Miller Cove thrust sheet was active in both the Taconian and Alleghanian orogenies, although it is unclear how much of the base of the earlier Miller Cove thrust sheet was removed by Alleghanian thrusting.

TACONIAN THRUST FAULT GEOMETRIES

Figure 2.3A is a cross section through the study area based on surface structural data and stratigraphic thicknesses of Hamilton (1961), Hadley and Goldsmith (1963), and recent mapping. To best illustrate the early (pre-Miller Cove) thrust fault geometries, a partially restored cross section is presented in Figure 2.3B in which Alleghanian and latest Taconian deformation has been removed. Removal of Alleghanian deformation involves translation of the Great Smoky thrust sheet 350 km or more to the southeast, removal of minor displacement on high-angle Gatlinburg system faults, and removal of open folds resulting from late folding of the Great Smoky thrust sheet. Removal of latest Taconian deformation is also required to establish the early thrust fault geometries. This involves removal of map-scale folds and imbricate faults (Fig. 2.3B) and an unknown amount of Taconian displacement along the early Miller Cove fault. Although the internal straining of this thrust sheet occurred during emplacement, these strains are small in the foothills and are not considered in this restoration.

Figure 2.3. Cross section through line A-A' of Figure 2.1. Abbreviations same as those in Figure 2.1. No vertical exaggeration. A: Present-day cross section. B: Partially restored cross section following removal of Alleghanian and latest Taconian deformation. HR hanging-wall ramp; HF hanging-wall flat; FR footwall ramp; FF footwall flat. C: Cross section after removal of Dunn Creek thrusting. D: Cross section after removal of Greenbrier thrusting.

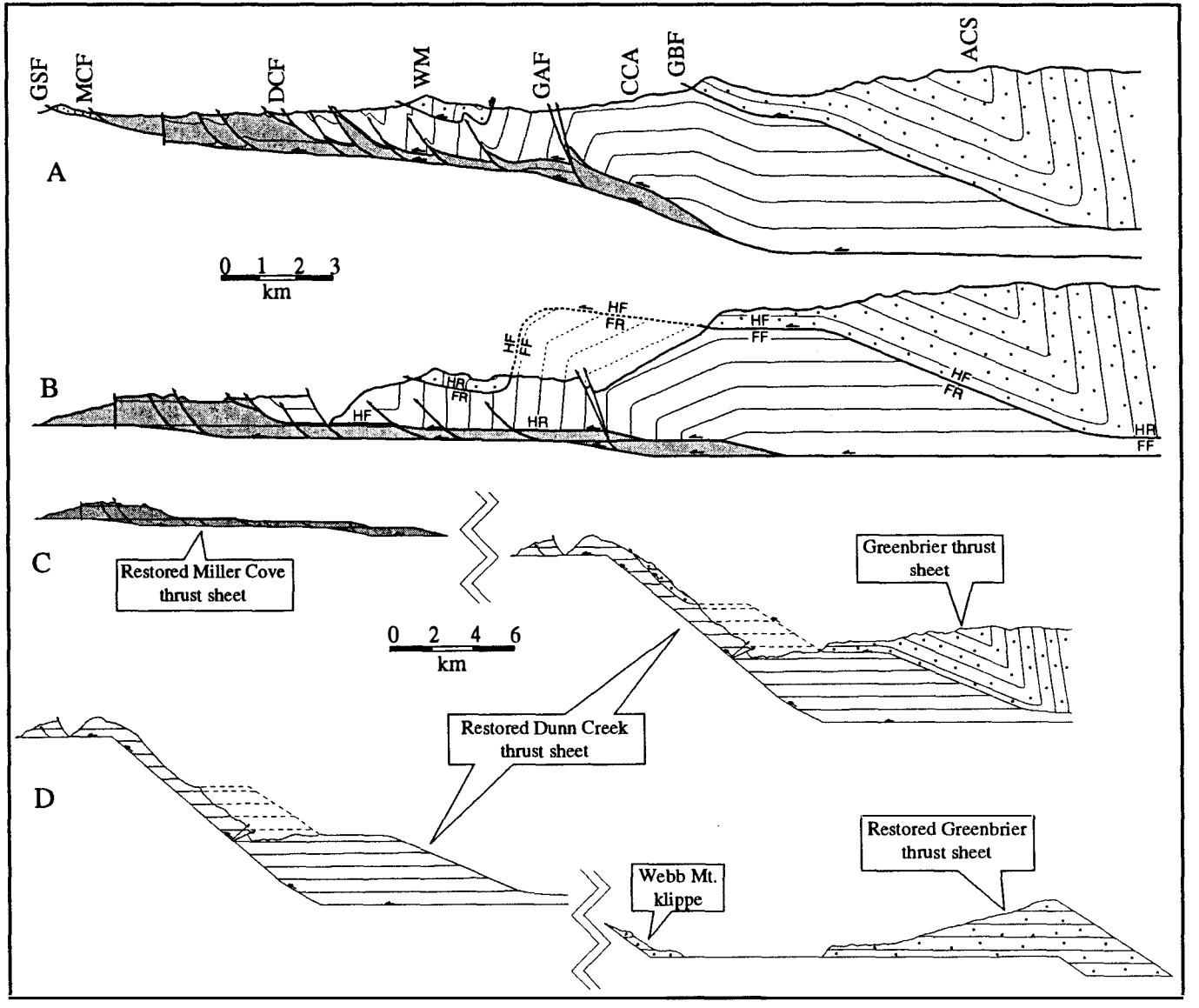
GSF
MCF
DCF
WM
GAF
CCA
GBF
ACS
A
0 1 2 3
km
B
HF
FR
FF
HR
C
Restored Miller Cove thrust sheet
0 2 4 6
km
Greenbrier thrust sheet
D
Restored Dunn Creek thrust sheet
Webb Mt. klippe
Restored Greenbrier thrust sheet

Examination of the partially restored cross section in Figure 2.3B shows structural geometries typically associated with foreland fold-thrust belts. The folded Greenbrier fault at the Webb Mountain klippe is steeply dipping and parallel to bedding on the south, but gently dipping and at a high angle to bedding on the north. A transition from a hanging-wall flat to a hanging-wall ramp geometry is therefore preserved here (Fig. 2.3B). The steeply dipping segment of the Greenbrier fault results from later folding of the fault by the Copeland Creek anticline.

The Greenbrier fault is approximately parallel to bedding along much of its trace, including a large area west of the axial trace of the Copeland Creek anticline (Fig. 2.1), but it truncates the Copeland Creek anticline in most other areas (Hadley and Goldsmith, 1963). The fault also cuts younger strata in the hinge of the Waterville syncline and older strata on the limbs (Hadley and Goldsmith, 1963). These relations led earlier workers to suggest that the Copeland Creek anticline and the Waterville syncline preceded emplacement of the Greenbrier fault (e.g., Hadley and Goldsmith, 1963; Keller, 1980; Witherspoon, 1981).

The above relations also can be explained, however, in terms of simple ramp-flat thrust geometries. Nowhere does the Greenbrier fault cut down section in the direction of thrust transport. We explain the "truncation" of the Copeland Creek anticline by the Greenbrier fault as a folded footwall ramp (Fig. 2.3B). We also suggest that the Greenbrier fault cuts up section to the east across a lateral ramp (north-trending footwall cutoff) that is folded by the Waterville syncline (Fig. 2.1). Emplacement of the Greenbrier fault into previously folded strata is therefore not required.

Given these simple geometric interpretations, the steeply dipping southern limb of the Alum Cave syncline (Fig. 2.3) may also represent the northern limb of a large hanging-wall ramp anticline where the Greenbrier thrust sheet ramps up from basement into the Ocoee Supergroup. This ramp anticline overlies additional horses of basement and cover in the Ravensford anticline south of the cross section line. The extent of this

hanging-wall ramp to the south is not clear because of extensive modification by late folds.

The dip of the Greenbrier thrust sheet steepens in the middle of the north limb of the Alum Cave syncline (Fig 2.3A). Such sheet-dip changes commonly reflect buried flat-to-ramp transitions in foreland areas and may reflect a footwall trailing-edge ramp through the upper Snowbird Group beneath the Greenbrier thrust. The Snowbird Group thins stratigraphically to the south, as only a very thin layer of Snowbird Group is present in the southeastern Great Smoky Mountains (Hadley and Goldsmith, 1963).

As many as four ramps can therefore be identified in this restoration of the Greenbrier thrust sheet. An upper hanging-wall ramp through Great Smoky Group strata is preserved at the Webb Mountain klippe, where, from south to north, a folded flat-to-ramp transition is present (Fig. 3B). A footwall ramp is represented by the large area where the Greenbrier fault cuts up-section through the Snowbird Group (Fig. 2.3B). This ramp was subsequently folded by the underlying Copeland Creek anticline. A footwall ramp through the Snowbird Group now underlying the Alum Cave syncline also may be present (Fig. 2.3B). The area south of the Alum Cave syncline represents the leading edge of another large hanging-wall ramp anticline.

A single major hanging-wall ramp can be identified within the Dunn Creek thrust sheet that underlies the Cartertown and Copeland Creek anticlines (Fig. 2.3B). An upper hanging-wall flat at the upper Snowbird Group level (bedding parallel to faults) is preserved north of these anticlines (Fig. 2.3B). These anticlines folded the overlying Greenbrier fault and indicate that the Greenbrier fault was emplaced earlier than the Dunn Creek fault ("in sequence"). The Dunn Creek fault may ramp down into basement like the Greenbrier fault, or it may branch from the Greenbrier fault at depth to the southeast.

Thrust Sheet Restoration

Because a hanging-wall ramp anticline within the Dunn Creek thrust sheet has folded the Greenbrier fault, the Dunn Creek thrust sheet must be restored first. Restoration

of this thrust sheet involves unfolding of the Copeland Creek anticline, which restores to a large ramp south of the Miller Cove thrust sheet (Fig. 2.3C). Unfolding of this anticline unfolds the overlying Greenbrier fault, making the ramp-flat geometry more apparent. The Greenbrier thrust sheet preserves two hanging-wall ramps: one at the Webb Mountain klippe and one at the south limb of the Alum Cave syncline (Fig. 2.3B). Restoration of the Greenbrier thrust sheet requires that the ramp-to-flat transition preserved at the Webb Mountain klippe restore to the base of a ramp (Fig. 2.3D), and that the lower ramp eventually enter basement southeast of the cross section.

The type of reconstruction presented above is instructive because it allows us to make minimum estimates of displacement for these early thrust sheets. For example, this reconstruction allows for a minimum of 23 km of displacement for the Greenbrier thrust sheet. This is comparable to the 24 km of displacement estimated by Hadley and Goldsmith (1963) on the basis of stratigraphic criteria. A similar minimum displacement of about 22 km is also estimated for the Dunn Creek thrust sheet.

DISCUSSION

The earliest two thrust sheets within the Great Smoky Mountains were emplaced with little internal deformation, and were later overprinted by both ductile and brittle fault systems. Removal of deformation related to these overprinting fault systems reveals thrust fault geometries characteristic of foreland fold-thrust belts and allows restoration of these thrust systems by means typically restricted to foreland areas. This foreland style of deformation has not been previously demonstrated in the southern Appalachians for rocks deformed prior to the Alleghanian orogeny, and suggests that the earliest deformation in the Great Smoky Mountains occurred in an orogenic foreland rather than hinterland.

Overprinting of foreland-style deformation by metamorphism and hinterland-style polyphase deformation may be a common process within orogenic belts as a result of the migration of metamorphism and ductile deformation towards the foreland. This style and sequence of deformation should be expected as a transitional zone between foreland and

hinterland portions of other orogenic belts. At higher metamorphic grades than those in the present study area, however, the early structural styles may not be recognized.

REFERENCES CITED

Connelly, J. B., and Dallmeyer, R. D., 1991, Polymetamorphic evolution of the western Blue Ridge, Tennessee and North Carolina: Evidence from ^{40}Ar / ^{39}Ar ages: Geological Society of America Abstracts with programs, v. 23, no. 1, p. 18.

Connelly, J. B., Woodward, N. B., and Walters, R. R., 1989, Polyphase early Paleozoic tectonism preserved in the western Blue Ridge; example from the Great Smoky Mountains National Park: Geological Society of America Abstracts with Programs, v. 21, p. 65.

Cook, F. A., Albaugh, D. S., Brown, L. D., Kaufman, S., Oliver, J. E., and Hatcher, R. D., Jr., 1979, Thin-skinned tectonics in the crystalline southern Appalachians; COCORP seismic-reflection profiling of the Blue Ridge and Piedmont: Geology, v. 7, p. 563-567.

Çoruh, C., Costain, J. K., Hatcher, R. D., Jr., Pratt, T. L., Williams, R. T., and Phinney, R. A., 1987, Results from regional vibroseis profiling: Appalachian ultra-deep core hole site study: Geophysical Journal of the Royal Astronomical Society, v. 89, p. 473-474.

Costello, J. O., 1984, Relationships between the Cartersville fault and Great Smoky fault in the southern Appalachians: A reinterpretation [M.S. thesis]: Columbia, University of South Carolina, 75 p.

Hadley, J. B., and Goldsmith, R., 1963, Geology of the eastern Great Smoky Mountains, North Carolina and Tennessee: U.S. Geological Survey Professional Paper 349-B, 118 p.

Hamilton, W., 1961, Geology of the Richardson Cove and Jones Cove quadrangles, Tennessee: U.S. Geological Survey Professional Paper 349-A, 55 p.

Harris, L. D., Harris, A. G., DeWitt, W., Jr., and Bayer, K. C., 1981, Evaluation of the southern eastern overthrust belt beneath the Blue Ridge-Piedmont thrust: American Association of Petroleum Geologists Bulletin, v. 65, p. 2497-2505.

Hatcher, R. D. Jr., 1989, Tectonic synthesis of the U.S. Appalachians, *in* Hatcher, R. D., Jr., Thomas, W. A., and Viele, G. W., eds., The Appalachian-Ouachita orogen in the United States: Boulder, Colorado, Geological Society of America, The Geology of North America, v. F-2, p. 511-535.

Hatcher, R. D., Jr., Thomas, W. A., Geiser, P. A., Snoke, A. W., Mosher, S., and Wiltschko, D. V., 1989, Alleghanian orogen, *in* Hatcher, R. D., Jr., Thomas, W. A., and Viele, G. W., eds., The Appalachian-Ouachita orogen in the United

States: Boulder, Colorado, Geological Society of America, The Geology of North America, v. F-2, p. 233-318.

Keller, F. B., 1980, Late Precambrian stratigraphy, depositional history, and structural chronology of part of the Tennessee Blue Ridge [Ph.D. thesis]: New Haven, Connecticut, Yale University, 353 p.

King, P. B., 1964, Geology of the central Great Smoky Mountains, Tennessee: U. S. Geological Survey Professional Paper 349-C, 148 p.

King, P. B., Hadley, J. B., Neuman, R. B., and Hamilton, W., 1958, Stratigraphy of the Ocoee Series in the Great Smoky Mountains, Tennessee and North Carolina: Geological Society of America Bulletin, v. 69, p. 947-966.

King, P. B., Neuman, R. B., and Hadley, J. B., 1968, Geology of the Great Smoky Mountains National Park, Tennessee and North Carolina: U.S. Geological Survey Professional Paper 587, 23 p.

Rast, N.,and Kohles, K. M., 1986, The origin of the Ocoee Supergroup: American Journal of Science, v. 286, p. 593-616.

Sack, W. R., 1988, Geometric analysis and kinematics of folding associated with overthrusting: Blue Ridge Province, Tennessee [M.S. thesis]: East Lansing, Michigan State University, 158 p.

Witherspoon, W. D., 1981, Structure of the Blue Ridge thrust front, Tennessee, southern Appalachians [Ph.D. thesis]: Knoxville, University of Tennessee, 165 p.

PART 3

TECTONIC EVOLUTION OF THE GREAT SMOKY MOUNTAINS

INTRODUCTION

The Great Smoky Mountains area of Tennessee and North Carolina preserves several fault systems of different ages. Interactions between these various thrust fault systems and thrust related structures has complicated structural and stratigraphic relations in this area. To better understand these complexities, a significant change in thrust system interpretation in the Great Smoky Mountains area is suggested here. In North America, emphasis in mapping is usually placed on fault-tracing and naming, usually from the perspective of the footwall strata. Thus, the Great Smoky fault is that fault which places old rocks, commonly Precambrian ones, over younger Valley and Ridge strata. In Alpine tectonics (e.g., Trumpy, 1969), however, the emphasis is placed on identifying and segregating the "nappes", or thrust sheets, with much less emphasis on the fault surfaces that bound them. This approach will be used for the Great Smoky Mountains because there are multiple thrust and extensional fault systems within the western Blue Ridge. Late thrust and extension faults truncate early low-angle faults and commonly cover the basal thrust surfaces which underlie the older thrust blocks. Thus, the new structural reconstructions suggested for the Great Smoky Mountains region are based on restoration of thrust sheets whose interpretation rests on key areas where initial thrust relationships are preserved. Emphasis lies in sequential restorations of the area based on structures such as transecting cleavage and faults. This is done by restoring the complex deformation history from youngest to oldest.

The Great Smoky Mountains area occupies the best mapped large area in the western Blue Ridge province (Hamilton, 1961; Hadley and Goldsmith, 1963; King, 1964;

Figure 3.1. Regional map of the Great Smoky Mountains area (modified from King and others, 1968; Hadley and Nelson, 1971, Walters, 1988, and Keller, 1980). ACS=Alum Cave syncline; BR=Big Ridge; CA=Cartertown anticline; CC=Cades Cove; CCA=Copeland Creek anticline; CGF=Colan Ground fault; CM=Cove Mountain; CRF=Chestnut Ridge fault; DCF=Dunn Creek fault; FBR=French Broad River; G=Gatlinburg; GAF=Gatlinburg fault; GBF=Greenbrier fault; GSF=Great Smoky fault; HF=Hayesville fault; LPR=Little Pigeon River; LSF=Line Springs fault; LTR=Little Tennessee River; MCF=Miller Cove fault; OF=Oconaluftee fault; PBF=Parsons Branch fault; PFF=Pigeon Forge fault; RCF=Rabbit Creek fault; RK=Roundtop klippe; TC=Tuckaleechee Cove; WC=Wear Cove; WM=Webb Mountain. Thrust faults with open teeth late and with closed teeth early. Cross-section lines are shown for Figures 3.5, 3.6 and 3.7.

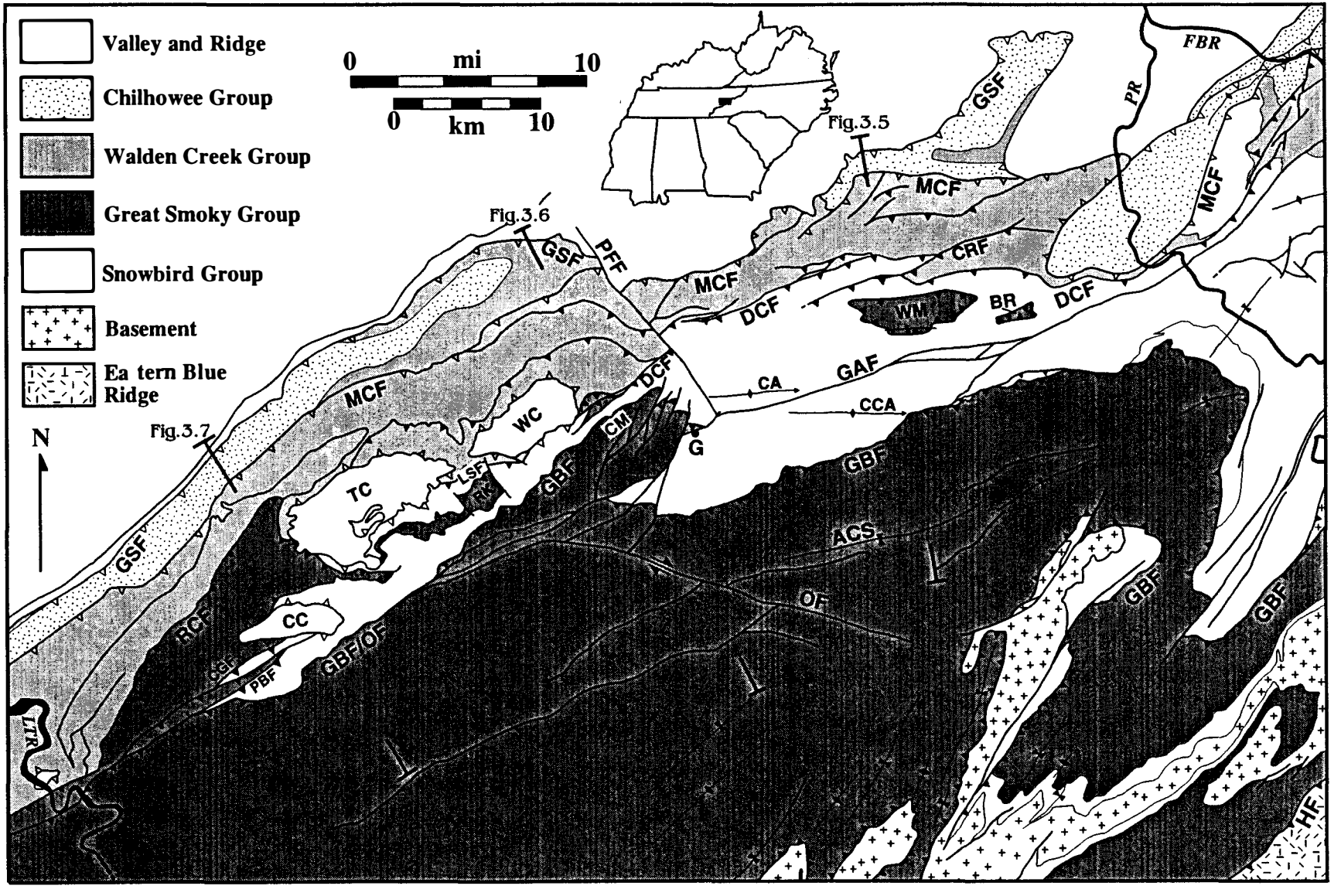
Valley and Ridge
Chilhowee Group
Walden Creek Group
Great Smoky Group
Snowbird Group
Basement
Ea tern Blue Ridge
0 mi 10
0 km 10
N
Fig.3.5
Fig.3.6
Fig.3.7
GSF
PFF
MCF
DCF
CRF
FBR
PR
WM
BR
CA
GAF
CCA
G
WC
CM
TC
LSF
GBF
ACS
OF
RCF
CC
PBF
GBF/OF
ITR
HF

Neuman and Nelson, 1965; Fig. 3.1). Recent work on kinematics of structural fabrics in parts of the area (Lewis, 1988; Walters, 1988; Connelly and Woodward, 1992) has added significantly to our understanding of the previously mapped structural geometries. This contribution builds on this existing map framework by adding fault fabric data, strain data, and cleavage studies to better understand the kinematic evolution of the Great Smoky Mountains structural belt. Until other parts of the western Blue Ridge are equally well mapped, the Great Smoky Mountains area will remain a principal index area for structural geometries and fabrics that may occur elsewhere in the western Blue Ridge.

REGIONAL GEOLOGY

Stratigraphy

The Ocoee Supergroup was divided into three groups by King and others (1958) based largely on the lithologic successions exposed along the French Broad (Oriel, 1950; Ferguson and Jewell, 1951), Pigeon (Hadley and Goldsmith (1963), Little Pigeon (Hamilton, 1961), Little (King, 1964), and Little Tennessee Rivers (Neuman and Nelson, 1965) (Fig. 3.2). The successions are not entirely compatible. The Snowbird Group underlies both the Great Smoky Group (Pigeon River) and the Walden Creek Group (French Broad River). The Walden Creek Group also overlies the Great Smoky Group in Ocoee Gorge (Costello and Hatcher, 1986). There are no chronostratigraphic markers which can be used to correlate the lithostratigraphic successions. Based on superposition of stratigraphic units, it appears likely that the Snowbird may be chronostratigraphically equivalent to lower parts of the Great Smoky Group and the Walden Creek Group may be similarly equivalent to parts of the upper Great Smoky Group.

Because of uncertain stratigraphic relations, several "unclassified" lithostratigraphic units remained after the work of King and others (1958). The

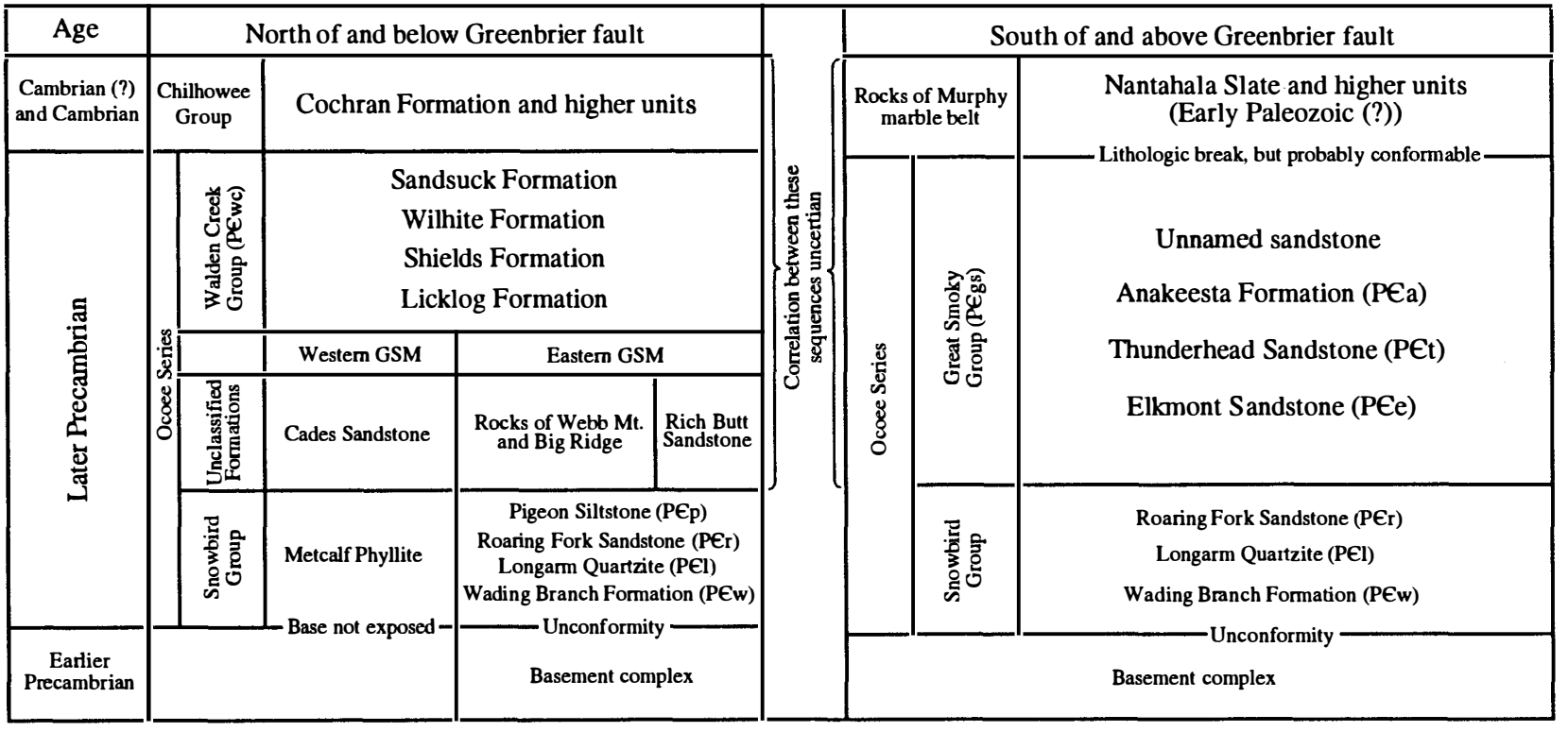

Figure 3.2. Stratigraphic units of the Ocoee Supergroup.

contribution of this paper to Ocoee stratigraphy is the assignation of most of these previously unclassified units to the established formations based on structural criteria (Walters and Woodward, 1987; Connelly and Woodward, 1990). Most of the unclassified formations (Cades Sandstone, Rocks of Webb Mountain and Big Ridge) are assigned to the lithologically similar Great Smoky Group (Fig. 3.1).

Structural Geology

Thrust faults are the dominant geologic structures within the Great Smoky Mountains area (Fig. 3.1). The older thrust faults in this area are interpreted to be Ordovician (Taconic) in age (e.g., Hadley and Goldsmith, 1963; King, 1964; Connelly and Dallmeyer, 1993). During the Carboniferous-Permian Alleghanian orogeny, this stack of Taconic thrust sheets was emplaced into its current position by the Great Smoky fault, and later folded (King, 1964; Neuman and Nelson, 1965) into a basin and dome (window) pattern by Alleghanian thrust structures of the Valley and Ridge (Boyer and Elliott, 1982; Woodward, 1985). In order to understand the geometry of the Taconic thrust sheets in the Great Smoky Mountains area, we must first remove the effects of the younger deformation event.

The major fault systems in the Great Smoky Mountains area are 1) the post-Great Smoky Gatlinburg fault system; 2) the Alleghanian Great Smoky fault system, including the Miller Cove fault. The Miller Cove fault separates cleaved rocks on the southeast from uncleaved rocks of the Chilhowee Mountain block, the English Mountain block, and the Valley and Ridge to the northwest (Fig. 3.1); 3) the Taconian early Miller Cove fault system that bounds the cleaved and faulted rocks of the Miller Cove thrust sheet, but that is now occupied by the Alleghanian Miller Cove fault; 4) the Taconian Dunn Creek-Line Springs-Rabbit Creek fault system; and 5) The Taconian Greenbrier fault.

Cleavage

Hadley and Goldsmith (1963) and King (1964) recognized that metamorphic isograds cross the major structures within the Great Smoky Mountains region, and are truncated by the Miller Cove and Great Smoky faults (Fig. 3.3). Two additional elements of the rock fabric evolution of this area are key to interpreting the structural history. Hamilton (1961) recognized that throughout most of the eastern Great Smoky Mountains, cleavage diverges from the axial planes of many folds and therefore may have been superimposed on these folds. This cleavage is axial planar to folds within the Miller Cove thrust sheet (Witherspoon, 1981; Sack, 1988) but transects most other structures within the Dunn Creek and Greenbrier thrust sheets (Hamilton, 1961; Connelly and Woodward, 1992) (Fig. 3.3). The structures within the overlying Dunn Creek and Greenbrier thrust sheets can therefore be placed in a hinterland to foreland sequence of deformation.

Connelly and Dallmeyer (1993) reported $^{40}Ar/^{39}Ar$ whole rock and muscovite results from a transect across the eastern Great Smoky Mountains. Metamorphic cooling ages range from ~460 Ma to 440 Ma from the chlorite metamorphic zone and ~380 Ma to 340 Ma for rocks from the biotite to kyanite zones. These ages were interpreted to indicate a polymetamorphic history in which a ~460 Ma (Taconic) event responsible for regional cleavage development was variably overprinted at higher metamorphic grades by a largely thermal ~380 Ma (Acadian?) event in which porphyroblasts overgrew earlier foliation (Connelly and Dallmeyer, 1991, 1993). The Great Smoky Mountains area therefore preserves a rare record of a Taconian low-grade thrust system which has been only slightly overprinted by later deformation.

Figure 3.3. Cleavage form lines and metamorphic isograds from the eastern Great Smoky Mountains (northeast corner of Figure 3.1). Cleavage and isograds transect the major structures of the Greenbrier and Dunn Creek thrust sheets and are axial planar to folds in the Miller Cove thrust sheet (based on data from Hamilton, 1961; Hadley and Goldsmith, 1963; King, 1964; Keller, 1980).

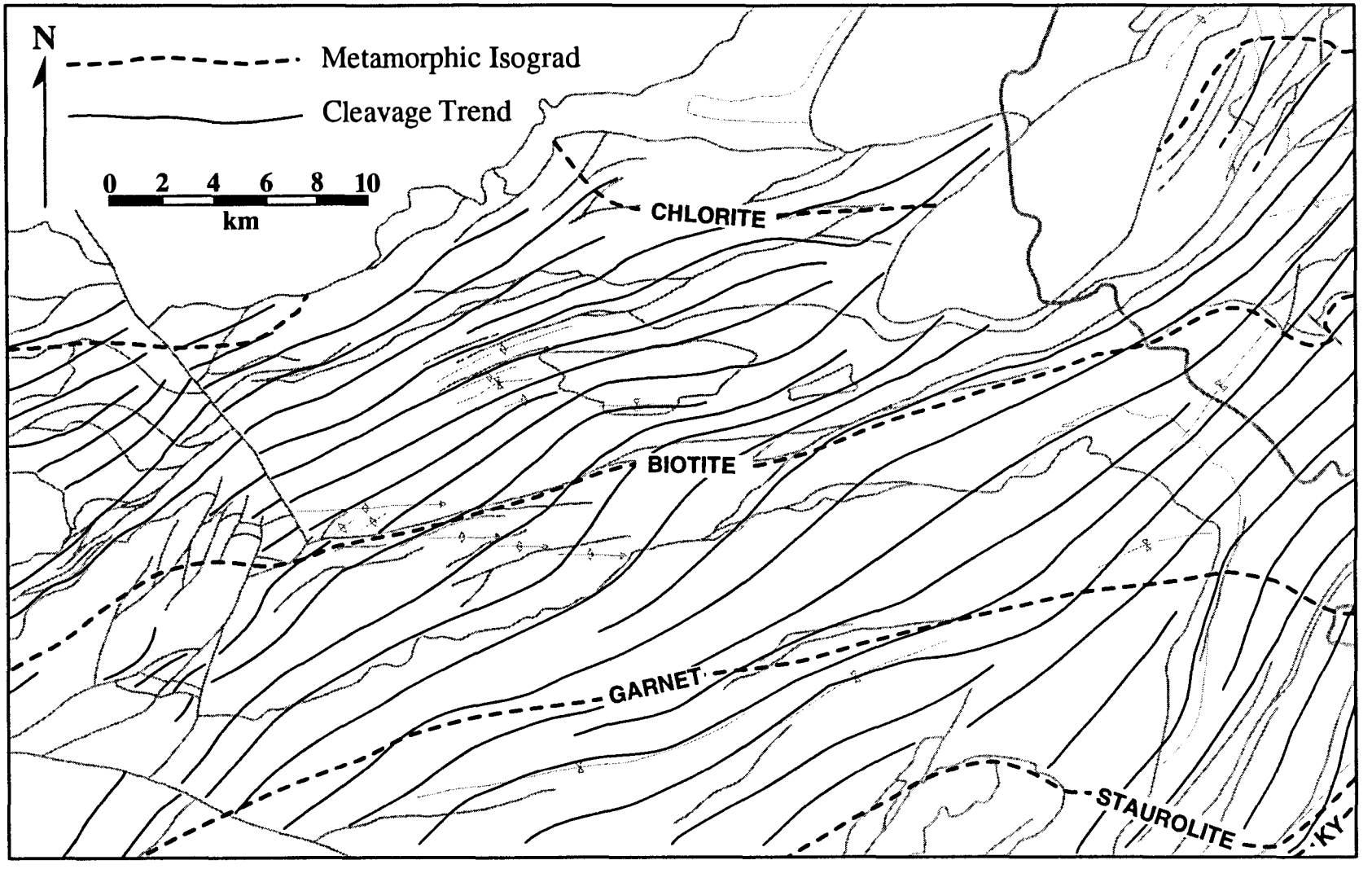
N
Metamorphic Isograd
Cleavage Trend
0 2 4 6 8 10
km
CHLORITE
BIOTITE
GARNET
STAUROLITE
KY

FAULT SYSTEMS

Gatlinburg Fault

The Gatlinburg fault system trends east-northeast and cuts across all of the earlier fold and thrust structures in the Great Smoky Mountains (Fig. 3.1). King (1964) suggested that it is a late high-angle reverse fault system, but displacements are relatively minor and no ramp-related folding, typical of thrusts, has been recognized. If high-angle reverse motion had consistently occurred on Gatlinburg-system faults, repetition of the low-angle fault structures, such as those of the Dunn Creek fault at the Pigeon River, would be expected, but this is not observed.

The Gatlinburg system faults roughly parallel the major east-northeast late fold trends that dome the overlying Great Smoky thrust sheet even where they transect structures within it. Strata of different groups within the Ocoee are rarely juxtaposed by Gatinburg system faults; where units are juxtaposed, the offsets omit strata as commonly as they duplicate strata. The geographic distribution of faults that omit strata is one of symmetry along the domal trends of the folded Great Smoky thrust sheet, with the culmination-side block up thrown in almost all cases. Fault zones along Gatlinburg system faults generally contain incohesive breccias (King, 1964; Robert, 1987). These brittle fault fabrics contrast with the ductile fabrics observed within most other thrust zones in the Great Smoky Mountains. These lines of evidence suggested to Woodward (1986) that the Gatlinburg faults are dominantly extensional in origin and related to post-emplacement extension of the crystalline Great Smoky thrust sheet as it was folded over subthrust duplex horses. In some areas these extensional motions reactivated earlier thrusts or partially truncated them, and in other areas all earlier thrusts and folds are truncated.

Other late high-angle faults that offset all other structures include the Pigeon Forge fault and the Oconaluftee fault (Fig. 3.1). These faults diverge from the east-northeast trend of the main Gatlinburg system faults, but likely formed at approximatly the same time and may be included in the Gatlinburg fault system.

Great Smoky Fault

The Great Smoky fault is part of the Blue Ridge-Piedmont thrust system and emplaces rocks of the Blue Ridge province over the Valley and Ridge province. Paleozoic strata from the Cambrian Chilhowee Group up through the Cambro-Ordovician Knox Group are present in different places within the Blue Ridge thrust sheet. In the Great Smoky Mountains region, only rocks as young as the Rome Formation are preserved in the Chilhowee Mountain and English Mountain fault blocks. In northeastern Tennessee, rocks as young as the Knox Group are exposed within the allochthonous Shady Valley synclinorium. Rocks this young within the Blue Ridge thrust sheet require that the footwall cutoffs of these units beneath the Blue Ridge must extend nearly to the Brevard zone or beyond (Harris and others, 1981) no matter how the subthrust structural details are drawn (Boyer and Elliott, 1982; Woodward, 1985; Hatcher and others, 1987; 1990).

Displacement along the Great Smoky fault has been estimated by Hatcher (1989) to be between 350 and 500 km. Final emplacement of the Great Smoky thrust sheet occurred during the Alleghanian orogeny, but the estimated magnitude of this displacement suggests that transport occurred over an extended period of time. As will be discussed in greater detail later, the Great Smoky fault observed today occupies and/or truncates earlier ductile deformation zones in a number of areas. Thus, the base of the Great Smoky sheet in a number of areas may truncate any of the earlier thrust sheets. Where well exposed, the basal Great Smoky thrust zone appears to be a mesoscopically faulted process zone (Hatcher and Milici, 1986) similar to that observed along Valley and

Ridge faults (Harris and Milici, 1977; Wojtal, 1986). A major component of deformation in these mesoscopically faulted process zones is partitioned into extension of the fault zone during thrust motion (Wojtal, 1986; Woodward and others, 1988; Erickson and Wiltschko, 1991). It is not clear if the lowest parts of the Taconian thrust stack have been variably removed in different places by this mesoscopic faulting, or if the Great Smoky fault simply truncated the Taconian thrust stack at different levels in different places.

Miller Cove Fault

The most external major structural boundary preserved within the Blue Ridge is the Miller Cove fault, which juxtaposes cleaved Walden Creek Group strata on the south and southeast with uncleaved Chilhowee and Walden Creek Group strata on the north and northwest (King, 1964; Costello, 1984; Figs. 3.1, 3.4A). Hamilton (1961) called the fault that juxtaposes these same rocks south of English Mountain the Great Smoky fault, and called the fault juxtaposing the Chilhowee strata and Valley and Ridge strata the English Mountain fault. In this paper, Great Smoky fault name is reserved for the northwesternmost Blue Ridge bounding fault (e.g., Costello, 1984; Hatcher and others, 1989). Because both the Miller Cove fault and Great Smoky fault of Hamilton (1961) south of English Mountain juxtapose the same stratigraphic sequences a short distance along strike from one another, we consider them to be (have been) continuous, with their branch line with the Great Smoky fault partially eroded where cleaved Ocoee strata are in direct contact with Valley and Ridge rocks, such as east of the Pigeon Forge fault (Fig. 3.1). This Miller Cove fault (in the broad sense) must be post-Taconic because it separates rocks with Taconian cleavage from those without it. It most likely formed early in the motion of the Great Smoky thrust system, juxtaposing previously thrust faulted and deformed Ocoee strata against the undeformed footwall ramp of uncleaved Chilhowee and Sandsuck strata.

Figure 3.4. Outline maps of the Miller Cove, Dunn Creek, and Greenbrier thrust sheets. Abbreviations the same as those in Figure 1. A: Outline map of the Miller Cove thrust sheet. Solid barbed lines indicate the Miller Cove thrust and its imbricates. Dashed lines show the trailing edges of the thrust sheet; CR-Chestnut Ridge fault. B: Outline map of the Dunn Creek-Line Springs-Rabbit Creek thrust sheet. The major hanging wall structure in the eastern Great Smoky Mountains is the Cartertown-Copeland Creek anticline (CA-CCA). The Dunn Creek-Greenbrier leading edge branch line is exposed on Cove Mountain (branch point BP1) and on the southwest edge of Tuckaleechee Cove (BP2). The Parsons Branch, Coalen Ground and Sinks faults are ductile imbricates of the Dunn Creek-Line Springs-Rabbit Creek thrust zone because they all transect and repeat parts of Metcalf Phyllite and the overlying Greenbrier thrust sheet. C: Outline Map of the Greenbrier thrust sheet including the Cades Sandstone, and the rocks of Webb Mountain and Big Ridge. There is a leading edge hanging-wall ramp anticline exposed as the Rabbit Creek nappe at Cove Mountain and at Webb Mountain. It has been folded by deformation in the Dunn Creek thrust sheet.

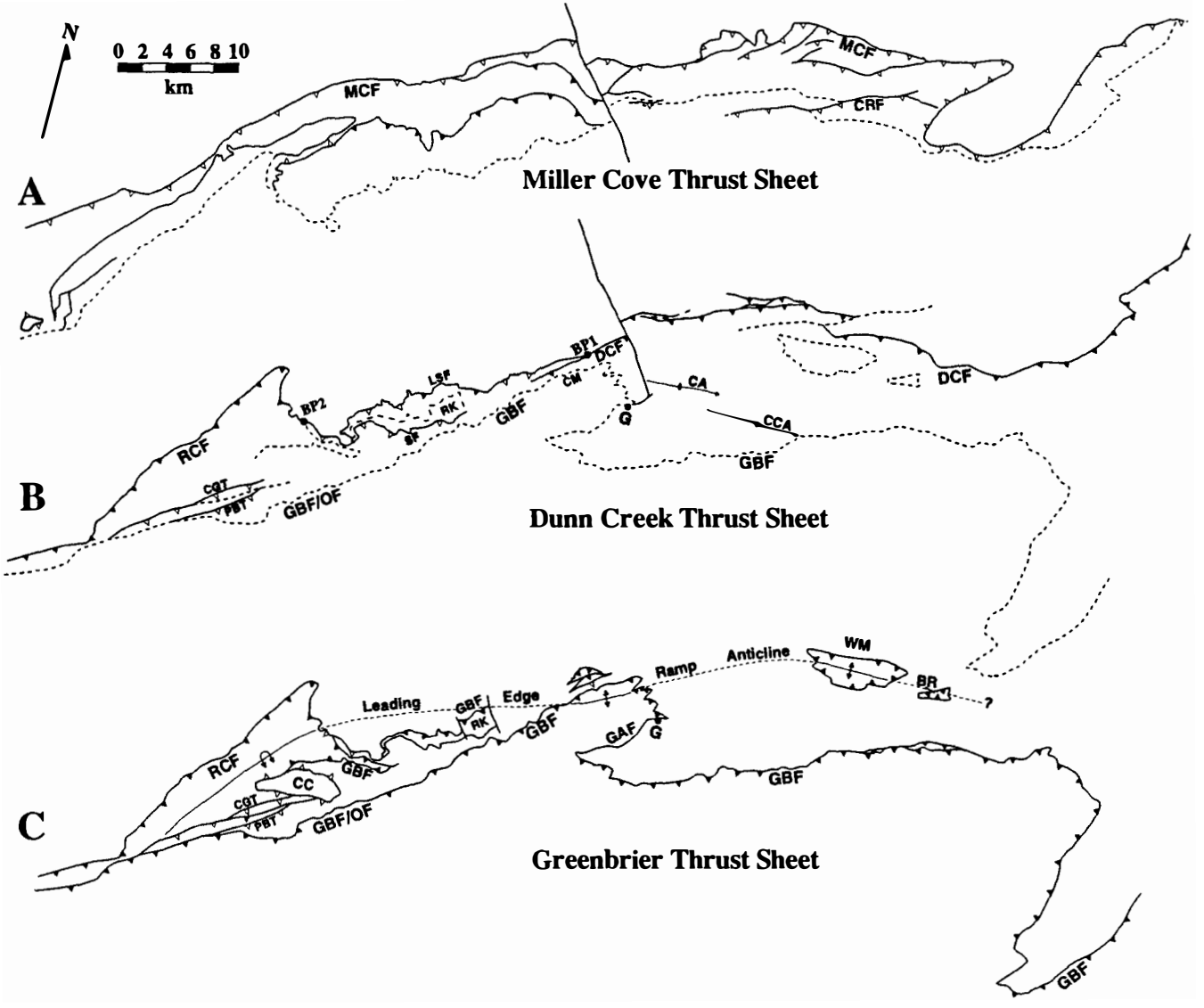
N
0 2 4 6 8 10
km
A
MCF
MCF
CRF
Miller Cove Thrust Sheet
B
RCF
CGT
PBT
GBF/OF
BP2
LSF
RK
SF
GBF
BP1
DCF
CM
Q
CA
CCA
GBF
DCF
Dunn Creek Thrust Sheet
C
RCF
CGT
PBT
GBF/OF
CC
GBF
Leading
GBF
RK
Edge
GBF
Ramp
Anticline
WM
BR
?
GAF
Q
GBF
GBF
Greenbrier Thrust Sheet

Early Miller Cove Fault

Cleavage within the Walden Creek Group strata of the Miller Cove thrust sheet parallels many small-displacement ductile thrust faults and is axial planar to folds associated with these faults. The ductile Chestnut Ridge fault (Figs. 3.1, 3.4A) is a well exposed example that truncates the overlying Dunn Creek fault north of Webb Mountain. Given the geometries of the cleavage, folds, and thrusts, the cleavage is interpreted to be related to body deformation within a moving thrust sheet deformed under ductile conditions (see Mitra and Elliott [1980] for an example of similar cleavage-thrust relationships in the Virginia Blue Ridge). It is inferred, therefore, that the base of this Taconian "early Miller Cove" thrust sheet was either reactivated as, and/or tuncated by, the brittle Miller Cove fault during the Alleghanian. It is unclear how much of the early ductile thrust zone may be preserved at the base of the early Miller Cove sheet given the relatively small preserved regional area of this thrust sheet.

Early Miller Cove thrust sheet deformation trends northeast across all earlier-formed structures in the Great Smoky Mountains (Witherspoon, 1981; Fig. 3.3). The late folds refold the more east-west trending structures in the Dunn Creek and Greenbrier sheets steepening the plunge of early fold hinges and causing small fold hinge offsets across related late minor faults.

Dunn Creek - Line Springs - Rabbit Creek Fault System

A broad belt of Pigeon Siltstone (Snowbird Group) within the Dunn Creek thrust sheet separates the Miller Cove thrust sheet from the Greenbrier thrust sheet in the eastern Great Smoky Mountains (Figs. 3.1, 3.4B). Just west of Gatlinburg, however, the Greenbrier thrust sheet extends northward around an eastwardly concave reentrant and directly overlies the Miller Cove thrust sheet north of Cove Mountain (Fig. 3.1). Although

many of the present boundaries between the Greenbrier sheet and structurally lower thrust sheets are late Gatlinburg-system faults, the Dunn Creek sheet clearly thins northward and westward to become a horse block bounded by the Greenbrier and Dunn Creek-Line Springs thrust faults. Down-dip plunging folds within the Pigeon Siltstone become much more common from east to west as this reentrant is approached, and the Pigeon grades into the more highly tectonized (but probably equivalent) Metcalf Phyllite of the Snowbird Group.

Southwest of Wear Cove, the Line Springs fault forms the base of the Metcalf Phyllite. Bedding within the Metcalf becomes less recognizable, and in many areas the fabric is dominated by shear bands (King, 1964; Witherspoon, 1981; Woodward and others, 1989). A zone of shear-banded Metcalf Phyllite between the Line Springs fault and the Roundtop klippe of the Greenbrier thrust sheet approaches half a kilometer in thickness (Lewis, 1988). The Great Smoky fault occupies the position of the the older Line Springs fault zone on the southeast side of Wear and Tuckaleechee Coves. The Rabbit Creek fault branches from the Line Springs fault zone on the west side of Tuckaleechee Cove and places Cades Sandstone over the Wilhite Formation (Walden Creek Group) of the Miller Cove sheet from there southwestward to beyond the Little Tennessee River at Chilhowee Lake.

The broad Dunn Creek thrust sheet east of Gatlinburg is relatively little affected by the folds, faults, and cleavage of underlying thrust sheets. The internal structural geometry of this sheet is therefore of great interest. The major fold structure of the Dunn Creek thrust sheet is the Cartertown-Copeland Creek anticline. Hinge regions of this fold have been modified by superimposed strains, which have also tightened interlimb angles. It is a major east-plunging box anticline that extends westward into the reentrant in the Greenbrier thrust sheet at Gatlinburg. Webb Mountain and Big Ridge preserve coarse unclassifed formation sandstones on the north side of this anticline and coarse

Thunderhead Sandstone in the Greenbrier thrust sheet overlies the southern limb of the fold (Fig. 3.1). Because the Dunn Creek sheet was emplaced prior to significant cleavage formation, it is attractive to treat it as a foreland-style thrust sheet in which major anticlines are interpreted to overlie the positions of major hanging-wall ramps (Dahlstrom, 1970; Connelly and Woodward,1990, 1992). If this interpretation as applied to the Dunn Creek thrust sheet is correct, then the Cartertown-Copeland Creek anticline marks the hanging wall segment of the major ramp through the Snowbird Group. The reentrant in the Greenbrier thrust sheet, although dissected by later faults, roughly follows the shape of this anticline in the underlying thrust sheet, suggesting that the Greenbrier thrust sheet is simply folded over it. Similar styles of thrust sheet deformation were observed by Jones (1971) in the Alberta foothills.

Greenbrier Fault

The Greenbrier thrust sheet is comprised of Great Smoky Group strata of the Thunderhead, Elkmont and Anakeesta Formations throughout the Great Smoky Mountains area (Figs. 3.1, 3.4C). The leading edge of the Greenbrier thrust sheet contains segments of the Greenbrier, Gatlinburg, and Oconoluftee fault systems. The Greenbrier thrust as mapped (King, 1964) underlies several klippen in front of the main fault trace north of Cove Mountain and the Roundtop Klippe (Fig. 3.4C). The Greenbrier fault is also believed to underlie the Cades Sandstone north of Cades Cove (Walters and Woodward, 1987) and the rocks of Webb Mountain and Big Ridge (Connelly and Woodward, 1990, 1992) (Fig. 3.4C).

The rocks of Webb Mountain and Big Ridge in the eastern Great Smoky Mountains were found to everywhere overlie a mylonitic (Greenbrier) fault zone that juxtaposes them with underlying Snowbird Group rocks. Bedding in sandstones at Webb Mountain and Big Ridge is at a high angle to the basal fault (hanging-wall ramp cutoff on

footwall ramp) on the north side of the mountains and is roughly parallel to the fault across the mylonitic zone on the south side of the mountains (hanging-wall flat on footwall flat). These structural geometries are interpreted as the leading-edge hanging-wall ramp anticline of the Greenbrier thrust sheet that was later folded by underlying structures, but is now mostly eroded away.

Great Smoky Group strata near the front of the main Greenbrier thrust sheet dip homoclinally southward in most areas. King (1964, cross section I'-I") showed that bedding in the Thunderhead Sandstone on Cove Mountain, however, dips steeply into the thrust forming a hanging-wall ramp anticline over the leading cutoff of the Elkmont Sandstone. This anticline lies along strike from the fragment of ramp anticline inferred at Webb Mountain (Fig. 3.4C). Southwest of Cove Mountain, King (1964, cross section J"-J'") illustrarts that bedding within the Greenbrier sheet is again approximately parallel to the thrust surface in front of the ramp anticline. Thus, the Roundtop klippe at the Sinks north of the main Greenbrier thrust sheet preserves the hanging-wall flat-footwall flat relationship expected to be behind the hanging wall ramp on Cove Mountain (Fig. 3.4C). This flat-on-flat relationship has been folded and truncated by the later ductile Sinks fault, which is inferred to be one of the Line Springs (Dunn Creek system) imbricates (Lewis, 1988).

Walters (1988) remapped the Cades Cove area and documented that the Cades Sandstone everywhere overlies the Metcalf Phyllite along a mylonitic fault zone. A recumbent fold (Rabbit Creek nappe) defined by the Cades Sandstone north of Cades Cove occupies the present leading edge of the Greenbrier thrust sheet. Mylonites in the Greenbrier fault zone on the north side of Cades Cove appear truncated by the fault that underlies the Rabbit Creek nappe. Thus, although the recumbent fold is believed to have initiated as the leading edge ramp anticline of the Greenbrier thrust sheet, it has been

significantly modified by subsequent motion on the Rabbit Creek fault (Dunn Creek system).

Superimposed Imbricate Faulting

Because the Rabbit Creek and Greenbrier thrust sheets are very thin at their leading edges in the western Great Smoky Mountains, the senses of the various fault generations can be identifed. The major fault contacts of the area are 1) the Greenbrier (Oconoluftee) system, which bounds the northern side of the Great Smoky Group outcrop belt; 2) the Rabbit Creek fault, which emplaces the overturned Cades Sandstone onto the Walden Creek Group of the Miller Cove thrust sheet; and 3) the Great Smoky fault, which underlies the Metcalf Phyllite and Cades Sandstone around the Cades Cove window.

In the western Great Smoky Mountains, Neuman and Nelson (1965) observed that the Metcalf Phyllite appears to stratigraphically overlie the Cades Sandstone in some exposures and stratigraphically underlie it in others. Thus, they suggested that the two units may intertongue. Fault-rocks and structures along the contacts, however, indicate that the lithologic contacts in the area are faults rather than stratigraphic contacts (Walters, 1988).

The Metcalf Phyllite overlies the Cades Sandstone in two outcrop belts on the southwest side of Cades Cove. The Metcalf along the southern contact shows a well-developed shear band structure indicating a reverse (top to the northwest) sense of displacement. Walters (1988) called this the Parsons Branch thrust (Figs. 3.1, 3.4C). The Cades Sandstone in the Coalen Ground thrust sheet beneath the Parsons Branch thrust is upright and southeast dipping although relatively highly strained (2.7:1 X/Z axial ratio measured on conglomerate clasts; Walters, 1988). This unit in turn overlies shear-banded Metcalf Phyllite along a repeated segment of the Greenbrier thrust. The Metcalf

beneath this segment of the Greenbrier is again thrust above overturned Cades Sandstone along the Coalen Ground fault (Figs. 3.1, 3.4C).

The most important contact relation in the western Great Smoky Mountains that demonstrates the stratigraphic relationships of these unclassified units is on the north side of Cades Cove, where the Metcalf Phyllite dips to the northwest beneath the Cades Sandstone. This was shown as a stratigraphic contact by Neuman and Nelson (1965), but the contact has shear-bands and ribbon quartz indicating that it is a northwest-vergent ductile thrust fault. The Greenbrier fault in this area dips toward and is cut off by the Great Smoky/Rabbit Creek fault. Thus, the Rabbit Creek fault as exposed, juxtaposes the overturned limb of the recumbent fold within the Rabbit Creek thrust sheet with the Miller Cove sheet, and therefore cannot simply be a continuation of the Greenbrier fault. The Greenbrier fault is cut by both the Parsons Branch and Coalen Ground faults south of Cades Cove and by the Sinks fault farther east (Fig. 3.4B). It appears that that the Rabbit Creek fault also truncates the Greenbrier fault, but at a lower angle and with substantially greater displacement. It is likely that many out-of-sequence ductile imbricate thrust faults in the Great Smoky Mountains root in the Rabbit Creek-Line Springs-Dunn Creek fault zone regionally, but can only be uniquely be identified in a few areas.

Southwest of Cades Cove, tracing any of the previously discussed faults continuously along strike for any distance is difficult, if not impossible. Neuman and Nelson (1965) showed the Oconaluftee fault trending more southward than the Rabbit Creek fault. Hardeman and others (1966) showed the Oconaluftee-Greenbrier fault cutting across the southern end of the Rabbit Creek fault, and Rodgers (1953) called the fault continuing across the Little Tennessee River the Gatlinburg fault.

The Oconaluftee and Gatlinburg faults are late brittle faults with variable displacement sense, and the Rabbit Creek system faults, whether in sequence or out-of-sequence, are ductile reverse faults. The late, ductile, high-angle reverse faults of the

Parsons Branch-Coalen Ground-Sinks system truncate and repeat the leading edge of the Greenbrier sheet southwest of Cades Cove (Walters, 1988). Unrecognized members of this fault system are probably present within the Greenbrier thrust sheet and elsewhere, but they may be difficult to map unless they juxtapose different rock units. It is likely that there are multiple fault systems that truncate the leading edge of the Greenbrier thrust sheet, and that the trailing upright limb of the Rabbit Creek nappe may be emplaced entirely over the leading edge anticline south of the Little Tennessee River.

THRUST SEQUENCES

As noted previously, the regional slaty cleavage of the Great Smoky Mountains foothills belt transects, and therefore postdates, most of the major early fault and fold structures. Because the eastern Great Smoky Mountains region preserves ramp anticlines in both the Dunn Creek and Greenbrier thrust sheets, a reconstuction of thrust patterns of this area is possible (Fig. 3.5). The reconstruction is presented in four steps, from youngest to oldest. 4) The Great Smoky and Miller Cove thrusts are restored, as are late brittle extension faults of the Gatlinburg fault system (Fig. 3.5A). 3) The early Miller Cove fault and ductile imbricate faults within the Miller Cove and Dunn Creek thrust sheets are restored (Fig. 3.5B). Within the eastern Great Smoky Mountains foothills area, internal strains associated with the emplacement of the early Miller Cove thrust sheet are low and are not accounted for in this restoration. 2) Dunn Creek thrust movement is restored returning the hanging-wall flat leading edge and the hanging-wall ramp beneath the Cartertown-Copeland Creek anticline to the top of the Snowbird Group ramp (Fig. 3.5C). Unfolding of the Cartertown-Copeland Creek anticline also unfolds the Greenbrier thrust sheet as exposed at Webb Mountain and Big Ridge. Based on this restoration, minimum displacement of the Dunn Creek thrust sheet is ~22 km. 1) Webb Mountain, Big Ridge, and Cove Mountain all expose the leading-edge hanging-wall ramp anticline of

Figure 3.5. Cross section across the eastern Great Smoky Mountains through Webb Mountain. A: Present day (deformed) cross section. B: Cross section restored to pre-early Miller Cove deformed section. C: Cross section restored to pre-Dunn Creek deformed section. D: Fully restored section. HR=hangingwall ramp; HF=hangingwall flat; FR=footwall ramp; FF=footwall flat. Other abbreviations and patterns same as those in Figure 3.1.

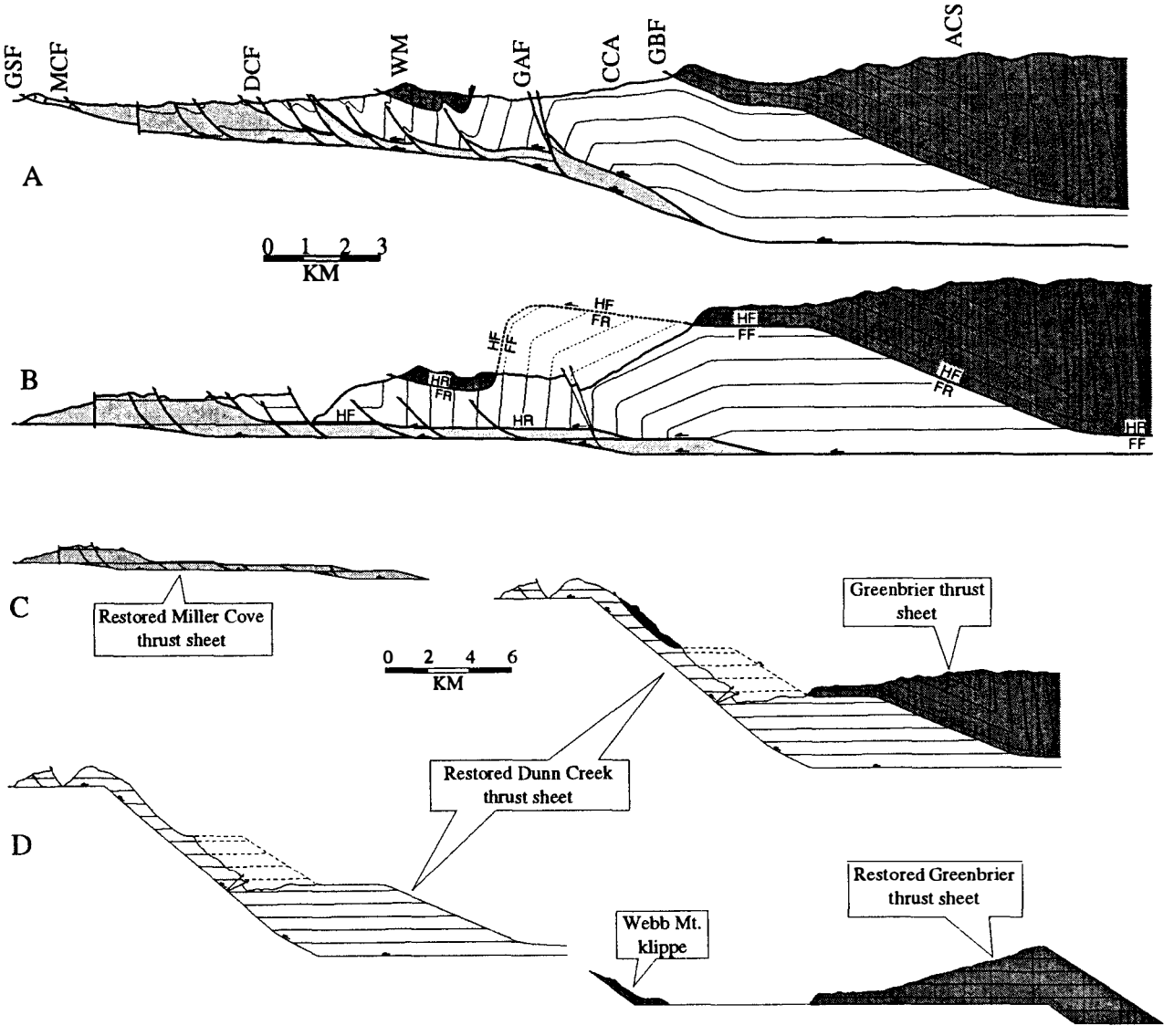
GSF
MCF
DCF
WM
GAF
CCA
GBF
ACS
A
0 1 2 3
KM
B
HF
FR
HF
FF
HR
C
Restored Miller Cove thrust sheet
0 2 4 6
KM
Greenbrier thrust sheet
Restored Dunn Creek thrust sheet
D
Webb Mt. klippe
Restored Greenbrier thrust sheet

the Great Smoky Group within the Greenbrier thrust sheet (Fig. 3.5, 3.6). Restoration of the Greenbrier thrust sheet to its origin returns these klippen to the top of the Great Smoky Group ramp southeast of the Snowbird Group-Great Smoky Group facies change (Fig. 3.5D). A minimum displacement of 23 km is estimated for the Greenbrier thrust sheet.

The Cades Cove area in the western Great Smoky Mountains region can similarly be reconstructed in six stages (Fig. 3.7). 6) The Great Smoky thrust sheet is unfolded and late brittle faults (Gatlinburg-Oconoluftee) are restored. This requires removal of displacement on all Valley and Ridge thrusts beneath the Great Smoky fault (Fig. 3.7B). 5) Alleghanian Great Smoky and Miller Cove thrusting is restored, returning the Chilhowee Mountain block to the Chilhowee-level footwall cutoff and returning the Miller Cove thrust to its position of last probable Ordovician movement (probably on top of other Ocoee strata). This requires that ductile fault rocks once present at the base of the Miller Cove, Rabbit Creek and Greenbrier thrust sheets be restored to the base of the Alleghanian allochthon (Fig. 3.7C). 4) Displacement on the Taconian early Miller Cove fault is then removed, as well as the associated ductile faulting, folding, and cleavage formation within the Miller Cove and overlying thrust sheets. A steeply-dipping second cleavage within the Rabbit Creek nappe present near the Rabbit Creek fault north of Cades Cove is believed to be of this generation, although it has not been dated. This restores the Walden Creek Group of the Miller Cove thrust sheet to the Walden Creek upper footwall cutoff (Fig. 3.7D). 3) The Parsons Branch, Coalen Ground, Sinks, and other late ductile faults that splay up from the Rabbit Creek-Line Springs fault zone and truncate the trailing edges of the Rabbit Creek nappe and the Roundtop klippe are restored (Fig. 3.7D). 2) Restore the ductile Rabbit Creek thrusting and overfolding that caused the high strains within the leading edge of the Greenbrier thrust sheet. This restores the folded and truncated Greenbrier fault beneath the Cades Sandstone north of Cades Cove to its position of last movement. The leading edge of the Greenbrier thrust sheet is present at depth at the

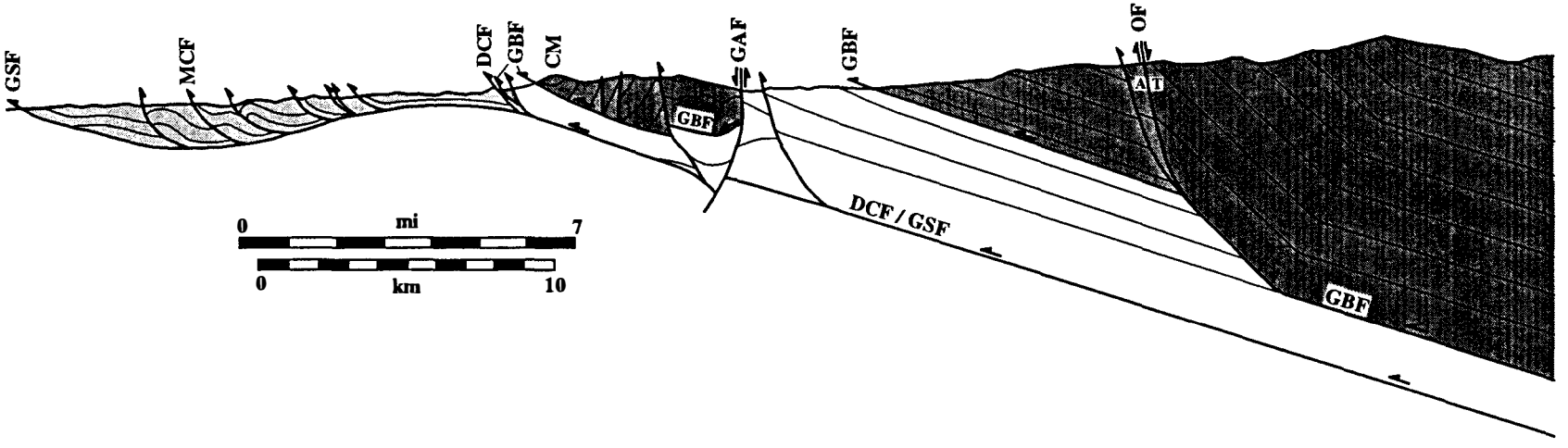

Figure 3.6. Cross section across Cove Mountain in the Central Great Smoky Mountains (after Knig, 1964, section G-G'''). Abbreviations and patterns same as those in Figure 3.1.

Figure 3.7. Cross section across Cades Cove in the western Great Smoky Mountains (after Neuman and Nelson, 1965, section D-D'). A: Deformed section. B: Deformed section after removal of Alleghanian folding. C: Section restored to pre-Early Miller Cove deformed section. D: Section restored to pre-ductile imbrication. E: Section restored to pre-Rabbit Creek faulting. Abbreviations and patterns same as those in Figure 3.1.

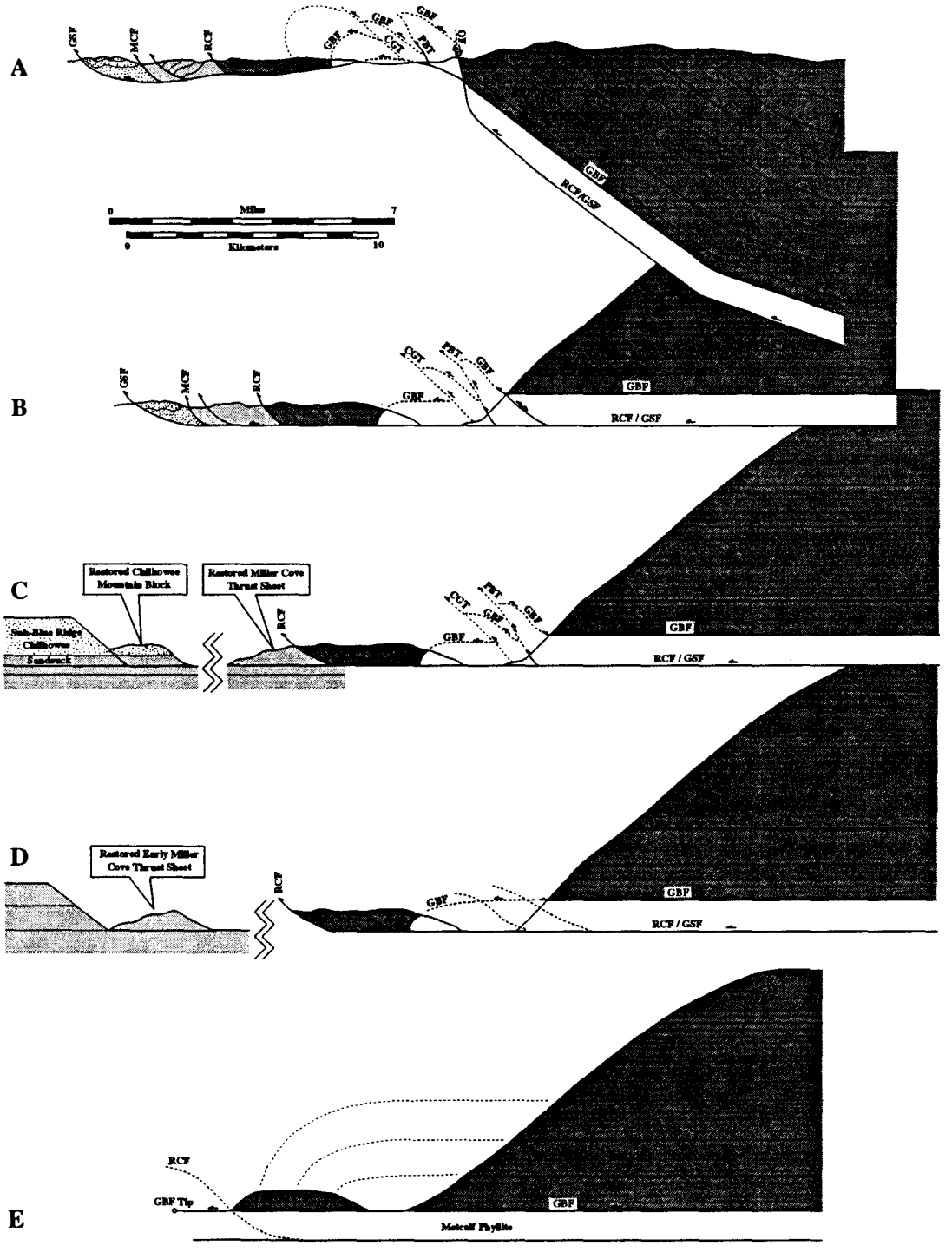
A
GSF
MCF
RCF
GBF
CGT
PBT
10
GBF
RCF/GSF
0
Miles
7
0
Kilometers
10
B
GSF
MCF
RCF
CGT
PBT
GBF
GBF
GBF
RCF / GSF
C
Restored Chilhowee Mountain Block
Restored Miller Cove Thrust Sheet
Sub-Blue Ridge Chilhowee Sandrock
RCF
CGT
PBT
GBF
GBF
GBF
RCF / GSF
D
Restored Early Miller Cove Thrust Sheet
RCF
GBF
GBF
RCF / GSF
E
RCF
GBF Tip
GBF
Metcalf Phyllite

Rabbit Creek footwall cutoff of the Rabbit Creek fault (Fig. 3.7E). 1) By analogy with the eastern Great Smoky Mountains, 23 km of displacement on the Greenbrier fault is restored, returning the leading-edge hanging-wall ramp anticline to a footwall ramp through the Elkmont and Thunderhead Sandstone southeast of the Snowbird Group-Great Smoky Group facies change.

IMPLICATIONS FOR THRUST SHEET RESTORATION

The structural patterns that can now be documented significantly simplify the stratigraphic patterns within the Great Smoky Mountains region and suggest a minimum restoration of this part of the Ocoee basin based on restorable cross-sections (Fig. 3.8). This schematic restoration requires that the Great Smoky Group and Snowbird Group are in part chronostratigraphically equivalent. This reconstruction is similar to the model of Neuman and Nelson (1965), although the restored cross sections have allowed dimensions to be placed on the present reconstruction.

SUMMARY

The Great Smoky Mountains area is a paradigm for Taconian foreland-style deformation in the southern Appalachians, as well as an interesting case study of a cleaved and metamorphosed imbricate thrust stack. It is comprised of three stacked thrust sheets which have been collectively transported and folded together during Alleghanian emplacement of the Great Smoky thrust system.

Many of the thrust sheet boundaries in the Great Smoky Mountains area are not thrust faults, but the distribution of the lithologies and an understanding of the kinematics of the truncating faults does allow the original thrust systems to be reconstructed accurately. The present emphasis on the positions of the thrust sheets and the kinematics

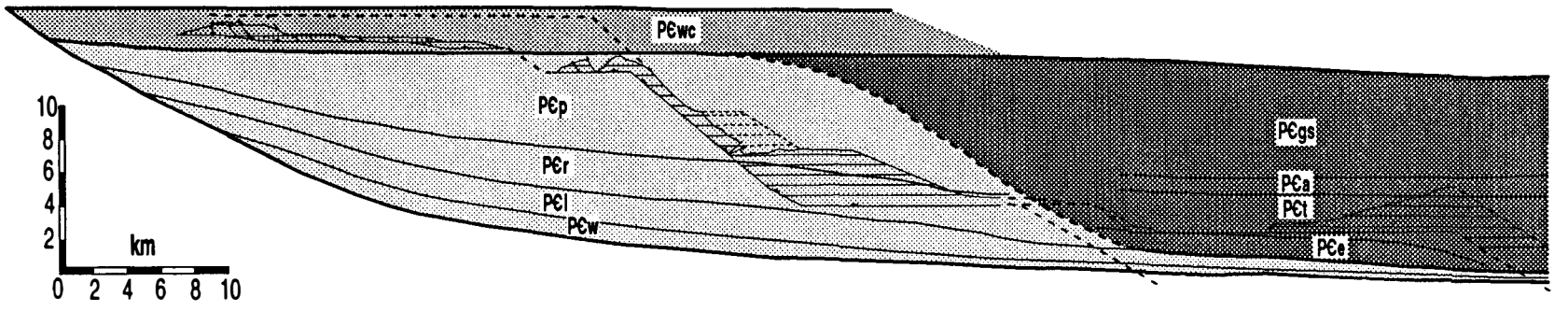

Figure 3.8. Schematic restored Ocoee basin prior to Ordovician deformation based on Figure 3.5. Positions of preserved thrust sheets and inferred fault trajectories shown. Abbreviations same as those in Figure 3.2. Patterns same as those in Figure 3.1.

of the faults which separate them suggests that simply trying to trace individual faults to other areas of the Blue Ridge probably will not improve the understanding of the regional geology without simultaneous kinematic studies.

REFERENCES CITED

Boyer, S. E., and Elliott, D., 1982, Thrust systems: American Association of Petroleum Geologists Bulletin, v. 66, p. 1196-1230.

Connelly, J. B., and Dallmeyer, R. D., 1990, Ordovician or Silurian metamorphism in the western Blue Ridge, Tennessee ?: Evidence from ^{40}Ar / ^{39}Ar whole rock phyllite ages: Geological Society of America Abstracts with Programs, v. 22, p. 231.

Connelly, J. B., and Dallmeyer, R. D., 1991, Polymetamorphic evolution of the western Blue Ridge, Tennessee and North Carolina; Evidence from ^{40}Ar / ^{39}Ar ages: Geological Society of America Abstracts with Programs, v. 23, p. 18.

Connelly, J. B., Woodward, N. B., and Walters, R. R., 1989, Polyphase early Paleozoic tectonism preserved in the western Blue Ridge; example from the Great Smoky Mountains National Park: Geological Society of America Abstracts with Programs v. 21, p. 65.

Connelly, J. B., and Woodward, N. B., 1990, Sequential restoration of early Paleozoic deformation; Great Smoky Mountains foothills, Tennessee: Geological Society of America Abstracts with Programs v. 22, p. 8.

Connelly, J. B., and Woodward, N. B., 1991, Tectonic evolution of the Blue Ridge in east-central Tennessee: Geological Society of America Abstracts with Programs, v. 23, p. 18.

Connelly, J. B., and Woodward, N. B., 1992 Taconian foreland-style thrust system in the Great Smoky Mountains, Tennessee: Geology, v. 20, p. 177-180.

Cook, F. A., Brown, L. D., Kaufman, S., and Oliver, J. E., 1983, The COCORP seismic reflection traverse across the southern Appalachians: American Association of Petroleum Geologists Studies in Geology, no. 14, 61 p.

Costello, J. O., 1984, Relationships between the Cartersville fault and Great Smoky fault in the southern Appalachians: a reinterpretation [M.S. thesis]: Columbia, University of South Carolina, 75 p.

Costello, J. O., and Hatcher, R.D., Jr., 1986, Contact relations between the Walden Creek Group and Great Smoky Group in Ocoee Gorge, Tennessee: Implications for the regional extent of the Greenbrier fault: Geological Society of America Abstracts with Programs, v. 18, p. 216.

Dahlstrom, C. D. A., 1970, Structural geology in the eastern margin of the Canadian Rockies: Bulletin of Canadian Petroleum Geology, v. 18, p. 332-406.

Erickson, S. G., and Wiltschko, D. V., 1991, Spatially heterogeneous strength in thrust fault zones: Journal of Geophysical Research, v. 96, p. 8427-8439.

Ferguson, H. W., and Jewell, W. B., 1951, Geology and barite deposits of the Del Rio district, Cocke County, Tennessee: Tennessee Division of Geology Bulletin 57, 235 p.

Hadley, J. B., and Goldsmith, R., 1963, Geology of the eastern Great Smoky Mountains, North Carolina and Tennessee: U.S. Geological Survey Professional Paper 349-B, 118 p.

Hadley, J. B., and Nelson, A. E., 1971, Geologic map of the Knoxville quadrangle, North Carolina, Tennessee, and South Carolina: U.S. Geological Survey Miscellaneous Investigations Map I-654, 1:250,000.

Hamilton, W. B., 1961, Geology of the Richardson Cove and Jones Cove quadrangles, Tennessee: U.S. Geological Survey Professional Paper 349-A, 55 p.

Hardeman, W. D., 1966, Geologic Map of Tennessee: four sheets, Tennessee Division of Geology, 1:250,000.

Harris, L. D., and Milici, R. C., 1977, Characteristics of thin-skinned deformation style in the southern Appalachians and potential hydrocarbon traps: U.S. Geological Survey Professional Paper 1018, 40 p.

Harris, L. D., Harris, A. G., DeWitt, W., Jr., and Boyer, K. C., 1981, Evaluation of southern eastern overthrust belt beneath the Blue Ridge-Piedmont thrust: American Association of Petroleum Geologists Bulletin, v. 65, p. 2497-2505.

Hatcher, R. D., Jr., 1989, Tectonic synthesis of the U.S. Appalachians, *in* Hatcher, R. D., Jr., Thomas, W. A., and Viele, G. W., eds., The Appalachian-Ouachita orogen in the United States: Boulder, Colorado, Geological Society of America, The Geology of North America, v. F-2, p. 511-535.

Hatcher, R. D., Jr., and Milici, R. C., 1986, Ocoee Gorge; Appalachian Valley and Ridge to Blue Ridge transition: Geological Society of America Centennial Field Guide, Southeastern Section, p. 265-270.

Hatcher, R. D., Jr., Williams, R. T., Costain, J. K., Coruh, C., Thomas, W. A., 1987, Palinspastic reconstruction of the southern Appalachians: Geological Society of America Abstracts with Programs, v. 19, p. 696.

Hatcher, R. D., Jr., Thomas, W. A., Geiser, P. A., Snoke, A. W., Mosher, S., and Wiltscho, D. V., 1989, Alleghanian orogen, *in* Hatcher, R. D., Jr., Thomas, W. A., and Viele, G. W., eds., The Appalachian-Ouachita orogen in the United States: Boulder, Colorado, Geological Society of America, The Geology of North America, v. F-2, p. 233-318.

Hatcher, R. D., Jr., Osberg, P. H., Drake, A.A., Jr., Robinson, P., and Thomas, W. A., 1990, Tectonic map of the U.S. Appalachians, *in* Hatcher, R. D., Jr., Thomas, W. A., and Viele, G. W., eds., 1989, The Appalachian-Ouachita orogen in the United States: Boulder, Colorado, Geological Society of America, The Geology of North America, v. F-2, Plate 1.

Jones, P. B., 1971, Folded faults and sequence of thrusting in Alberta Foothills: American Association of Petroleum Geolgists Bulletin, v. 55, p. 292-306.

Keller, F. B., 1980, Late Precambrian stratigraphy, depositional history, and structural chronology of part of the Tennessee Blue Ridge [Ph.D. thesis]: New Haven, Connecticut, Yale University, 353 p.

King, P. B., 1964, Geology of the central Great Smoky Mountains, Tennessee: U.S. Geological Survey Professional Paper 349-C, 148 p.

King, P. B., Neuman, R.B., and Hadley, J.B., 1968, Geology of the Great Smoky Mountains National Park, Tennessee and North Carolina: U.S. Geological Survey Professional Paper 587, 23 p.

Lewis, J. C., 1988, Structural geology and finite strain analysis of the Precambrian Thunderhead Sandstone along the Greenbrier fault and Roundtop klippe: Great Smoky Mountains, Tennessee [M.S. Thesis]: Knoxville, Tennessee, University of Tennessee, 186 p.

Mitra, G., and Elliott, D., 1980, Deformation of basement in the Blue Ridge and the development of the South Mountain cleavage, *in* Wones, D.R., ed., The Caledonides in the U.S.A.: Blacksburg, Virginia, Virginia Polytechnic Institute and State University Memoir 2, p. 307-311.

Neuman, R. B., and Nelson, W. H., 1965, Geology of the western part of the Great Smoky Mountains, Tennessee: U.S. Geological Survey Professional Paper 349-D, 81 p.

Oriel, S. S., 1950, Geology and mineral resources of the Hot Springs window, Madison County, North Carolina: North Carolina Division of Mineral Resources Bulletin 60, 70 p.

Rast, N., and Kohles, K. M., 1986, The origin of the Ocoee Supergroup: American Journal of Science, v. 286, p. 593-616.

Robert, L., 1987, Structural geology and geometries of the Denton duplex along the frontal Blue Ridge, near Hartford, Tennessee [M.S. thesis]: Knoxville, Tennessee, University of Tennessee, 147 p.

Rodgers, J., 1953, Geologic map of East Tennessee with explanatory text: Tennessee Division of Geology Bulletin 58, Part II, 168 p.

Trumpy, R., 1969, The Helvetic nappes of eastern Switzerland: Ecolgae Geologicae Helvetiae, v. 62, p.105-142.

Walters, R. R., 1988, Structural Geometries, fabrics and stratigraphic relationships in the Cades Cove region, Great Smoky Mountains National Park, Tennessee [M.S. thesis]: Knoxville, Tennessee, University of Tennessee, 145 p.

Walters, R. R., and Woodward, N. B., 1987, Structural relationships in the Cades Cove area, Great Smoky Mountains National Park, Tennessee: Geological Society of America Abstracts with Programs, v. 19, p. 880.

Witherspoon, W. D., 1981, Structure of the Blue Ridge thrust front, Tennessee, southern Appalachians [Ph.D. thesis]: Knoxville, Tennessee, University of Tennessee, 165 p.

Wojtal, S., 1986, Deformation within foreland thrust sheets by populations of minor faults: Journal of Structural Geology, v. 8, p. 341-360.

Woodward, N. B., ed., 1985, Valley and Ridge thrust belt: Balanced structural sections, Pennsylvania to Alabama: Appalachian Basin Industrial Associates, University of Tennessee Department of Geological Sciences Studies in Geology no. 12, 64 p.

Woodward, N. B., 1986, Fault geometries and tectonic reconstructions of the Tennessee Blue Ridge: Geological Society of America Abstracts with Programs, v. 18, p. 273.

Woodward, N. B., Wojtal, S. F., Mitra, G., Dunne, W., Simpson, C., Evans, M., and Costello, J., 1989, Geometry and deformation fabrics in the central and southern Appalachian Valley and Ridge and Blue Ridge: IGC field trip T 357, American Geophysical Union, 105 p.

Woodward, N. B., Wojtal, S., Paul., J.B., and Zadins, Z., 1988, Partitioning of deformation within several external thrust zones of the Appalachian orogen: Journal of Geology, v. 96, p. 351-361.

PART 4

STRAIN VARIATIONS AND STRAIN FACTORIZATION WITHIN AN EARLY PALEOZIOC THRUST SYSTEM, EASTERN GREAT SMOKY MOUNTAINS FOOTHILLS, TENNESSEE

INTRODUCTION

The eastern Great Smoky Mountains foothills area (Fig. 4.1) preserves a foreland-style thrust belt that was subsequently internally deformed during early Paleozoic thrust faulting. These early formed thrust sheets were transported along a major thrust fault and later folded by underlying thrust sheets during the late Paleozoic. Despite this complex deformational history, regionally penetrative internal deformation was restricted to a single (early Paleozoic) thrusting event. This internal deformation is largely in the form of a variably developed slaty cleavage that transects earlier structures of the foreland-style thrust system and is locally folded by late Paleozoic thrust-related deformation. Cleavage dips consistently moderately southeastward toward the hinterland and appears to be unaffected by earlier structures of the foreland-style thrust belt or structural position. The consistent hinterland-dipping geometry of the regional cleavage observed in the study area has been interpreted in other areas as resulting from simple shear parallel to a basal thrust fault during transport (Mitra and Elliott, 1980).

The three-dimensional finite strain geometry recorded in sandstones from the various thrust sheets was determined to provide additional insight into the origin of the penetrative strains from this area unavailable from cleavage geometries alone. Knowledge of the orientations and magnitudes of the finite strain ellipses allows strain to be factorized into different strain events. Strain factorization is a type of forward modeling of a series of strain events that attempt to reproduce the observed finite strains (Ramsay and Huber, 1983; Kligfield and others, 1984). It is a mathematical technique

Figure 4.1. Geologic map of the eastern Great Smoky Mountains. BR=Big Ridge; CA=Cartertown anticline; CCA=Copeland Creek anticline; CRF=Chestnut Ridge fault; DCF=Dunn Creek fault; GAF=Gatlinburg fault; GBF=Greenbrier fault; GSF=Great Smoky fault; MCF=Miller Cove fault; WM=Webb Mountain. Area of Figure 4.2 shown by box. Cross sections shown in Figure 4.9. (modified from King and others, 1968; Keller, 1980).

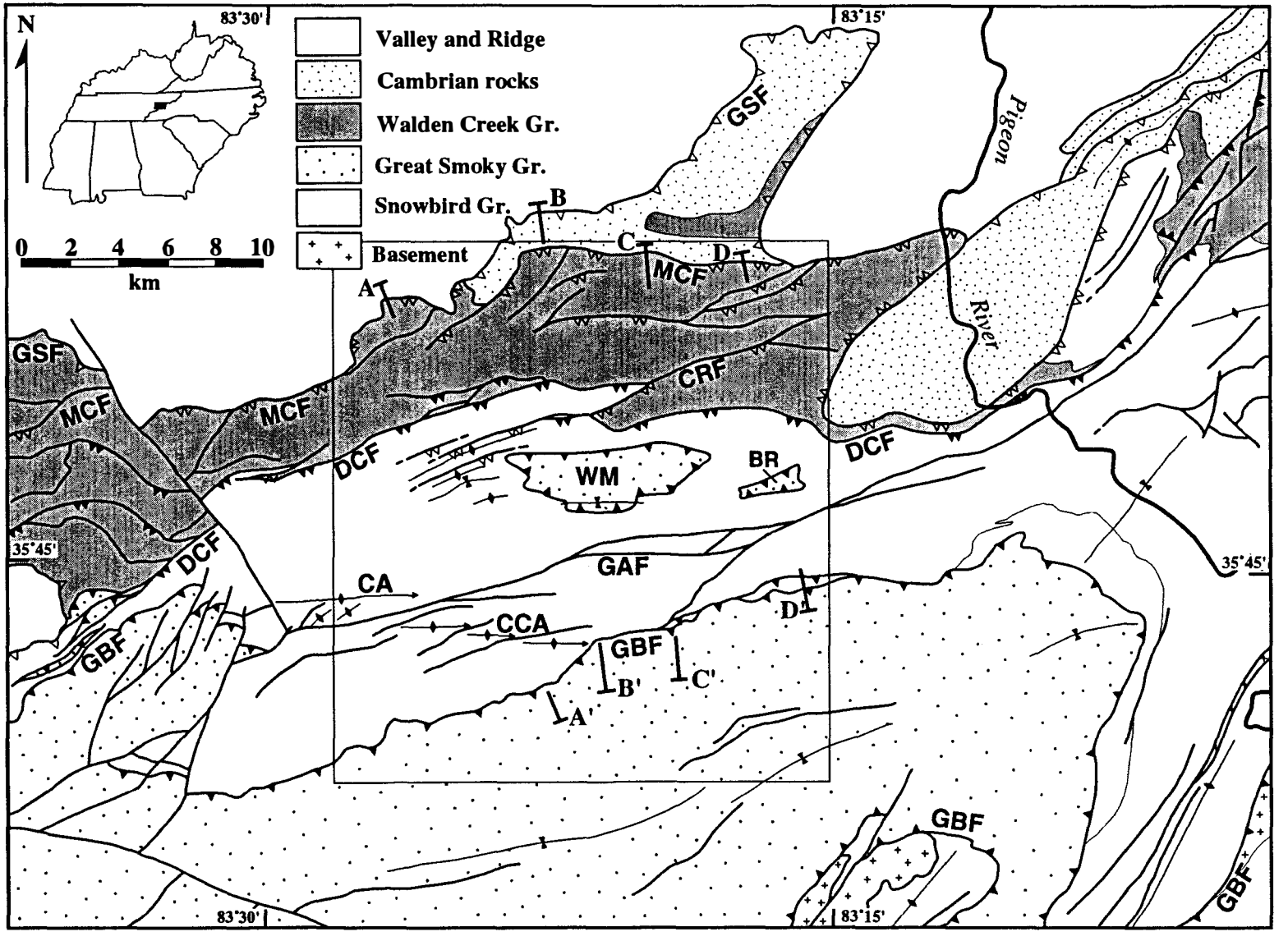
N
83°30'
83°15'
Valley and Ridge
Cambrian rocks
Walden Creek Gr.
Great Smoky Gr.
Snowbird Gr.
Basement
0 2 4 6 8 10
km
GSF
MCF
CRF
DCF
GAF
CA
CCA
GBF
WM
BR
Pigeon
River
A
B
C
D
A'
B'
C'
D'
35°45'

for finding the deformation components or factors to describe finite strain in terms of the superposition (matrix multiplication) of 2 or more strains (Ramsay and Huber, 1987). The choice of type and sequence of events is constrained by the style and sequence of deformation recognized in the region. Strain factorization in other thrust belts has been successful in elucidating the deformational history that have contributed to the finite strain of various areas (e.g., Coward and Kim, 1981; Fisher and Coward, 1982; Sanderson, 1982; Evans and Dunne, 1990; Couzens and others, 1993).

The purposes of this study are to: 1) determine the orientations and magnitudes of finite strains within three major early Paleozoic thrust sheets; 2) determine the deformation mechanisms that accommodated this strain; and 3) factorize the finite strain using simple kinematic models to attempt to determine deformation events that may have contributed to the finite strain. The regional and local geology of the study area have been discussed in Parts 1, 2, and 3 of this dissertation.

SAMPLE DESCRIPTION

The sandstone samples used for finite strain analysis were collected from thrust sheets internally deformed during early Paleozoic orogenesis, including the Miller Cove, Dunn Creek, and Greenbrier thrust sheets (Figs. 4.1 and 4.2). Sandstones in each thrust sheet differ because each sheet is comprised of a different group of the Ocoee Supergroup. Sandstones from each group, and therefore each thrust sheet, differ in grain size, texture, and composition. Within each thrust sheet, however, composition and grain size of sandstones are similar. Because of similar lithology and deformation conditions, a similar suite of tectonic microstructures is also characteristic of each thrust sheet. Percent estimates of components and microstructures listed below are visual estimates.

Rock units present in the Miller Cove thrust sheet belong to the Licklog, Shields, Wilhite, and Sandsuck Formations of the Walden Creek Group. The Walden Creek

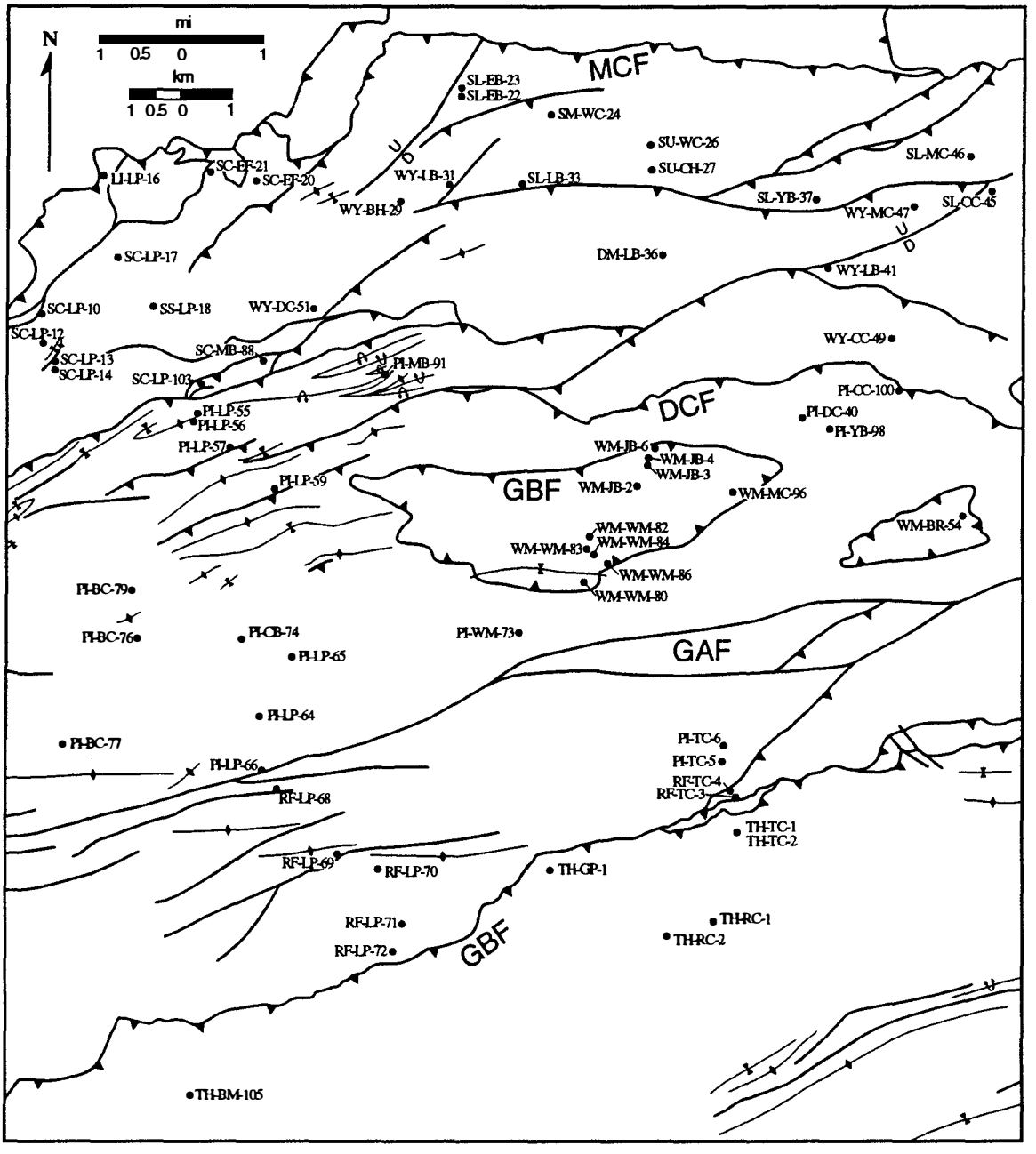

Figure 4.2. Geologic map of the eastern Great Smoky Mountains foothills area showing locations of samples used for strain analysis. DCF=Dunn Creek fault; GAF=Gatlinburg fault; GBF=Greenbrier fault; MCF=Miller Cove fault (modified from Hamilton, 1961).

Group consists of widely varied clastic rocks and minor carbonates (Hamilton, 1961). Grain size of sampled sandstone ranges from fine sand (0.125-0.25 mm) to coarse sand (0.5-1mm), although most samples contain medium sand (0.25-0.5 mm). Compositionally, quartz is the dominant component with feldspar comprising between 1 and 25 percent of grains. Feldspar is commonly replaced by sericite and carbonate. Clastic biotite (0-5 percent) is the only other significant component. The matrix is composed of clay in the samples from the northern Miller Cove thrust sheet. As recrystallization increases southward, sericite and fine-grained chlorite become increasingly important matrix components. Matrix percentage present ranges from approximately 1 to 35 percent, and is inversely related to grain size. Carbonate cement is present in many samples, with coarser grains visibly twinned.

Rocks in the Dunn Creek thrust sheet belong to the Snowbird Group, which in the study area consists of siltstones and fine-grained sandstones of the Pigeon Siltstone and fine- to medium-grained sandstones of the Roaring Fork Sandstone. Sandstone samples collected for strain analysis range in grain size from very fine sand (0.0625-0.125 mm) to medium sand, although most samples are fine sand. Compositionally, quartz is the most abundant component, although feldspar comprises up to 40 percent of grains in the finest grained samples. Detrital muscovite and biotite represent 0 to 10 percent of grains. The matrix is composed of sericite and fine-grained chlorite. The percent of matrix ranges from approximately 5 to 50 percent. Like rocks from the Miller Cove thrust sheet, the finer grained rocks typically have a larger percentage of matrix. Feldspar and detrital biotite are commonly replaced by sericite and chlorite.

Rocks within the Greenbrier thrust sheet belong to the Great Smoky Group, which consists of a thick sequence of conglomerate, sandstone, and slate. Samples collected for strain analysis are from the Thunderhead Sandstone and the rocks of Webb Mountain, a previously unclassified unit here included with the Great Smoky Group (Parts 2 and 3).

Samples used for strain analysis range from medium to coarse sand size, with most samples being coarse grained. Samples are typically poorly sorted and grains are angular to subangular. Most grains are quartz, with feldspar comprising from 10 to 30 percent of grains. Detrital muscovite and biotite compose only 0 to 5 percent of the grains. The percent matrix ranges from 15 to 35 percent and is composed of fine-grained chlorite and sericite, which commonly replaces feldspar. Finely crystalline carbonate comprises up to 10 percent of some samples apparently replacing sericite.

Microstructures

Observed tectonic microstructures in quartz include undulatory extinction, patchy extinction/subgrains, deformation lamellae, deformation bands, intragranular microfractures, transgranular microfractures, stylolites, sutured grain boundaries, serrated grain boundaries, and fibrous overgrowths. Microstructural types and abundances differ between each thrust sheet reflecting differences in both lithology and deformation conditions.

Within Walden Creek Group lithologies of the Miller Cove thrust sheet, undulatory extinction occurs in nearly all quartz grains. Patchy extinction is much less common but was observed in all samples. Microfractures in quartz grains are commonly fluid inclusion planes (FIP's) (Fig. 4.3a), but they vary greatly in abundance between samples. Many feldspar grains show open or sericitized microfractures (Fig. 4.3b). Deformation lamellae were observed in approximately half of the samples, and deformation bands are observed in several samples (Fig. 4.3b). The presence and abundance of these microstructures appears to show a general relationship with matrix abundance. Deformation lamellae and deformation bands were absent from those samples with greater than approximately 15 percent matrix. Pressure solution features, either stylolites (Fig. 4.3a) or sutured grain boundaries (Fig. 4.3c), were observed in

Figure 4.3. Photomicrographs of microstructures from the Miller Cove thrust sheet (Walden Creek Group). a) Sandstone from the Shields Conglomerate (sample SC-LP-17) showing fluid inclusion planes (dipping steeply to the left) that have formed approximately normal to stylolites (dipping gently to the right). Bedding is horizontal. b) Deformation lamellae (DL) and deformation band (DB) within a quartz grain and sericitized fractures (F) in feldspar grains from the middle Sandsuck Formation (sample SM-WC-24). c) Sutured quartz grain boundaries from the lower Sandsuck Formation (sample SL-CC-45). d) Fibrous overgrowths (O) from sandstone of the Shields Formation (sample SC-LP-10). Bedding is horizontal. Field of view of a) is 2.5 mm. Field of view of b), c), and d) is 1.2 mm.

a)

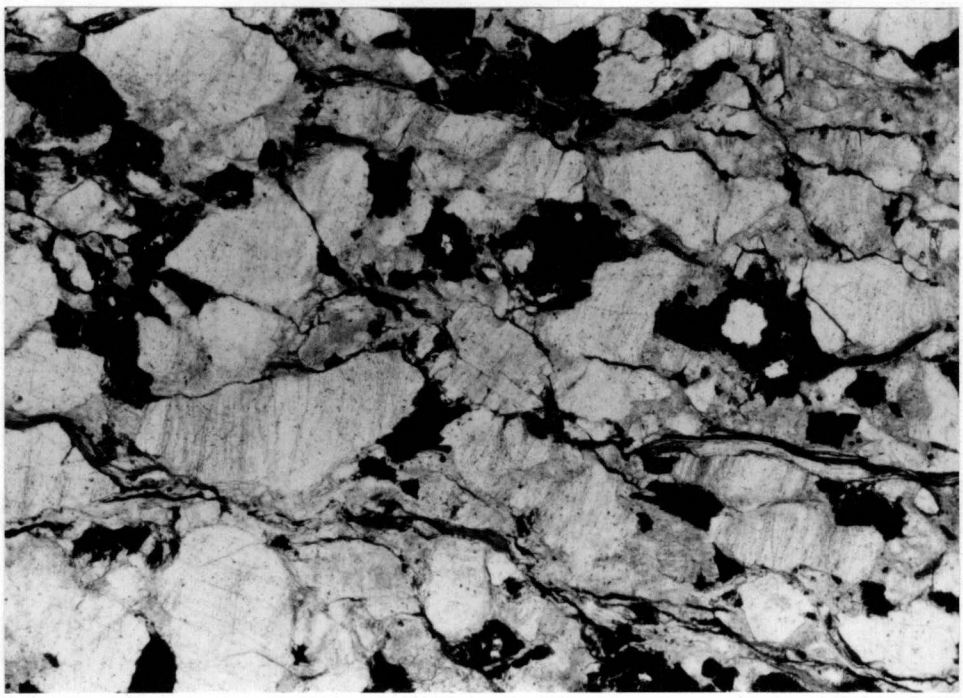

b)

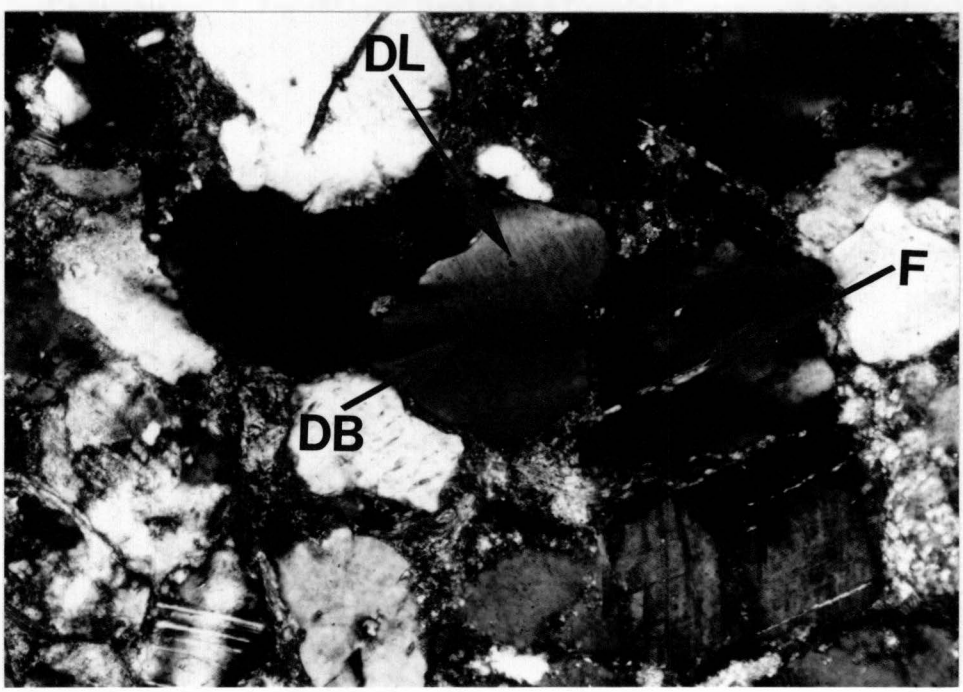

c)

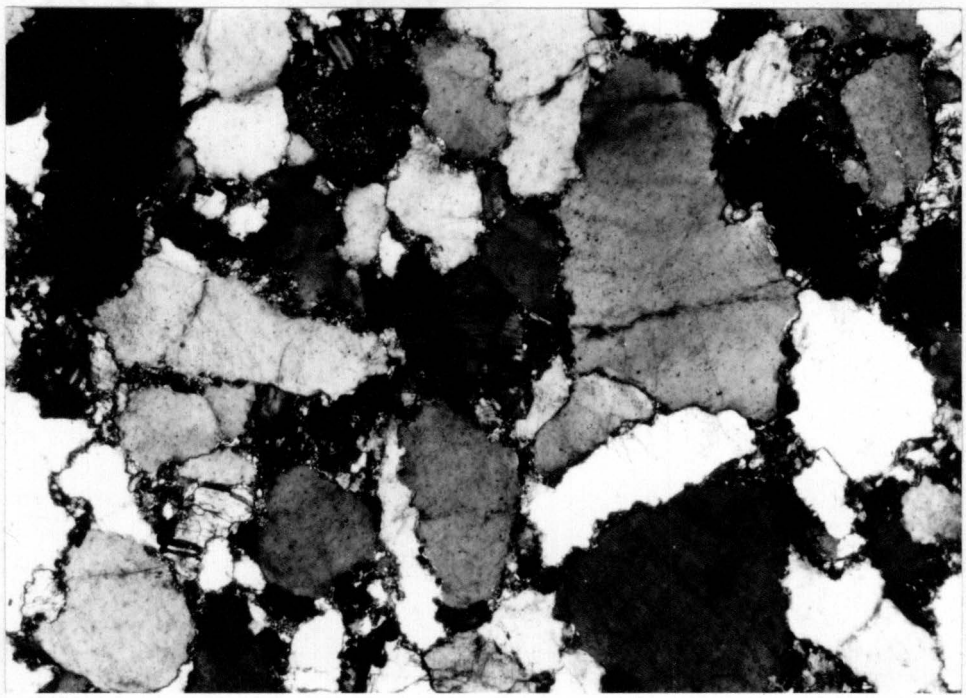

d)

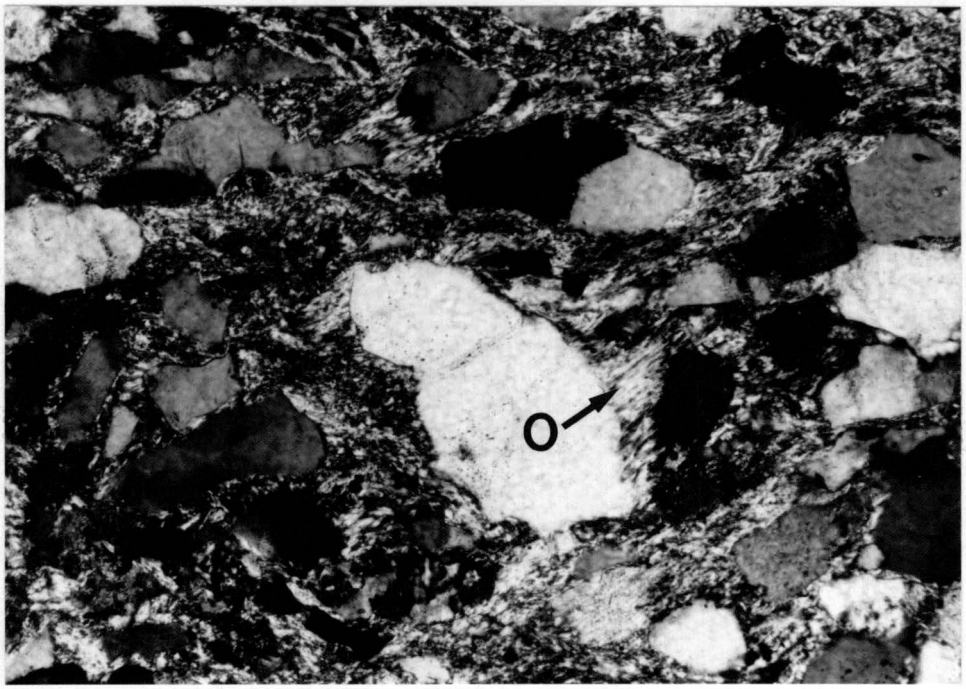

nearly all samples. Sutured grain boundaries occur in those samples with less than approximately 15 percent matrix, whereas stylolites occur in samples with greater than approximately 15 percent matrix. Stylolites are characterized by smooth, anastomosing seams of insoluble residue (Fig. 4.3b), and occur both subparallel and oblique to bedding. Within the southern Miller Cove thrust sheet, where cleavage is more strongly developed, sericite and fine-grained chlorite have recrystallized subparallel to some stylolite seams. Fibrous overgrowths (beards) of quartz, chlorite, and muscovite (Fig. 4.3d) are present around quartz and feldspar grains in several samples and are typically parallel to stylolites where both occur. Pressure shadows around pyrite grains, some curved, are rare but were observed in two samples.

Microstructures and microstructural abundances in Snowbird Group lithologies of the Dunn Creek thrust sheet differ from those in the Miller Cove thrust sheet reflecting the finer grain size, more abundant matrix, and slightly higher temperature of deformation. Undulatory extinction occurs in nearly all quartz grains. Patchy extinction is present in nearly all samples, and becomes more prevalent southward. Microfractures are rare. Sutured grain boundaries, deformation lamellae, and deformation bands (Fig. 4.4a) are rare and occur only in those samples with approximately 15 percent or less matrix (Fig. 4.4a). Serrated grain boundaries were observed in some samples from the southern Dunn Creek thrust sheet. Stylolites (Fig. 4.4b) are the most prevalent microstructure present, reflecting the abundant matrix present in Snowbird Group lithologies. Stylolites parallel and oblique to bedding are present, sometimes occurring in the same sample (Fig. 4.4c). Fibrous overgrowths of quartz, chlorite, and muscovite are present around quartz and feldspar grains and are parallel to stylolites and aligned sericite. Aligned fine-grained muscovite (Fig. 4.4d) is common in the southern Dunn Creek thrust sheet south of the Gatlinburg fault.

Figure 4.4. Photomicrographs of microstructures from the Dunn Creek thrust sheet (Snowbird Group). a) Deformation lamellae (DL) and deformation band (DB) in quartz grain from sandstone within the Pigeon Siltstone (sample PI-BC-79). b) Stylolites within the Pigeon Siltstone (sample PI-CC-100). c) Bedding parallel (horizontal) and bedding oblique stylolites from the Pigeon Siltstone (sample PI-LP-55). d) Metamorphic muscovite aligned subparallel to long dimension of detrital grains from the Roaring Fork Sandstone (sample RF-TC-4). Field of view of a) is 0.6 mm. Field of view of b) and c) is 2.5 mm. Field of view of d) is 1.2 mm.

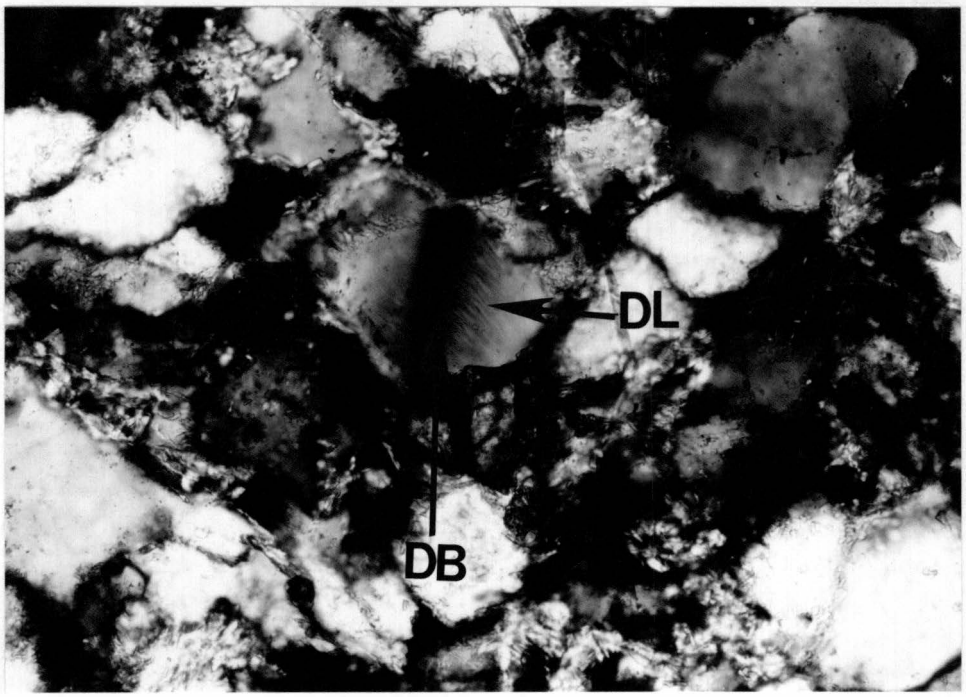

a)

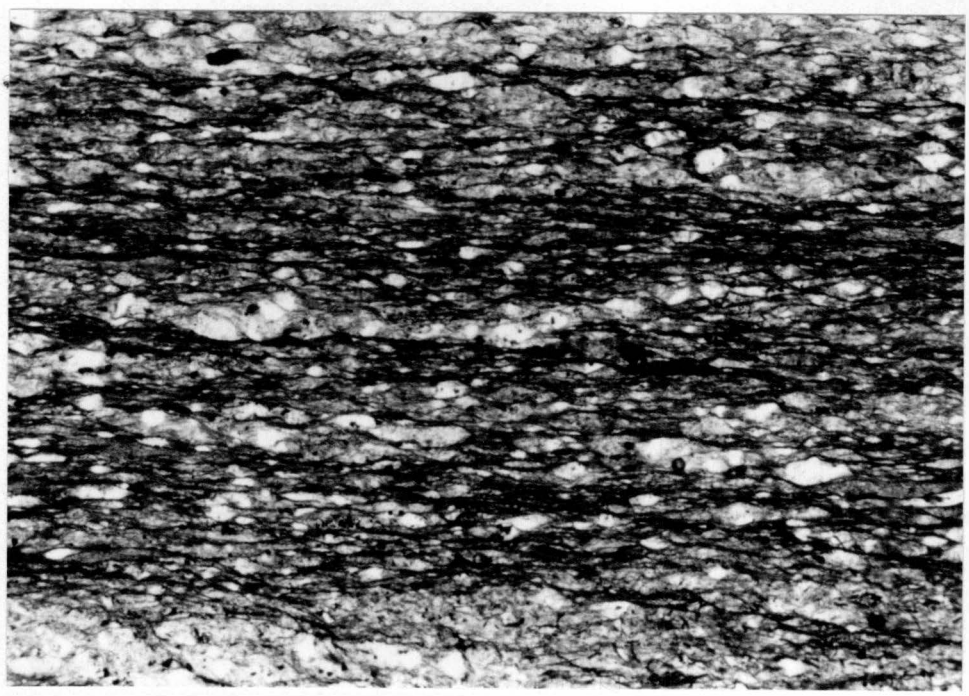

b)

c)

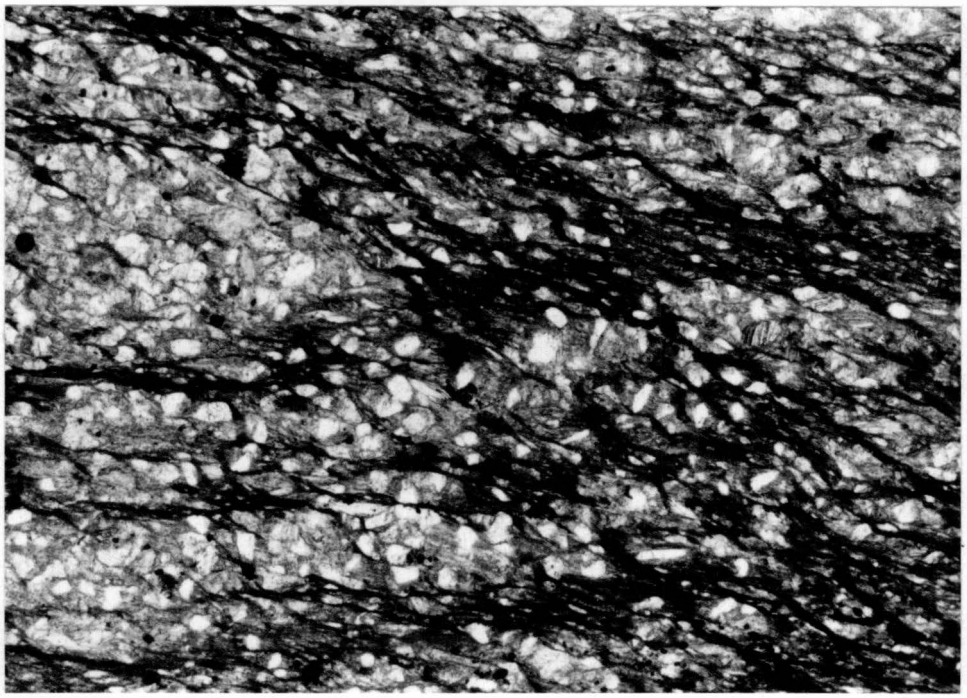

d)

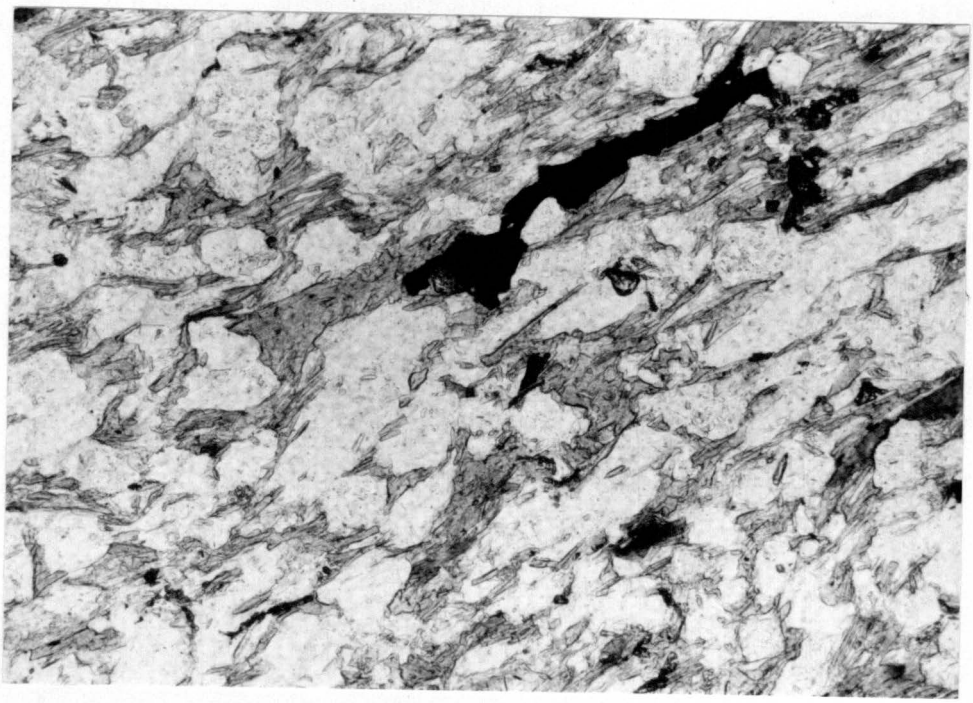

Microstructures and microstructural abundances observed within Great Smoky Group lithologies of the Greenbrier thrust sheet differ between the klippes and the main thrust sheet. These differences are likely a result of different structural positions (hanging-wall ramp versus hanging-wall flat) and higher temperatures during deformation affecting the rocks in the main thrust sheet. Undulatory extinction is present in nearly all grains. Patchy extinction occurs in all samples, but is more common in rocks from the main thrust sheet. Deformation lamellae and deformation bands (Fig. 4.5a) are common in quartz grains from both the klippes and the main thrust sheet. Microfractures, both FIP's (Fig. 4.5b) and sericite-filled extension fractures, are common in samples from the klippes and rare in samples from the main thrust sheet. Sutured grain boundaries are rare in rocks from the klippes and common in rocks from the main thrust sheet. Serrated grain boundaries (Fig. 4.5c) were only observed in samples from the main thrust sheet where they are common. Stylolites (Fig. 4.5d) are present in some samples from the klippes and are generally subparallel to bedding. Stylolites are present in all samples from the main thrust sheet. Small fibrous overgrowths (Fig. 4.5d) were observed only in a few samples from the klippes and are approximately parallel to stylolites. Weakly aligned fine-grained metamorphic muscovite and larger randomly oriented biotite porphyroblasts are present in the main Greenbrier thrust sheet.

FINITE STRAIN ANALYSIS

Methods

Sixty nine oriented sandstone samples were collected for strain analysis from the Miller Cove, Dunn Creek, and Greenbrier thrust sheets in eastern Great Smoky Mountains foothills (Figs. 4.1 and 4.2). Three mutually perpendicular thin sections were cut from each sample and photographed. For each thin section, the shapes and positions

Figure 4.5. Photomicrographs of microstructures from the Greenbrier thrust sheet (Great Smoky Group). a) Deformation lamellae and deformation bands from the Thunderhead Sandstone (sample TH-BM-105). b) Fluid inclusion planes (subvertical) in quartz grains from the Thunderhead Sandstone (sample TH-BM-105). c) Serrated grain boundaries between quartz grains within the Thunderhead Sandstone (sample TH-BM-105). d) Stylolites subhorizontal) and fibrous overgrowths (F) within rocks of Webb Mountain sandstones (sample WM-JB-2). Bedding is horizontal. Field of view for all samples is 2.5 mm.

a)



b)

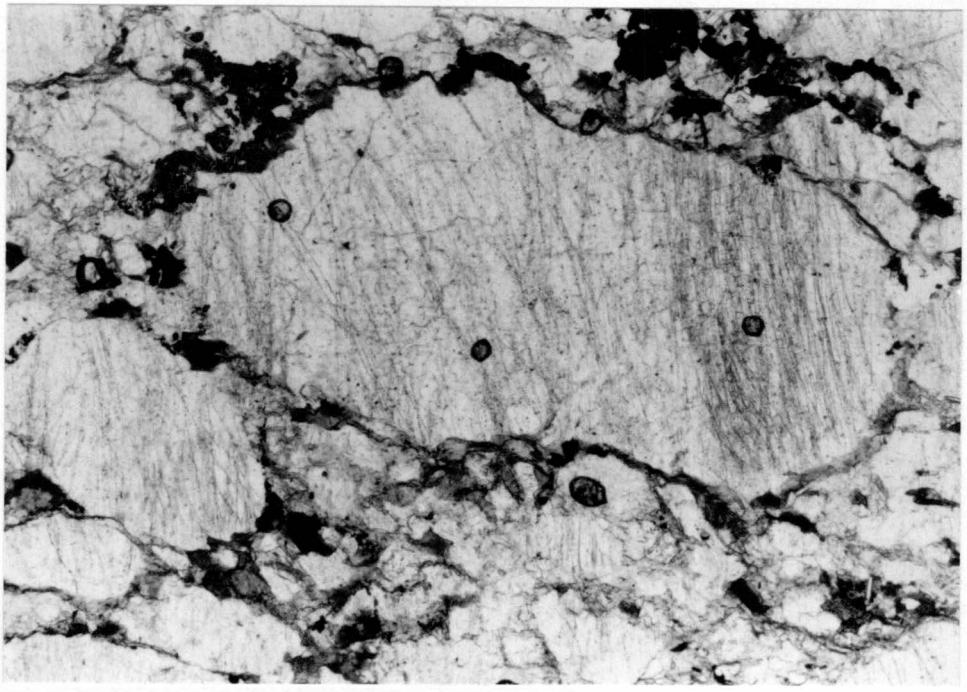

c)

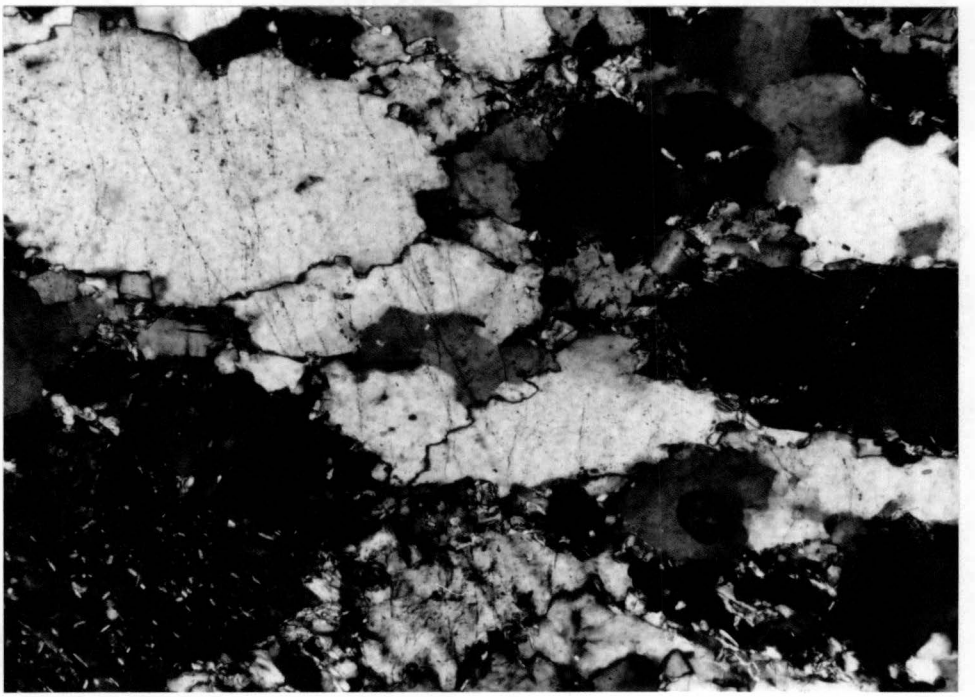

d)

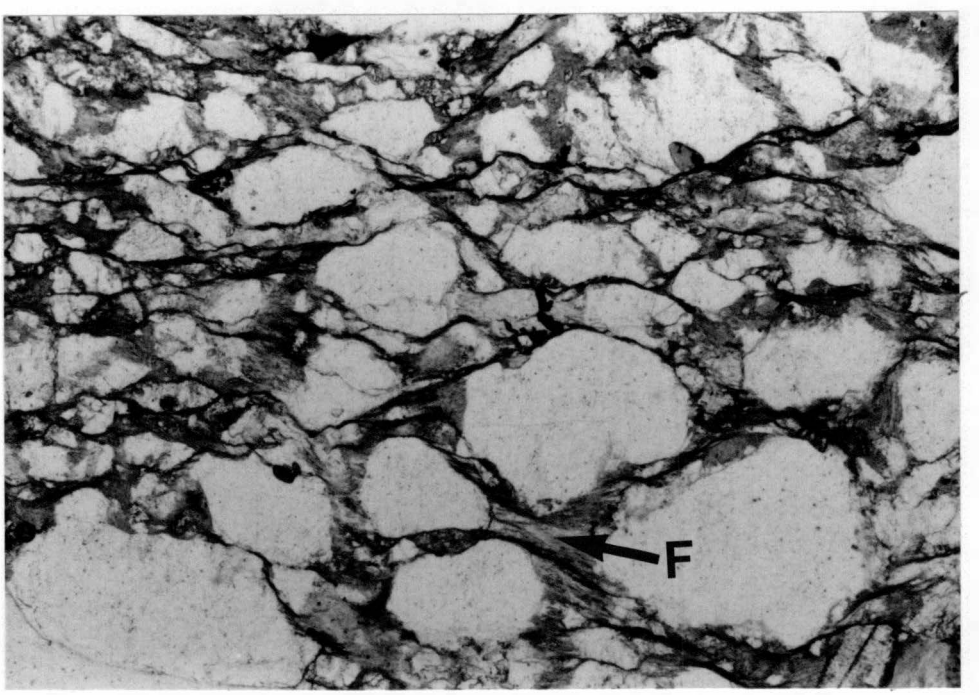

of approximately 200 grains were digitized. Both R_f/ϕ (Dunnet, 1969; Dunnet and Siddans, 1971; Lisle, 1977; Lisle, 1985) and normalized Fry (Fry, 1979; Erslev, 1988) methods were used to determine the strain ellipse for each thin section. The R_f/ϕ technique determines strain based on marker shape, whereas the Fry method determines strain based on the spatial distribution of markers in a deformed rock. The R_f/ϕ method yields strain for only the markers whereas the Fry method yields a value for whole-rock strain. Thus, the two methods should yield different results for inhomogeneously strained rocks, such as where strain is concentrated in the matrix rather than in the framework markers. Strain ellipsoids were calculated from the three mutually perpendicular thin sections for both the R_f/ϕ and normalized Fry methods using the method of Owens (1984).

Results

R_f/ϕ X/Y, X/Z, and Y/Z ratios ($X \geq Y \geq Z$) vary between 1.01 and 1.79 with means and standard deviations of 1.14 ± 0.11, 1.33 ± 0.16, and 1.17 ± 0.08, respectively (Appendix). R_f/ϕ ratios show a general increase in strain magnitude from north to south. Mean X/Z ratios and standard deviations from the Miller Cove, Dunn Creek, and Greenbrier thrust sheets are 1.29 ± 0.11, 1.32 ± 0.14, and 1.42 ± 0.21 respectively (Appendix). Ellipsoid shapes are variable, but most samples (65 percent) plot in the field of apparent flattening on a Flinn plot (Fig. 4.6). Apparent flattening is most pronounced in the Miller Cove thrust sheet where 77 percent of samples plot in the flattening field, and least pronounced in the Dunn Creek thrust sheet where 54 percent of samples plot in the flattening field (Fig. 4.6).

Strain ratios determined by the Fry method are typically 5 to 20 percent higher than those determined by the R_f/ϕ method for all thrust sheets and nearly all samples (Fig. 4.7). Fry X/Y, X/Z, and Y/Z ratios vary between 1.03 and 3.24 with means and

Figure 4.6. Flinn plot of Fry and R_f/ϕ strain data separated by thrust sheet. MCTS=Miller Cove thrust sheet, DCTS=Dunn Creek thrust sheet, GBTS=Greenbrier thrust sheet. For data from the Greenbrier thrust sheet, squares indicate samples from the main Greenbrier thrust sheet and circles indicate klippes.

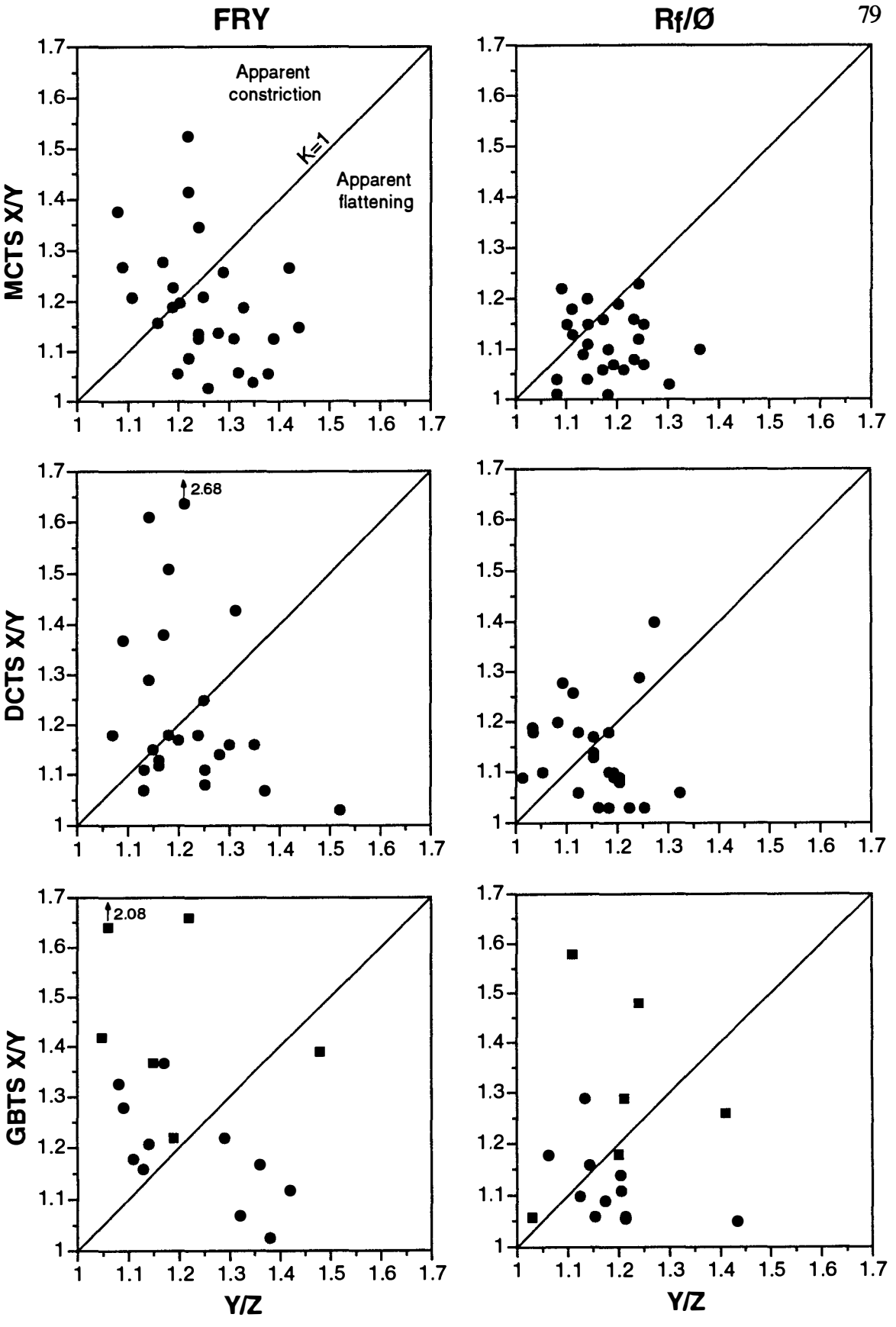
FRY
Rf/Ø
Apparent constriction
K=1
Apparent flattening
MCTS X/Y
DCTS X/Y
GBTS X/Y
2.68
2.08
Y/Z
Y/Z

Figure 4.7. Comparison of Fry X/Z strain magnitudes and R_f/ϕ X/Z strain magnitudes separated by thrust sheet. MCTS=Miller Cove thrust sheet, DCTS=Dunn Creek thrust sheet, GBTS=Greenbrier thrust sheet. Lines represent percentage of Fry magnitude determined by the R_f/ϕ method.

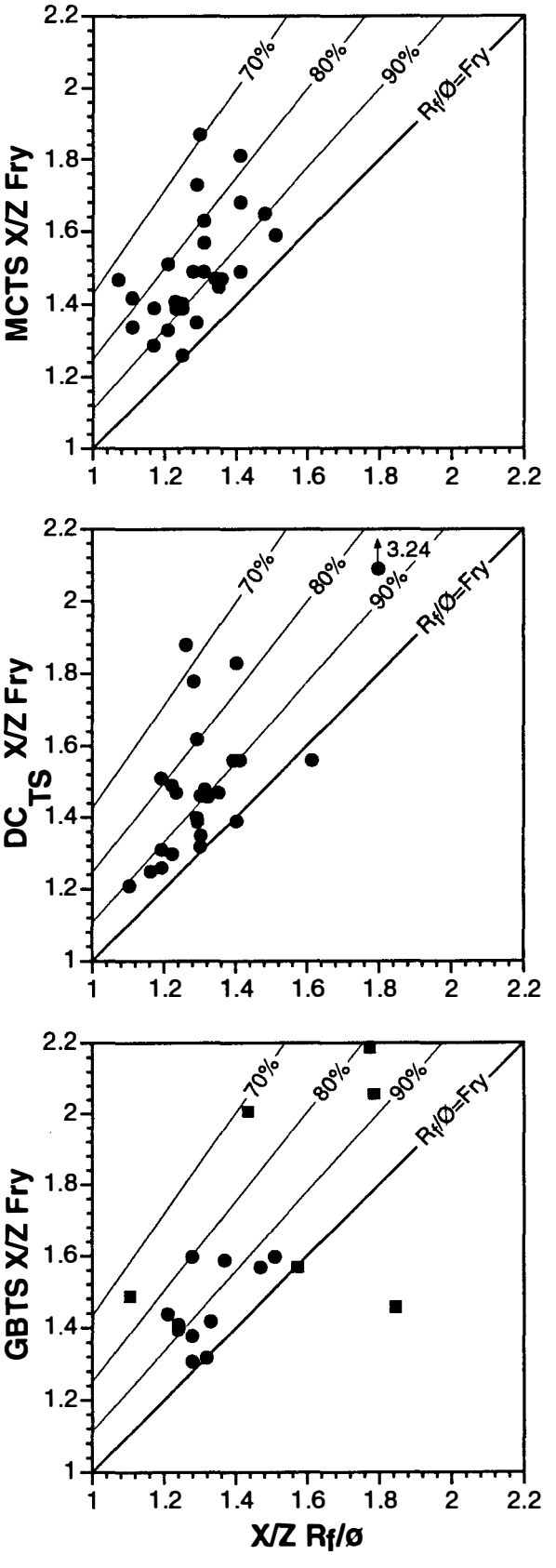
MCTS X/Z Fry
DC TS X/Z Fry
GBTS X/Z Fry
X/Z Rf/ø
70%
80%
90%
Rf/Ø=Fry
3.24
1
1.2
1.4
1.6
1.8
2
2.2

standard deviations of 1.25 ± 0.24, 1.53 ± 0.28, and 1.23 ± 0.11, respectively (Appendix). Like ratios determined by the R_f/ϕ method, Fry ratios show a general increase in strain magnitude from north to south (Figs. 4.8 and 4.9). X/Z ratios and standard deviations from the Miller Cove, Dunn Creek, and Greenbrier thrust sheets are 1.50 ± 0.15, 1.54 ± 0.39, and 1.58 ± 0.25 respectively. Ellipsoid shapes are more variable than those determined by the R_f/ϕ method, although 57 percent of samples plot in the field of apparent flattening on a Flinn plot (Fig. 4.6). Like ellipsoid shapes determined by the R_f/ϕ method, apparent flattening strains are most pronounced in the Miller Cove thrust sheet where 68 percent of samples plot in the apparent flattening field. Within the Greenbrier thrust sheet, although, 65% of the samples plot in the field of apparent constriction (Fig. 4.6).

The orientations of principal strain axes are variable, but a general pattern can be recognized. X axes are typically subhorizontal and strike parallel; Y axes are subhorizontal and strike normal, although other orientations are common; Z axes are steeply dipping to subvertical and most commonly plunge steeply to the north or northwest (Figs. 4.10, 4.11, 4.12, and 4.13). Principal strain axes determined using the R_f/ϕ method show more consistent orientations than those determined by the Fry method (Figs. 4.12; 4.13).

The orientations of the principal strain axes within each thrust sheet vary. The Miller Cove thrust sheet shows the most consistent pattern, with subhorizontal strike parallel X axes, subhorizontal strike-normal Y axes (Fry Y axes are more variable than R_f/ϕ), and subvertical to steeply northwest-plunging Z axes (Figs. 4.10, 4.11, 4.12, and 4.13). The Greenbrier thrust sheet shows a similar although less consistent pattern (Figs. 4.10, 4.11, 4.12, and 4.13).

Strain patterns within the Dunn Creek thrust sheet are more complicated. Both X and Y principal strain axes within the Dunn Creek thrust sheet exhibit similar patterns,

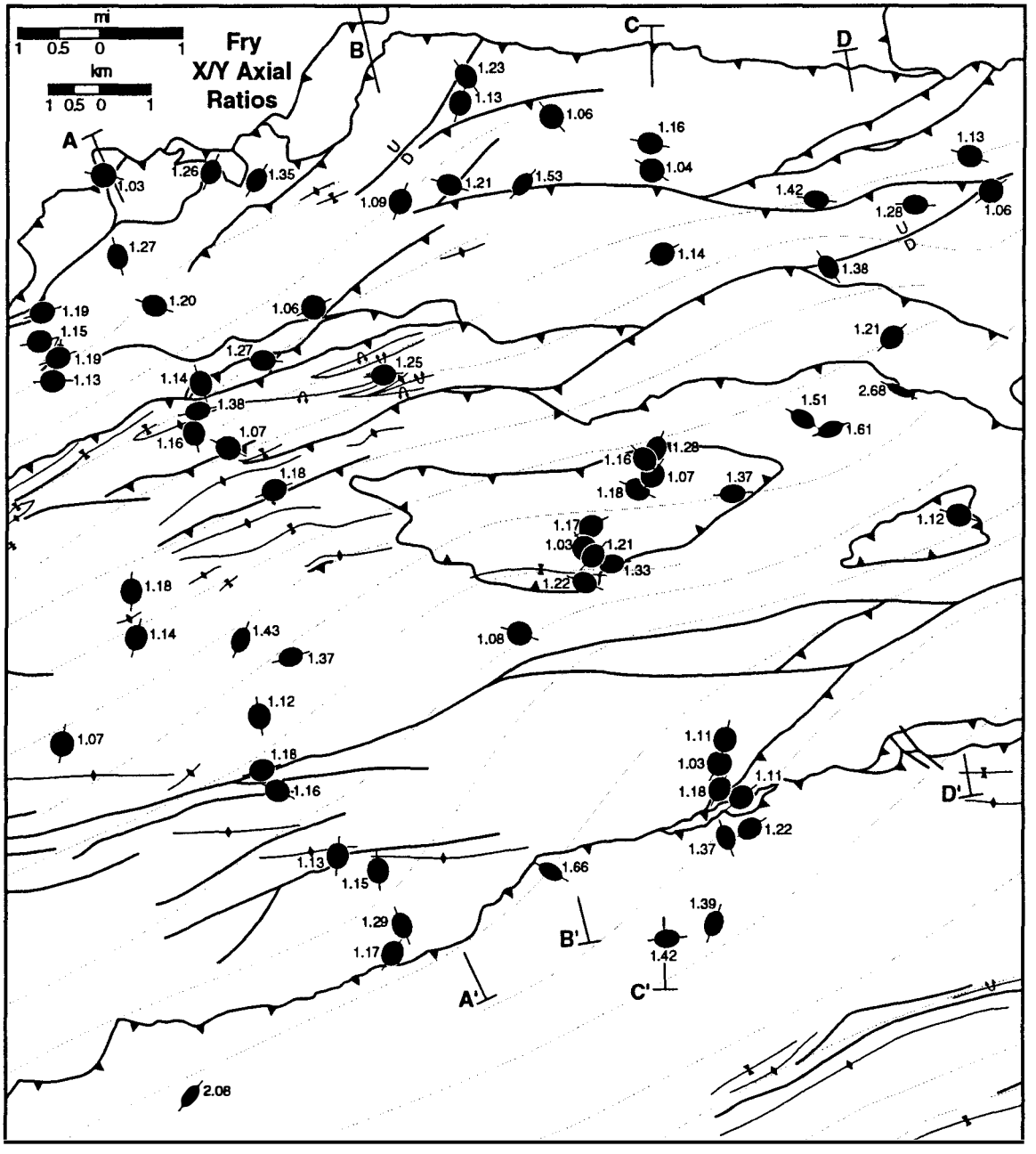

Figure 4.8. X/Y axial ratios as determined by the fry method. Trends of the X axes are indicated for each ellipse. Cross section lines for figure 4.9 are indicated.

Figure 4.9. Cross sections through the study area with X/Z ellipses as determined by the Fry method shown. X axis for each ellipse indicated. Bedding for each ellipse is indicated by two parallel lines. Patterns are the same as those used in Figure 4.1.

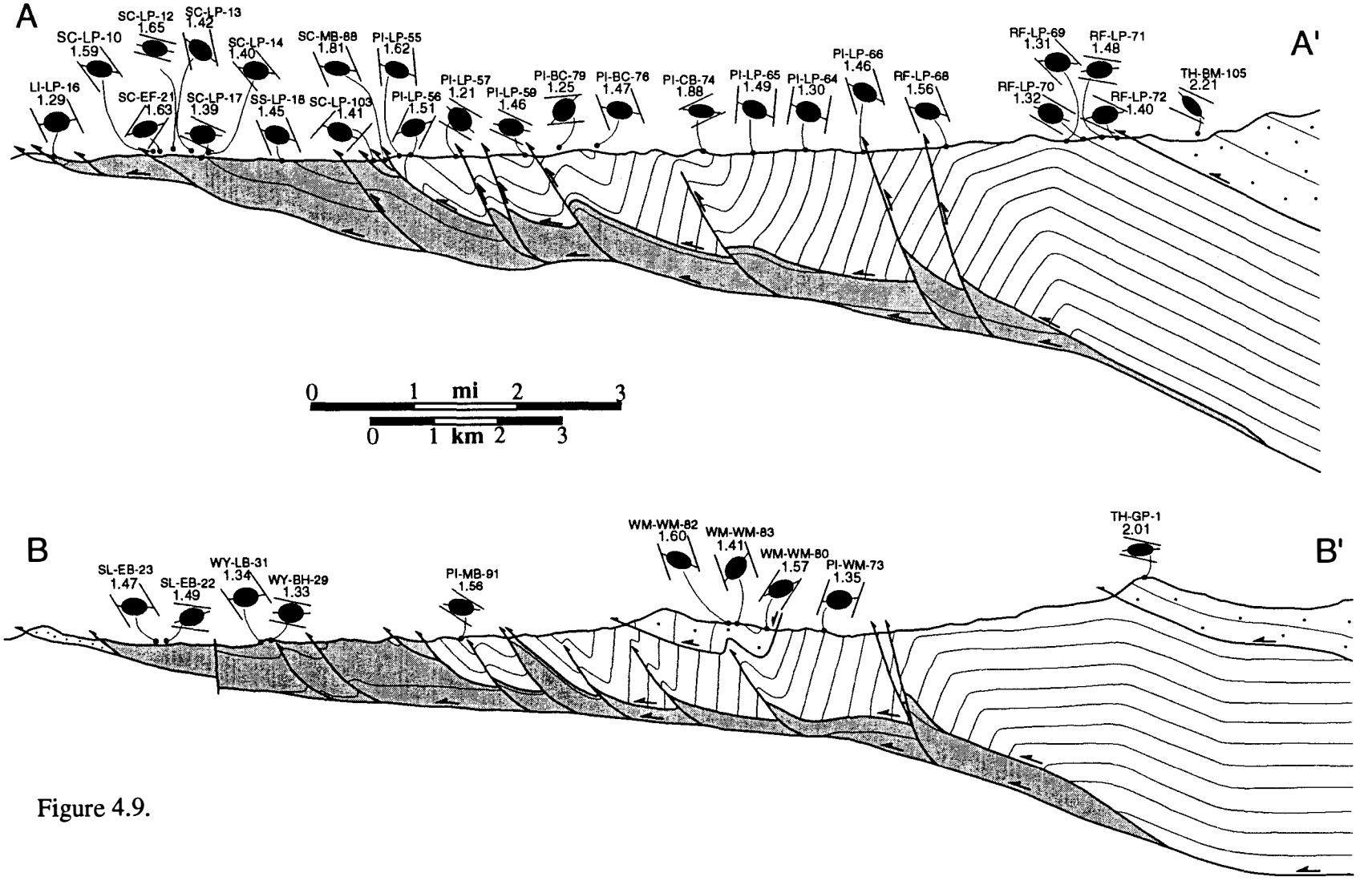
A
A'
SC-LP-12 1.65
SC-LP-13 1.42
SC-LP-10 1.59
SC-LP-14 1.40
SC-MB-88 1.81
PI-LP-55 1.62
LI-LP-16 1.29
SC-EF-21 1.63
SC-LP-17 1.39
SS-LP-18 1.45
SC-LP-103 1.41
PI-LP-56 1.51
PI-LP-57 1.21
PI-LP-59 1.46
PI-BC-79 1.25
PI-BC-76 1.47
PI-CB-74 1.88
PI-LP-65 1.49
PI-LP-64 1.30
PI-LP-66 1.46
RF-LP-68 1.56
RF-LP-69 1.31
RF-LP-71 1.48
RF-LP-70 1.32
RF-LP-72 1.40
TH-BM-105 2.21
0 1 mi 2 3
0 1 km 2 3
B
B'
SL-EB-23 1.47
SL-EB-22 1.49
WY-LB-31 1.34
WY-BH-29 1.33
PI-MB-91 1.56
WM-WM-82 1.60
WM-WM-83 1.41
WM-WM-80 1.57
PI-WM-73 1.35
TH-GP-1 2.01

Figure 4.9.

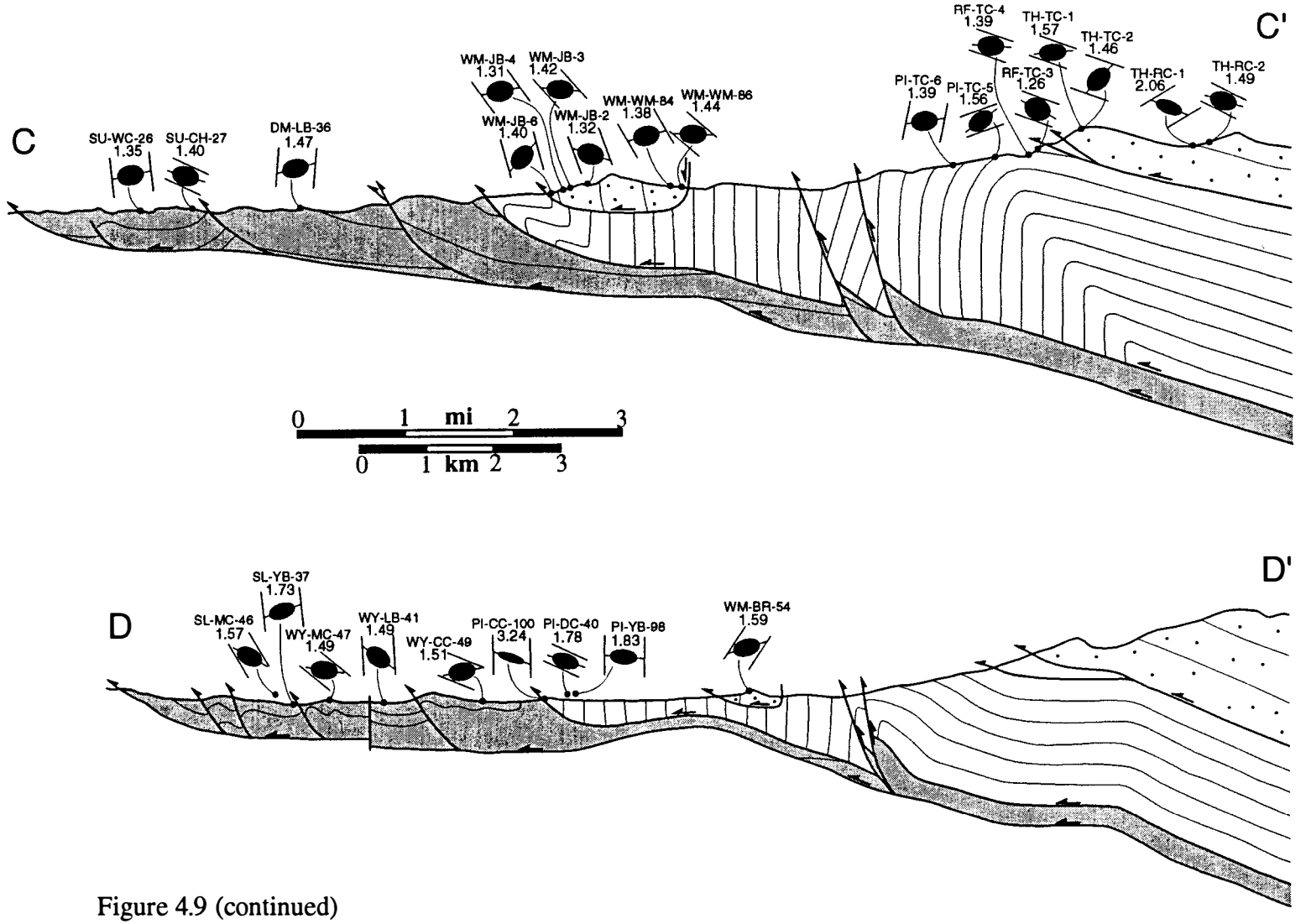

Figure 4.9 (continued)

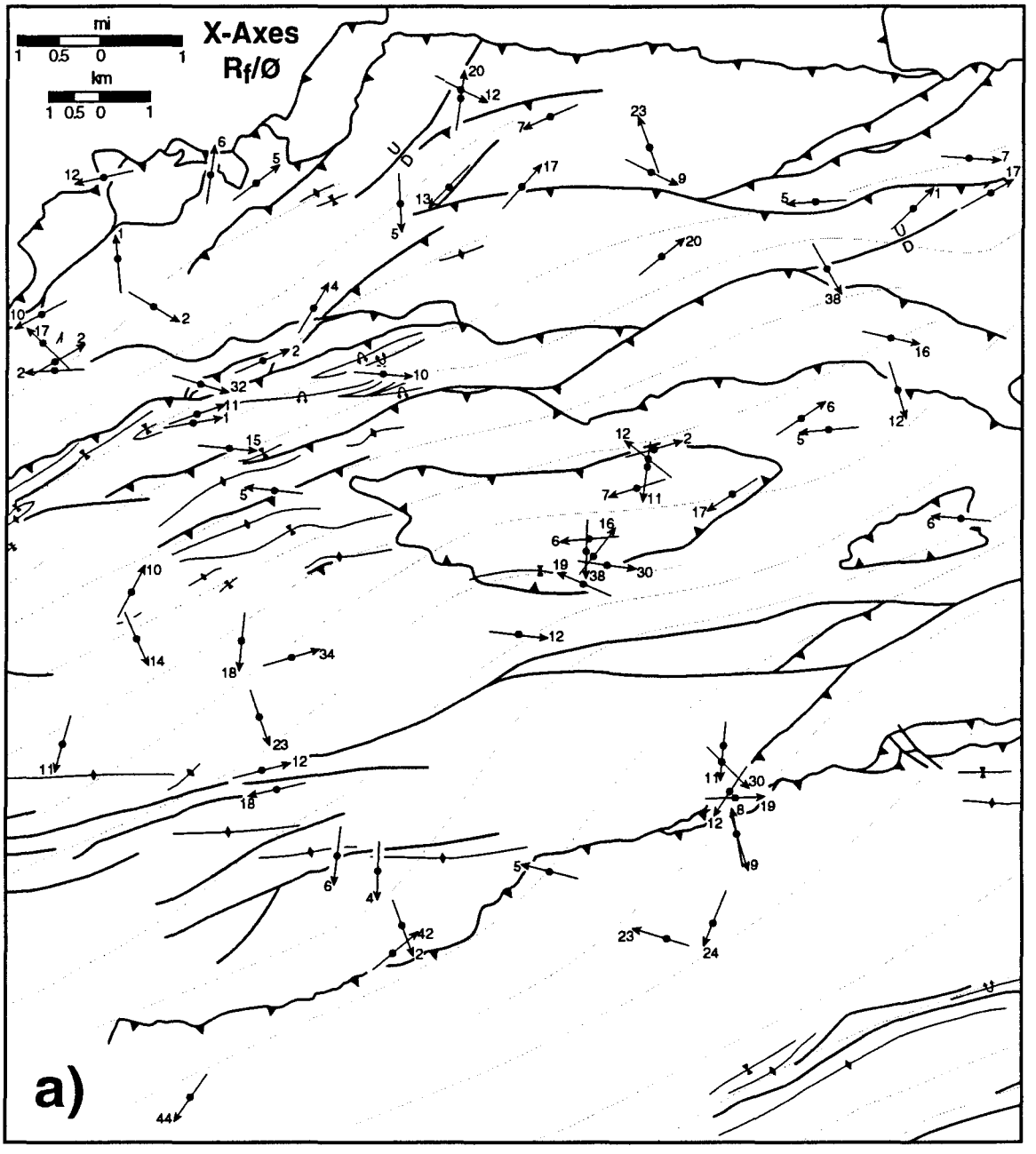

Figure 4.10. Trend and plunge of principal strain axes for each sample as determined by the $R_f/Ø$ method. Light-colored lines are cleavage form lines. a) Trend and plunge of X axes. b) Trend and plunge of Y axes. c) Trend and plunge of Z axes.

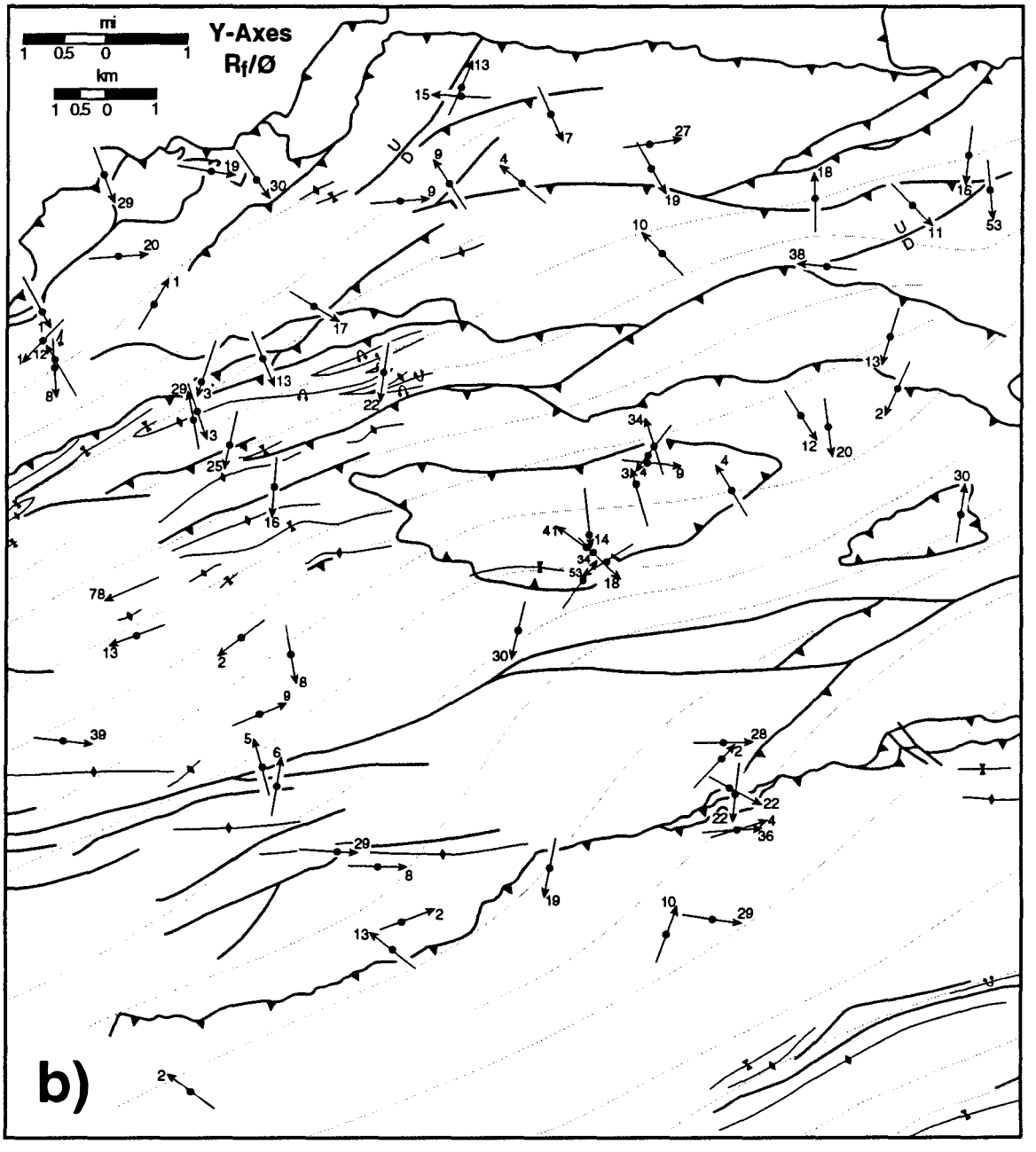

Figure 4.10 (continued)

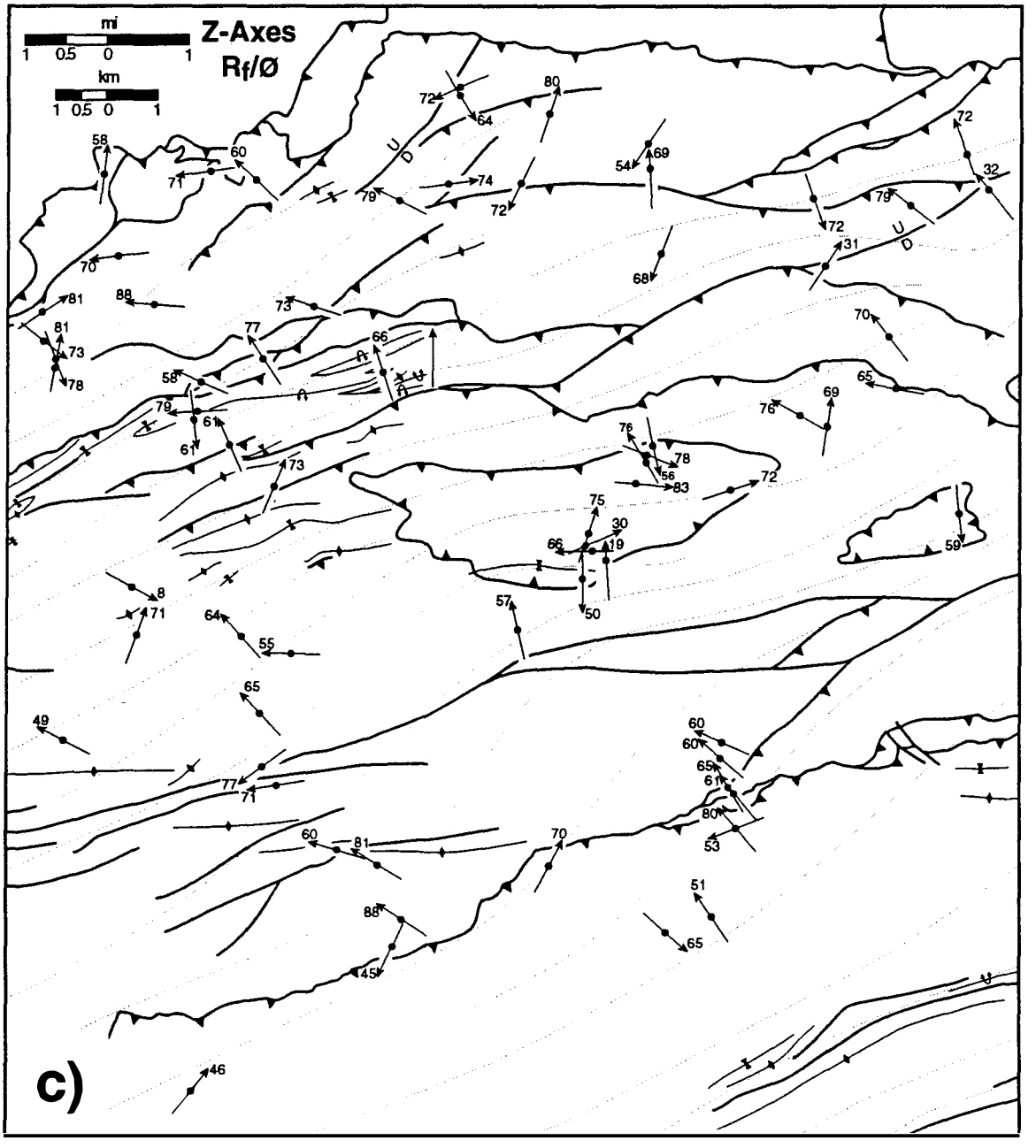

Figure 4.10 (continued)

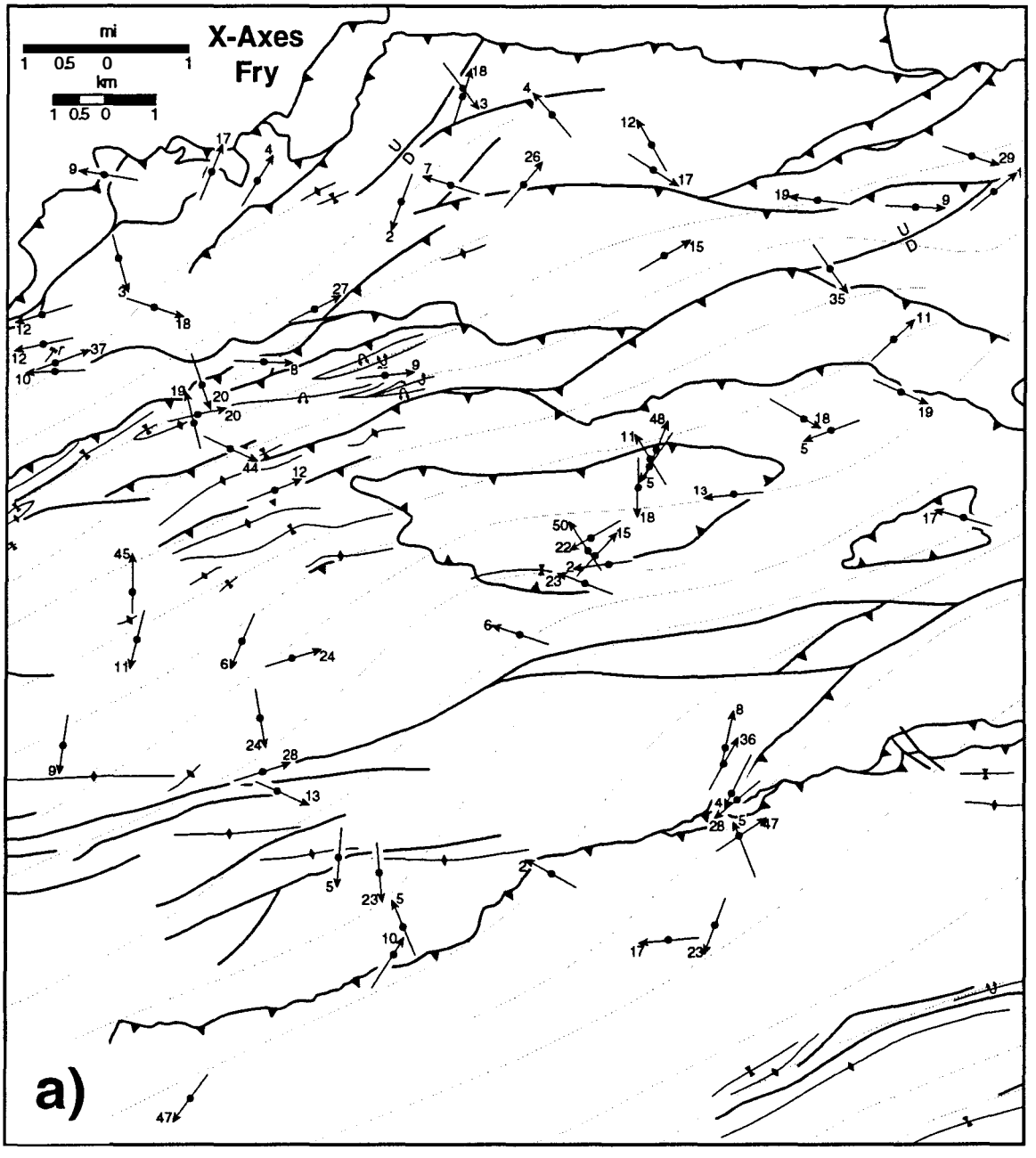

Figure 4.11. Trend and plunge of principal strain axes for each sample as determined by the Fry method. Light-colored lines are cleavage form lines. a) Trend and plunge of X axes. b) Trend and plunge of Y axes. c) Trend and plunge of Z axes.

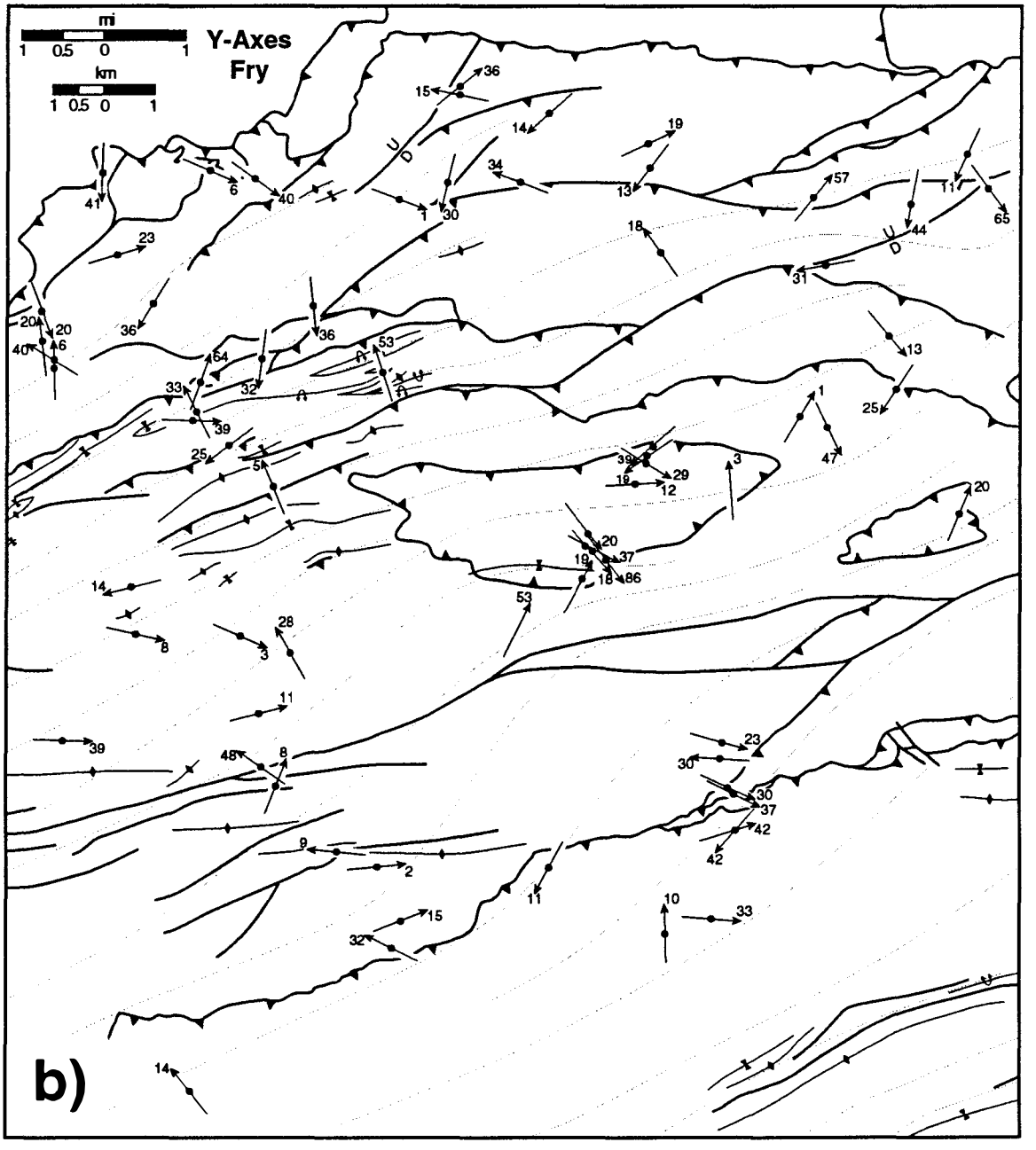

Figure 4.11 (continued)

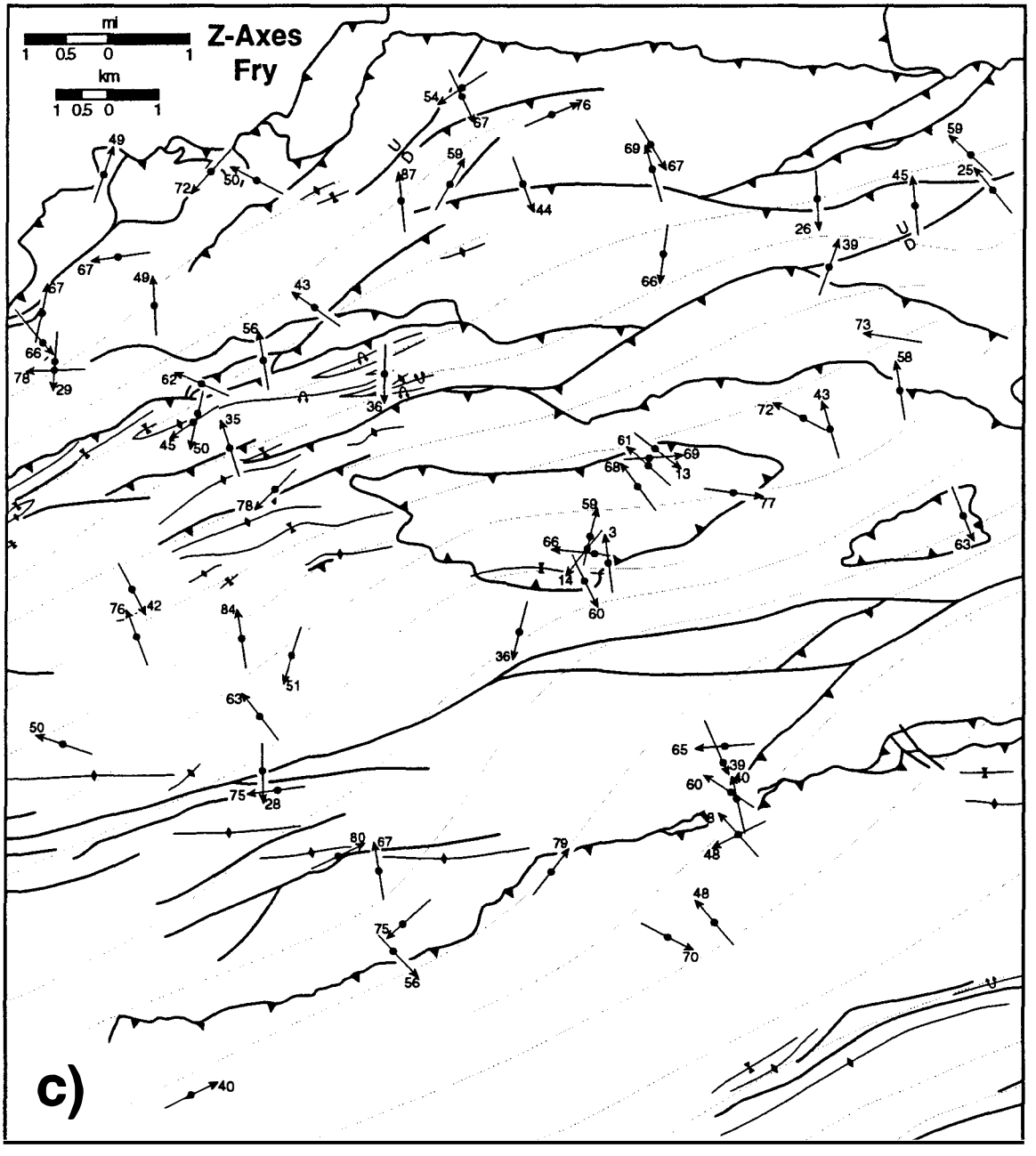

Figure 4.11 (continued)

Figure 4.12. Equal-area lower hemisphere stereonets depicting orientations of principal strain axes as determined by the R_f/ϕ method ($X \geq Y \geq Z$). Data are plotted for all strain data and separated by thrust sheet. Data are contoured using the Kamb (1959) method with the first contour line equal to 3σ (95 percent confidence level) and a contour interval of 2σ.

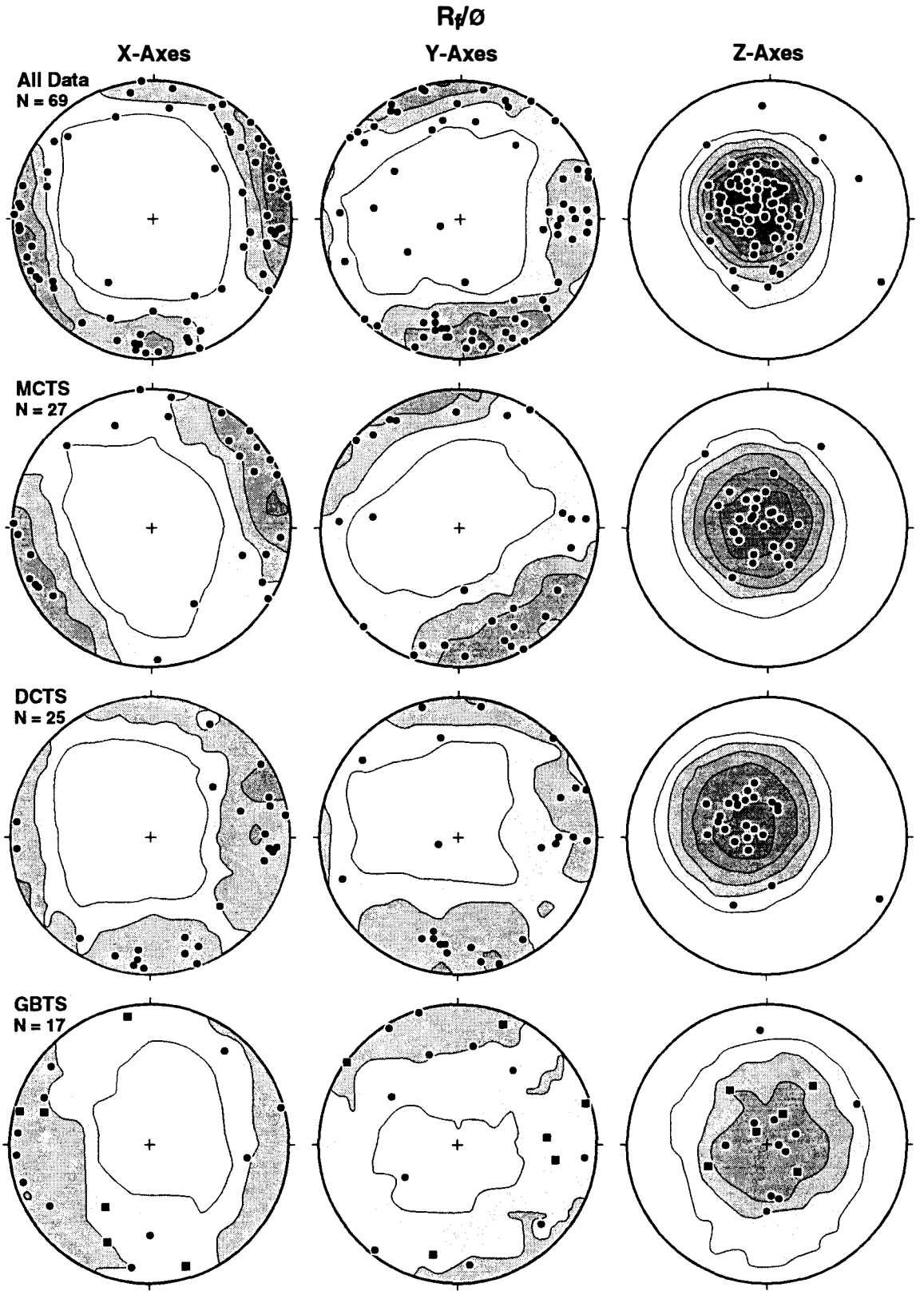
Rf/Ø
X-Axes
Y-Axes
Z-Axes
All Data
N = 69
MCTS
N = 27
DCTS
N = 25
GBTS
N = 17

Figure 4.13. Equal-area lower hemisphere stereonets depicting orientations of principal strain axes as determined by the Fry method ($X \geq Y \geq Z$). Data are plotted for all strain data and separated by thrust sheet. Data are contoured using the Kamb (1959) method with the first contour line equal to 3σ (95 percent confidence level) and a contour interval of 2σ.

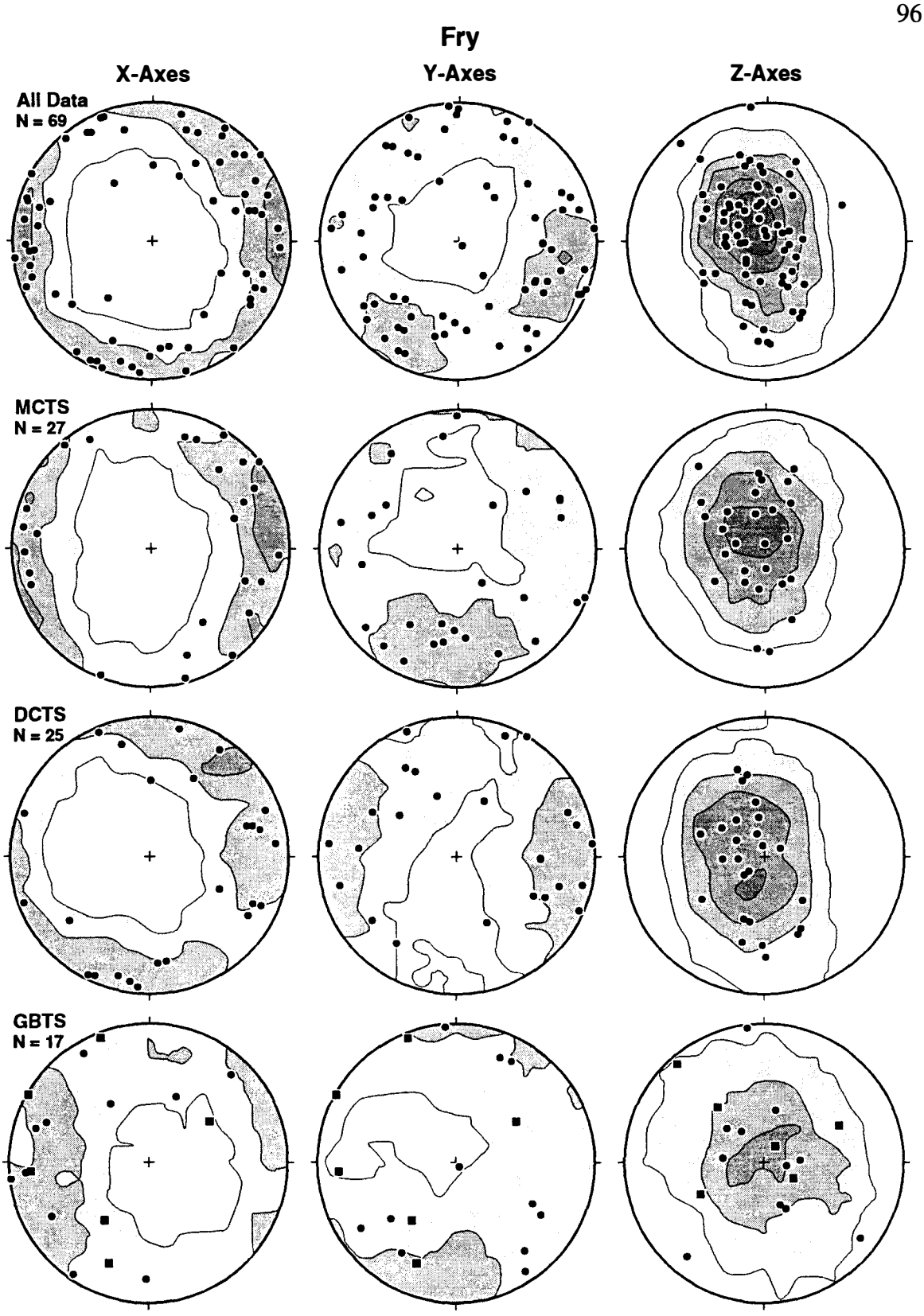
Fry
X-Axes
Y-Axes
Z-Axes
All Data
N = 69
MCTS
N = 27
DCTS
N = 25
GBTS
N = 17

with each showing a group of axes plunging both gently to the east (strike parallel) and gently to the south (strike normal) (Figs. 4.10, 4.11, 4.12, and 4.13). Those samples with X axes that plunge gently eastward have Y axes that plunge gently southward, and those with X axes that plunge gently southward have Y axes that plunge gently eastward (Figs. 4.12 and 4.13). Strike-parallel X axes and strike-normal Z axes predominate in the northern Dunn Creek thrust sheet, where a hanging-wall flat has been modified by later imbricate faulting and folding. This area therefore shows a similar strain pattern to the Miller Cove and Greenbrier thrust sheets. Strike-normal X axes and strike-parallel Z axes predominate in the southern Dunn Creek thrust sheet (Figs. 4.10, 4.11, 4.12, and 4.13), where a large hanging-wall ramp anticline has been overprinted by internal strain. Most Z axes plunge steeply northwestward throughout the entire Dunn Creek thrust sheet (Figs. 4.12 and 4.13).

In order to evaluate the possibility of a dominant compactional strain recognized in some foreland thrust belts (Couzens and others, in press), bedding for all samples, along with principal strain axes, was restored to horizontal. Rotated principal strain axes determined by both R_f/ϕ and Fry methods show less consistent orientations than unrotated samples (Figs. 4.14 and 4.15) indicating that tectonic strains have contributed to the finite strain of the sandstones.

DISCUSSION

Strain magnitudes throughout the study area are small and relatively consistent, with only one sample (PI-CC-100) clearly influenced by fault zone strains. The measured finite-strain geometry determined by strain analysis of sandstones is somewhat different than that expected based on regional cleavage geometries measured primarily in slates from the study area. Regional cleavage dips moderately (40 to 70 degrees) to the southeast and is generally unaffected by structural position (Hamilton, 1961). Poles

Figure 4.14. Equal-area lower hemisphere stereonets depicting orientations of rotated principal strain axes as determined by the R_f/ϕ method ($X \geq Y \geq Z$). Principal strain axes have been rotated along with bedding to a horizontal bedding orientation. Data are plotted for all strain data and separated by thrust sheet. Data are contoured using the Kamb (1959) method with the first contour line equal to 3σ (95 percent confidence level) and a contour interval of 2σ.

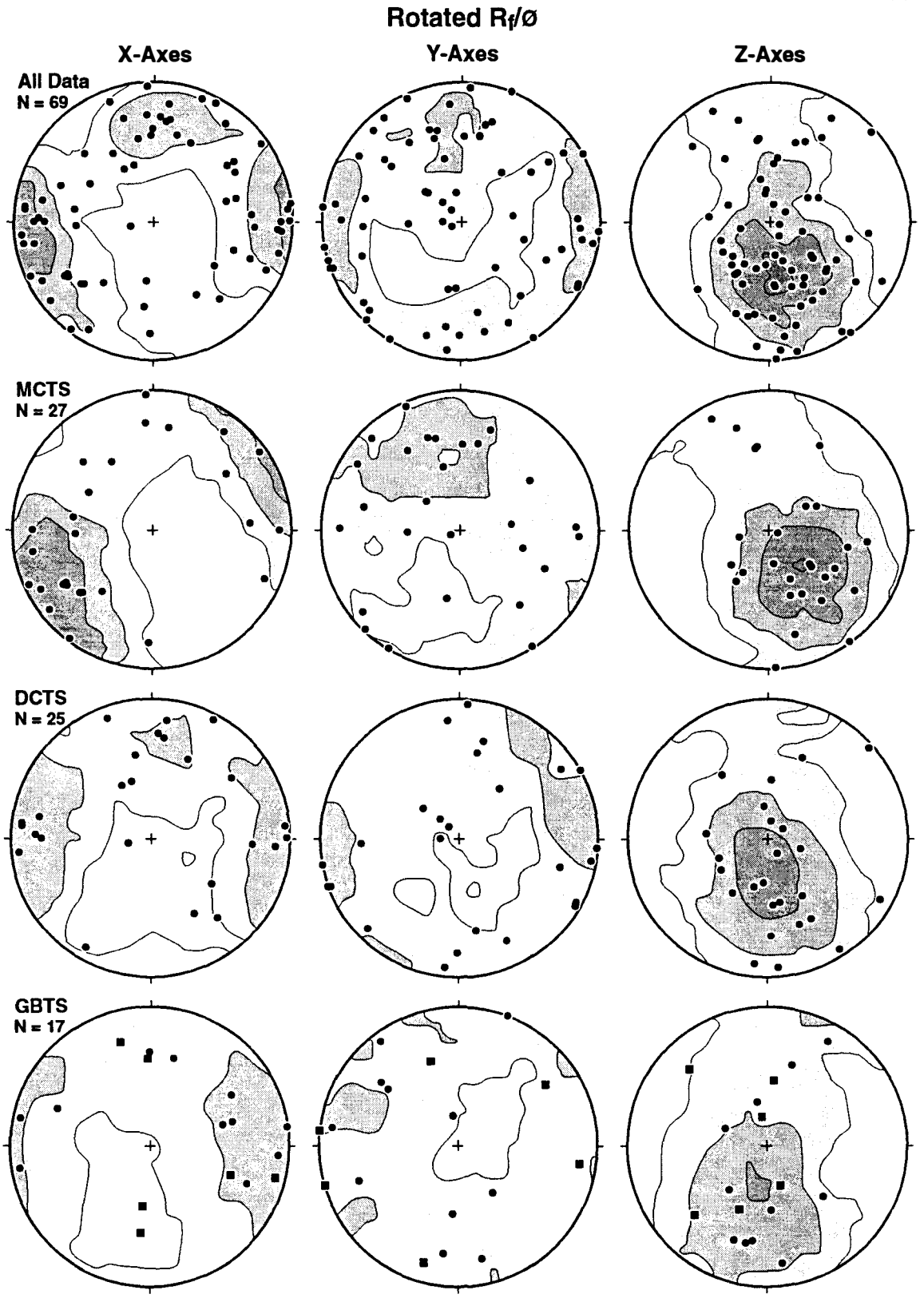
Rotated Rf/ø
X-Axes
Y-Axes
Z-Axes
All Data
N = 69
MCTS
N = 27
DCTS
N = 25
GBTS
N = 17

Figure 4.15. Equal-area lower hemisphere stereonets depicting orientations of rotated principal strain axes as determined by the Fry method ($X \geq Y \geq Z$). Principal strain axes have been rotated along with bedding to a horizontal bedding orientation. Data are plotted for all strain data and separated by thrust sheet. Data are contoured using the Kamb (1959) method with the first contour line equal to 3σ (95 percent confidence level) and a contour interval of 2σ.

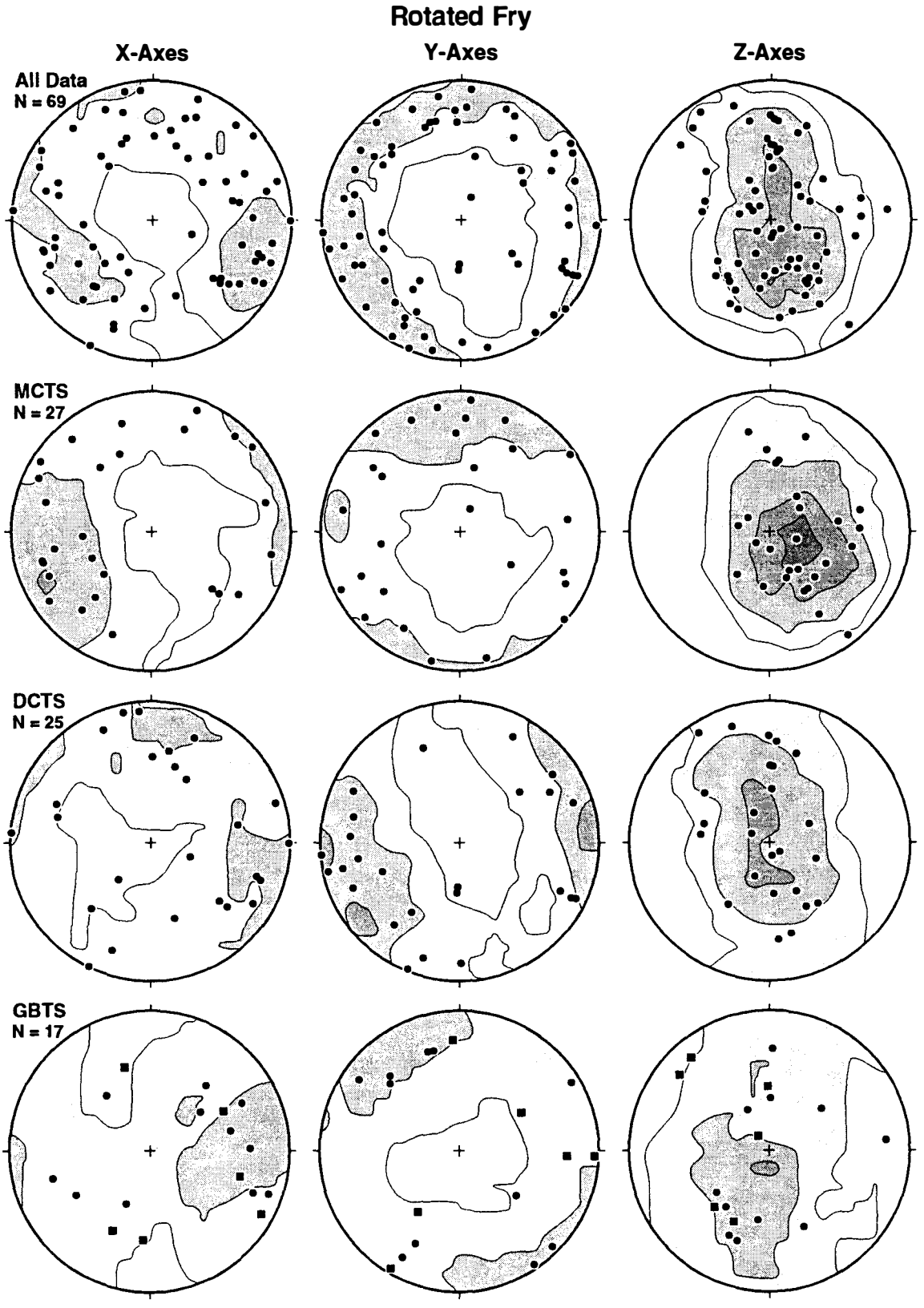
Rotated Fry
X-Axes
Y-Axes
Z-Axes
All Data
N = 69
MCTS
N = 27
DCTS
N = 25
GBTS
N = 17

to cleavage plunge somewhat more gently to the northwest than Z axes determined in this study (Hamilton, 1961, Fig. 25), and X and Y principal strain axes appear to be controlled somewhat by structural position (X axes are generally parallel to strike in hanging-wall flat areas and normal to strike in hanging-wall ramp areas). The most conspicuous aspects of the finite strain geometry are the subvertical to steeply northwest plunging Z axes and the subhorizontal strike parallel X axes, both of which suggest compaction may be an important part of the finite strain. As indicated previously, however, increased scatter observed in rotated plots of principal strain axes (Figs. 4.14, 4.15) indicates that tectonic strains were also important.

Strain Factorization

To quantitatively evaluate the importance of the deformation events that may have contributed to the finite strain of the sandstones, strain was factorized into three events typical of low grade thrust belts. Two simple models were considered. Samples from the Miller Cove thrust sheet and those parts of the Dunn Creek thrust sheet with hanging-wall flat geometries were modeled for compaction by volume loss, layer-parallel shortening/extension (both plane strain and axial symmetric flattening), and transport parallel simple shear (Fig. 4.16a). Samples from the hanging-wall ramp portion of the Dunn Creek thrust sheet that were fault-bend folded prior to superposition of cleavage strains (section 2) were modeled as compaction by volume loss, rigid-body rotation (bedding rotated from horizontal to vertical) from fault-bend folding, horizontal shortening/extension (both axial symmetric flattening and plane strain), and transport-parallel simple shear (Fig. 4.16b). Because the strain geometries are more complicated and less data are available, strains from the Greenbrier thrust sheet were not modeled.

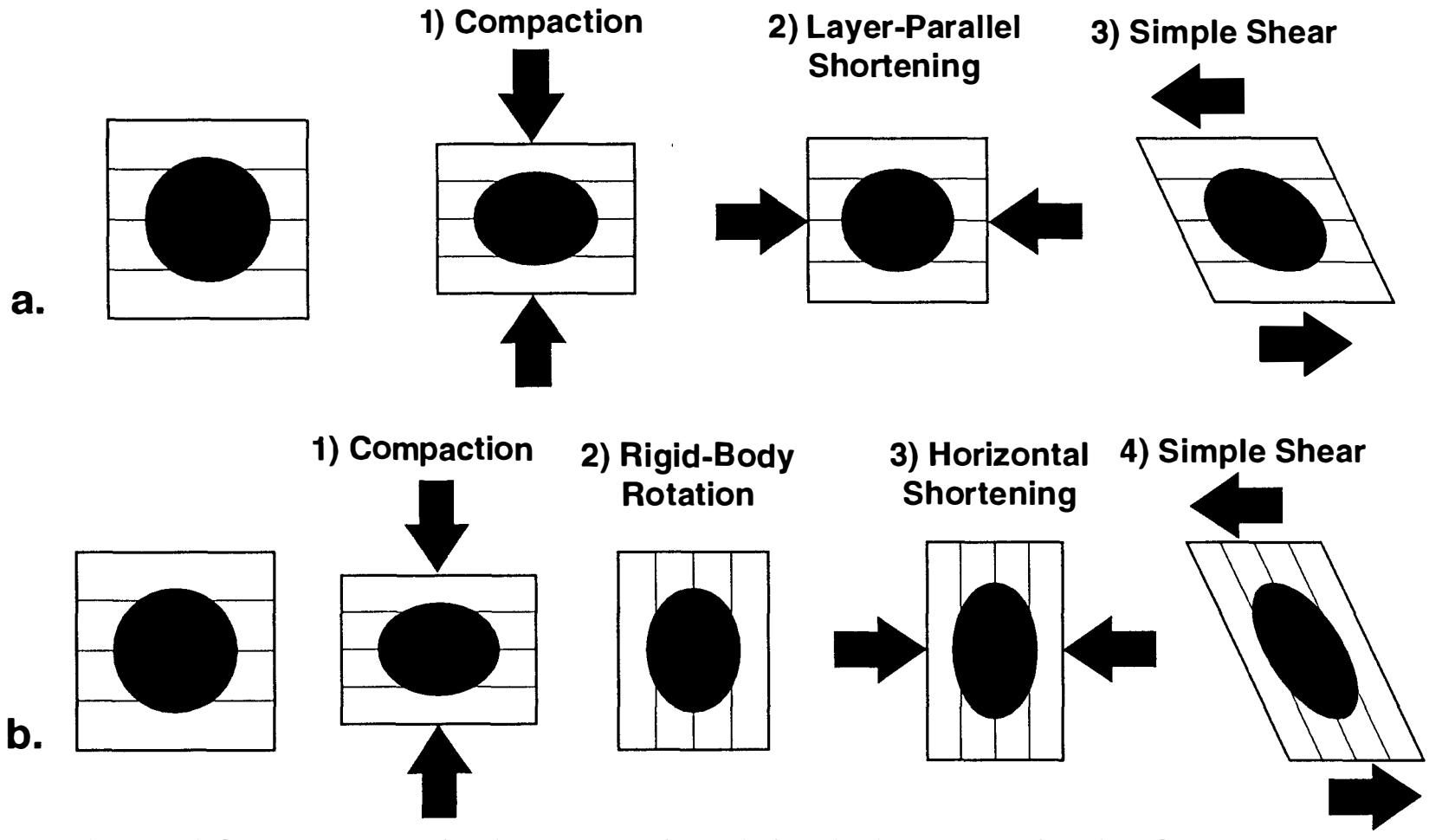

Figure 4.16. Conceptual model of strain events used for strain factorization. a) Model for Miller Cove thrust sheet and those parts of the Dunn Creek thrust sheet with hanging-wall flat geometries. b) Model for hanging-wall ramp portion of the Dunn Creek thrust sheet.

Before strain factorization is attempted, a coordinate system must be defined. The chosen system has *a* parallel to strike, *b* perpendicular to strike, and *c* vertical. Strain events are defined in terms of the deformation matrix:

$$\boldsymbol{D} = \begin{bmatrix} aa & ab & ac \\ ba & bb & bc \\ ca & cb & cc \end{bmatrix}$$

which is used to map points in a volume from original positions to strained positions (Ramsay, 1967; Means, 1976; Ramsay and Huber, 1987; Couzens, 1992). Superposition of the various strain components involves matrix multiplication of two or more strain events. Because matrix multiplication is not commutative, strain events must be multiplied in the inferred sequence of deformation. Matrices multiplied for the two models considered in this study are presented in Table 4.1. These matricies were evaluated for different values of compaction, horizontal shortening (α), and shear strain (γ). Ellipsoid shape and orientation were calculated using a spreadsheet for three-dimensional strain factorization from Couzens (1992). Curves were plotted of equal values of α and γ for various values of compaction on a graph of measured strain ratios (R) and angle between the longer axis and horizontal in the transport profile (θ). The long axis of the ellipse in the profile direction (θ for X or Y axis) and the ellipticity in the profile direction (R = X/Z or X/Y) of the measured strain results were plotted on each graph.

In the case of no compactional strain, most measured strains plot in the vicinity of $\gamma = 0.1$ and $\alpha = 1.1$ for both the axial flattening and plane strain cases (Fig. 4.17). Thus, low values of shear strain combined with low values of horizontal extension could explain the observed strain magnitudes and geometries. As indicated previously, however, most strain results indicate apparent extension (X axes) parallel to strike. Thus,

Table 4.1. Matricies multiplied for the two models evaluated in this study; γ = shear strain, S = stretch, Δ = dilation. a) Model for Miller Cove thrust sheet and those parts of the Dunn Creek thrust sheet with hanging-wall flat geometries. b) Model for hanging-wall ramp portions of the Dunn Creek thrust sheet.

---

a) 3) Simple shear 2) Layer Parallel Shortening Axial Flattening 1) Compaction

$$\begin{bmatrix} 1 & 0 & 0 \\ 0 & 1 & 0 \\ 0 & \gamma & 1 \end{bmatrix} X \begin{bmatrix} 1/\sqrt{S} & 0 & 0 \\ 0 & S & 0 \\ 0 & 0 & 1/\sqrt{S} \end{bmatrix} X \begin{bmatrix} 1 & 0 & 0 \\ 0 & 1 & 0 \\ 0 & 0 & 1+\Delta \end{bmatrix} = \mathbf{D}$$

or

2) Layer-Parallel Shortening Plane Strain

$$\begin{bmatrix} 1 & 0 & 0 \\ 0 & S & 0 \\ 0 & 0 & 1/S \end{bmatrix}$$

b) 3) Simple shear 2) Horizontal Shortening Axial Flattening 1) Simulates Compaction with 90° Rotation

$$\begin{bmatrix} 1 & 0 & 0 \\ 0 & 1 & 0 \\ 0 & \gamma & 1 \end{bmatrix} X \begin{bmatrix} 1/\sqrt{S} & 0 & 0 \\ 0 & S & 0 \\ 0 & 0 & 1/\sqrt{S} \end{bmatrix} X \begin{bmatrix} 1 & 0 & 0 \\ 0 & 1+\Delta & 0 \\ 0 & 0 & 1 \end{bmatrix} = \mathbf{D}$$

or

2) Horizontal Shortening Plane Strain

$$\begin{bmatrix} 1 & 0 & 0 \\ 0 & S & 0 \\ 0 & 0 & 1/S \end{bmatrix}$$

Figure 4.17. Plot of strain ratio (R) in the profile direction (X/Z or Y/Z) against the angle between the longer axis of the ellipse in the profile direction (X or Y axis) and the shear direction. Solid lines are equal values of stretch (α) in the profile direction (layer-parallel shortening/extension). Dashed lines are equal values of shear strain (γ). Values for both axial flattening and plane strain layer parallel shortening cases have been determined. No compaction strains have been applied. Strain results from the R_f/ϕ method are plotted. Unfilled symbols are those samples in which Y/Z ellipses parallel the profile direction, and filled symbols are those samples in which the X/Z ellipses parallel the profile direction. Circles are samples from the Miller Cove thrust sheet, triangles are samples from hanging-wall flat portions of the Dunn Creek thrust sheet, and squares are from the hanging-wall ramp portions of the Dunn Creek thrust sheet.

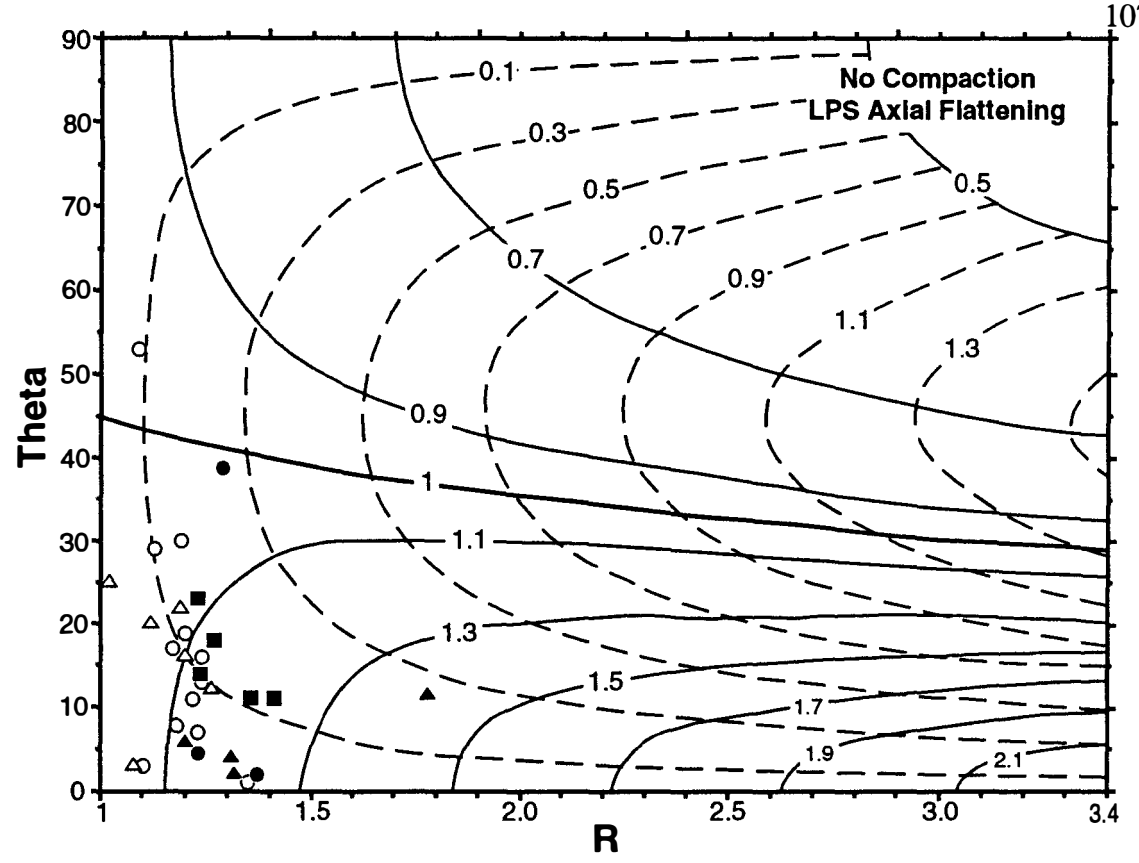
No Compaction
LPS Axial Flattening
Theta
R
0.1
0.3
0.5
0.7
0.9
1.1
1.3
1.5
1.7
1.9
2.1

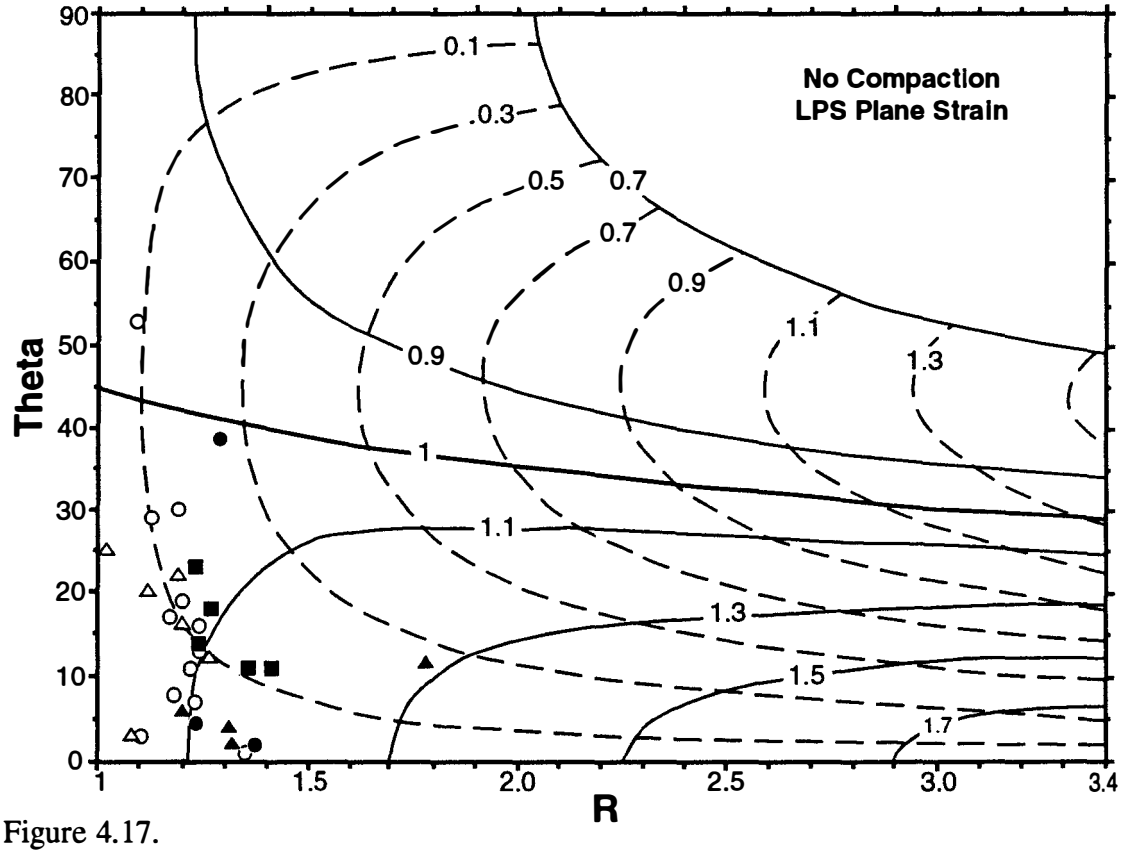
No Compaction
LPS Plane Strain
Theta
R
0.1
0.3
0.5
0.7
0.9
1.1
1.3
1.5
1.7

Figure 4.17.

most ellipses in the profile direction (and plotted on the graphs) are Y/Z axial ratios, unlike the model results which produce X axes in the transport profile.

To model successfully Y/Z ellipses in the profile direction, graphs were constructed with compaction strains of 20, 30, and 40 percent (Fig. 4.18). For these graphs, α curves are identical to those produced without compaction, although γ curves differ because a non-zero compaction produces a field on the graphs where Y/Z ellipses are parallel to the profile direction (shaded area on graphs) and X/Z ellipses are normal to the profile direction (parallel to strike). This field is larger for the axial flattening models and grows with increasing compaction values (Fig. 4.18). For the measured strains to match the modeling results, samples from the Miller Cove and northern Dunn Creek thrust sheet, where X axes are parallel to strike, should plot in the Y/Z ellipse field. In addition, those samples from the southern most Dunn Creek thrust sheet, where X axes are normal to strike, should plot in the X/Z ellipse field. These conditions are best satisfied by the 20 percent compaction (either axial flattening or plane strain LPS) model (Fig. 4.18a). The measured strain magnitudes and geometries in this part of the study area can therefore be produced by 20 percent vertical volume loss compaction strains followed by a small amount of layer parallel shortening ($\alpha \approx 0.95$) and small amounts of shear strain ($\gamma \approx 0.1$).

For areas where bedding was steeply dipping prior to superimposing cleavage strains (hanging-wall ramp area within the Dunn Creek thrust sheet), a second set of graphs were constructed in which compaction was applied horizontally to simulate vertical compaction and 90 degree rigid-body rotation (Fig. 4.19). These models produce identical γ curves to previously discussed graphs but α values differ significantly. Using the simplest assumption of a homogeneous deformation across both subdomains, the modeled strain history of the first subdomain should account for the finite strains in the second domain, but it does not. It yields appropriate strain ratios but produces steeply

Figure 4.18. Plot of strain ratio (R) in the profile direction (X/Z or Y/Z) against the angle between the longer axis of the ellipse in the profile direction (X or Y axis) and the shear direction for various values of compaction. Solid lines are equal values of stretch (α) in the profile direction (layer-parallel shortening/extension). Dashed lines are equal values of shear strain (γ). Shaded area is field of Y/Z axes parallal to the profile direction. Values for both axial flattening and plane strain layer parallel shortening cases have been determined. Strain results from the R_f/ϕ method are plotted. Unfilled symbols are those samples in which Y/Z ellipses parallel the profile direction, and filled symbols are those samples in which the X/Z ellipses parallel the profile direction. Circles are samples from the Miller Cove thrust sheet and triangles are samples from hanging-wall flat portions of the Dunn Creek thrust sheet. a) 20 percent compaction. b) 30 percent compaction. c) 40 percent compaction.

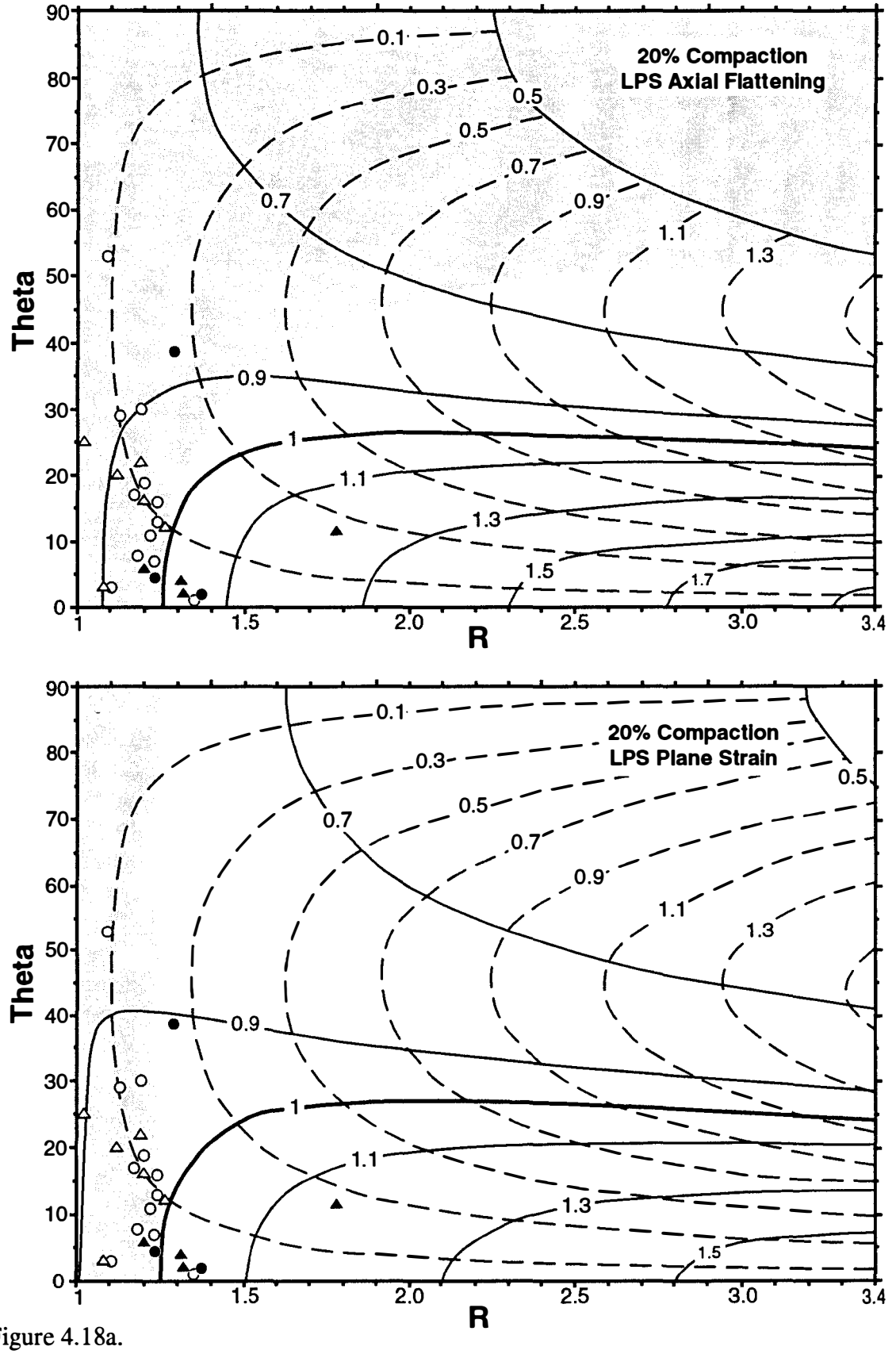
20% Compaction
LPS Axial Flattening
Theta
R
0.1
0.3
0.5
0.7
0.9
1.1
1.3
1.5
1.7
20% Compaction
LPS Plane Strain
Theta
R
0.1
0.3
0.5
0.7
0.9
1
1.1
1.3
1.5

Figure 4.18a.

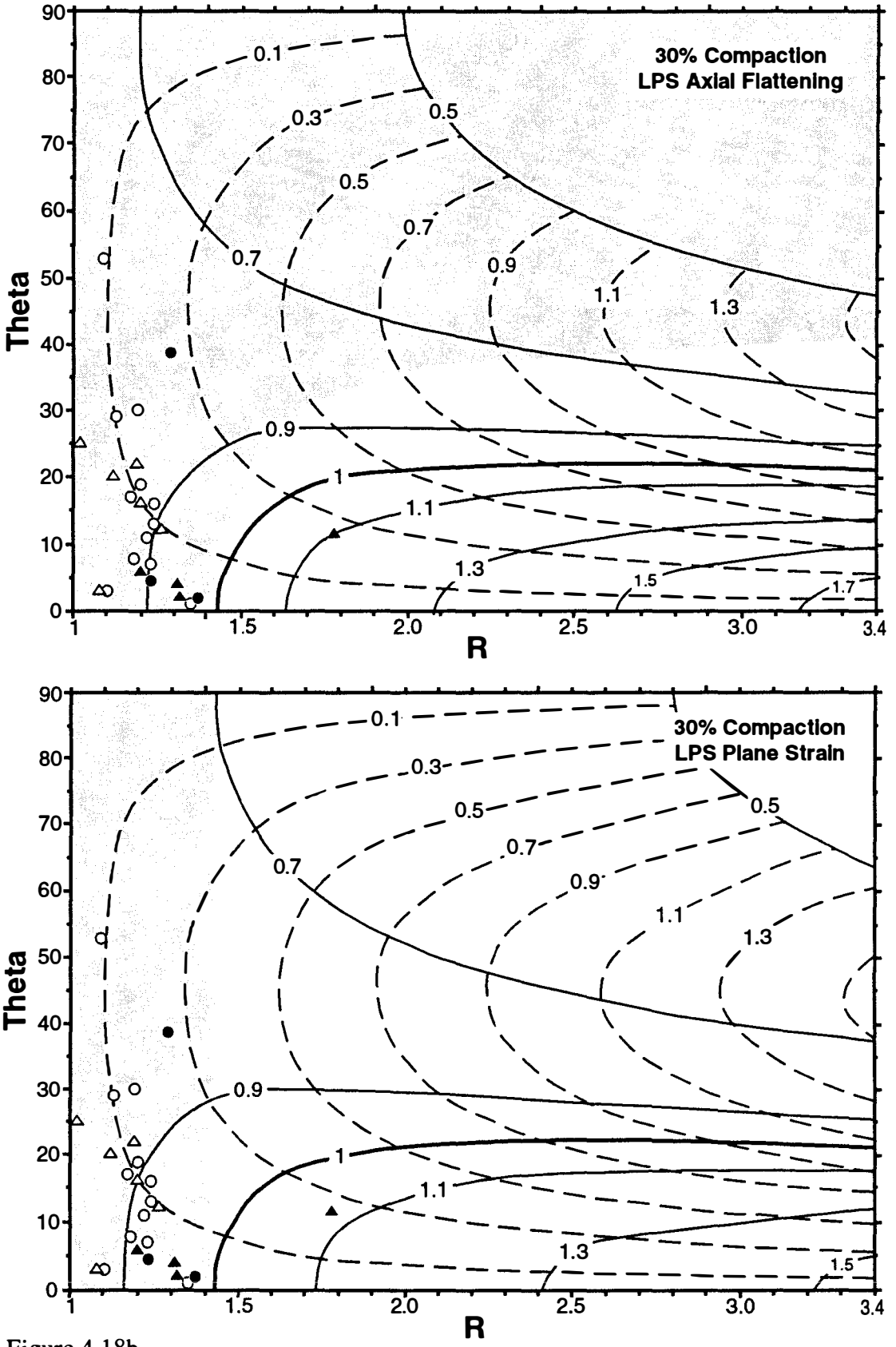
30% Compaction
LPS Axial Flattening
Theta
R
0.1
0.3
0.5
0.7
0.9
1.1
1.3
1.5
1.7
30% Compaction
LPS Plane Strain
Theta
R
0.1
0.3
0.5
0.7
0.9
1.1
1.3
1.5

Figure 4.18b.

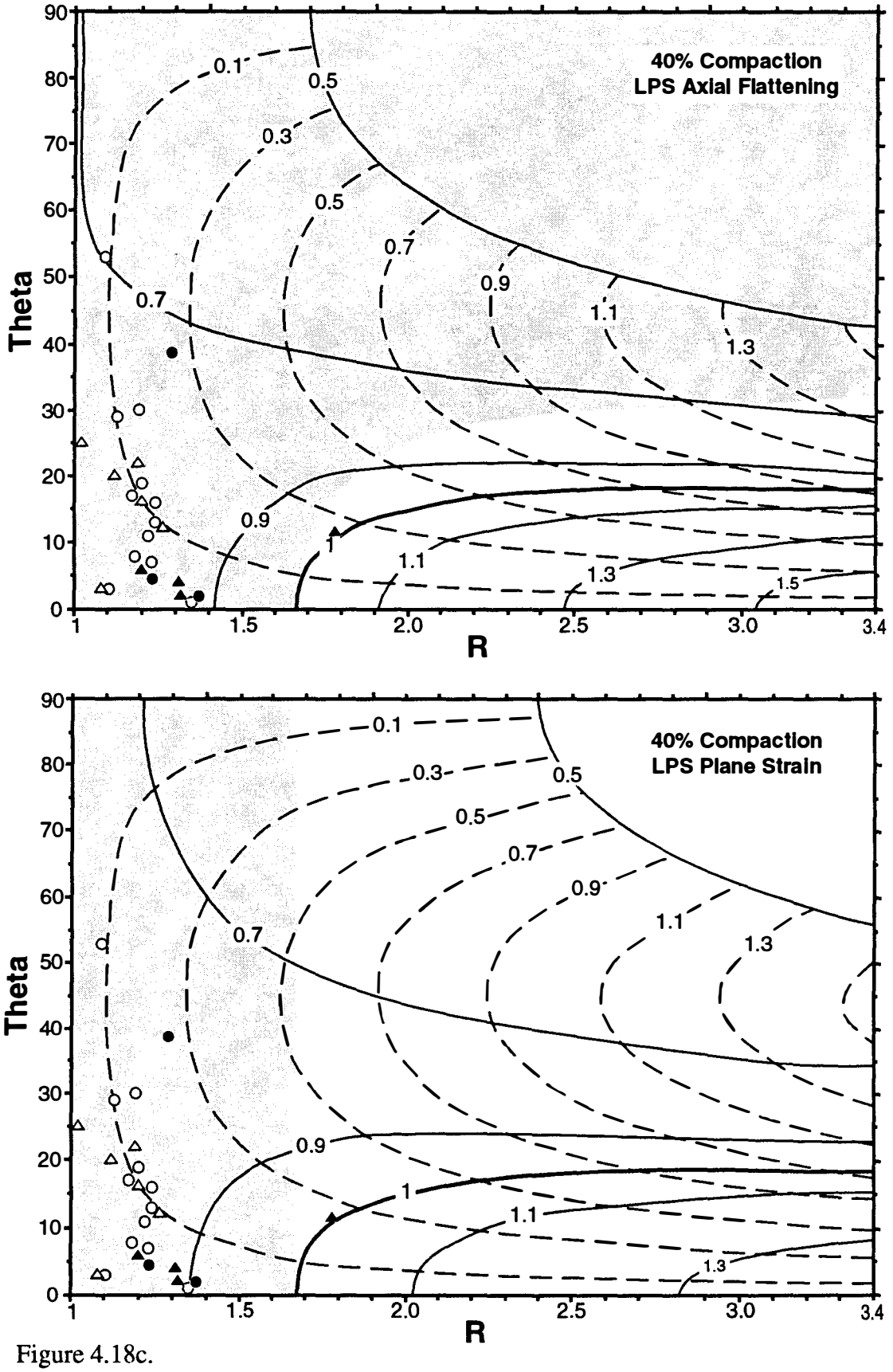
40% Compaction
LPS Axial Flattening
Theta
R
0.1
0.3
0.5
0.7
0.9
1.1
1.3
1.5
40% Compaction
LPS Plane Strain
Theta
R
0.1
0.3
0.5
0.7
0.9
1
1.1
1.3

Figure 4.18c.

Figure 4.19. Plot of strain ratio (R) in the profile direction (X/Z or Y/Z) against the angle between the longer axis of the ellipse in the profile direction (X or Y axis) and the shear direction for different values of horizontal compaction (to simulate vertical compaction and 90 degree rigid body rotation). Solid lines are equal values of stretch (α) in the profile direction (horizontal shortening/extension). Dashed lines are equal values of shear strain (γ). Shaded area is field of Y/Z axes parallal to the profile direction. Values for both axial flattening and plane strain layer parallel shortening cases have been determined. Strain results from the R_f/ϕ method with X or Y axes that plunge approximatly parallel to the profile direction are plotted. Samples plotted (squares) are from the hanging-wall ramp portions of the Dunn Creek thrust sheet. a) 20 percent compaction. b) 30 percent compaction.

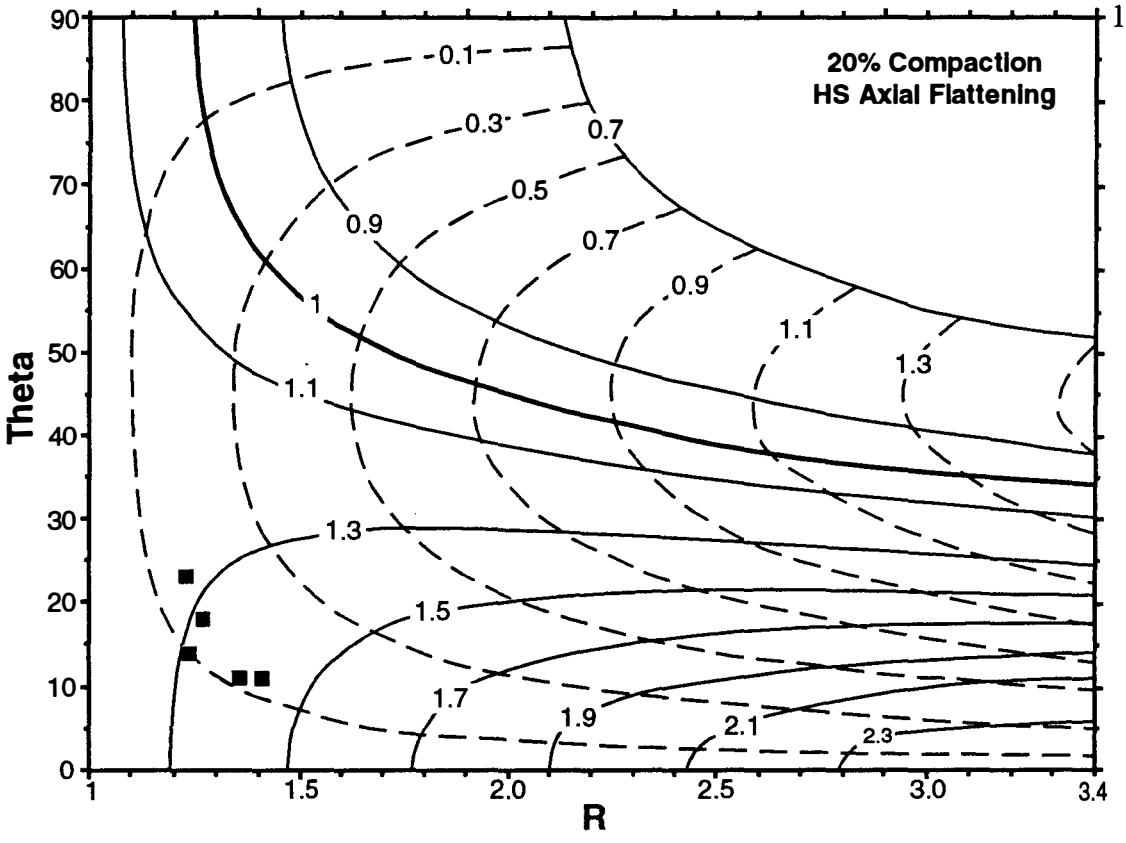
20% Compaction
HS Axial Flattening
Theta
R
0.1
0.3
0.5
0.7
0.9
1
1.1
1.3
1.5
1.7
1.9
2.1
2.3

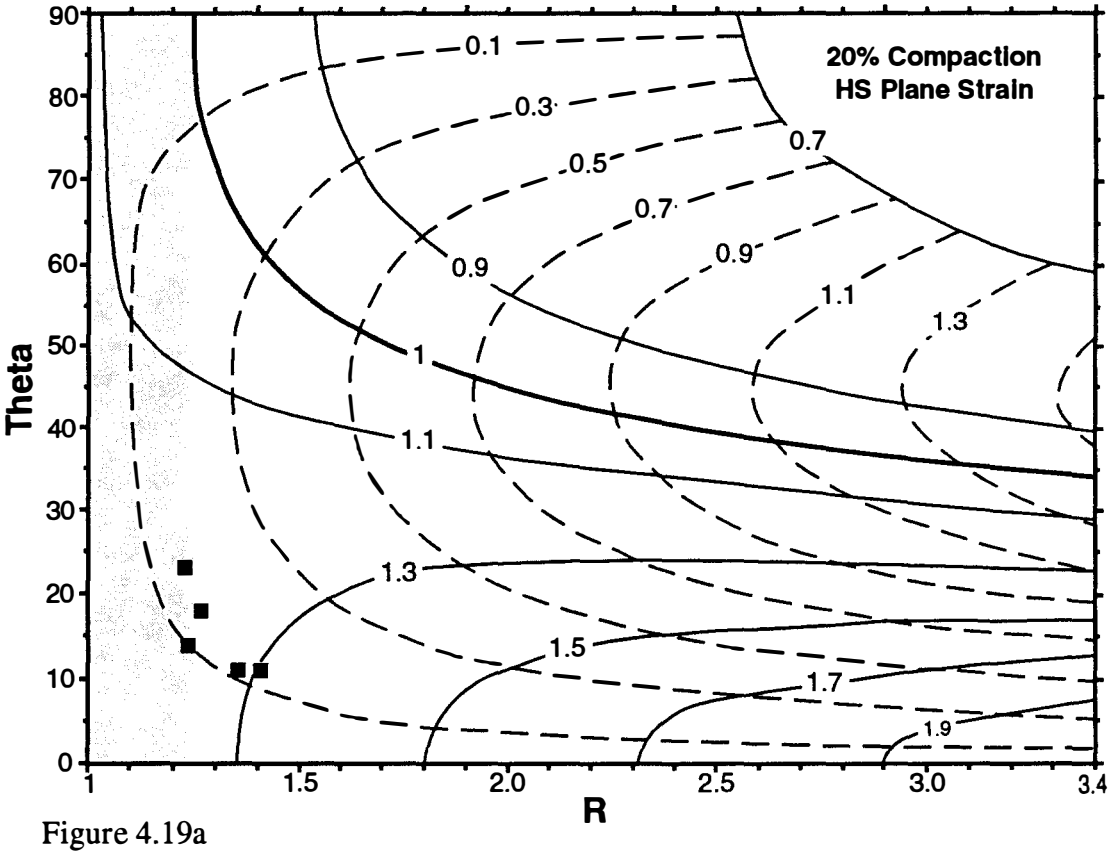
20% Compaction
HS Plane Strain
Theta
R
0.1
0.3
0.5
0.7
0.9
1
1.1
1.3
1.5
1.7
1.9

Figure 4.19a

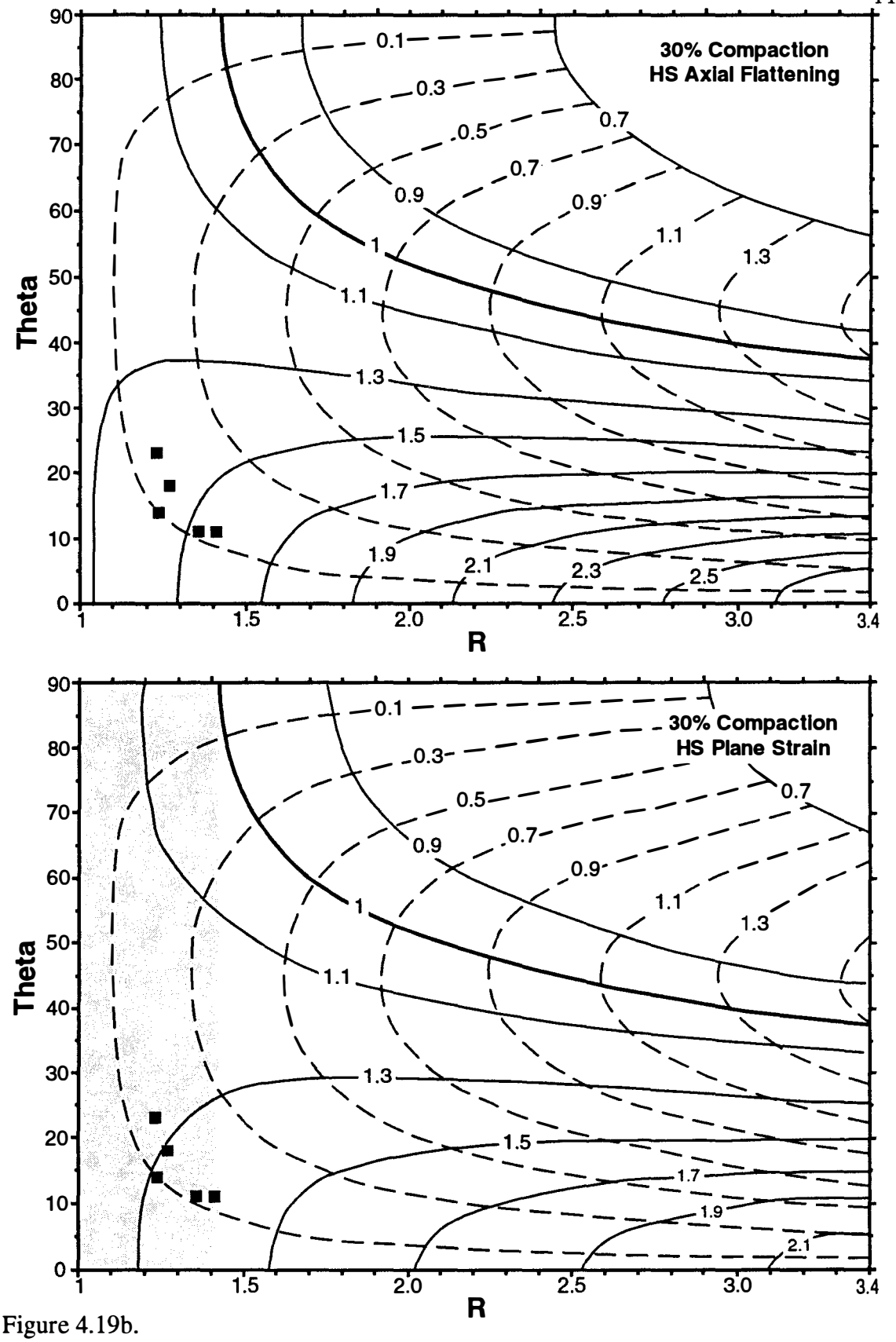
30% Compaction
HS Axial Flattening
0.1
0.3
0.5
0.7
0.7
0.9
0.9
1
1.1
1.1
1.3
1.3
1.5
1.7
1.9
2.1
2.3
2.5
Theta
R
90
80
70
60
50
40
30
20
10
0
1
1.5
2.0
2.5
3.0
3.4
30% Compaction
HS Plane Strain
0.1
0.3
0.5
0.7
0.7
0.9
0.9
1
1.1
1.1
1.3
1.3
1.5
1.7
1.9
2.1
Theta
R

Figure 4.19b.

plunging X axes (~80°) rather than the actual gently plunging measured values (~10° to 30°). Instead, the measured finite strains require relatively large amounts of horizontal extension ($\alpha \approx 1.2$ to 1.3) to yield the observed strain ellipse orientation and magnitude (Fig. 4.19a).

The failure of a single homogeneous strain history to account for the finite strains in both subdomains may result from: 1) The assumption of a single homogeneous strain history across both subdivisions may be inappropriate; 2) Compaction strains were not important or not recorded in the sandstones. This factor would explain the relatively consistent strain magnitudes between the hanging-wall flat and hanging-wall ramp areas. It would not, however, provide an explanation for the dominance of strike-parallel X axes recorded throughout most of the study area that can be simply be explained by compaction. Also, compaction strains are known to be an important part of the diagenetic history of sandstones (Pryor, 1973); 3) The unreliable nature of the strain markers within the hanging-wall ramp area. Most sandstones from this part of the Dunn Creek thrust sheet belong to the Pigeon Siltstone. Sandstones from this unit are fine to very fine sand size and have abundant matrix (20 to 50 percent) and feldspar grains (20 to 40 percent). These sandstones may be considered unreliable for strain analysis because they are not framework supported. Strain results from the hanging-wall ramp area may therefore be suspect; and 4) The simplicity of the strain models. Bedding within the hanging-wall ramp area was modeled as vertical prior to superposition of cleavage strains. Although bedding in this area is commonly steeply dipping to slightly overturned (Fig. 4.9), those samples used for strain factorization dip an average of 48 degrees southeast and are overturned. This would result in pretectonic ellipse long axis plunges of 48 degrees southeast rather than vertical. Less horizontal extension would therefore be required to produce the observed gently southeast-plunging ellipse orientations. In addition, overturning of this fold limb with layer-parallel attenuation

provides a likely cause for the subhorizontal extension required to produce the measured strains. More complex strain factorization models are required to evaluate this possibility.

CONCLUSIONS

1) Finite strain magnitudes recorded within sandstones of the three Early Paleozoic thrust sheets are low and increase from north to south. Mean strain ratios determined by the R_f/ϕ method for the Miller Cove, Dunn Creek, and Greenbrier thrust sheets are 1.29, 1.32, and 1.42 respectively. Strain ratios determined by the Fry method are typically 5 to 20 percent higher. Most ellipsoid shapes fall in the apparent flattening field of a Flinn plot.

2) Microstructural observations indicate that strain was accommodated by those deformation mechanisms typical of low grade metamorphic conditions including dislocation flow (undulatory extinction, deformation lamellae, deformation bands, patchy extinction, serrated grain boundaries), pressure solution (stylolites, sutured grain boundaries), and brittle fracturing (microfractures, fluid inclusion planes).

3) Most principal strain axes within all three thrust sheets show a consistent pattern in which X axes are subhorizontal and strike parallel, Y axes are subhorizontal and transport parallel, and Z axes are steeply northwest plunging. An important exception is the hanging-wall ramp portion of the Dunn Creek thrust sheet, where most X axes are transport parallel and most Y axes are strike parallel. Principal strain axis orientations determined by both the R_f/ϕ and Fry methods are similar but those determined by the R_f/ϕ method are more consistent.

4) The finite strains within the Miller Cove thrust sheet and hanging-wall flat portions of the Dunn Creek thrust sheet are most simply modeled by a series fo strain events that include 20 percent vertical compaction by volume loss followed by a small amount of layer parallel shortening ($\alpha \approx 0.95$) (either axial flattening or plane strain) and small amounts of shear strain ($\gamma \approx 0.1$).

5) The finite strains within the hanging-wall ramp portion of the Dunn Creek thrust sheet cannot be explained using similar strain values to those of the first model. The measured finite strains require large values of horizontal extension ($\alpha \approx 1.2$ to 1.3) to yield the observed ellipse orientation and magnitude. The failure of a single model to account for the observed strain magnitudes in the separate subdomains may be explained by incorrectly assuming a single homogeneous strain across both subdomains, the absence of compaction strains, unreliable strain markers, or the simplicity of the strain models.

REFERENCES CITED

Connelly, J. B., and Woodward, N. B., 1992, Taconian foreland-style thrust system in the Great Smoky Mountains, Tennessee: Geology, v. 20, p. 177-180.

Coward, M. P., and Kim, J. H., 1981, Strain within thrust sheets, *in* McClay, K. R., and Price, N. J., eds., Thrust and nappe tectonics, Geological Society of London Special Publication 9: p. 275-292.

Couzens, B. A., 1992, Strain transitions across the junction of the southern and central Appalachians, Virgina and West Virgina [M.S. Thesis]: Knoxville, Tennessee, University of Tennessee, 197 p.

Couzens, B. A., Dunne, W. M., Onasch, C. M., and Glass, R., in press, Strain variations and three-dimensional strain factorization at the transition from the southern to the central Appalachians: Journal of Structural Geology, v. 15.

Dunnett, D., 1969, A technique of finite strain analysis using elliptical particles: Tectonophysics, v. 12, p. 117-136.

Dunnett, D., and Siddans, A. W. B., 1971, Non-random sedimentary fabrics and their modification by strain: Tectonophysics, v. 12, p. 307-325.

Erslev, E. A., 1988, Normalized center-to-center strain analysis of packed aggregates: Journal of Structural Geology, v. 10, p. 201-209.

Fry, N., 1979, Random point distributions and strain measurement in rocks: Tectonophysics, v. 60, p. 89-105.

Hamilton, W., 1961, Geology of the Richardson Cove and Jones Cove quadrangles, Tennessee: U.S. Geological Survey Professional Paper 349-A, 55 p.

Kamb, W. B., 1959, Ice petrofabric observations from Blue Glacier, Washington, in relation to theory and experiment: Journal of Geophysical Research, v. 67, p. 153-170.

Keller, F. B., 1980, Late Precambrian stratigraphy, depositional history, and structural chronology of part of the Tennessee Blue Ridge [Ph.D. thesis]: New Haven, Connecticut, Yale University, 353 p.

King, P. B., Neuman, R.B., and Hadley, J.B., 1968, Geology of the Great Smoky Mountains National Park, Tennessee and North Carolina: U.S. Geological Survey Professional Paper 587, 23 p.

Kligfield, R., Crespi, J., Naruk, S., and Davis, G. I. H., 1984, Displacement and strain patterns of extensional orogens: Tectonics, v. 3, p. 577-609.

Lisle, R. J., 1977, Clastic grain shape and orientation in relation to cleavage from the Aberystwyth Grits, Wales: Tectonophysics, v. 39, p. 381-395.

Lisle, R. J., 1985, Geological strain analysis: A mauual for the R_f/ϕ method: Pergamon Press, New York, 99 p.

Mitra, G., and Elliott, D., 1980, Deformation of basement in the Blue Ridge and the development of the South Mountain cleavage, in Wones, D. R., ed., The Caledonides in the U.S.A: Blacksburg, Virginia, Virginia Polytechnic Institute and State University Memoir 2, p. 307-311.

Means, W. D., 1976, Stress and strain: Basic concepts of continuum mechanics for geologists: Springer-Verlag, New York.

Owens, W. H., 1984, The calculation of the best-fit ellipsoid from elliptical sections on arbitrarily oriented planes: Journal of Structural Geology, v. 6, p. 571-578.

Pryor, W. A., 1973, Permeability-porosity patterns and variations in some Holocene sand bodies: American Association of Petroleum Geologists Bulletin, v. 57, p. 162-189.

Ramsay, J. G., 1967, Folding and fracturing of rocks: McGraw Hill, New York, 568 p.

Ramsay, J. G., and Huber, M. I., 1987, The techniques of Modern Structural geology, Volume 2: Folds and Fractures: Academic Press, New York, p. 309-700.

Sanderson, D. J, 1982, Models of strain variation in nappes and thrust sheets: A review: Tectonophysics, v. 88, p. 201-233.

APPENDIX

Rf/ø and Fry strain data. TS=thrust sheet (G=Greenbrier; GW=Greenbrier Webb Mountain klippe; D=Dunn Creek; M=Miller Cove); Str.= structural position (1=hanging-wall flat; 2=hanging-wall ramp); X, Y, Z = principal strain axes (X≥Y≥Z); az=azimuth; pl=plunge.

$R_f/ø$ Data

Sample	TS	Str.	X	Y	Z	X/Y	X/Z	Y/Z	X(az)	X(pl)	Y(az)	Y(pl)	Z(az)	Z(pl)
RF-TC-3	D	2	1.07	1.06	0.89	1.01	1.20	1.19	89	19	187	22	322	61
RF-TC-4	D	2	1.12	1.03	0.86	1.09	1.30	1.20	214	12	119	22	330	65
PI-TC-5	D	2	1.28	0.99	0.79	1.29	1.62	1.25	135	30	44	2	312	60
PI-TC-6	D	2	1.14	1.08	0.81	1.06	1.41	1.33	186	11	90	28	295	60
PI-DC-40	D	1	1.10	1.07	0.85	1.03	1.29	1.26	57	6	148	12	300	77
PI-LP-55	D	1	1.16	0.97	0.89	1.20	1.30	1.09	72	11	162	3	267	79
PI-LP-56	D	1	1.07	1.04	0.89	1.03	1.20	1.17	81	2	350	29	173	61
PI-LP-57	D	1	1.07	0.98	0.96	1.09	1.11	1.02	96	15	193	25	337	61
PI-LP-59	D	1	1.13	1.03	0.86	1.10	1.31	1.20	276	5	185	16	23	73
PI-LP-64	D	2	1.08	1.05	0.88	1.03	1.23	1.19	161	23	68	9	318	65
PI-LP-65	D	2	1.13	0.96	0.92	1.18	1.23	1.04	74	34	170	8	272	55
PI-LP-66	D	2	1.16	0.98	0.87	1.18	1.33	1.13	76	12	345	5	234	77
RF-LP-68	D	2	1.22	0.95	0.86	1.28	1.42	1.10	102	18	10	6	262	71
RF-LP-69	D	1	1.08	1.02	0.90	1.06	1.20	1.13	187	6	94	29	287	60
RF-LP-70	D	1	1.13	1.04	0.86	1.09	1.31	1.21	182	4	92	8	301	81
RF-LP-71	D	1	1.15	1.01	0.87	1.14	1.32	1.16	160	2	70	2	303	88
RF-LP-72	D	1	1.12	1.04	0.86	1.08	1.30	1.21	51	42	309	13	206	45
PI-WM-73	D	2	1.14	1.01	0.87	1.13	1.31	1.16	97	12	194	30	347	57
PI-CB-74	D	2	1.09	1.06	0.86	1.03	1.27	1.23	142	26	233	2	326	64
PI-BC-76	D	2	1.14	0.96	0.92	1.19	1.24	1.04	157	14	250	13	21	71
PI-BC-77	D	2	1.17	1.00	0.86	1.17	1.36	1.16	196	11	97	39	298	49
PI-BC-79	D	2	1.09	0.99	0.93	1.10	1.17	1.06	28	10	247	78	119	8
PI-MB-91	D	1	1.18	1.00	0.84	1.18	1.40	1.19	95	10	189	22	342	66
PI-YB-98	D	1	1.21	0.96	0.86	1.26	1.41	1.12	265	5	173	20	9	69
PI-CC-100	D	1	1.36	0.97	0.76	1.40	1.79	1.28	114	17	205	2	301	73
TH-TC-1	G	1	1.26	0.98	0.81	1.29	1.56	1.21	350	8	86	36	249	53
TH-TC-2	G	1	1.39	0.94	0.76	1.48	1.83	1.24	163	9	73	4	320	80
TH-BM-105	G	1	1.41	0.89	0.80	1.58	1.76	1.11	215	44	307	2	39	46
TH-RC-1	G	1	1.31	1.04	0.74	1.26	1.77	1.41	203	24	99	29	326	51
TH-RC-2	G	1	1.05	0.99	0.96	1.06	1.09	1.03	287	23	21	10	132	65
TH-GP-1	G	1	1.19	1.01	0.84	1.18	1.42	1.20	284	5	192	19	29	70
WM-BR-54	GW	2	1.16	1.02	0.84	1.14	1.38	1.21	275	6	9	30	174	59
WM-WM-80	GW	1	1.24	0.96	0.84	1.29	1.48	1.14	294	19	37	34	180	50
WM-WM-82	GW	1	1.17	1.11	0.77	1.05	1.52	1.44	265	6	174	14	18	75
WM-WM-83	GW	1	1.14	0.97	0.91	1.18	1.25	1.07	179	34	306	41	66	30
WM-WM-84	GW	1	1.11	1.05	0.86	1.06	1.29	1.22	39	16	134	18	269	66
WM-WM-86	GW	1	1.09	1.03	0.89	1.06	1.22	1.16	98	30	238	53	357	19
WM-MC-96	GW	2	1.11	1.05	0.86	1.06	1.29	1.22	238	17	329	4	73	72
WM-JB-2	GW	2	1.16	1.00	0.87	1.16	1.33	1.15	253	7	344	3	95	83
WM-JB-3	GW	2	1.14	1.03	0.85	1.11	1.34	1.21	188	11	96	9	329	76
WM-JB-4	GW	2	1.12	1.03	0.87	1.09	1.29	1.18	308	12	218	4	112	78
WM-JB-6	GW	2	1.11	1.01	0.89	1.10	1.25	1.13	74	2	343	34	168	56
SC-LP-10	M	1	1.23	1.00	0.81	1.23	1.52	1.23	242	10	152	1	57	81
SC-LP-12	M	1	1.18	1.07	0.79	1.10	1.49	1.35	314	17	224	1	129	73
SC-LP-13	M	1	1.05	1.01	0.94	1.04	1.12	1.07	60	2	330	12	159	78
SC-LP-14	M	1	1.10	1.03	0.87	1.07	1.26	1.18	267	2	177	8	11	81
LI-LP-16	M	1	1.07	1.03	0.91	1.04	1.18	1.13	257	12	160	29	8	58

SC-LP-17	M	1	1.12	1.01	0.89	1.11	1.26	1.13	355	1	86	20	263	70
SS-LP-18	M	1	1.18	0.98	0.87	1.20	1.36	1.13	121	2	31	1	275	88
SC-EF-20	M	1	1.19	1.00	0.84	1.19	1.42	1.19	53	5	146	30	314	60
SC-EF-21	M	1	1.11	1.08	0.84	1.03	1.32	1.29	9	6	100	19	262	71
SL-EB-22	M	1	1.21	1.04	0.85	1.16	1.42	1.22	9	20	273	15	149	64
SL-EB-23	M	1	1.03	1.02	0.95	1.01	1.08	1.07	116	12	24	13	246	72
SM-WC-24	M	1	1.15	1.03	0.84	1.12	1.37	1.23	247	7	156	7	19	80
SU-WC-26	M	1	1.12	0.95	0.86	1.18	1.30	1.10	340	23	82	27	215	54
SU-CH-27	M	1	1.10	1.04	0.87	1.06	1.26	1.20	244	9	151	19	357	69
WY-BH-29	M	1	1.09	1.03	0.89	1.06	1.22	1.16	177	5	86	9	297	79
WY-LB-31	M	1	1.05	1.01	0.94	1.04	1.12	1.07	235	16	327	9	85	72
SL-LB-33	M	1	1.17	0.96	0.89	1.22	1.31	1.08	42	17	310	4	207	72
DM-LB-36	M	1	1.16	1.00	0.86	1.16	1.35	1.16	51	20	317	10	202	68
SL-YB-37	M	1	1.14	0.99	0.88	1.15	1.30	1.13	267	5	359	18	161	72
WY-LB-41	M	1	1.12	1.02	0.87	1.10	1.29	1.17	151	38	277	38	34	31
SL-CC-45	M	1	1.13	0.98	0.90	1.15	1.26	1.09	61	17	175	53	320	32
SL-MC-46	M	1	1.12	1.05	0.85	1.07	1.32	1.24	94	7	187	16	340	72
WY-MC-47	M	1	1.12	1.04	0.85	1.08	1.32	1.22	45	1	136	11	308	79
WY-CC-49	M	1	1.10	1.01	0.90	1.09	1.22	1.12	103	16	197	13	323	69
WY-DC-51	M	1	1.06	1.05	0.90	1.01	1.18	1.17	31	4	122	17	288	73
SC-MB-88	M	1	1.18	1.03	0.83	1.15	1.42	1.24	67	2	158	13	327	77
SC-LP-103	M	1	1.12	0.99	0.90	1.13	1.24	1.10	107	32	199	3	294	58
Mean						1.14	1.33	1.17						
Standard Dev.						0.11	0.16	0.08						
Mean MCTS						1.11	1.29	1.17						
Std. Dev. MCTS						0.06	0.11	0.07						
Mean DCTS						1.14	1.32	1.17						
Std. Dev. DCTS						0.10	0.14	0.08						
Mean GBTS						1.18	1.42	1.20						
Std. Dev. GBTS						0.15	0.21	0.10						

Fry Data

Sample	TS	Str.	X	Y	Z	X/Y	X/Z	Y/Z	X(az)	X(pl)	Y(az)	Y(pl)	Z(az)	Z(pl)
RF-TC-3	D	2	1.12	1.01	0.89	1.11	1.26	1.13	231	28	117	37	348	40
RF-TC-4	D	2	1.18	1.00	0.85	1.18	1.39	1.18	207	4	115	30	303	60
PI-TC-5	D	2	1.17	1.14	0.75	1.03	1.56	1.52	30	36	274	30	156	39
PI-TC-6	D	2	1.15	1.04	0.83	1.11	1.39	1.25	13	8	106	23	266	65
PI-DC-40	D	1	1.39	0.92	0.78	1.51	1.78	1.18	121	18	31	1	298	72
PI-LP-55	D	1	1.31	0.95	0.81	1.38	1.62	1.17	77	18	334	33	193	50
PI-LP-56	D	1	1.21	1.04	0.80	1.16	1.51	1.30	346	19	92	39	236	45
PI-LP-57	D	1	1.09	1.02	0.90	1.07	1.21	1.13	115	44	233	25	342	35
PI-LP-59	D	1	1.20	1.02	0.82	1.18	1.46	1.24	69	12	338	5	226	78
PI-LP-64	D	2	1.13	1.01	0.87	1.12	1.30	1.16	171	24	76	11	322	63
PI-LP-65	D	2	1.27	0.93	0.85	1.37	1.49	1.09	74	24	330	28	198	51
PI-LP-66	D	2	1.20	1.02	0.82	1.18	1.46	1.24	73	28	305	48	179	28
RF-LP-68	D	2	1.22	1.05	0.78	1.16	1.56	1.35	114	13	22	8	263	75
RF-LP-69	D	1	1.14	1.01	0.87	1.13	1.31	1.16	185	5	276	9	65	80
RF-LP-70	D	1	1.15	1.00	0.87	1.15	1.32	1.15	175	23	85	2	351	67
RF-LP-71	D	1	1.24	0.96	0.84	1.29	1.48	1.14	337	5	69	15	229	74
RF-LP-72	D	1	1.18	1.01	0.84	1.17	1.40	1.20	33	10	297	32	138	56
PI-WM-73	D	2	1.13	1.05	0.84	1.08	1.35	1.25	289	6	27	53	195	36
PI-CB-74	D	2	1.39	0.97	0.74	1.43	1.88	1.31	204	6	114	3	352	84
PI-BC-76	D	2	1.19	1.04	0.81	1.14	1.47	1.28	194	11	103	8	340	76
PI-BC-77	D	2	1.16	1.08	0.79	1.07	1.47	1.37	189	9	92	39	289	50
PI-BC-79	D	2	1.14	0.97	0.91	1.18	1.25	1.07	1	45	256	14	153	42
PI-MB-91	D	1	1.25	1.00	0.80	1.25	1.56	1.25	84	9	342	53	181	36
PI-YB-98	D	1	1.43	0.89	0.78	1.61	1.83	1.14	250	5	155	47	344	43
PI-CC-100	D	1	2.04	0.76	0.63	2.68	3.24	1.21	115	19	214	25	351	58
TH-TC-1	G	1	1.29	0.94	0.82	1.37	1.57	1.15	339	5	73	42	243	48
TH-TC-2	G	1	1.21	0.99	0.83	1.22	1.46	1.19	57	47	222	42	319	8
TH-BM-105	G	1	1.66	0.80	0.75	2.08	2.21	1.07	217	47	322	14	65	40
TH-RC-1	G	1	1.42	1.02	0.69	1.39	2.06	1.48	201	24	95	33	320	48
TH-RC-2	G	1	1.28	0.90	0.86	1.42	1.49	1.05	265	17	359	10	118	70
TH-GP-1	G	1	1.49	0.90	0.74	1.66	2.01	1.22	299	2	209	11	38	79
WM-BR-54	GW	2	1.21	1.08	0.76	1.12	1.59	1.42	287	17	23	20	159	63
WM-WM-80	GW	1	1.24	1.02	0.79	1.22	1.57	1.29	291	23	29	19	154	60
WM-WM-82	GW	1	1.23	1.05	0.77	1.17	1.60	1.36	241	22	142	20	14	59
WM-WM-83	GW	1	1.13	1.10	0.80	1.03	1.41	1.38	327	50	118	37	219	14
WM-WM-84	GW	1	1.19	0.98	0.86	1.21	1.38	1.14	43	15	138	18	276	66
WM-WM-86	GW	1	1.24	0.93	0.86	1.33	1.44	1.08	263	2	143	86	353	3
WM-MC-96	GW	2	1.30	0.95	0.81	1.37	1.60	1.17	265	13	356	3	99	77
WM-JB-2	GW	2	1.15	0.99	0.88	1.16	1.31	1.13	181	18	87	12	324	68
WM-JB-3	GW	2	1.15	1.07	0.81	1.07	1.42	1.32	214	5	122	29	312	61
WM-JB-4	GW	2	1.17	1.01	0.84	1.16	1.39	1.20	329	11	235	19	87	69
WM-JB-6	GW	2	1.22	0.95	0.87	1.28	1.40	1.09	23	48	229	39	128	13
SC-LP-10	M	1	1.24	1.04	0.78	1.19	1.59	1.33	253	12	159	20	12	67
SC-LP-12	M	1	1.24	1.08	0.75	1.15	1.65	1.44	258	12	353	20	139	66
SC-LP-13	M	1	1.19	1.00	0.84	1.19	1.42	1.19	70	37	302	40	185	29
SC-LP-14	M	1	1.16	1.03	0.83	1.13	1.40	1.24	268	11	359	6	118	78
LI-LP-16	M	1	1.10	1.07	0.85	1.03	1.29	1.26	280	9	182	41	19	48
SC-LP-17	M	1	1.21	0.95	0.87	1.27	1.39	1.09	165	3	74	23	262	67
SS-LP-18	M	1	1.20	1.00	0.83	1.20	1.45	1.20	109	18	212	36	357	49
SC-EF-20	M	1	1.31	0.97	0.78	1.35	1.68	1.24	33	4	126	40	298	50
SC-EF-21	M	1	1.27	1.01	0.78	1.26	1.63	1.29	23	17	114	6	222	72
SL-EB-22	M	1	1.19	1.05	0.80	1.13	1.49	1.31	17	18	282	15	155	67
SL-EB-23	M	1	1.22	0.99	0.83	1.23	1.47	1.19	143	3	51	36	237	54
SM-WC-24	M	1	1.16	1.09	0.79	1.06	1.47	1.38	320	4	229	14	67	76
SU-WC-26	M	1	1.19	0.96	0.87	1.24	1.37	1.10	331	12	65	19	211	67
SU-CH-27	M	1	1.13	1.09	0.81	1.04	1.40	1.35	123	17	217	13	344	69
WY-BH-29	M	1	1.13	1.04	0.85	1.09	1.33	1.22	201	2	111	1	354	87
WY-LB-31	M	1	1.17	0.97	0.87	1.21	1.34	1.11	288	7	194	30	30	59
SL-LB-33	M	1	1.42	0.93	0.76	1.53	1.87	1.22	41	26	291	34	160	44
DM-LB-36	M	1	1.19	1.04	0.81	1.14	1.47	1.28	60	15	325	18	188	66
SL-YB-37	M	1	1.35	0.95	0.78	1.42	1.73	1.22	277	19	39	57	177	26
WY-LB-41	M	1	1.27	0.92	0.85	1.38	1.49	1.08	145	35	260	31	20	39

SL-CC-45	M	1	1.10	1.04	0.87	1.06	1.26	1.20	52	1	144	65	321	25
SL-MC-46	M	1	1.21	1.07	0.77	1.13	1.57	1.39	109	29	205	11	314	59
WY-MC-47	M	1	1.24	0.97	0.83	1.28	1.49	1.17	93	9	191	44	354	45
WY-CC-49	M	1	1.22	1.01	0.81	1.21	1.51	1.25	47	11	140	13	280	73
WY-DC-51	M	1	1.14	1.08	0.82	1.06	1.39	1.32	63	27	174	36	306	43
SC-MB-88	M	1	1.32	1.04	0.73	1.27	1.81	1.42	93	8	188	32	350	56
SC-LP-103	M	1	1.17	1.03	0.83	1.14	1.41	1.24	161	20	64	19	294	62
Mean						1.25	1.53	1.23						
Standard Dev.						0.24	0.28	0.11						
Mean MCTS						1.20	1.50	1.25						
Std. Dev. MCTS						0.12	0.15	0.10						
Mean DCTS						1.27	1.54	1.22						
Std. Dev. DCTS						0.32	0.39	0.10						
Mean GBTS						1.31	1.58	1.22						
Std. Dev. GBTS						0.24	0.25	0.13						

PART 5

POLYMETAMORPHIC EVOLUTION OF THE WESTERN BLUE RIDGE PROVINCE: EVIDENCE FROM $^{40}Ar/^{39}Ar$ WHOLE-ROCK SLATE/PHYLLITE AND MUSCOVITE AGES

INTRODUCTION

Multiple periods of metamorphism and deformation are well documented in the northern Appalachians by several lines of evidence. Textures indicative of polymetamorphism are common (Rosenfeld, 1968; Laird and Albee, 1981), and geochronologic evidence for Ordovician, Devonian, and Carboniferous events has been presented (Dallmeyer, 1982; Laird and others, 1984; Hames and others, 1991). Furthermore, geochrologic results are compatible with paleontologic controls (Billings and Cleaves, 1934; Brookins, Berdan, and Stewart, 1973; Lyons and Darrah, 1978), and a clear sedimentary expression of these events is preserved in the Appalachian foreland (Colton, 1970; Hatcher and others, 1990). The record of deformation and metamorphism within the crystalline southern Appalachians, however, is not as well established. In large part this reflects erosion of most sedimentary cover sequences, rarity of documented fossils within metasedimentary rocks, and telescoping of metamorphic assemblages by extensive late Paleozoic thrust faulting.

Previous geochronologic studies in the southern Appalachians have suggested that most metamorphism and ductile deformation occurred in the Ordovician ("Taconic"). Devonian ("Acadian") and younger effects were believed to be recorded only in localized, retrogressive overprinting of earlier ductile fabrics. The importance of Ordovician metamorphism in this area, however, has recently been questioned because of reported fossil discoveries in the western Blue Ridge (Unrug and Unrug, 1990; Unrug and others, 1991; Tull and others, in press) and the Talladega belt (Tull and others, 1988) that indicate protoliths of some metamorphosed clastic rocks were deposited during the early to middle

Paleozoic. In addition, lithostratigraphic correlations between rocks exposed in the Murphy belt (western Blue Ridge) and fossiliferous Early Devonian strata in the adjacent Talladega belt have been suggested (Tull and Guthrie, 1985; Tull and Groszos, 1988). These interpretations imply that all deformation and metamorphism in the western Blue Ridge must be middle Paleozoic or younger. This is contrary to much of the previous geochronology reported for the southern Appalachians and a stratigraphic record of Ordovician tectonic instability in the Appalachian foreland.

In an attempt to evaluate these apparently contradictory results, a program of $^{40}Ar/^{39}Ar$ geochronology and structural analysis was undertaken in the Great Smoky Mountains in the western Blue Ridge. Samples from the lowest grade rocks exposed in the western Blue Ridge were analyzed to minimize potential effects of post-metamorphic cooling. These results are presented here and provide important constraints on the metamorphic evolution of the western Blue Ridge.

Paleozoic metamorphic episodes in the Appalachians have generally been correlated with the Taconic, Acadian, and Alleghanian orogenies. These events were defined largely on the basis of the stratigraphic record in the adjacent foreland areas. Because of the tectonic resolution now available, however, we believe the simple division of Paleozoic Appalachian orogenesis into the Taconic, Acadian, and Alleghanian is no longer adequate. For example, the Alleghanian orogeny is now known to include a sequence of events that are diachronous and discontinuous along the Appalachian orogenic belt, and has been expanded to include a period of > 80 Ma (Dallmeyer and others, 1986; Secor and others, 1986; Hatcher and others, 1989). These divisions will therefore not be emphasized and focus will simply be on the ages of deformation.

REGIONAL GEOLOGIC SETTING

The Blue Ridge structural province (Fig. 5.1) is bounded on the northwest by the Blue Ridge fault system (Holston-Iron Mountain, Great Smoky, Cartersville) and on the southeast by the Brevard fault zone (King, 1955; Hatcher, 1972). The Blue Ridge thrust transported imbricated crystalline thrust sheets composed of Precambrian basement, Late Proterozoic-early Paleozoic metasedimentary and metavolcanic rocks, and Paleozoic plutonic units northwestward over Paleozoic sedimentary rocks during Carboniferous-Permian (Alleghanian) orogenesis (Hatcher and others, 1989). Seismic reflection characteristics (Cook and others, 1979; Harris and others, 1981; Çoruh and others, 1987) suggest that most of the Blue Ridge thrust sheet is separated from autochthonous basement by 1 to 5 km of duplicated (duplexed) lower Paleozoic rocks with or without Proterozoic sedimentary rocks or basement. Following emplacement, the Blue Ridge thrust sheet was folded as a result of duplex thrusting within underlying thrust sheets (Boyer and Elliott, 1982; Woodward, 1985; Hatcher, 1991).

The Blue Ridge is divided into two contrasting lithostratigraphic terranes by the Hayesville-Gossan Lead fault (Fig. 5.1), which represents a regional terrane boundary separating rocks initially deposited on North American continental basement from sequences deposited on oceanic or attenuated continental crust of uncertain palinspastic affinities (Hatcher, 1978). This boundary is believed to have been at least locally tectonically active immediately prior to attainment of maximum metamorphic conditions. It was locally reactivated following metamorphism (Hatcher and Goldberg, 1991).

Rocks within the western Blue Ridge comprise a complex sequence of basement gneisses, plutonic units, metasedimentary and metavolcanic rift sequences, together with rifted continental margin and platform successions. Basement rocks consist of polymetamorphic gneisses and associated granitic intrusives that record radiometric ages range between 1000 to 1200 Ma (Davis and others, 1962; Fullagar and Odom, 1973)

Figure 5.1. Regional tectonic map of the southern Appalachian orogen. EBR, eastern Blue Ridge; WBR, western Blue Ridge; MB, Murphy belt; TB, Talladega belt (modified from Hatcher and others, 1990).

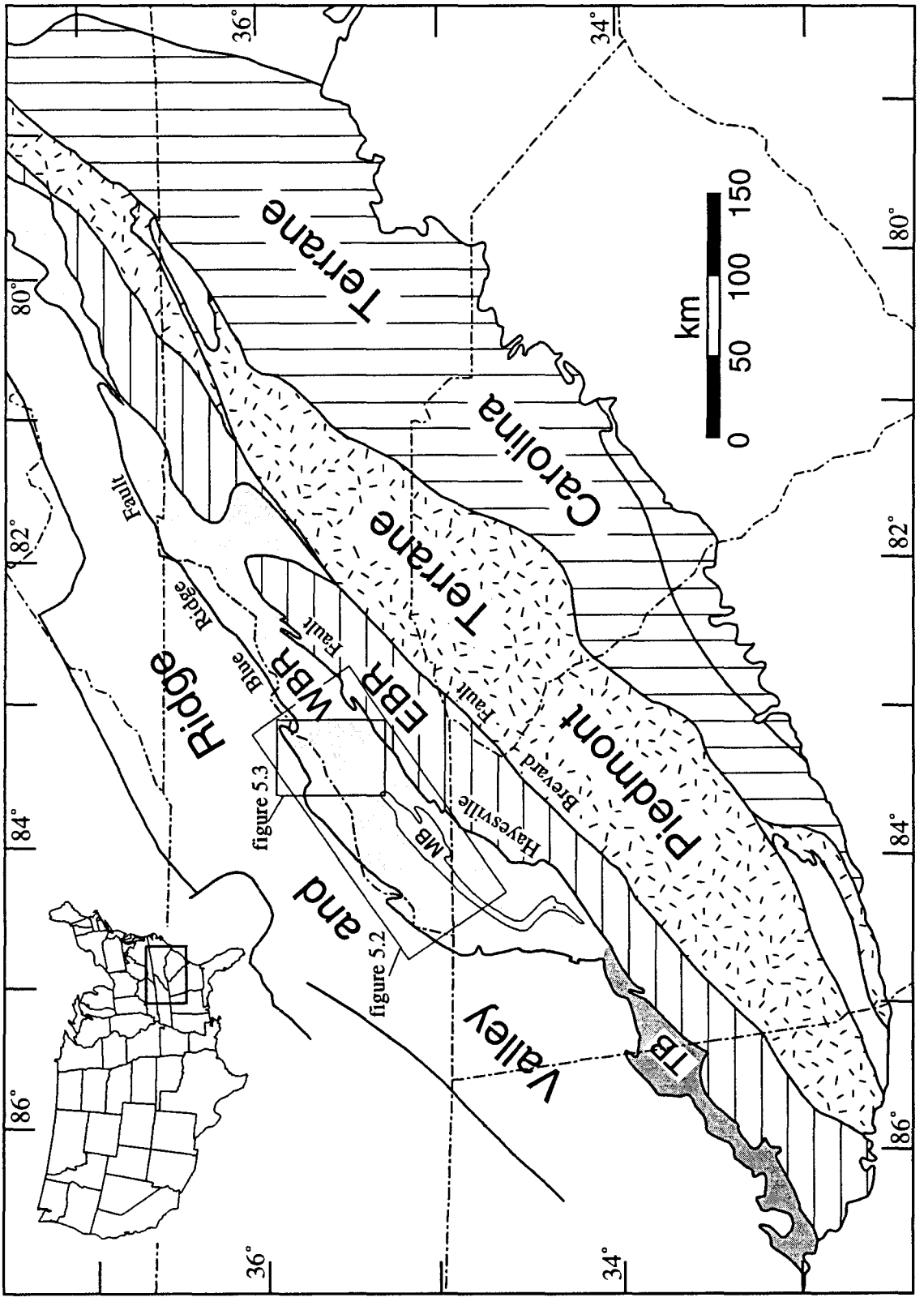
Terrane
Carolina
Terrane
Piedmont
Ridge
and
Valley
EBR
WBR
MB
TB
Blue Ridge Fault
Brevard Fault
Hayesville
figure 5.3
figure 5.2
km
0
50
100
150
36°
34°
80°
82°
84°
86°

indicating a Grenville affinity. Nonconformably overlying basement are Late Proterozoic rift-related sequences including metasedimentary and metavolcanic rocks of the Mount Rogers and Grandfather Mountain Formations, and metasedimentary rocks of the Ocoee Supergroup (King and others, 1958; Hadley, 1970). Along the western edge of the Blue Ridge, these Late Proterozoic sequences are overlain both conformably and unconformably by shelf deposits of the Cambrian Chilhowee Group and overlying Shady Dolomite and Rome Formation (Colton, 1970). In eastern segments of the western Blue Ridge, the Ocoee Supergroup is also conformably overlain by the Murphy Group, a diverse sequence of variably metamorphosed clastic and carbonate lithologies (Fig. 5.1).

The structure of the western Blue Ridge is dominated by numerous northwest-vergent thrust faults of contrasting age and character. The earliest thrust faults display ductile fabrics that formed prior to attainment of peak metamorphic conditions and mylonites developed along these fault zones are typically annealed (Hatcher and Goldberg, 1991). Younger faults, such as those along the frontal Blue Ridge thrust zone, postdate metamorphism and are characterized by predominantly brittle fabrics. Younger faults commonly truncate earlier faults and have been locally reactivated.

The earliest folds recognized in the western Blue Ridge occur in the Great Smoky Mountains area and are east to east-northeast trending and premetamorphic (Hamilton, 1961; Hadley and Goldsmith, 1963). They have been overprinted by one or more generations of more northeasterly-trending ductile folds. The dominant foliation postdates the earliest folding and is commonly crenulated or transposed in more internal portions of the western Blue Ridge.

Rock units exposed in the western Blue Ridge were affected by a progressive Paleozoic Barrovian-type regional metamorphism (Carpenter, 1970). Metamorphic grade (Fig. 5.2) generally increases from the northwest (unmetamorphosed or sub-greenschist facies) to the southeast (at least kyanite grade). The pattern of metamorphism is more

Figure 5.2. Generalized geologic map of the southern Appalachian western Blue Ridge in the vicinity of the study area showing the approximate positions of metamorphic isograds and locations and results of previous geochronologic studies (modified from Hardeman, 1966; North Carolina Geological Survey, 1985; Hatcher and Goldberg, 1991). A, amphibole; B, biotite; H, hornblende; M, muscovite; W, whole rock. Circles from K-Ar results compiled in Kish (1991); triangles from $^{40}Ar/^{39}Ar$ results from Dallmeyer (1975, 1988); squares indicate sample locations from the present study. DT, Ducktown; LTR, Little Tennessee River; OR, Ocoee River; PR, Pigeon River; TC, Tuckaleechee Cove; TP, Tellico Plains.

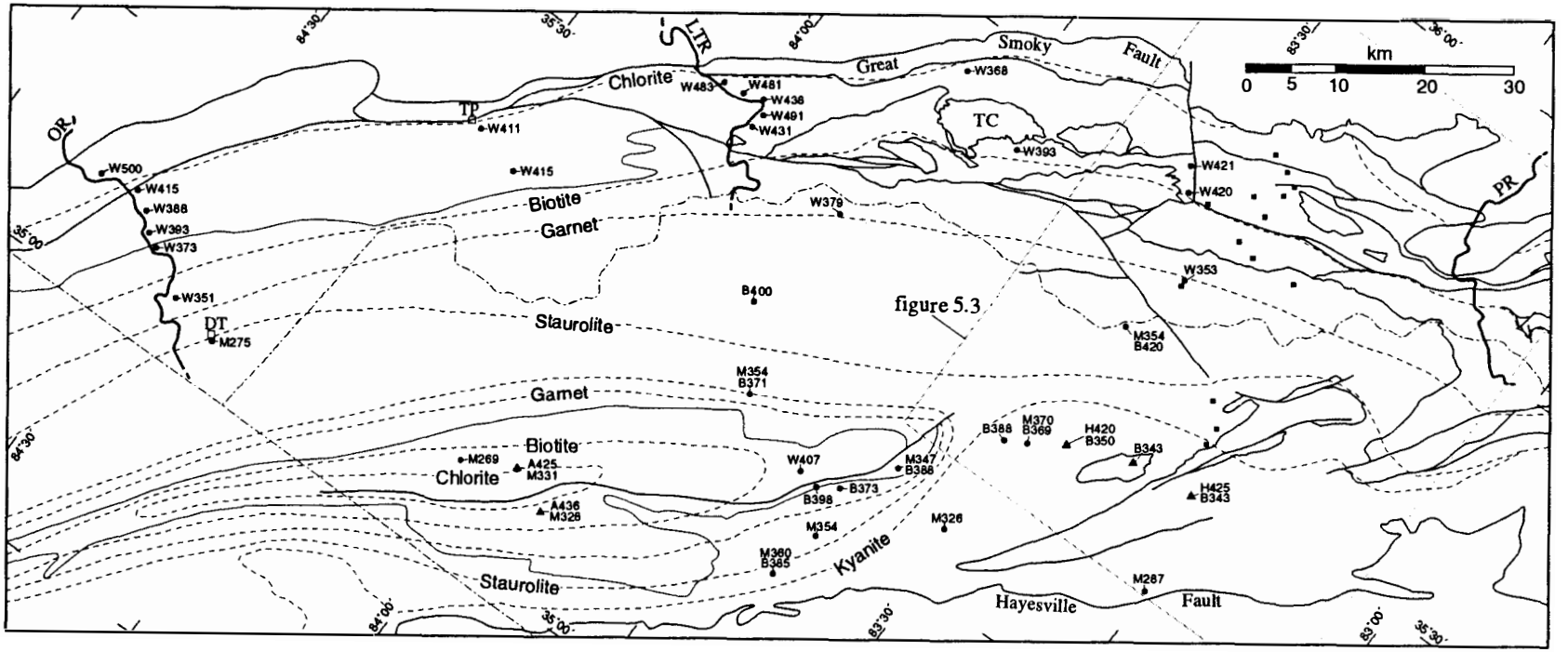
km
0 5 10 20 30
Great Smoky Fault
Chlorite
Biotite
Garnet
Staurolite
Kyanite
Hayesville Fault
LTR
TP
TC
OR
DT
PR
W500
W415
W388
W393
W373
W351
M275
W411
W415
W483
W481
W436
W491
W431
W368
W393
W421
W420
W379
W353
B400
M354
B420
M354
B371
M269
A425
M331
A436
M328
W407
M347
B388
B373
B398
M354
M360
B385
M326
B388
M370
B369
H420
B350
B343
H425
B343
M287
84°30'
35°30'
84°00'
83°30'
36°00'
35°00'
83°00'

figure 5.3

complex in the Murphy syncline where grade decreases inward toward the synclinal axis (Fig. 5.2). Retrogressive metamorphic textures have been described throughout the western Blue Ridge. They have generally been attributed to either prolonged cooling following an initial early Paleozoic metamorphism (Dallmeyer and others, 1978) or a distinct later regional metamorphic overprint (Hatcher, 1978; Hatcher and Odom, 1980).

ORDOVICIAN TECTONISM IN THE SOUTHERN APPALACHIANS

The record of Ordovician orogenic activity in eastern North America, now known as the Taconic orogeny, was first described in the Hudson Valley of New York on the basis of an angular unconformity separating folded rocks as young as Middle Ordovician from overlying Early to Late Silurian units. A similar but slightly older orogenic event was also recognized in the southern Appalachians and termed by Kay (1942) and Rodgers (1953) the Blountian phase of the Taconic orogeny. Drake and others (1989) suggested that the Blountian phase was a separate and distinct tectonic event that occurred prior to the Taconic.

Ordovician orogenesis has also been considered important within internal parts of the southern Appalachian orogen (Butler, 1972; Hatcher, 1972, 1978; Dallmeyer, 1975; Butler, 1991). This interpretation was based both on the stratigraphic record in the foreland and geochronologic data reported from internal portions of the orogen. As discussed previously, however, fossil evidence and proposed stratigraphic correlations have questioned the existence of pre-Devonian tectonothermal activity (Tull and Guthrie, 1985; Unrug and Unrug, 1990). Evidence presented both for and against Ordovician orogenic activity in the southern Appalachian western Blue Ridge is discussed below.

Evidence For Ordovician Tectonic Activity in the Southern Appalachians

The foreland stratigraphic record. Kay (1942) first recognized the significance of extensive early Middle Ordovician clastic rocks in the eastern Valley and Ridge province (Blountian clastic wedge), and suggested that these sediments were derived from an eastern highlands that had developed during the Blountian disturbance. This clastic wedge was deposited in the Sevier basin of eastern Tennessee, and overlies a major unconformity developed at the top of the Lower Ordovician-Upper Cambrian Knox Group. The clastic sequence includes shallow shelf, debris flows, pelagic, turbidite, and shallow water-subaerial deposits (Shanmugan, 1980). Coarse polymictic conglomerates occur within turbiditic sequences of the Blountian wedge that contain fragments derived from most of the Lower Paleozoic units stratigraphically down to and including the Chilhowee Group (Kellberg and Grant, 1956; Lowry, 1972; Mack, 1985). This has been interpreted to suggest substantial structural relief adjacent to the basin had developed prior to deposition. An easterly source is indicated for the conglomerates and associated turbidite deposits (Shanmugan, 1980). Orogenic activity prior to conglomerate deposition is also indicated by the internal deformation and metamorphism displayed within some of the rock fragments within the conglomerates. Kellberg and Grant (1956) recognized that fragments of Lower Cambrian clastics were "altered from sandstone to vitreous quartzite." Mack (1985) described metapelitic slate and phyllite fragments within sandstones of the Blountian clastic wedge indicating a low-grade metamorphic source.

Geochronologic evidence. Available radiometric ages for the western Blue Ridge in the vicinity of the study area are summarized in Figure 5.2. Summaries of geochronology available in this area may be found in Glover and others (1983) Drake and others (1989), Osberg and others (1989), Butler (1991), and Kish (1991). Initial geochronologic studies in the Blue Ridge recognized a limited area of early Paleozoic (450 Ma) metamorphism within lower grade rocks exposed within the western Blue Ridge, and

a more extensive area of middle Paleozoic (350 Ma) metamorphism was documented within higher grade parts of the southern Appalachians (Long and others, 1959; Kulp and Eckelman, 1961). These authors concluded that two distinct early Paleozoic regional metamorphic events were recorded. The younger was believed to have culminated at 350 Ma, and appeared to have variably rejuvenated micas that had initially crystallized at 460 Ma. More recent interpretations proposed that the younger ages may date post-metamorphic uplift and cooling through appropriate closure temperatures; they therefore represent only minimum ages for metamorphism (Hadley, 1964; Armstrong, 1966; Butler, 1972). The 350 Ma ages have therefore commonly been interpreted to record regionally diachronous cooling following a single phase of tectonothermal activity at 450 to 480 Ma.

Rb-Sr whole-rock results were reported by Fullagar and Bottino (1970) from Ducktown, Tennessee, and Ore Knob, North Carolina. These results indicated that Paleozoic metamorphism in the Blue Ridge occurred prior to 475 Ma. Kish and others (1976) reported 440 ± 13 Ma Rb-Sr whole-rock ages for unmetamorphosed pegmatites exposed near Bryson City, North Carolina, and ages of ~ 400 Ma were listed for pegmatites from the Spruce Pine district of North Carolina. These dates were interpreted to reflect minimum dates for regional metamorphism in the western Blue Ridge.

Kish and Harper (1973) reported conventional K-Ar whole-rock ages for slate and phyllite from the western Blue Ridge (northwest of the biotite isograd). These ranged from 420 to 400 Ma, and were interpreted to indicate that regional metamorphism occurred at $\geq$400 Ma ago. A wide range of K-Ar whole-rock ages for lower greenschist facies slates from the western Great Smoky Mountains were grouped at ~ 480 Ma and at 430 to 370 Ma (Kish, 1982). The relatively wide range in the younger group of K-Ar ages was interpreted to reflect either slow cooling and/or partial rejuvanation by a 390 Ma recrystallization event.

Dallmeyer (1975) reported $^{40}Ar/^{39}Ar$ ages for hornblende and biotite from recrystallized basement rocks from the western Blue Ridge in North Carolina. Hornblende concentrates displayed internally concordant spectra which defined plateau ages of 420 to 425 Ma (recalculated from the initially published results using the decay constants proposed by Steiger and Jäger, 1977). Biotite concentrates yielded plateau ages of 350 to 360 Ma. The spectra provided no indication of extraneous argon contamination, and were interpreted by Dallmeyer (1975) to date times of post-metamorphic cooling through the contrasting temperatures required for intracrystalline retention of argon. The hornblende dates were considered to represent a minimum age for the high-grade Paleozoic metamorphism recorded in the area and were used to develop a post-metamorphic thermal model that suggested attainment of peak metamorphic conditions at 480 Ma.

Dallmeyer (1988) reported $^{40}Ar/^{39}Ar$ data on amphibole and muscovite concentrates from rocks within the Murphy belt. Amphibole results suggested post-metamorphic cooling through argon closure temperatures at 425 to 440 Ma. Discordant age spectra were interpreted to result from a distinct later thermal overprint that locally effected partial argon loss from amphibole at 325 to 350 Ma. The overprint was of sufficient magnitude to completely rejuvenate muscovite within interlayered pelitic schist which records plateau ages of ~330 Ma. These results were interpreted by Dallmeyer (1988) to indicate a polymetamorphic evolution that involved both Ordovician and Carboniferous thermal events.

Evidence Precluding Ordovician Orogenic Activity in the Southern Appalachians

Fossil evidence. Unrug and Unrug (1990) reported a fossil assemblage within regionally metamorphosed rocks of the Walden Creek Group (Ocoee Supergroup)

exposed along westernmost sections of the Blue Ridge in Tennessee. This assemblage is reported as trilobite, ostracode, bryozoan, and microcrinoid fragments, and agglutinated foraminifera. The foraminiferal assemblage was interpreted to be Silurian or younger. More recently, Unrug and others (1991) reported additional fossil assemblages from the Walden Creek Group that include calcispheres and calcareous foraminifera. These fossils were interpreted to reflect a Late Devonian (Frasnian) to earliest Mississippian age, suggesting that the previously assumed Late Proterozoic depositional age for the Walden Creek Group, and possibly the entire Ocoee, be abandoned (Unrug and others, 1992). In addition, the new paleontologic age assignment questions the geologic significance of most previously reported geochronology from the western Blue Ridge (Dallmeyer, 1975; Kish and others, 1976; Dallmeyer, 1988). A Late Devonian to earliest Mississippian age for the Walden Creek Group requires that recorded metamorphism must be Carboniferous or younger and leaves only a remote possibility that some of the earliest (premetamorphic) deformation occurred during Devonian orogenesis.

The validity and interpretation of the fossils described by Unrug and Unrug (1990) and Unrug and others (1991) have been questioned because of: (1) inconsistencies with previously documented stratigraphic relationships (King and others, 1958; Keller, 1980); (2) other fossil evidence (Knoll and Keller, 1979); and (3) lack of confirmation by other workers (Broadhead and Hatcher, 1992). A conformable contact between the Sandsuck Formation (uppermost unit of the Walden Creek Group) and overlying Chilhowee Group argues against a middle Paleozoic age for the Walden Creek Group because an Early Cambrian age for the Chilhowee Group has been clearly documented (Walcott, 1890; Laurence and Palmer, 1963; Simpson and Sundberg, 1987; Walker and Driese, 1991). Although stratigraphic relations between the Chilhowee Group and upper portions of the Walden Creek Group are equivocal in the Great Smoky Mountains (King and others, 1958; Hamilton, 1961), stratigraphic relations immediately east of the Great Smoky

Mountains are certain. Detailed mapping in this area (Ferguson and Jewell, 1951; Keller, 1980) has documented that the Walden Creek Group (including the Sandsuck Formation) stratigraphically underlies the Chilhowee Group (Fig. 5.3). A continuous, possibly unconformable, succession from the Sandsuck Formation to the Chilhowee Group is also exposed northeast and within and adjacent to the Hot Springs window (Oriel, 1951; Bearce, 1969; Walker and Simpson, 1991). Stratigraphic evidence therefore appears to preclude a post-Early Cambrian age for the Walden Creek Group.

The detailed taxonomic identification of fossils presented by Unrug and Unrug (1990) and Unrug, Unrug, and Palmes (1991) has been questioned (Rodgers, 1991; Broadhead and others, 1991). Because of their small size and poor preservation, it has been suggested that these fossils cannot be confirmed as different from Ordovician and Cambrian fossils. For example, similar foraminifera have been reported from Lower Cambrian rocks of west Africa (Culver and others, 1990; Culver, 1991). Rodgers (1991) suggested that the fossils described by Unrug and Unrug (1990) may belong to the Tommotian stage, the lowest known fossiliferous stage of the Cambrian. In addition, nonfossil allochems similar to the calcareous foraminifera and calcispheres reported by Unrug and others (1991) have been described by Broadhead and Hatcher (1992) from a carbonate horizon within the Sandsuck Formation that clearly underlies Early Cambrian rocks of the Chilhowee Group along the Parksville reservoir. These authors suggested that the structures described by Unrug and others (1991) within other units of the Walden Creek Group may be peripherally micritized and diagenetically recrystallized inorganic grains. Broadhead and others (1991), however, suggested that the bryozoan and crinoid fragments pictured in Unrug and Unrug (1990) and Unrug and others (1991) are not known before the Middle Ordovician.

Other problems arising from a middle to late Paleozoic depositional age suggested for the Walden Creek Group include: (1) lack of megafossils within carbonate units

Figure 5.3. Geologic map of the eastern Great Smoky Mountains area showing sample localities and metamorphic isograds. ACS, Alum Cave syncline; BD, Bryson dome; CA, Cataloochee anticlinorium; CCA, Copeland Creek anticline; DCF, Dunn Creek fault; GAF, Gatlinburg fault; GBF, Greenbrier fault; GSF, Great Smoky fault; HF, Hayesville fault; MCF, Miller Cove fault; MS, Murphy syncline; RA, Ravensford anticline (modified from King and others, 1968).

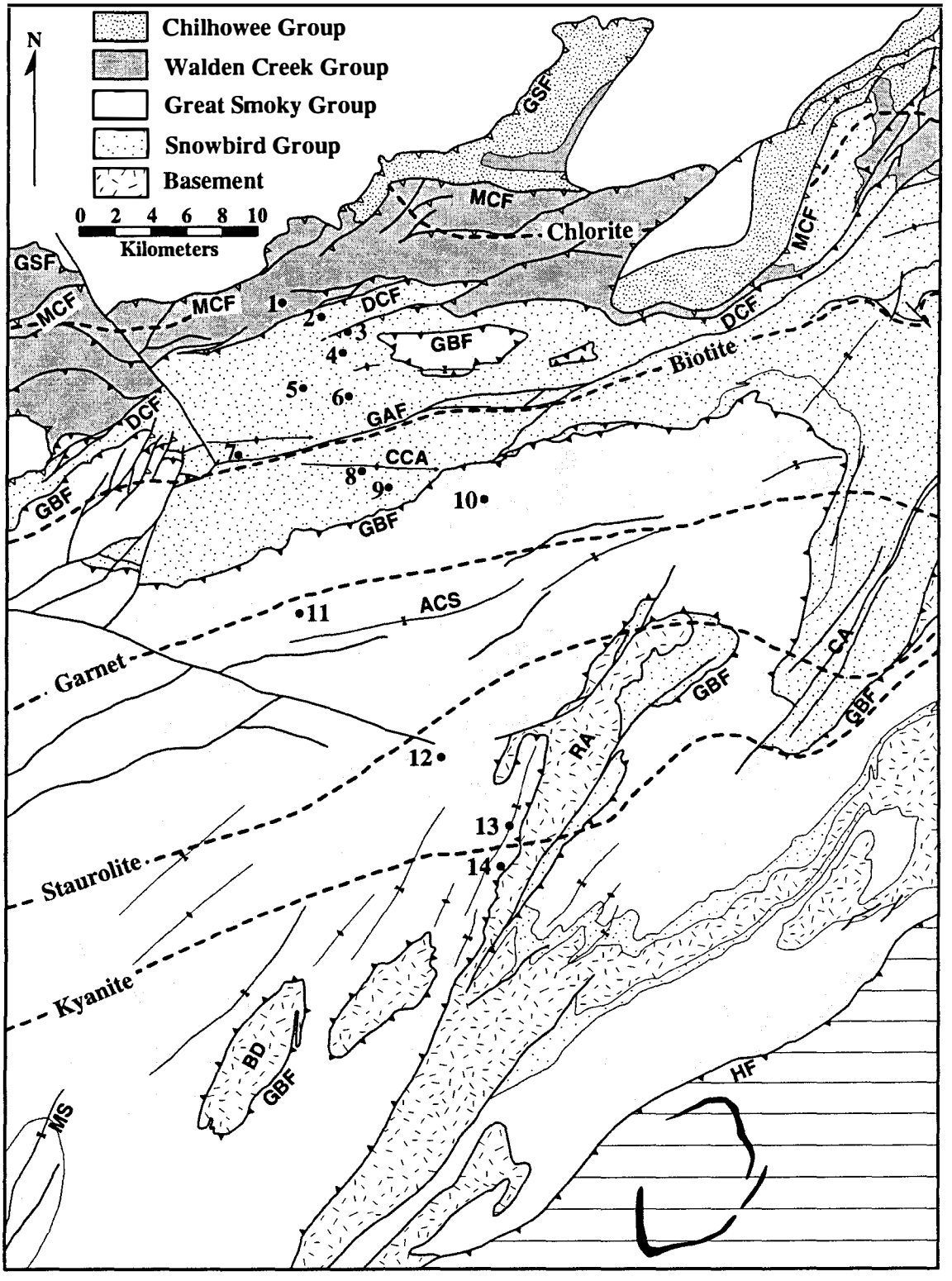
N
Chilhowee Group
Walden Creek Group
Great Smoky Group
Snowbird Group
Basement
0 2 4 6 8 10
Kilometers
GSF
MCF
DCF
GBF
GAF
CCA
ACS
RA
BD
HF
MS
Chlorite
Biotite
Garnet
Staurolite
Kyanite
1
2
3
4
5
6
7
8
9
10
11
12
13
14

interpreted to represent platform margin deposits (Rodgers, 1991; Broadhead and others, 1991); and (2) absence of conodonts that are common microfossils in Silurian and Devonian carbonate rocks formed in a wide variety of facies (Broadhead, Hatcher, and Costello, 1991). A middle to late Paleozoic age assignment also conflicts with other fossil evidence from the Walden Creek Group. Knoll and Keller (1979) suggested a late Precambrian age on the basis of acritarchs, particularly *Bavlinella faveolata* (Shepleva); a species now known to range into the Cambrian (Knoll and Swett, 1985). Broadhead and others (1991) recently relocated and described soft-bodied metazoan macrofossils originally discovered by Phillips (1952) in the Sandsuck Formation. This confirms that the Sandsuck Formation can be no younger than Early Cambrian. Thus, as indicated by Broadhead and others (1991), evaluating the true geologic significance of the reports of Unrug and Unrug (1990) and Unrug and others (1991) awaits both independent confirmation and careful taxonomic investigation of the fossils in order to determine the biostratigraphic significance of these fossils.

Stratigraphic evidence. Several workers have suggested a correlation between the Murphy belt (western Blue Ridge) and nearby Talladega belt (e.g., Crickmay, 1936; Stose and Stose, 1944; Hadley, 1970; Tull and Guthrie, 1985). The Talladega belt, situated in the southwest part of the western Blue Ridge, occupies a structurally equivalent position between the foreland thrust belt and the eastern Blue Ridge (Fig. 5.1). Fossiliferous Lower Devonian strata within the Talladega belt have been regionally metamorphosed to lower greenschist facies. Whole-rock conventional K-Ar dates for slate from the Talladega belt yielded a mean age of 399 ± 17 Ma (Kish, 1990). These are compatible with paleontologic controls that indicate Early to Middle Devonian metamorphism in the Talladega belt.

Tull and Guthrie (1985) and Tull and Groszos (1988) have argued that uppermost stratigraphic levels of the Murphy Group (Mineral Bluff Formation) are correlative with

lithologically similar clastic sequences exposed in the Talladega belt (Talladega Group). Upper portions of the Talladega Group (upper Lay Dam Formation and Jemison Chert) are paleontologically restricted to the Silurian-Early Devonian (Tull and others, 1988). In addition, these authors proposed that a major unconformity separates the uppermost Mineral Bluff Formation from underlying formations of the Murphy Group. This unconformity has been correlated with a similar post-Early Ordovician unconformity in the Talladega belt. This unconformity was suggested to have developed prior to metamorphism and significant deformation because of the low angle and continuity of structural fabrics below the unconformity into overlying higher-grade units of the Murphy belt rocks and Great Smoky Group (Dallmeyer and others, 1978; Tull and Groszos, 1988). If these stratigraphic correlations are correct, regional metamorphism in the western Blue Ridge must have been post-Silurian.

Despite gross lithologic similarities between rocks of the Talladega Group and Mineral Bluff Formation (Tull and Groszos, 1988), other correlations are possible. An alternative possibility suggested by Tull and Groszos (1988) is that deposition of the Mineral Bluff clastic sequence pre-dated the Talladega Group. This would require that the Talladega Group be missing within the Murphy belt. Based on analogies with known deep-water stratigraphic successions exposed in other areas, Thomas and Hatcher (1988) suggested that the Murphy succession may represent deep-water proximal deposits of the Middle Ordovician Blountian clastic wedge. Similarly, Hatcher and Broadhead (1992) suggested that the Murphy belt sequence could represent a more distal facies of the platform sequence that was deposited later (time-transgressively) eastward. In this interpretation, the clastic sequence above the proposed unconformity in the Murphy belt is part of the Blountian clastic wedge. A post-Ordovician age for rocks of the Murphy belt has therefore not been stratigraphically demonstrated.

GEOLOGY OF THE STUDY AREA

Stratigraphy

The present study area is located in the eastern Great Smoky Mountains of the western Blue Ridge (Figs. 5.1, 5.3). The dominant stratigraphic unit exposed in this area is the Ocoee Supergroup, which consists of a 12 to 15 km thick sequence of predominantly clastic metasedimentary rocks (King and others, 1958; Hadley, 1970; Rast and Kohles, 1986). Numerous thrust faults are present in the study area affecting both basement rocks and units within the overlying Ocoee Supergroup. Although faulting locally complicates regional stratigraphic relations, the Ocoee Supergroup has been divided into three major and contrasting lithologic sequences. In ascending stratigraphic order, these include the Snowbird Group, the Great Smoky Group, and the Walden Creek Group (King and others, 1958). The Snowbird Group is generally considered the oldest because locally it nonconformably overlies basement and is itself conformably overlain by the Great Smoky Group. The Great Smoky Group, however, also locally nonconformably overlies basement (Hadley and Goldsmith, 1963). The Walden Creek Group conformably succeeds both the Snowbird Group (Ferguson and Jewell, 1951; Keller, 1980) (Fig. 5.3) and the Great Smoky Group (Hurst and Schlee, 1962; Hernon, 1964; Costello and Hatcher, 1986, 1991) in different areas.

Fault Systems

The Great Smoky Mountains area records the effects at least two major deformational events that have produced five distinct fault systems (Woodward and others, 1991). These include the Great Smoky, Gatlinburg, Miller Cove, Dunn Creek, and Greenbrier fault systems (Fig. 5.3). The Great Smoky and Gatlinburg systems are regarded as late Paleozoic in age. The Dunn Creek and Greenbrier fault systems are

premetamorphic and are believed to have been active in the early Paleozoic. An additional early Paleozoic thrust sheet, now floored by the Miller Cove fault, was emplaced during regional cleavage development (Connelly and Woodward, 1992). Early Paleozoic structures may be distinguished from late Paleozoic structures on the basis of their relations to regional cleavage and metamorphic isograds, and on the ductile nature of the early fault fabrics. Predominantly brittle fabrics are characteristic of late Paleozoic faults in this area.

The Great Smoky thrust fault forms the northwestern boundary of the western Blue Ridge province in the vicinity of the study area and is part of the Blue Ridge thrust system. The Great Smoky fault is dominantly brittle and internal deformation of late Paleozoic age within the Great Smoky thrust sheet in this area is minor.

The younger Gatlinburg fault system is a primarily east-northeast trending system of brittle, high-angle structures (Fig. 5.3). Both dip-slip and strike-slip motion are recognized; however, dip slip predominates in the study area. Maximum displacement is approximatly 2000 m (King, 1964). Although King (1964) described these faults as thrusts, Woodward and others (1991) noted that normal separations also occur. Woodward and others (1991) interpreted these faults as "late" structures related to folding of the Great Smoky thrust sheet because they parallel the post-emplacement folding.

The predominantly brittle Miller Cove fault branches from the Great Smoky fault (Fig. 5.3) and separates cleaved and metamorphosed rocks of the Ocoee Supergroup from generally uncleaved and unmetamorphosed rocks of the upper Ocoee Supergroup, Chilhowee Group, and younger strata (Costello, 1984; Hatcher and others, 1989). The Miller Cove fault locally represents the frontal Blue Ridge fault where the branch line between the Great Smoky and Miller Cove faults has been eroded. Pre-late Paleozoic cleavage, folds, and ductile thrust faults within the Miller Cove thrust sheet, however,

suggest that this thrust sheet was at least locally active prior to the late Paleozoic (Connelly and Woodward, 1992).

The Greenbrier fault is a folded, low-angle thrust separating rocks of the Great Smoky Group from the underlying Snowbird Group (Fig. 5.3). A horizontal displacement of at least 24 km has been estimated based on stratigraphic criteria (Hadley and Goldsmith, 1963) and structural reconstructions (Connelly and Woodward, 1992). Because the Greenbrier fault does not offset metamorphic isograds or affect regional cleavage, it has been considered a premetamorphic structure (Hadley and Goldsmith, 1963; King, 1964; Milton, 1983).

The Dunn Creek thrust fault separates Walden Creek Group footwall rocks from Snowbird Group hanging wall rocks throughout most of the foothills area (Fig. 5.3). A premetamorphic age for the Dunn Creek fault is indicated by truncation of this fault by later synmetamorphic thrust faults (Connelly and Woodward, 1992), and lack of offset of the chlorite isograd northeast of the study area (Keller, 1980).

Folds

The earliest post-Grenville folds recognized in the Great Smoky Mountains include the east-trending F_1 Cartertown-Copeland Creek anticline (Dunn Creek thrust sheet) and the Alum Cave syncline (Greenbrier thrust sheet) (Fig. 5.3). They are transected by and predate a regional S_1 foliation (Hamilton, 1961; Connelly and Woodward, 1992). These folds have been described as truncated by the Greenbrier fault, and thus were interpreted to predate emplacement. Connelly and Woodward (1992), however, reinterpreted them as rootless, ramp-related folds that formed during emplacement of the Greenbrier and Dunn Creek thrust sheets. They suggested that a foreland-style thrust belt existed prior to overprinting by regional cleavage, metamorphism, and ductile folding.

Early folds and faults were affected by a second generation of folds (F_2) that exhibit axial-planar S_1 cleavage and include most of the mesoscopic and some map-scale folds in the Miller Cove and Dunn Creek thrust sheets. Some folds are cored by ductile thrust faults that locally truncate premetamorphic faults (Connelly and Woodward, 1992). Within the Miller Cove thrust sheet, cleavage is axial planar to folds (Witherspoon, 1981; Sack, 1988) and is commonly parallel to the ductile thrust faults. Within the Dunn Creek thrust sheet, however, cleavage transects most east-trending folds, and is axial planar to northeast-trending second-generation folds. Interference between these two fold generations occurs throughout the Dunn Creek thrust sheet and results in steeply plunging second-generation folds with axial-planar cleavage. Connelly and Woodward (1992) suggested that these F_2 folds and the S_1 regional cleavage formed during pre-late Paleozoic movement of the present Miller Cove thrust sheet.

Third-generation (F_3) folds in this area trend north-northeast and include the Ravensford anticline, Cataloochee anticlinorium, and many smaller associated folds that occur primarily within the Greenbrier thrust sheet (Fig. 5.3). These are the second-generation folds described by Hadley and Goldsmith (1963). Larger F_3 anticlines locally expose basement rocks. These folds are typically open but may be isoclinal and most are asymmetric with axial planes dipping southeastward (Hadley and Goldsmith, 1963). Folding of regional S_1 foliation by F_3 folds indicates that they postdated regional metamorphism (Hadley and Goldsmith, 1963; Witherspoon, 1981). S_2 crenulation cleavage is parallel to axial planes of F_3 folds (Hadley and Goldsmith, 1963; Mohr, 1973). Nonpenetrative S_2 cleavage is locally present north of the Greenbrier fault and becomes progressively more penetrative south of the garnet isograd. At higher metamorphic grades, S_2 cleavage becomes the dominant foliation (Hadley and Goldsmith, 1963).

Metamorphism

Isograds in the eastern Great Smoky Mountains suggest a progressive Barrovian-type metamorphism that generally increases from sub-chlorite grade (within frontal units) to at least kyanite grade (Fig. 5.3). In detail, however, the metamorphic history of this area is complex. Hadley and Goldsmith (1963) recognized that the peak of thermal metamorphism was both preceded and followed by deformation and a lower-grade metamorphism. Petrographic evidence suggests that S_1 regional cleavage and schistosity formed during an early kinematic phase of metamorphism. This was followed by a higher-grade, static recrystallization that involved formation of porphyroblasts of chloritoid, biotite, garnet, staurolite, and/or kyanite. Porphyroblasts are randomly oriented and overgrow all preexisting foliations (Hadley and Goldsmith, 1963; King, 1964). Following porphyroblast growth, an S_2 crenulation cleavage locally formed and fractured, offset, and rotated porphyroblasts. Minor quartz and chlorite formed in pressure shadows adjacent to some porphyroblasts (Hadley and Goldsmith, 1963).

Mohr (1973) described similar textural characteristics within garnet and lower metamorphic grades west of Bryson dome (Fig. 5.3). Above garnet grade, however, snowball textures suggest that porphyroblasts grew during development of S_2. One or more post-S_2 minor retrograde events are indicated by the local presence of chlorite and white mica selvages over kyanite crystals and local pseudomorphic replacement of staurolite and kyanite by sericite and/or chlorite (Mohr, 1973). Textures indicative of polymetamorphism were also described by Power and Forrest (1971) within the Murphy belt. Early foliation was overgrown by garnet. Subsequent folding was followed by growth of sillimanite, staurolite, and biotite. Garnets are commonly included within staurolite.

ANALYTICAL METHODS

Muscovite concentrates were prepared from three samples of argillaceous Thunderhead metasandstone collected within high-grade portions of the western Blue Ridge in Tennessee and North Carolina (staurolite and kyanite zones). Eleven slate/phyllite samples were collected for whole-rock analysis from lower grade areas along an approximately north-south (across strike) transect. Lithologies included the Walden Creek, Snowbird, and Great Smoky Groups. Sample localities are indicated in Figure 5.3. Location coordinates of the dated samples are provided in Table 5.1.

Table 5.1. Location coordinates of dated samples.

Sample	Latitude	Longitude
1	35°48'27"	83°27'33"
2	35°48'04"	83°25'48"
3	35°47'35"	83°24'24"
4	35°47'15"	83°24'17"
5	35°45'47"	83°26'46"
6	35°45'27"	83°24'19"
7	35°43'38"	83°29'07"
8	35°43'10"	83°23'24"
9	35°43'03"	83°23'13"
10	35°42'25"	83°19'01"
11	35°39'03"	83°26'34"
12	35°34'40"	83°20'45"
13	35°32'38"	83°18'09"
14	35°31'23"	83°18'24"

Illite Crystallinity

The seven slate/phyllite samples from the chlorite zone were crushed and sieved following wire-brush removal of weathered surfaces and thorough washing. They were prepared for determination of illite crystallinity by desegregation in a shatter box for 20 sec. Bulk < 2 μm size-fractions were isolated by differential settling in Atterberg cylinders and centrifugation following techniques listed in Reuter (1985). Illite crystallinity of the < 2 μm size fractions was determined from oriented sedimentation slides by comparison of the (001) illite and (100) quartz (internal standard) reflections following the methods of Weber (1972). Cross-calibration of 28 samples (correlation coefficient = 0.97) from Reuter (1985, 1987) suggests that the following boundary values are appropriate for the equipment setting employed at the University of Georgia (compared with the calibrations of Teichmüller and others, 1979): greenschist/anchizone = 115; anchizone/diagenesis = 350. In the present study, boundaries between the upper anchizone/middle anchizone and middle anchizone/lower anchizone are defined at crystallinity values of, 190 and 270 respectively (Fig. 5.4). According to Kubler (1967) and Dunoyer de Segonzac (1969, 1970), minimum illite crystallinity values are reached within the epizone whereas Teichmüller and others (1979) define the greenschist/anchizone boundary by the first appearance of minimum crystallinity values. As a result, rocks suggested to reflect epizonal metamorphism according to Kubler (1967) and/or Dunoyer de Segonzac (1969, 1970) are classified as upper anchizone by Teichmüller and others (1979) (Fig. 5.4).

$^{40}Ar/^{39}Ar$ Analyses

Techniques used during $^{40}Ar/^{39}Ar$ analyses generally followed those described in detail by Dallmeyer and Gil-Ibarguchi (1990). The whole-rock slate/phyllite samples were prepared by crushing and sieving to 80/100 mesh followed by thorough washings.

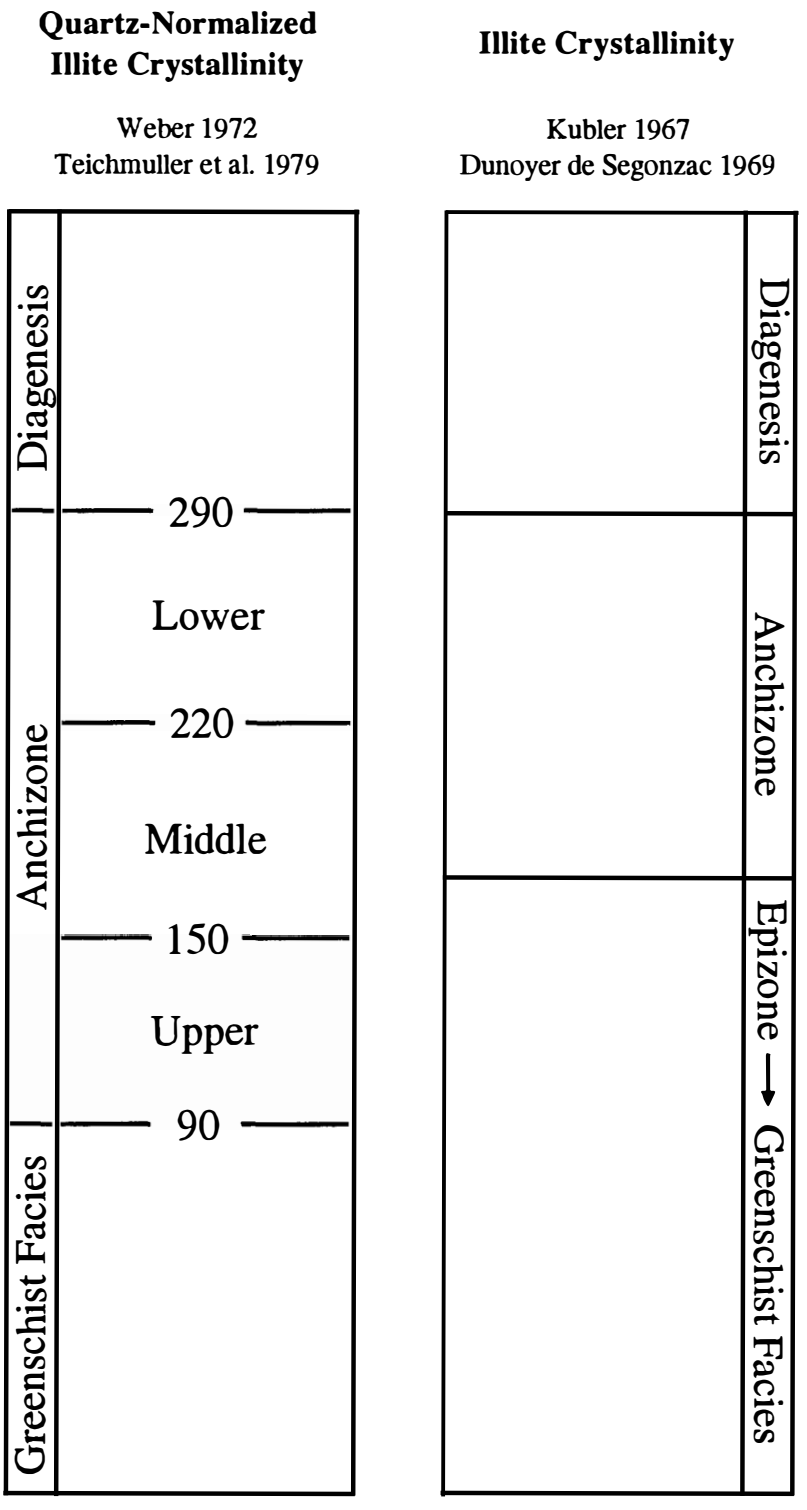

Figure 5.4. Comparison of illite crystallinity based on the contrasting methods of Kubler (1967) and Teichmüller and others (1979).

Muscovite concentrates (> 99 percent) were prepared from crushed and sized rock powders using flotation and magnetic separation. Mineral concentrates and whole-rock powder were wrapped in aluminum-foil packets, encapsulated in sealed quartz vials, and irradiated for 40 hours at the TRIGA reactor at the U.S. Geological Survey in Denver, Colorado. Variations in the flux of neutrons along the length of the irradiation assembly were monitored with several mineral standards, including MMhb-1 (Samson and Alexander, 1987). The samples were incrementally heated until fusion in a double-vacuum, resistance-heated furnace. Measured isotopic ratios were corrected for total system blanks and the effects of mass discrimination. Interfering isotopes produced during irradiation were corrected using factors reported by Dalrymple and others (1981) for the TRIGA reactor. Apparent $^{40}Ar/^{39}Ar$ ages were calculated from corrected isotopic ratios using the decay constants and isotopic abundance ratios listed by Steiger and Jäger (1977) following the methods described in Dallmeyer and Keppie (1987).

Intralaboratory uncertainties have been calculated by statistical propagation of uncertainties associated with measurement of each isotopic ratio (at two standard deviations of the mean) through the age equation. Interlaboratory uncertainties are ± 1.25-1.5 precent of the quoted age. Total-gas ages have been computed for each sample by appropriate weighting of the age and percentage ^{39}Ar released within each temperature increment. A "plateau" is considered to be defined if the ages recorded by two or more contiguous gas fractions (with similar apparent K/Ca ratios) each representing > 4 precent of the total ^{39}Ar evolved (and together constituting > 50 percent of the total quantity of ^{39}Ar evolved) are mutually similar within a ± 1 percent intralaboratory uncertainty. Analysis of the MMhb-1 monitor indicates that apparent K/Ca ratios may be calculated through the relationship 0.518 (± 0.005) x ($^{39}Ar/^{37}Ar$) corrected.

RESULTS

Illite Crystallinity

The quartz-normalized illite crystallinity indices for the bulk < 2 μm size fractions isolated from the slate/phyllite samples collected within the chlorite zone range between 116 and 436 (Table 5.2). The results correlate with metamorphic conditions ranging from lower greenschist facies to the diagenesis zone (following the classification of Teichmüller and others, 1979; Fig. 5.4).

$^{40}Ar/^{39}Ar$

Whole-rock slate/phyllite. Eleven whole-rock slate/phyllite samples from the western Blue Ridge were analyzed with $^{40}Ar/^{39}Ar$ incremental-release techniques. The analytical data are listed in Table 5.3 and portrayed as age spectra in Figures 5.5 and 5.6.

Seven whole-rock samples (1-7) have been analyzed from the chlorite zone (diagenesis to uppermost anchizone/lowermost greenschist). These display variably discordant $^{40}Ar/^{39}Ar$ spectra (Fig. 5.5) that define total-gas ages ranging between 499 and 389 Ma. In general, only minor intrasample variation in the apparent $^{40}Ar/^{39}Ar$ ages is recorded by most intermediate-temperature gas fractions. Considerable intersample variation, however, exists in the intermediate-temperature ages. For the lowest grade sample (1: diagenesis) these are ~ 500 Ma. For samples from the middle-upper anchizone (2-5) they are ~ 450 Ma (plateaux are defined for samples 3-5). For samples from the upper anchizone/lowermost greenschist facies (6-7), intermediate temperature ages are 380 to 420 Ma. The intermediate temperature fractions are all characterized by similar intrasample apparent K/Ca ratios (Fig. 5.5) indicating that experimental evolution of gas occurred from compositionally uniform populations of intracrystalline "sites". These are interpreted to correspond with constituent, very fine-grained white mica. Low-temperature

Table 5.2. Quartz-Normalized Illite Crystallinity Determined on Bulk <2 μm Size Fractions at the Locations Sampled for $^{40}Ar/^{39}Ar$ Dating in the Chlorite Zone of the Eastern Great Smoky Mountains, Western Blue Ridge.

Sample	Crystallinity
1	436
2	195
3	187
4	147
5	138
6	116
7	144

Note. Comparison of (001) reflection in illite and (100) reflection in internal quartz standard (after Weber, 1972).

Table 5.3. $^{40}Ar/^{39}Ar$ analytical data for incremental heating experiments on whole-rock slate/phyllite samples from the western Blue Ridge, Tennessee-North Carolina.

Release Temp. (°C)	$(^{40}Ar/^{39}Ar)^*$	$(^{36}Ar/^{39}Ar)^*$	$(^{37}Ar/^{39}Ar)^c$	^{39}Ar % of total	^{40}Ar non-atm.$^+$	$^{36}Ar_{Ca}$ %	Apparent Age (Ma)**
			Diagenesis-Lower Anchizone				
Sample	**1.**	J=0.010522					
425	18.04	0.00563	0.013	6.59	90.76	0.06	286.8 ± 2.2
450	21.34	0.00126	0.018	6.88	98.24	0.39	359.5 ± 2.7
475	27.37	0.00099	0.028	5.71	98.92	0.78	452.2 ± 2.0
505	29.92	0.00059	0.024	14.03	99.40	1.09	491.1 ± 2.0
535	30.79	0.00074	0.026	13.33	99.28	0.97	503.0 ± 1.3
565	30.75	0.00079	0.023	13.59	99.22	0.79	502.2 ± 1.2
590	30.89	0.00084	0.025	13.18	99.18	0.81	503.9 ± 1.4
615	31.85	0.00067	0.024	8.05	99.36	0.97	518.4 ± 1.2
635	33.71	0.00033	0.026	5.23	99.70	2.11	546.2 ± 1.8
650	36.31	0.00051	0.032	4.10	99.58	1.69	581.5 ± 2.7
675	39.75	0.00070	0.036	3.06	99.47	1.41	627.4 ± 3.9
705	43.75	0.00099	0.035	2.40	99.32	0.95	679.2 ± 4.5
735	49.27	0.00167	0.036	2.12	98.99	0.59	747.2 ± 4.3
Fusion	53.60	0.00306	0.044	1.73	98.31	0.39	795.6 ± 4.3
Total	30.83	0.00114	0.025	100.00	98.65	0.91	499.3 ± 1.5
			Middle-Upper Anchizone				
Sample	**2.**	J=0.010302					
425	10.93	0.00594	0.017	3.58	83.90	0.08	162.8 ± 3.2
450	11.81	0.00176	0.022	4.89	95.56	0.34	198.3 ± 2.6
475	18.19	0.00139	0.020	4.01	97.72	0.39	303.4 ± 1.8
505	27.32	0.00052	0.028	7.95	99.43	1.48	445.0 ± 1.9
535	28.35	0.00063	0.033	7.78	99.34	1.42	459.5 ± 2.2
565	27.99	0.00061	0.027	11.07	99.34	1.19	454.4 ± 1.6
590	27.24	0.00052	0.026	9.80	99.42	1.37	443.9 ± 1.9
615	26.65	0.00020	0.027	11.25	99.76	3.57	436.7 ± 2.1
635	26.34	0.00042	0.029	11.29	99.51	1.84	431.1 ± 1.9
655	26.38	0.00017	0.029	6.45	99.79	4.47	432.8 ± 2.0
675	26.63	0.00046	0.029	6.26	99.47	1.68	435.2 ± 1.3
705	27.30	0.00011	0.032	4.59	99.87	7.69	446.5 ± 2.1
735	28.57	0.00089	0.036	3.49	99.07	1.10	461.5 ± 3.8
770	30.24	0.00111	0.038	2.28	98.91	0.94	484.5 ± 3.7
815	31.41	0.00038	0.059	3.14	99.64	4.24	504.1 ± 2.9
Fusion	33.51	0.00066	0.148	2.15	99.44	6.10	532.3 ± 3.3
Total	25.84	0.00076	0.031	100.00	98.67	2.21	420.6 ± 1.8

Table 5.3 (Continued)

Release Temp. (°C)	$(^{40}Ar/^{39}Ar)^*$	$(^{36}Ar/^{39}Ar)^*$	$(^{37}Ar/^{39}Ar)^c$	^{39}Ar % of total	^{40}Ar non-atm.$^+$	$^{36}Ar_{Ca}$ %	Apparent Age (Ma)**
			Middle-Upper Anchizone				
Sample 3.	J=0.009965						
425	11.60	0.00595	0.022	3.07	84.81	0.10	168.7 ± 1.9
450	12.24	0.00123	0.013	3.54	97.00	0.28	201.8 ± 1.8
475	18.80	0.00039	0.015	3.09	99.37	1.08	308.0 ± 2.1
505	25.11	0.00060	0.041	4.95	99.28	1.86	400.3 ± 1.6
535	27.18	0.00036	0.042	8.18	99.60	3.19	430.9 ± 0.8
56μ	28.45	0.00048	0.045	9.16	99.49	2.50	448.2 ± 2.2
590	28.65	0.00066	0.045	7.03	99.32	1.87	450.4 ± 1.8
615	28.42	0.00045	0.042	11.88	99.52	2.55	447.9 ± 1.6
635	28.39	0.00043	0.041	10.59	99.55	2.62	447.7 ± 2.1
655	28.36	0.00029	0.039	10.46	99.69	3.72	447.8 ± 0.9
675	28.02	0.00029	0.037	9.65	99.69	3.53	443.0 ± 2.0
700	28.12	0.00037	0.038	7.15	99.60	2.82	444.1 ± 2.1
730	29.89	0.00023	0.033	4.41	99.77	4.01	469.4 ± 1.5
765	32.45	0.00021	0.049	3.39	99.80	6.41	504.5 ± 2.0
800	35.82	0.00087	0.094	2.07	99.29	2.92	547.3 ± 2.2
Fusion	34.66	0.00069	0.233	1.38	99.45	9.20	532.7 ± 2.3
Total	27.16	0.00061	0.042	100.00	99.01	2.85	428.0 ± 1.2
Total without 425-535 °C, 730 °C-fusion				65.92			447.0 ± 1.1
			Upper Anchizone				
Sample 4.	J=0.009662						
375	8.58	0.00857	0.043	0.23	70.44	0.14	102.3 ± 6.3
400	9.48	0.00309	0.002	1.67	90.32	0.01	143.4 ± 4.0
425	12.55	0.00137	0.003	2.46	96.74	0.05	200.1 ± 2.7
450	13.23	0.00064	0.040	2.89	98.55	1.70	214.1 ± 1.6
475	18.57	0.00084	0.045	3.08	98.65	1.47	293.9 ± 1.8
500	22.40	0.00081	0.046	4.91	98.92	1.54	349.9 ± 1.3
525	28.39	0.00027	0.082	4.54	99.72	8.29	436.2 ± 2.0
545	30.37	0.00043	0.070	5.93	99.58	4.48	462.4 ± 1.9
565	30.49	0.00039	0.071	6.55	99.62	4.91	464.1 ± 2.2
585	30.21	0.00043	0.065	8.50	99.58	4.09	460.2 ± 1.9
605	30.01	0.00047	0.074	8.09	99.54	4.30	457.4 ± 2.1
625	29.97	0.00051	0.062	8.93	99.49	3.30	456.6 ± 2.2
645	29.82	0.00033	0.056	9.54	99.67	4.68	455.4 ± 1.8
670	29.50	0.00021	0.055	9.21	99.78	7.03	451.4 ± 2.1
695	29.75	0.00042	0.053	6.97	99.58	3.46	454.0 ± 1.6
720	29.88	0.00041	0.052	5.20	99.59	3.41	455.8 ± 1.2
745	30.50	0.00066	0.057	3.26	99.36	2.33	463.3 ± 2.2
775	31.36	0.00009	0.050	2.61	99.91	15.54	477.0 ± 2.6
810	31.76	0.00057	0.065	3.48	99.47	3.13	480.5 ± 1.9
Fusion	31.27	0.00055	0.087	1.95	99.49	4.29	474.1 ± 2.6
Total	28.01	0.00053	0.059	100.00	99.22	4.31	428.3 ± 1.5
Total without 375-500 °C, 745 °C-fusion				68.91			457.2 ± 1.3

Table 5.3 (Continued)

Release Temp. (°C)	$(^{40}Ar/^{39}Ar)^*$	$(^{36}Ar/^{39}Ar)^*$	$(^{37}Ar/^{39}Ar)^c$	^{39}Ar % of total	^{40}Ar non-atm.$^+$	$^{36}Ar_{Ca}$ %	Apparent Age (Ma)**
			Upper Anchizone				
Sample	**5.**	J=0.009953					
500	16.00	0.00180	0.043	5.56	96.66	0.65	258.3 ± 1.2
540	26.88	0.00046	0.059	6.44	99.49	3.50	425.7 ± 1.5
570	27.38	0.00022	0.062	7.73	99.76	7.79	433.8 ± 1.6
590	27.48	0.00022	0.057	9.69	99.76	7.08	435.1 ± 1.3
610	27.50	0.00005	0.063	6.19	99.95	37.23	436.1 ± 1.6
630	27.57	0.00015	0.055	11.12	99.84	10.13	436.7 ± 0.9
660	27.66	0.00033	0.059	13.44	99.64	4.85	437.3 ± 1.1
690	27.87	0.00013	0.055	10.73	99.86	11.54	441.0 ± 1.1
720	28.05	0.00013	0.056	9.53	99.86	11.55	443.5 ± 1.3
750	28.47	0.00009	0.057	5.51	99.90	16.85	449.6 ± 1.0
780	28.79	0.00043	0.067	2.90	99.56	4.27	452.7 ± 2.6
830	29.08	0.00004	0.082	4.51	99.96	55.78	458.3 ± 1.8
900	29.09	0.00109	0.097	5.01	98.90	2.42	454.2 ± 2.1
Fusion	28.98	0.00027	0.373	1.63	99.81	37.31	456.4 ± 3.1
Total	27.20	0.00034	0.065	100.00	99.56	12.27	430.2 ± 1.1
Total without 500-540 °C				68.4			437.8 ± 0.9
			Upper Anchizone-Lower Greenschist				
Sample	**6.**	J=0.010095					
500	20.49	0.00186	0.034	5.64	97.30	0.50	330.9 ± 1.7
540	25.22	0.00062	0.048	12.78	99.27	2.11	406.4 ± 1.3
570	25.68	0.00029	0.049	8.28	99.65	4.52	414.6 ± 1.5
600	25.75	0.00020	0.048	17.56	99.77	6.59	416.0 ± 2.2
630	26.04	0.00028	0.046	11.07	99.68	4.53	419.9 ± 2.5
660	26.35	0.00023	0.048	9.93	99.73	5.58	424.5 ± 1.5
690	26.69	0.00038	0.041	8.56	99.57	2.98	428.8 ± 2.4
720	26.71	0.00040	0.042	6.06	99.55	2.83	429.0 ± 2.0
760	27.15	0.00065	0.042	5.27	99.28	1.74	434.1 ± 3.0
800	27.38	0.00071	0.050	3.78	99.23	1.92	437.3 ± 3.6
860	27.33	0.00009	0.049	5.00	99.90	15.49	439.1 ± 2.5
920	28.04	0.00041	0.064	5.21	99.56	4.25	448.0 ± 3.2
Fusion	29.44	0.00057	0.213	0.87	99.46	10.16	467.2 ± 4.2
Total	25.98	0.00045	0.048	100.00	99.46	4.56	418.0 ± 2.1

Table 5.3 (Continued)

Release Temp. (°C)	$(^{40}Ar/^{39}Ar)^*$	$(^{36}Ar/^{39}Ar)^*$	$(^{37}Ar/^{39}Ar)^c$	^{39}Ar % of total	^{40}Ar non-atm.$^+$	$^{36}Ar_{Ca}$ %	Apparent Age (Ma)**
			Upper Anchizone-Lower Greenschist				
Sample 7.	J=0.010111						
450	17.21	0.00240	0.044	4.34	95.87	0.50	278.2 ± 2.0
500	23.63	0.00027	0.054	4.74	99.66	5.47	385.3 ± 1.8
540	23.38	0.00026	0.047	16.00	99.66	4.87	381.6 ± 1.7
570	23.38	0.00009	0.047	12.00	99.88	14.40	382.4 ± 2.1
600	23.71	0.00031	0.044	7.22	99.60	3.80	386.3 ± 2.2
630	23.68	0.00023	0.043	8.32	99.70	5.00	386.1 ± 2.1
660	23.93	0.00032	0.047	8.74	99.60	4.07	389.5 ± 2.0
690	24.04	0.00028	0.043	8.19	99.64	4.13	391.2 ± 2.3
720	24.22	0.00022	0.050	6.84	99.73	6.32	394.2 ± 2.6
750	24.40	0.00036	0.049	7.72	99.56	3.75	396.3 ± 2.0
780	24.92	0.00039	0.063	5.10	99.53	4.39	403.6 ± 2.1
840	25.64	0.00087	0.069	4.81	98.99	2.16	412.1 ± 2.9
900	26.81	0.00033	0.147	4.23	99.66	12.07	431.4 ± 2.5
Fusion	32.60	0.00138	1.416	1.74	99.08	28.00	510.3 ± 2.3
Total	23.90	0.0004	0.077	100.00	99.46	6.22	388.5 ± 1.7
			Biotite Zone				
Sample 8.	J=0.010470						
450	49.25	0.14428	0.136	1.80	13.44	0.03	120.8 ± 7.2
500	18.51	0.00674	0.027	6.60	89.22	0.11	287.8 ± 1.6
540	21.23	0.00212	0.035	8.55	97.03	0.45	352.3 ± 1.2
565	21.13	0.00105	0.034	8.43	98.52	0.87	355.7 ± 0.8
590	20.76	0.00094	0.034	6.86	98.65	0.99	350.5 ± 1.3
615	20.53	0.00088	0.032	6.79	98.72	0.99	347.1 ± 2.6
645	20.41	0.00080	0.032	9.37	98.83	1.08	345.7 ± 0.9
675	20.52	0.00072	0.036	6.41	98.95	1.35	347.7 ± 1.0
710	20.67	0.00021	0.044	9.71	99.69	5.65	352.4 ± 1.2
745	20.95	0.00056	0.089	7.23	99.21	4.32	355.2 ± 1.2
780	21.23	0.00049	0.129	5.87	99.33	7.12	359.9 ± 1.1
815	21.51	0.00045	0.094	7.13	99.38	5.65	364.4 ± 1.0
860	22.31	0.00065	0.115	10.10	99.15	4.79	375.8 ± 1.0
Fusion	23.61	0.00097	0.207	5.13	98.83	5.78	394.4 ± 1.2
Total	21.52	0.00380	0.067	100.00	96.68	2.91	348.8 ± 1.3

Table 5.3 (Continued)

Release Temp. (°C)	$(^{40}Ar/^{39}Ar)^*$	$(^{36}Ar/^{39}Ar)^*$	$(^{37}Ar/^{39}Ar)^c$	^{39}Ar % of total	^{40}Ar non-atm.+	$^{36}Ar_{Ca}$ %	Apparent Age (Ma)**
			Biotite Zone				
Sample 9.	J=0.010291						
450	14.02	0.00734	0.019	1.77	84.50	0.07	207.5 ± 4.8
500	17.56	0.00666	0.022	1.72	88.76	0.09	268.3 ± 7.4
550	23.52	0.00223	0.012	3.37	97.17	0.14	381.0 ± 4.5
580	23.10	0.00092	0.003	2.65	98.79	0.10	380.5 ± 3.3
620	22.93	0.00066	0.006	3.88	99.12	0.25	379.2 ± 2.6
650	22.41	0.00034	0.006	5.71	99.53	0.50	372.8 ± 2.0
680	22.10	0.00073	0.007	5.29	99.00	0.26	366.3 ± 1.1
710	21.82	0.00024	0.005	9.40	99.65	0.58	364.3 ± 0.9
740	21.68	0.00011	0.006	8.54	99.82	1.54	362.7 ± 1.9
770	21.83	0.00074	0.005	9.11	98.97	0.19	362.1 ± 1.3
800	21.99	0.00033	0.006	7.30	99.53	0.51	366.3 ± 1.3
830	22.29	0.00073	0.014	4.44	99.01	0.54	369.2 ± 1.3
860	22.35	0.00007	0.018	5.39	99.88	6.67	373.0 ± 1.7
890	22.61	0.00013	0.012	8.08	99.80	2.34	376.7 ± 1.4
920	23.13	0.00005	0.011	7.95	99.92	6.65	384.8 ± 1.4
980	24.04	0.00036	0.012	10.14	99.53	0.88	397.1 ± 1.6
Fusion	29.12	0.00057	0.105	5.26	99.43	5.02	470.5 ± 1.8
Total	22.62	0.00067	0.014	100.00	98.96	1.76	374.1 ± 1.8
Sample 10.	J=0.010162						
450	17.00	0.00230	0.018	1.97	95.97	0.21	276.7 ± 3.6
500	21.17	0.00057	0.020	0.93	99.18	0.93	348.9 ± 3.8
540	21.29	0.00128	0.020	0.79	98.20	0.42	347.5 ± 7.0
565	21.32	0.00151	0.015	0.94	97.89	0.27	346.9 ± 2.0
590	21.26	0.00082	0.017	1.57	98.83	0.55	349.0 ± 2.6
615	21.11	0.00040	0.015	1.95	99.42	1.03	348.7 ± 2.8
645	20.95	0.00045	0.015	3.45	99.64	0.89	346.0 ± 1.8
675	20.78	0.00026	0.015	4.32	99.60	1.56	344.2 ± 1.2
710	20.57	0.00019	0.015	8.21	99.70	2.10	341.4 ± 0.7
740	20.38	0.00010	0.015	9.81	99.83	3.92	339.0 ± 0.7
780	20.33	0.00013	0.014	10.85	99.79	2.98	338.1 ± 0.7
815	20.46	0.00010	0.015	12.32	99.83	3.84	340.1 ± 0.6
850	20.76	0.00024	0.014	10.72	99.64	1.65	344.2 ± 0.9
920	21.22	0.00011	0.019	20.84	99.83	4.78	351.7 ± 0.4
Fusion	22.31	0.00009	0.038	11.33	99.87	11.82	368.1 ± 0.8
Total	20.86	0.00023	0.018	100.00	99.64	4.01	345.6 ± 0.9

Table 5.3 (Continued)

Release Temp. (°C)	$(^{40}Ar/^{39}Ar)^*$	$(^{36}Ar/^{39}Ar)^*$	$(^{37}Ar/^{39}Ar)^c$	^{39}Ar % of total	^{40}Ar non-atm.$^+$	$^{36}Ar_{Ca}$ %	Apparent Age (Ma)**
			Garnet Zone				
Sample 11.	J=0.010291						
450	38.02	0.04739	0.023	1.05	63.16	0.01	379.6 ± 2.8
500	23.20	0.00738	0.028	0.88	90.58	0.10	336.3 ± 4.1
550	20.37	0.00201	0.028	1.73	97.06	0.38	318.0 ± 1.8
600	19.96	0.00047	0.025	5.58	99.29	1.48	318.7 ± 1.4
640	20.43	0.00018	0.027	8.06	99.72	4.03	326.9 ± 1.5
670	21.71	0.00043	0.025	7.99	99.40	1.58	344.5 ± 1.4
700	21.93	0.00127	0.019	13.38	98.26	0.40	344.1 ± 1.1
730	21.53	0.00083	0.015	8.62	98.84	0.51	340.1 ± 1.6
760	21.29	0.00014	0.013	9.71	99.78	2.41	339.6 ± 0.9
790	21.26	0.00060	0.011	8.27	99.14	0.48	337.2 ± 0.8
820	21.46	0.00007	0.012	6.74	99.88	4.61	342.4 ± 1.0
850	21.50	0.00007	0.011	5.53	99.88	4.24	342.9 ± 1.2
885	21.46	0.00056	0.013	7.93	99.21	0.61	340.3 ± 0.6
920	21.41	0.00021	0.015	3.26	99.68	1.87	341.0 ± 1.5
980	21.57	0.00036	0.014	8.42	99.49	1.05	342.8 ± 1.1
Fusion	23.12	0.00050	0.065	2.87	99.35	3.50	364.6 ± 1.2
Total	21.58	0.00108	0.018	100.00	98.80	1.76	339.7 ± 1.2
Total without 450-600 °C and fusion				79.84			341.6 ± 1.0

*measured.

c corrected for post-irradiation decay of ^{37}Ar (35.1 day 1/2-life).

+$[^{40}Ar$ tot. - $(^{36}Ar$ atm.) (295.5)] / ^{40}Ar tot.

**calculated using correction factors of Dalrymple and others (1981); two sigma intralaboratory errors.

Figure 5.5. $^{40}Ar/^{39}Ar$ apparent age and apparent K/Ca spectra of whole-rock analyses of slate/phyllite samples from the chlorite zone, Miller Cove and Dunn Creek thrust sheets. Sample locations shown in Figure 5.3. Analytical uncertainties (two sigma intralaboratorary) are represented by vertical width of bars. Experimental temperatures increase from left to right.

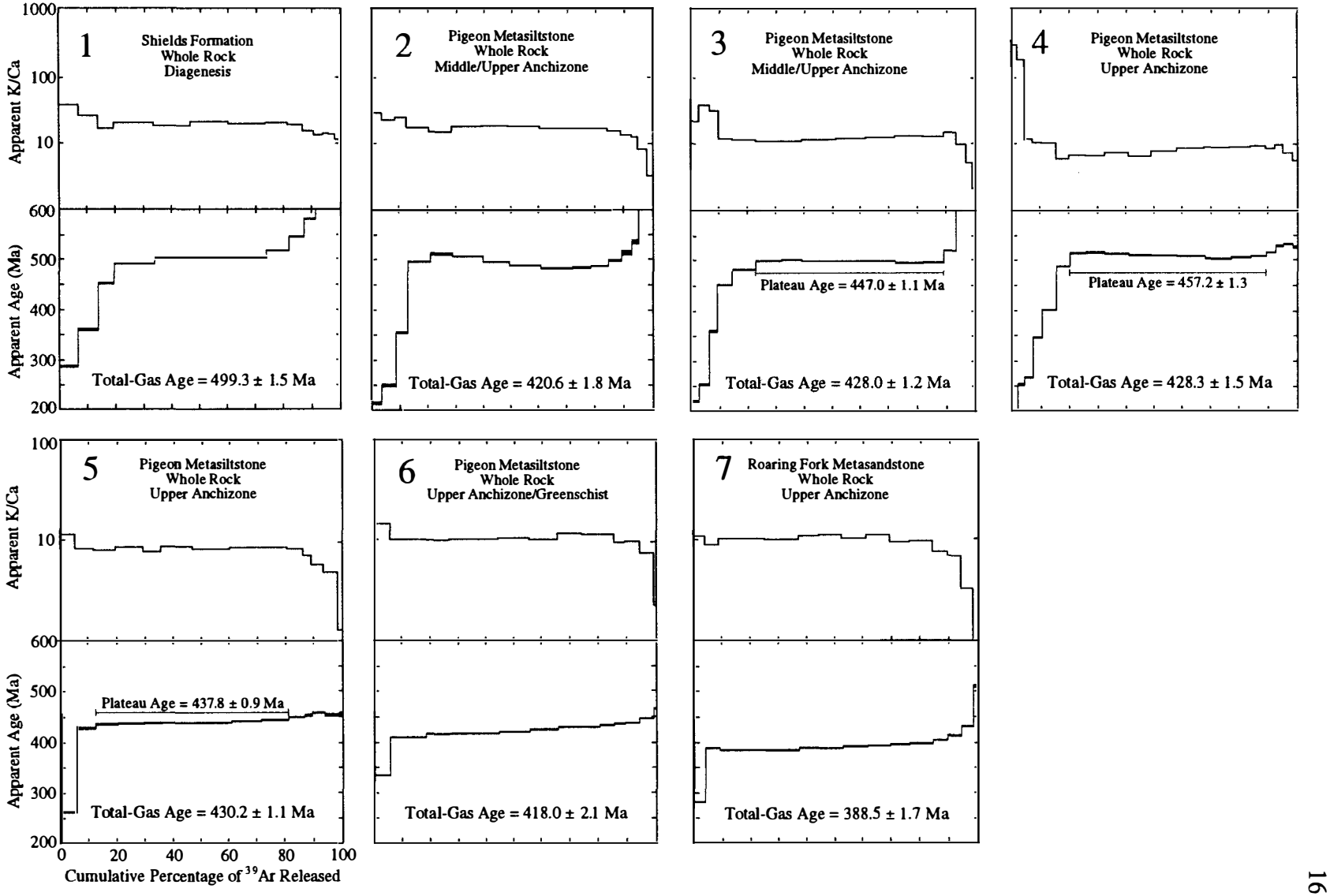
1
Shields Formation
Whole Rock
Diagenesis
Total-Gas Age = 499.3 ± 1.5 Ma
2
Pigeon Metasiltstone
Whole Rock
Middle/Upper Anchizone
Total-Gas Age = 420.6 ± 1.8 Ma
3
Pigeon Metasiltstone
Whole Rock
Middle/Upper Anchizone
Plateau Age = 447.0 ± 1.1 Ma
Total-Gas Age = 428.0 ± 1.2 Ma
4
Pigeon Metasiltstone
Whole Rock
Upper Anchizone
Plateau Age = 457.2 ± 1.3
Total-Gas Age = 428.3 ± 1.5 Ma
5
Pigeon Metasiltstone
Whole Rock
Upper Anchizone
Plateau Age = 437.8 ± 0.9 Ma
Total-Gas Age = 430.2 ± 1.1 Ma
6
Pigeon Metasiltstone
Whole Rock
Upper Anchizone/Greenschist
Total-Gas Age = 418.0 ± 2.1 Ma
7
Roaring Fork Metasandstone
Whole Rock
Upper Anchizone
Total-Gas Age = 388.5 ± 1.7 Ma
Apparent K/Ca
Apparent Age (Ma)
1000
100
10
600
500
400
300
200
0
20
40
60
80
100
Cumulative Percentage of ^{39}Ar Released

Figure 5.6. $^{40}Ar/^{39}Ar$ apparent age and apparent K/Ca spectra of whole-rock analyses of slate/phyllite samples from the biotite and garnet zones, Dunn Creek and Greenbrier thrust sheets. Sample locations shown in Figure 5.3. Data plotted as in Figure 5.5.

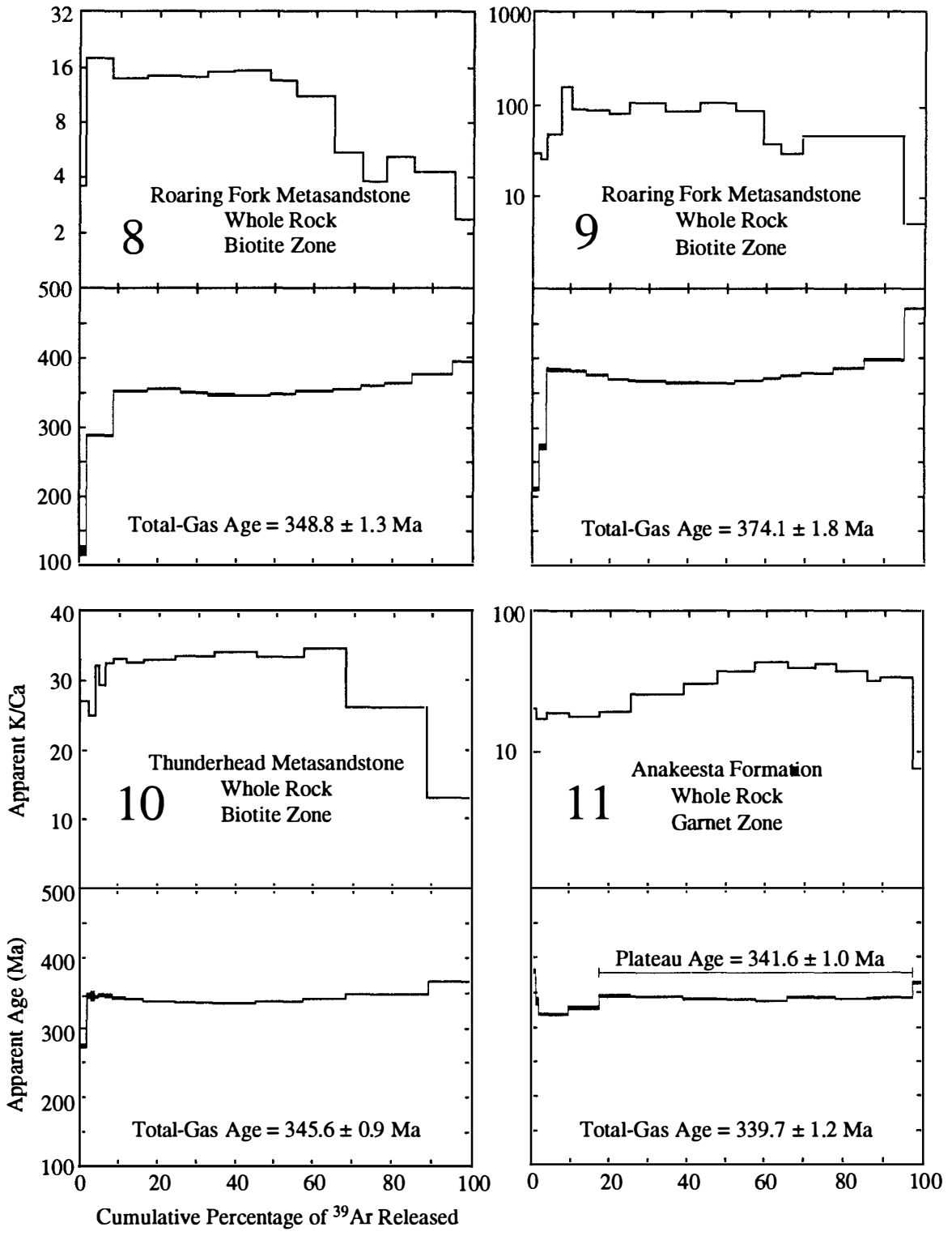
8
Roaring Fork Metasandstone
Whole Rock
Biotite Zone
Total-Gas Age = 348.8 ± 1.3 Ma
9
Roaring Fork Metasandstone
Whole Rock
Biotite Zone
Total-Gas Age = 374.1 ± 1.8 Ma
10
Thunderhead Metasandstone
Whole Rock
Biotite Zone
Total-Gas Age = 345.6 ± 0.9 Ma
11
Anakeesta Formation
Whole Rock
Garnet Zone
Plateau Age = 341.6 ± 1.0 Ma
Total-Gas Age = 339.7 ± 1.2 Ma
Apparent K/Ca
Apparent Age (Ma)
Cumulative Percentage of 39Ar Released

gas increments are characterized by systematically increasing apparent ages and variable apparent K/Ca ratios. Petrographic characteristics suggest that these increments correspond to experimental gas evolution from variably rejuvenated detrital potassium feldspar and chlorite. Systematically decreasing apparent K/Ca ratios are displayed by most high-temperature increments and are interpreted to reflect experimental evolution of gas from detrital plagioclase feldspar. In the lower grade samples (1-3: diagenesis and middle/upper anchizone), increasingly older apparent ages are recorded in the high-temperature increments, which likely relate to source ages. In the higher-grade samples (4-7: upper anchizone/lowermost greenschist facies), the high-temperature increase in apparent ages is much less marked, likely reflecting extensive Paleozoic metamorphic rejuvenation of the detrital plagioclase grains.

Four whole-rock phyllite samples (8-11) have been analyzed from the biotite and garnet zones. These display apparent K/Ca spectra with characteristics generally similar to those described for the lower grade slate/phyllite whole-rock samples (Fig. 5.6); however, there is generally much less variation in the apparent ages recorded by intermediate-temperature gas fractions. Most range between 340 Ma and 350 Ma.

Muscovite. Three muscovite concentrates were analyzed with $^{40}Ar/^{39}Ar$ incremental release techniques. The analytical data are listed in Table 5.4 and are presented as age spectra in Figure 5.7. These samples display only slightly discordant $^{40}Ar/^{39}Ar$ spectra (Fig. 5.7) that define plateau ages of 362 Ma (12), 372 Ma (13), and 377 Ma (14). Apparent K/Ca ratios are very large and display no significant or systematic intrasample variations. Therefore, they are not presented with the age spectra. The plateau ages are interpreted to date the last cooling through temperatures required for intracrystalline retention of argon. Although not fully calibrated experimentally, using the preliminary data of Robbins (1972) in the diffusion equations of Dodson (1973) suggests that temperatures of $350 \pm 25^{\circ}$ C are required for argon retention in muscovite.

Table 5.4. $^{40}Ar/^{39}Ar$ analytical data for incremental heating experiments on muscovite concentrates from the western Blue Ridge, Tennessee-North Carolina.

Release Temp. (°C)	$(^{40}Ar/^{39}Ar)^*$	$(^{36}Ar/^{39}Ar)^*$	$(^{37}Ar/^{39}Ar)^c$	^{39}Ar % of total	^{40}Ar non-atm.$^+$	$^{36}Ar_{Ca}$ %	Apparent Age (Ma)**
			Staurolite Zone				
Sample 12. J=0.009750							
550	19.63	0.01226	0.026	1.10	81.53	0.06	261.6 ± 7.9
600	22.29	0.00248	0.007	3.31	96.69	0.008	344.1 ± 2.7
630	22.18	0.00116	0.004	2.87	98.43	0.09	348.2 ± 2.0
660	22.02	0.00009	0.003	2.58	99.85	0.97	350.3 ± 1.6
690	21.99	0.00119	0.006	3.66	98.38	0.13	345.2 ± 2.5
720	22.14	0.00059	0.005	3.70	99.19	0.22	350.0 ± 2.4
750	22.48	0.00124	0.006	5.10	98.34	0.13	352.1 ± 1.6
780	22.91	0.00128	0.007	7.53	98.33	0.15	358.2 ± 1.1
810	23.13	0.00091	0.003	12.00	98.82	0.10	363.0 ± 0.6
840	22.65	0.00083	0.004	9.89	98.89	0.12	356.3 ± 0.9
870	22.64	0.00096	0.005	8.56	98.72	0.14	355.6 ± 0.9
900	22.89	0.00062	0.005	9.43	99.17	0.22	360.7 ± 1.0
950	23.31	0.00067	0.004	17.94	99.12	0.17	366.5 ± 0.6
Fusion	23.35	0.00034	0.006	12.33	99.55	0.46	368.6 ± 0.5
Total	22.83	0.00097	0.005	100.00	98.69	0.21	358.3 ± 1.1
Total without 550-750 °C				77.69			362.3 ± 0.7
Sample 13. J=0.009751							
550	22.31	0.00931	0.013	1.38	87.65	0.04	314.7 ± 5.9
600	24.91	0.00174	0.005	1.69	97.91	0.07	384.9 ± 5.5
630	24.22	0.00130	0.009	2.62	98.39	0.18	376.8 ± 5.2
660	23.34	0.00083	0.005	3.89	98.92	0.17	366.3 ± 1.7
690	22.97	0.00086	0.008	4.99	98.87	0.26	360.8 ± 1.7
720	23.65	0.00110	0.007	6.63	98.60	0.16	369.5 ± 1.4
750	24.08	0.00099	0.006	12.52	98.76	0.16	376.1 ± 0.6
780	23.90	0.00079	0.006	11.96	99.00	0.19	374.4 ± 0.7
810	23.63	0.00109	0.008	5.85	98.61	0.19	369.4 ± 1.9
840	23.65	0.00096	0.005	6.76	98.78	0.13	370.2 ± 1.4
870	23.64	0.00077	0.007	5.97	99.02	0.24	370.9 ± 1.2
900	23.40	0.00082	0.005	6.58	98.95	0.16	367.2 ± 1.4
940	23.46	0.00088	0.003	8.20	98.87	0.09	367.8 ± 1.4
980	23.68	0.00075	0.005	11.50	99.05	0.17	371.5 ± 0.8
Fusion	23.73	0.00047	0.005	9.47	99.39	0.28	373.4 ± 0.6
Total	23.68	0.00099	0.006	100.00	98.73	0.18	370.5 ± 1.3
Total without 550-690 °C				85.44			371.7 ± 0.9

Table 5.4 (Continued)

Release Temp. (°C)	$(^{40}Ar/^{39}Ar)^*$	$(^{36}Ar/^{39}Ar)^*$	$(^{37}Ar/^{39}Ar)^c$	^{39}Ar % of total	^{40}Ar non-atm.+	$^{36}Ar_{Ca}$ %	Apparent Age (Ma)**
			Kyanite Zone				
Sample 14.	J=0.009750						
550	25.98	0.04631	0.051	0.79	47.31	0.03	194.9 ± 10.2
600	25.62	0.00683	0.014	2.39	92.10	0.06	357.2 ± 6.8
630	26.78	0.00238	0.017	2.60	97.35	0.20	390.8 ± 3.1
660	25.93	0.00218	0.003	3.06	97.49	0.04	380.2 ± 2.1
690	25.20	0.00170	0.009	4.32	97.99	0.15	372.2 ± 2.6
720	25.16	0.00197	0.010	4.85	97.66	0.13	370.6 ± 1.3
750	25.77	0.00168	0.005	9.91	98.05	0.09	380.0 ± 2.0
780	25.81	0.00181	0.005	7.39	97.91	0.07	380.1 ± 1.4
810	25.71	0.00112	0.004	11.82	98.69	0.11	381.5 ± 0.6
840	25.51	0.00148	0.005	7.45	98.26	0.08	377.2 ± 1.7
870	25.33	0.00159	0.005	7.61	98.12	0.08	374.4 ± 1.9
900	25.21	0.00138	0.005	7.89	98.36	0.09	373.5 ± 2.0
950	25.22	0.00142	0.003	9.05	98.31	0.06	373.6 ± 1.9
1000	25.25	0.00110	0.003	7.19	98.69	0.08	375.3 ± 1.9
1050	25.52	0.00085	0.004	8.31	99.00	0.14	380.0 ± 1.7
Fusion	25.63	0.00052	0.005	5.39	99.68	0.25	382.8 ± 1.8
Total	25.53	0.00191	0.006	100.00	97.78	0.10	375.8 ± 0.8
Total without 550-600 °C				91.16			377.2 ± 0.7

*measured.

c corrected for post-irradiation decay of ^{37}Ar (35.1 day 1/2-life).

+$[^{40}Ar$ tot. - $(^{36}Ar$ atm.) (295.5)] / ^{40}Ar tot.

**calculated using correction factors of Dalrymple and others (1981); two sigma intralaboratory errors.

Figure. 5.7. $^{40}Ar/^{39}Ar$ apparent age spectra of muscovite concentrates from the staurolite and kyanite zones, Greenbrier thrust sheet. Sample locations shown in Figure 5.3. Data plotted as in Figure 5.5.

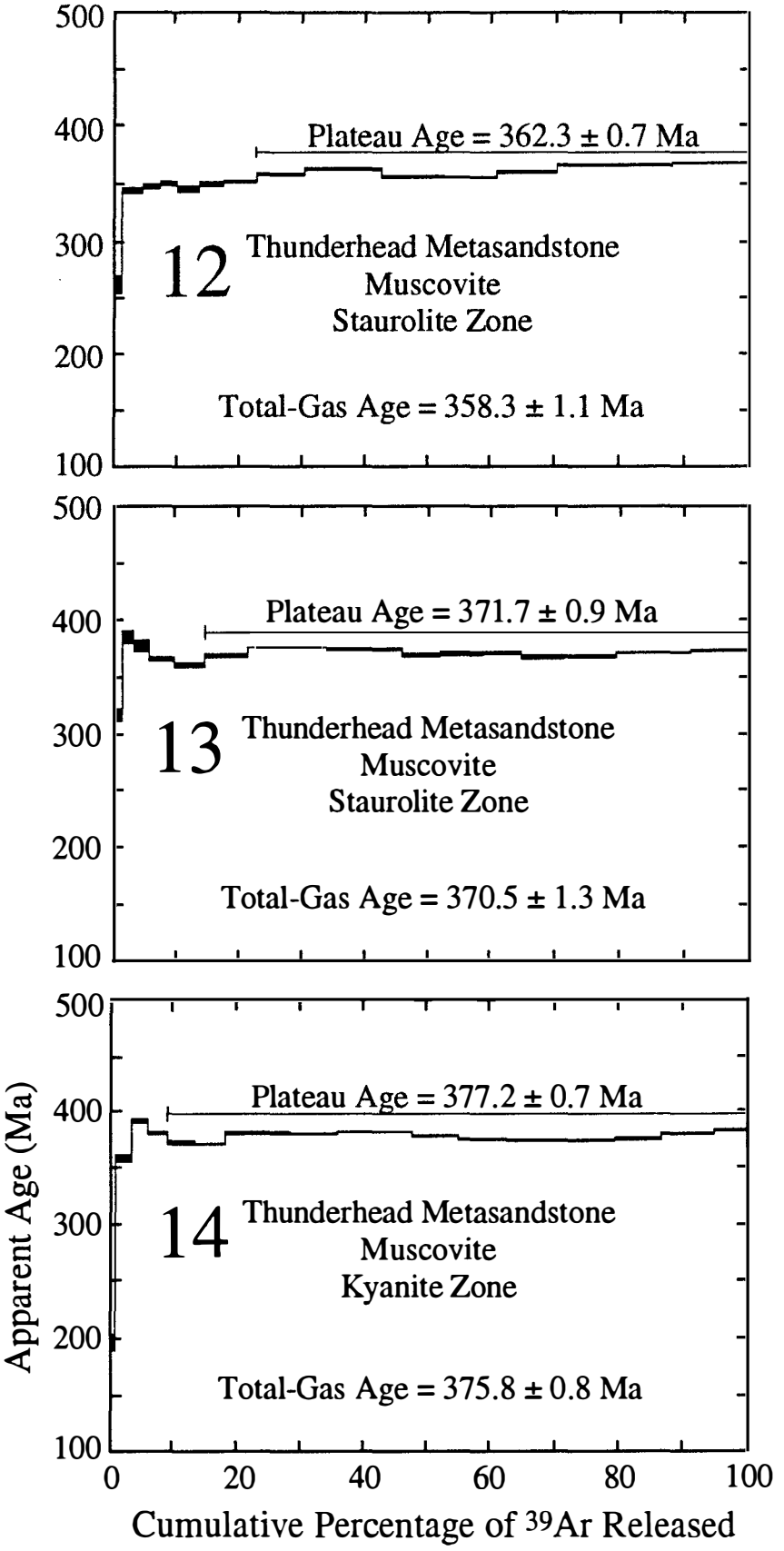
500
400
300
200
100
Plateau Age = 362.3 ± 0.7 Ma
12
Thunderhead Metasandstone
Muscovite
Staurolite Zone
Total-Gas Age = 358.3 ± 1.1 Ma
Plateau Age = 371.7 ± 0.9 Ma
13
Thunderhead Metasandstone
Muscovite
Staurolite Zone
Total-Gas Age = 370.5 ± 1.3 Ma
Plateau Age = 377.2 ± 0.7 Ma
14
Thunderhead Metasandstone
Muscovite
Kyanite Zone
Total-Gas Age = 375.8 ± 0.8 Ma
Apparent Age (Ma)
0
20
40
60
80
100
Cumulative Percentage of 39Ar Released

COMPARISON WITH PREVIOUS GEOCHRONOLOGY

The ^{40}Ar / ^{39}Ar results from the present study area are similar to and compatible with results from previous geochronological studies in adjacent areas of the western Blue Ridge. Whole-rock conventional K-Ar ages determined for Ocoee Supergroup slates and phyllites from the chlorite, biotite, and garnet metamorphic zones (Kish and Harper, 1973; Kish, 1982, 1991) yielded age patterns that are similar to those of the present study. Samples from a transect along the Little Tennessee River (chlorite and biotite zones) yield ages that range from 483 to 379 Ma and show a gradual younging to the southeast (Fig. 5.2). Samples from a transect along the Ocoee River (chlorite and biotite zones) yield somewhat younger ages between 415 and 351 Ma (Fig. 5.2). Two samples collected near Tellico Plains (chlorite zone) yield ages of 411 and 415 Ma, whereas samples from north of Tuckaleechee Cove (chlorite zone) show slightly younger ages of 393 and 368 Ma (Fig. 5.2). Two samples from several kilometers west of the present transect (chlorite zone) yield ages of 420 and 421 Ma (Fig. 5.2). A sample from Mt. LeConte (garnet zone) yielded an age of 353 Ma. This result is comparable to the plateau age of 342 Ma determined for sample 11 also collected from Mt. LeConte (Fig. 5.2).

Muscovite ages from the present study are similar to most previously determined muscovite ages from the western Blue Ridge which range from 350 to 370 Ma (Fig. 5.2). The 377 Ma age determined for sample 14, however, is the oldest muscovite age in this part of the western Blue Ridge and is believed to closely date peak metamorphic conditions in this area. $^{40}Ar/^{39}Ar$ muscovite ages from the Murphy belt area are ~ 330 Ma (Dallmeyer, 1988; Fig. 5.2) and somewhat younger than other areas of the western Blue Ridge. $^{40}Ar/^{39}Ar$ biotite ages from several kilometers south of the muscovite samples of the present study (Fig. 5.2) yield $^{40}Ar/^{39}Ar$ ages of 350 to 360 Ma (Dallmeyer, 1975; recalculated from the initially published results using the decay constants proposed by Steiger and Jäger, 1977). These slightly younger ages are likely the result of the lower

temperatures required for Ar retention in biotite. Most other biotite ages from the Blue Ridge are anomalously old compared to muscovite ages from the same sample suggesting the presence of excess ^{40}Ar in biotite in this area (Kish, 1989).

INTERPRETATION

Whole-rock slate/phyllite samples from the middle-upper anchizone (2-5) yield $^{40}Ar/^{39}Ar$ plateau and intermediate temperature ages of 450 Ma. These dates contrast with apparent ages of 350 Ma defined by intermediate-temperature increments of samples from the biotite and garnet zones (8-11). It is unlikely that samples collected only several kilometers apart could have experienced cooling histories after a single thermal event that would result in an 100 Ma difference in apparent ages. Results from the present study are therefore not consistent with previously reported models for the Blue Ridge that suggested prolonged maintenance of post-metamorphic temperatures in excess of those required for argon retention in higher grade parts of the Blue Ridge (Hadley, 1964; Dallmeyer, 1975) Alternative explanations include: (1) incomplete rejuvenation of detrital components at lowest metamorphic grades resulting in anomalously old apparent ages; and/or (2) polymetamorphism.

Geochronological resolution of detrital from authigenic very fine-grained white mica is difficult in very low-grade rocks. Dallmeyer and Takasu (1992) reported results of $^{40}Ar/^{39}Ar$ analyses of whole-rock slate/phyllite samples from a progressively metamorphosed sedimentary sequence in the Narragansett basin (Massachusetts-Rhode Island). They demonstrated that very fine-grained, pelitic slate/phyllite whole-rock systems (similar to those described herein from the western Blue Ridge) were completely rejuvenated during late Paleozoic metamorphism at grades above the middle anchizone (using illite crystallinity calibrations identical to those described herein). If appropriate for the western Blue Ridge, these controls suggest that except for sample 1 (diagenesis zone),

intracrystalline argon systems within detrital mica grains in all other samples were likely completely rejuvenated during Paleozoic metamorphism(s). This implies that the intermediate-temperature $^{40}Ar/^{39}Ar$ ages recorded by samples 2-11 relate to the time of metamorphic rejuvenation and/or an associated growth of newly-formed white mica. The results combine to suggest two distinct tectonothermal episodes; one at 440 to 460 Ma (recorded in samples 2-5) and another at 340 to 380 Ma (recorded in samples 8-14). The latter thermal event apparently partially rejuvenated intracrystalline argon systems formed during the earlier event in samples 6 and 7. Muscovite separates (samples 12-14) from the staurolite and kyanite zones display slightly older ages (360-380 Ma) than whole-rock samples (340-350 Ma) as a result of higher temperatures of argon retention for muscovite. The muscovite results are therefore believed to closely date the younger metamorphic event (growth of porphyroblasts) in this area.

Interpretation of the geochronologic results as a record of polymetamorphic evolution is consistent with textural characteristics described earlier. Although the distribution of metamorphic isograds suggests a progressive Barrovian-type metamorphism (Fig. 5.3), metamorphic textures from the study area and adjacent areas document a polymetamorphic history (Hadley and Goldsmith, 1963; King, 1964; Power and Forrest, 1971; Mohr, 1973; Labotka and Shireman, 1991). Hadley and Goldsmith (1963) recognized that peak metamorphic conditions were preceded by and followed by deformation and lower grade metamorphism. The regional S_1 cleavage developed during an early kinematic phase of deformation. Porphyroblasts overgrew S_1 cleavage during a higher grade static phase of metamorphism. Porphyroblast growth was followed by S_2 crenulation cleavage that forms a penetrative schistosity at higher metamorphic grades. It is therefore likely that the 440 to 460 Ma whole-rock ages recorded within the chlorite metamorphic zone (where textural evidence for polymetamorphism is lacking) record the development of the regional S_1 cleavage in the western Blue Ridge. The younger, 340 to

380 Ma ages recorded within biotite and higher metamorphic zones are interpreted to date the time of growth of porphyroblasts and thus the peak thermal conditions in this area. Together the $^{40}Ar/^{39}Ar$ results suggest that rocks of the western Blue Ridge experienced major periods of metamorphism at 440 to 460 Ma and at 360 to 380 Ma.

Thus, despite the apparently simple metamorphic isograd pattern in the western Blue Ridge (Fig. 5.2), the present geochronologic results and metamorphic textures suggest a polymetamorphic history for this area. Unlike areas such as the northern Appalachians, however, detailed metamorphic petrology has only locally been conducted in the western Blue Ridge (Nesbitt and Essene, 1982; Mohr and Newton, 1983; Eckert and others, 1989). Resolution of areas where peak Paleozoic metamorphic conditions occurred in the early Paleozoic from areas that experienced peak conditions during a later period is not yet possible and awaits detailed metamorphic petrology.

TECTONIC IMPLICATIONS

Interpreting the geologic significance of the $^{40}Ar/^{39}Ar$ results depends upon calibration of the Paleozoic time-scale (Palmer, 1983; Harland and others, 1989). Snelling (1985) and Kunk and others (1985) suggested that the Ordovician-Silurian boundary (base of the Llandovery) is 435 to 440 Ma. This together with a 420 Ma calibration of the Ludlow (Wyborn and others, 1982) is used for interpretation of the $^{40}Ar/^{39}Ar$ results from the western Blue Ridge. McKerrow and others (1980) proposed that the middle Devonian is bracketed by 396 and 382 Ma and that the Silurian-Devonian boundary is 412 Ma. Gale and others (1980) discussed this calibration and suggested a compromise that defined the base of the Devonian at 400 Ma and the Middle Devonian to be bracketed by 387 and 374 Ma. This proposition is consistent with more recent time-scale calibrations (Palmer, 1983; Harland and others, 1989) and is used here.

Samples 2 to 5 were metamorphosed to conditions of the middle/upper anchizone. These should be near or below closure temperature of Ar in muscovite (Dallmeyer and Takasu, 1992). The 440 to 460 Ma ages from these whole-rock samples therefore closely date metamorphism. The ages are in general agreement with, although slightly younger than, the filling of the presently adjacent Sevier foreland basin by Blountian synorogenic sediments. Initial downwarping of the Sevier basin (reflected by deposition of the Whitesburg Formation; Shanmugan and Lash, 1982) occurred in the early Llanvirnian (475-480 Ma; Drake and others, 1989) and probably reflected eastward loading of the crust by thrust sheets. The major premetamorphic faults in this area (Dunn Creek, Greenbrier, and Hayesville) may have propagated at this time. Downwarping was followed by deposition of pelagic (Blockhouse Formation) and distal turbidite (Sevier Formation) sediments (Shanmugan and Lash, 1982) during the early Llanvirnian to middle Llandeilian (475-465 Ma; Drake and others, 1989). The ages reported here, however, correspond most closely to deposition of the overlying molasse deposits (Bays Formation), which were deposited during the middle Llandeilian to early Caradocian (465-455 Ma; Drake and others, 1989). A similar correspondence between radiometric uplift ages and molasse sedimentation has been recognized in other orogenic belts (Trümpy, 1973; Eisbacher and Gabrielse, 1975).

A Late Devonian to earliest Mississippian paleontologic age assignment for regionally metamorphosed Walden Creek Group rocks of the western Blue Ridge by Unrug, Unrug, and Palmes (1991) is inconsistent with results from the present study that indicate a Middle to Late Ordovician metamorphism. It is also inconsistent with most previous geochronologic results in the western Blue Ridge, as well as previous paleontologic results and geologic mapping. The present $^{40}Ar/^{39}Ar$ results require that the Walden Creek Group be no younger than Late Ordovician, although stratigraphic arguments require an earlier (pre-Chilhowee) age. A Middle to Late Ordovician

metamorphic age is also inconsistent with proposed stratigraphic correlations between rocks of the Murphy belt and Early Devonian strata of the Talladega belt (Tull and Guthrie, 1985; Thompson and Tull, 1991). The present results require that all Murphy belt units are no younger than Late Ordovician.

The 340 to 380 Ma whole-rock and muscovite ages are interpreted to indicate a Middle-Late Devonian tectonothermal event. The nature and importance of middle Paleozoic tectonism is poorly understood in the southern Appalachians (Ferrill and Thomas, 1988; Osberg and others, 1989; Tull and Telle, 1989). In the northern and central Appalachians, a thick Devonian clastic sequence in the foreland is temporally associated with metamorphism in the hinterland (Osberg and others, 1989). In the southern Appalachians, however, only a thin Lower to Middle Devonian clastic sequence (Frog Mountain Formation) is locally preserved in the foreland (Ferrill and Thomas, 1988). Within the Tennessee foreland, most of the Devonian underlying the sub-Chattanooga shale unconformity is absent (Colton, 1970). Tull and others (1988), however, provided fossil evidence to link the thick Cambrian to Devonian predominately clastic sequence of the Talladega belt with the Appalachian foreland in Alabama. This suggests that the southernmost Apppalachian foreland may have once also contained a similar cover sequence. The stratigraphic record in the southern Appalachians therefore may not be inconsistent with a Middle to Late Devonian tectonothermal event.

REFERENCES CITED

Armstrong, R. L., 1966, K-Ar dating of plutonic and volcanic rocks in orogenic belts, *in* Schaeffer, O.A., and Zahringer, J., eds., Potassium-argon dating: New York, Springer-Verlag, p. 117-133.

Bearce, D. N., 1969, Geology of the southwestern Bald Mountains in the Blue Ridge province of Tennessee: Southeastern Geology, v. 11, p. 21-36.

Billings, M. P., and Cleaves, A. B., 1934, Paleontology of the Littleton area, New Hampshire: American Journal of Science, v. 28, p. 412-438.

Boyer, S. E., and Elliott, D., 1982, Thrust systems: American Association of Petroleum Geologists Bulletin, v. 66, p. 1196-1230.

Broadhead, T. W., and Hatcher, R. D., Jr., 1992, ?Fossil and nonfossil carbonate allochems: Importance for correlation and origin of limestone bodies of the western Blue Ridge, Tennessee: Geological Society of America Abstracts with Programs, v. 24, no. 2, p. 5.

Broadhead, T. W., Hatcher, R. D., Jr., and Costello, J. O., 1991, Tectonic and stratigraphic implications of mid-Paleozoic (?) fossils from the Late Proterozoic (?) Walden Creek Group rocks in the Foothills Belt, Eastern Tennessee, *in* Kish, S.A., ed., Studies of Precambrian and Paleozoic Stratigraphy in the western Blue Ridge: Carolina Geological Society Field Trip Guidebook, p. 39-44.

Brookins, D. G., Berdan, J.M., and Stewart, D. B., 1973, Isotopic and Paleontologic evidence for correlatng three volcanic sequences in the Maine coastal belt: Geological Society of America Bulletin, v. 48, p. 1619-1628.

Butler, J. R., 1972, Age of Paleozoic regional metamorphism in the Carolinas, Georgia, and Tennessee southern Appalachians: American Journal of Science, v. 273-A, p. 72-88.

Butler, J. R., 1991, Metamorphism, *in* Horton, J.W., Jr., and Zullo, V.A., eds., The Geology of the Carolinas-Carolina Geological Society 50th Anniversary Volume: Knoxville, University of Tennessee Press, p. 127-141.

Colton, G. W., 1970, The Appalachian basin-Its depositional sequences and their geologic relationships, *in* Fisher, G.W., Pettijohn, F. J., Read, J. C., Jr., and Weaver, K. N., eds., Studies of Appalachian geology: central and southern: New York, Wiley-Interscience, p. 5-47.

Connelly, J. B., and Woodward, N. B., 1992, Taconian foreland-style thrust system in the Great Smoky Mountains, Tennessee: Geology, v. 20, p. 177-180.

Cook, F. A., Albaugh, D. S., Brown, L. D., Oliver, J. E., Kaufman, S., and Hatcher, R. D., Jr., 1979, Thin-skinned tectonics in the crystalline southern Appalachians: COCORP seismic-reflection profiling of the Blue Ridge and Piedmont: Geology, v. 7, p. 563-568.

Çoruh, C., Costain, J. K., Hatcher, R. D., Jr., Pratt, T. L., Williams, R. T., and Phinney, R. A., 1987, Results from regional vibroseis profiling: Appalachian ultradeep core hole site study: Geophysical Journal of the Royal Astronomical Society, v. 89, p. 473-474.

Costello, J. O., 1984, Relationships between the Cartersville fault and Great Smoky fault in the southern Appalachians: A reinterpretation [M.S. thesis]: Columbia, South Carolina, University of South Carolina, 75 p.

Costello, J. O., and Hatcher, R. D., Jr., 1986, Contact relationships between the Walden Creek Group and Great Smoky Group in Ocoee Gorge, Tennessee: Implications on the regional extent of the Greenbrier fault: Geological Society of America Abstracts with Programs, v. 18, p. 216.

Costello, J. O., 1991, Problems of stratigraphic correlation between Great Smoky, Snowbird, and Walden Creek Groups between the Great Smoky Mountains National Park, Central east Tennessee, and Ocoee Gorge, southeastern Tennessee, *in* Kish, S.A., ed., Studies of Precambrian and Paleozoic Stratigraphy in the western Blue Ridge: Carolina Geological Society Field Trip Guidebook, p. 13-25.

Crickmay, G. W., 1936, Status of the Talladega Series in southern Appalachian stratigraphy: Geological Society of America Bulletin, v. 47, p. 1371-1392.

Culver, S. J., 1991, Early Cambrian foraminifera from west Africa: Science, v. 254, p. 689-691.

Culver, S. J., Repetski, J. E., Pojeta, J., Jr., and Hunt, D., 1990, Early Cambrian Foraminifera and metazoan shelly fossils from west Africa: Geological Society of America Abstracts with Programs, v. 22, no. 7, p. 221.

Dallmeyer, R. D., 1975, Incremental $^{40}Ar/^{39}Ar$ ages of biotite and hornblende from retrograde basement gneisses of the southern Blue Ridge: Their bearing on the age of Paleozoic metamorphism: American Journal of Science, v. 275, p. 444-460.

Dallmeyer, R. D., 1982, $^{40}Ar/^{39}Ar$ ages from the Narragansett basin and southern Rhode Island basement terrane: their bearing on the extent and timing of Alleghanian tectonothermal events in New England: Geological Society of America Bulletin, v. 93, p. 1118-1130.

Dallmeyer, R. D., 1988, Polymetamorphic evolution of the western Blue Ridge allocthon: evidence from $^{40}Ar/^{39}Ar$ mineral ages, *in* Fritz, W. J., and LaTour, E. L., eds., Geology of the Murphy belt and related rocks-Georgia and North Carolina: Georgia Geological Society Guidebook, v. 8, p. 95-101.

Dallmeyer, R. D., Courtney, P. S., and Wooten, R. M., 1978, Stratigraphy, structure, and metamorphism east of the Murphy syncline: Georgia Geological Society Guidebook 17, 74 p.

Dallmeyer, R. D., and Gil-Ibarguchi, I., 1990, Age of amphibolitic metamorphism in the ophiolitic unit of the Morais allochthon (Portugal): Implications for early Hercynian orogenesis in the Iberian Massif: Geological Society of London Journal, v. 147, p. 873-878.

Dallmeyer, R. D., and Keppie, J. D., 1987, Polyphase late Paleozoic tectonothermal evolution of the southwestern Meguma Terrane, Nova Scotia: evidence from $^{40}Ar/^{39}Ar$ mineral ages: Canadian Journal of Earth Sciences, v. 24, p. 1242-1254.

Dallmeyer, R. D., and Takasu, A., 1992, $^{40}Ar/^{39}Ar$ Ages of detrital muscovite and whole-rock slate/phyllite, Narragansett basin, RI-MA, USA: implications for rejuvination during very low-grade metamorphism: Contributions to Mineralogy and Petrology, v. 110, p. 515-527.

Dallmeyer, R. D., Wright, J. E., Secor, D. T., Jr., and Snoke, A. W., 1986, Character of the Alleghanian orogeny in the southern Appalachians: Part II. Geochronological constraints on the tectonothermal evolution of the eastern Piedmont in South Carolina: Geological Society of America Bulletin, v. 97, p. 1329-1344.

Dalrymple, G. B., Alexander, E. C., Lanphere, M. A., and Kraker, G. P., 1981, Irradiation of samples for $^{40}Ar/^{39}Ar$ dating using the Geological Survey TRIGA reactor: U.S. Geological Survey Professional Paper 1176, 55 p.

Davis, G. L., Tilton, G. R., and Wetherill, G. W., 1962, Mineral ages from the Appalachian province in North Carolina and Tennessee: Journal of Geophysical Research, v. 67, p., 1987-1996.

Dodson, M. H., 1973, Closure temperature in cooling geochronoligical and petrological systems: Contributions to Mineralogy and Petrology, v. 40, p. 259-274.

Drake, A. A., Jr., Sinha, A. K., Laird, J., and Guy, R. E., 1989, The Taconic orogen, *in* Hatcher, R.D., Jr., Thomas, W. A., and Viele, G. W., eds., The Appalachian-Ouachita Orogen in the United States: Boulder, Colorado, Geological Society of America, The Geology of North America, v. F-2, p. 101-177.

Dunoyer de Segonzac, G., 1969, Les minéraux argileux dans la diagenèse-Passage au metamorphisme: Service de la Carte Géologique Alsace et Lorraine Mémoires, v. 29, p. 320.

Dunoyer de Segonzac, G., 1970, The transformation of clay minerals during diagenesis and low-grade metamorphism: A review: Sedimentology, v. 15, p. 281-346.

Eckert, J. O., Hatcher, R. D., Jr., and Mohr, D. W., 1989, The Wayah granulite-facies metamorphic core, southwestern North Carolina: High grade culmination of Taconic metamorphism in the southern Blue Ridge: Geological Society of America Bulletin, v. 101, p. 1434-1447.

Eisbacher, G. H., and Gabrielse, H., 1975, The molasse facies of the Columbian orogen, Canadian Cordillera: Geologische Rundschau, v. 64, p. 85-100.

Ferguson, H. W., and Jewell, W. B., 1951, Geology and barite deposits of the Del Rio District, Cocke County, Tennessee: Tennessee Division of Geology Bulletin, v. 57, 228 p.

Ferrill, B. A., and Thomas, W. A., 1988, Acadian dextral transpression and synorogenic sedimentary successions in the Appalachians: Geology, v. 16, p. 604-608.

Fullagar, P. D., and Bottino, M. L., 1970, Sulfide mineralization and rubidium-strontium geochronology at Ore Knob, North Carolina and Ducktown, Tennessee: Economic Geology, v. 65, p. 541-550.

Fullagar, P.D., and Odom, A. L., 1973, Geochronology of Precambrian gneisses in the Blue Ridge Province of northwestern North Carolina and adjacent parts of Virginia and Tennessee: Geological Society of America Bulletin, v. 84, p. 3065-3080.

Gale, N. H., Beckinsale, R. D., Wadge, A. J., 1980, Discussion of a paper by McKerrow, Lambert and Chamberlain on the Ordovician, Silurian and Devonian time scales: Earth and Planetary Science Letters, v. 51, p. 9-17.

Glover, L., III; Speer, J. A., Russell, G. S., and Farrar, S. S., 1983, Ages of regional metamorphism and ductile deformation in the central and southern Appalachians: Lithos, v. 16, p. 223-245.

Hadley, J. B., 1964, Correlation of isotopic ages, crustal heating and sedimentation in the Appalachian region, *in* Lowry, W. D., ed., Tectonics of the Southern Appalachians: Virginia Polytechnical Institute, Department of Geological Sciences Memoir 1, p. 33-44.

Hadley, J. B., 1970, The Ocoee Series and its possible correlatives, *in* Fisher, G. S., Pettijohn, F. J., Reed, J. C., and Weaver, K. N., eds., Studies of Appalachian geology: Central and southern: New York, Wiley-Interscience, p. 247-259.

Hadley, J. B., and Goldsmith, R., 1963, Geology of the eastern Great Smoky Mountains, North Carolina and Tennessee: U.S. Geological Survey Professional Paper 349-B, 118 p.

Hames, W. E., Tracy, R. J., Ratcliffe, N. M., and Sutter, J. F., 1991, Petrologic, structural, and geochronologic characteristics of the Acadian metamorphic overprint on the Taconide zone in part of southwestern New England: American Journal of Science, v. 291, p. 887-913.

Hamilton, W. B., 1961, Geology of the Richardson Cove and Jones Cove quadrangles, Tennessee: U.S. Geological Survey Professional Paper 349-A, 55 p.

Hardeman, W. D., 1966, Geologic map of Tennessee: Tennessee Division of Geology, scale 1:250,000.

Harland, W. B., Armstrong, R. L., Cox, A. V., Craig, L. E., Smith, A. G., and Smith, D. G., 1989, A geologic time scale: Cambridge, England, Cambridge University Press, 263 p.

Harris, L. D., Harris, A. G., DeWitt, W., Jr., and Bayer, K. C., 1981, Evaluation of southern Eastern overthrust belt beneath Blue Ridge-Piedmont thrust: American Association of Petroleum Geologists Bulletin, v. 65, p. 2497-2505.

Hatcher, R. D., Jr., 1972, Developmental model for the southern Appalachians: Geological Society of America Bulletin, v. 83, p. 2735-2760.

Hatcher, R. D., Jr., 1978, Tectonics of the western Piedmont and Blue Ridge: Review and speculation: American Journal of Science, v. 278, p. 276-304.

Hatcher, R. D., Jr., 1991, Interactive property of large thrust sheets with footwall rocks-the subthrust interactive duplex hypothesis: A mechanism of dome formation in thrust sheets: Tectonophysics, v., 191, p. 237-242.

Hatcher, R. D., Jr., Costello, J. O., and Broadhead, T. W., 1992, Development of the Iapetan margin - Proterozoic to Ordovician (?) time-transgressive (?) sequences in the southern Appalachians: Geological Society of America Abstracts with Programs, v. 24, no. 2, p. 20.

Hatcher, R. D., Jr., and Goldberg, S. A., 1991, The Blue Ridge Province, *in* Horton, J.W., Jr., and Zullo, V.A., eds., The Geology of the Carolinas - Carolina Geological Society 50th Anniversary Volume: Knoxville, University of Tennessee Press, p. 11-35.

Hatcher, R. D., Jr., and Odom, A. L., 1980, Timing of thrusting in the southern Appalachians, USA: Model for orogeny?: Geological Society of London Journal, v. 137, p. 321-327.

Hatcher, R. D., Jr., Osberg, P. H., Drake, A. A., Jr., Robinson, P., and Thomas, W. A., 1990, Tectonic map of the U.S. Appalachians-Plate 1, *in* Hatcher, R. D., Jr., Thomas, W. A., and Viele, G. W., eds., The Appalachian-Ouachita orogen in the United States: Boulder, Colorado, Geological Society of America, The Geology of North America, v. F-2.

Hatcher, R. D., Jr., Thomas, W. A., Geiser, P. A., Snoke, A. W., Mosher, S., and Wiltschko, D. V., 1989, Alleghanian orogen, *in* R. D. Hatcher, J., Thomas, W. A., and Viele, G. W., eds., The Appalachian-Ouachita orogen in the United States: Boulder, Colorado, Geological Society of America, The Geology of North America, v. F-2, p. 233-318.

Hernon, R. M., 1964, Geologic maps and sections of the Ducktown, Isabella, and Persimmon Ceek quadrangles, Tennessee and North Carolina: U.S. Geological Survey Open File, scale 1:24,000.

Hurst, V. J., and Schlee, J. S., 1962, Field Excursion: Ocoee metasediments, north-central Georgia, southeastern Tennessee: Georgia Geological Society Guidebook 3, 28 p.

Kay, G. M., 1942, Development of the northern Allegheny synclinorium and adjoining region: Geological Society of America Bulletin, v. 53, p. 1601-1658.

Kellberg, J. M., and Grant, L. F., 1956, Coarse conglomerates of the Middle Ordovician in the southern Appalachian valley: Geological Society of America Bulletin, v. 67, p. 697-716.

Keller, F. B., 1980, Late Precambrian stratigraphy, depositional history, and structural chronology of part of the Tennessee Blue Ridge [Ph.D. thesis]: New Haven, Connecticut, Yale University, 363 p.

King, P. B., 1955, A geologic section across the southern Appalachians: An outline of the geology in the segment in Tennessee, North Carolina, and South Carolina, *in* Russell, R. J., ed., Guides to southeastern geology: Boulder, Colorado, Geological Society of America, p. 332-373.

King, P. B., 1964, Geology of the central Great Smoky Mountains, Tennessee: U.S. Geological Survey Professional Paper 349-C, 148 p.

King, P. B., Hadley, J. B., Neuman, R. B., and Hamilton, W. B., 1958, Stratigraphy of the Ocoee Series, Great Smoky Mountains, Tennessee and North Carolina: Geological Society of America Bulletin, v. 69, p. 947-967.

King, P. B., Neuman, R. B., and Hadley, J. B., 1968, Geology of the Great Smoky Mountains National Park, Tennessee and North Carolina: U.S. Geological Survey Professional Paper 587, 23 p.

Kish, S. A., 1982, The application of Potassium-Argon dating of slates to the study of the metamorphic history of the southern Appalachian Piedmont and Blue Ridge: Geological Society of America Abstracts with Programs, v. 14, p. 31.

Kish, S. A., 1989, Igneous and metamorphic history of the eastern Blue Ridge, southwestern North Carolina: K-Ar and Rb-Sr studies, *in* Fritz, W. J., Hatcher, R. D., Jr., and Hopson, J. L., eds., Geology of the eastern Blue Ridge of northeast Georgia and the adjacent Carolinas: Georgia Geological Society Guidebook, v. 8, p. 41-55.

Kish, S. A., 1990, Timing of middle Paleozoic (Acadian) metamorphism in the southern Appalachians: K-Ar studies in the Talladega belt, Alabama: Geology, v. 18, p. 650-653.

Kish, S. A., 1991, Potassium-Argon Dating in the western Blue Ridge of North Carolina and Tennessee, *in* Kish, S. A., ed., Studies of Precambrian and Paleozoic Stratigraphy in the western Blue Ridge: Carolina Geological Society Field Trip Guidebook, p. 69-77.

Kish, S. A., Fullagar, P. D., and Dabbagh, A. E., 1976, Paleozoic plutonic activity in the Blue Ridge of North Carolina: Geological Society of America Abstracts with Programs, v. 8, p. 211-212.

Kish, S. A., and Harper, C. T., 1973, Potassium-argon geochronology of a portion of the southwestern Blue Ridge: Geological Society of America Abstracts with Programs, v. 5, p. 409.

Knoll, A. H., and Keller, F. B., 1979, Late Precambrian microfossils from the Walden Creek Group, Ocoee Supergroup, Tennessee: Geological Society of America Abstracts with Programs, v. 11, p. 185.

Knoll, A. H., and Swett, K., 1985, Micropaleontology of the Late Proterozoic Veteranen Group, Spitsbergen: Palaeontology, v. 28, p. 451-473.

Kubler, B., 1967, La cristallinité de l'illite et les zones tout à fait supérieure du métamorphisme: Colloque sur les "Etages Tectoniques", 18-21 avril, 1966, Neuchâtel, Festschrift, p. 105-122.

Kulp, J. L., and Eckelman, F. D., 1961, Potassium-argon isotopic ages on micas from the southern Appalachians: New York Academy of Sciences Annals, v. 91, p. 408-419.

Kunk, M. J., Sutter, J. F., Obradivitch, J., and Lanphere, M. A., 1985, Age of biostratigraphic horizens within the Ordovician and Silurian systems, *in* Snelling, N. J., ed., The chronology of the Geological Record: Geological Society of London, Memoir 10, p. 89-92.

Laird, J., and Albee, A. L., 1981, Pressure, temperature, and time indicators in mafic schist: Their application to reconstructing the polymetamorphic history of Vermont: American Journal of Science, v. 281, p. 127-175.

Laird, J., Lanphere, M. A., and Albee, A. L., 1984, Distribution of Ordovician and Devonian metamorphism in mafic and pelitic schists from northern Vermont: American Journal of Science, v. 284, p. 376-413.

Labotka, T. C., and Shireman, J., 1991, Metamorphism in the Blue Ridge near Cullowhee, North Carolina: Geological Society of America Abstracts with Programs, v. 23, no. 1, p. 55.

Laurence, R. A., and Palmer, A. R., 1963, Age of the Murray Shale and Hesse Quartzite on Chilhowee Mountain, Blount County, Tennessee: U.S. Geological Survey Professional Paper 475-C, C53-C54 p.

Long, L. E., Kulp, J. L., and Eckelman, F. D., 1959, Chronology of major metamorphic events in the southeastern United States: American Journal of Science, v. 257, p. 585-603.

Lowry, W. D., 1972, The Diamond Hill and Fincastle conglomerates-evidence of great structural relief between the Blue Ridge anticlinorium and Salem synclinorium in Middle Ordivician time: Geological Society of America Abstracts with Programs, v. 4, p. 89.

Lyons, P. C., and Darrah, W. C., 1978, A late Middle Pennsylvanian flora of the Narragansett Basin, Massachusetts: Geological Society of America Bulletin, v. 89, p. 433-438.

Mack, G. H., 1985, Provenance of Middle Ordovician Blount clastic wedge, Georgia and Tennessee: Geology, v. 13, p. 299-302.

McKerrow, W. S., Lambert, R. St. J., and Chamberlain, V. E., 1980, The Ordovician, Silurian and Devonian time scales: Earth and Planetary Sciences Letters, v. 51, p. 1-8.

Milton, D. J., 1983, Garnet-biotite geothermometry confirms the premetamorphic age of the Greenbrier fault, Great Smoky Mountains, North Carolina: Geological Society of America Abstracts with Programs, v. 15, p. 90.

Mohr, D. W., 1973, Stratigraphy and structure of part of the Great Smoky and Murphy belt Groups, western North Carolina: American Journal of Science, v. 273-A, p. 41-71.

Mohr, D. W., and Newton, R. C., 1983, Kyanite-staurolite metamorphism in sulfidic schists of the Anakeesta Formation, Great Smoky Mountains, North Carolina: American Journal of Science, v. 283, p. 97-134.

Nesbitt, B. E., and Essene, E. J., 1982, Metamorphic thermometry and barometry of a portion of the southern Blue Ridge province: American Journal of Science, v. 282, p. 701-729.

North Carolina Geological Survey, 1985, Geologic Map of North Carolina: North Carolina Department of Natural Resources and Community Development, Raleigh, scale 1:500,000.

Oriel, S. S., 1951, Structure of the Hot Springs window, Madison County, North Carolina: American Journal of Science, v. 249, p. 1-31.

Osberg, P. H., Tull, J. F., Robinson, P., Hon, R., and Butler, J. R., 1989, The Acadian orogen, *in* Hatcher, R. D., Jr., Thomas, W. A., and Viele, G. W., eds., The Appalachian-Ouachita Orogen in the United States: Boulder, Colorado, Geological Society of America, The Geology of North America, v. F-2, p. 179-232.

Palmer, A. R., 1983, The Decade of North American Geology, 1983 geologic time scale: Geology, v. 11, p. 503-504.

Phillips, H. E., 1952, The geology of Starr Mountain, southeast Tennessee [M.S. thesis]: Knoxville, Tennessee, University of Tennessee, 61 p.

Power, W. R., and Forrest, J. T., 1971, Stratigraphy and Structure of the Murphy belt, North Carolina: Carolina Geological Society Guidebook, 29 p.

Rast, N., and Kohles, K. M., 1986, The origin of the Ocoee Supergroup: American Journal of Science, v. 286, p. 593-616.

Reuter, A., 1985, Korngrößenabhangigkeit von K-Ar Datierungen und Illit-Kristallinität anchizonaler Metapelite und assoziierter Metatuffe aus dem östlichen Rheinischen Schiefergebirge: Göttinger Arbeiten zur Geologie und Paläontologie, v. 27, p. 91.

Reuter, A., 1987, Implications of K-Ar ages of whole-rock and grain-size fractions of metapelites and intercalated metatuffs within an anchizonal terrane: Contributions to Mineralogy and Petrology, v. 97, p. 105-115.

Robbins, C. S., 1972, Radiogenic argon diffusion in muscovite under hydrothermal conditions [M.S. thesis]: Providence, Rhode Island, Brown University, 88 p.

Rodgers, J., 1953, Geologic map of east Tennessee with explanatory text: Tennessee Division of Geology Bulletin 58, Part II, p. 168.

Rodgers, J., 1991, Evolution of ideas about the Ocoee conglomerates and slates, *in* Kish, S.A., ed., Studies of Precambrian and Paleozoic stratigraphy in the western Blue Ridge: Carolina Geological Society Field Trip Guidebook, p. 1-12.

Rosenfeld, J. L., 1968, Garnet rotations due to the major Paleozoic deformations in southeast Vermont, *in* Zen, E-an, White, W. S., Hadley, J. B., Jr., eds., Studies of Appalachian Geology: Northern and maritime: New York, Wiley Interscience, p. 185-202.

Sack, W. R., 1988, Geometric analysis of folding associated with overthrusting: Blue Ridge province, Tennessee [M.S. thesis]: East Lansing, Michigan, Michigan State University, 157 p.

Samson, S. D., and Alexander, E. C., 1987, Calibration of the interlaboratory $^{40}Ar/^{39}Ar$ dating standard, MMhb-1: Chemical Geology, v. 66, p. 27-34.

Secor, D. T., Jr., Snoke, A. W., Bramlett, K. W., Costello, O. P., and Kimbrell, O. P., 1986, Character of the Alleghanian orogeny in the southern Appalachians: Part I. Alleghanian deformation in the eastern Piedmont of South Carolina: Geological Society of America Bulletin, v. 97, p. 1319-1328.

Shanmugam, G., 1980, Rhythms in deep-sea, fine-grained turbidite and debris-flow sequences, Middle Ordovician, eastern Tennessee: Sedimentology, v. 27, p. 419-432.

Shanmugam, G., and Lash, G. G., 1982, Analogous tectonic evolution of the Ordovician foredeeps, southern and central Appalachians: Geology, v. 10, p. 562-566.

Simpson, E. L., and Sundberg, F. A., 1987, Early Cambrian age for synrift deposits of the Chilhowee Group of southwestern Virginia: Geology, v. 15, p. 123-126.

Snelling, N. J., 1985, The chronology of the geological record: Geological Society of London, Memoir 10, 162 p.

Steiger, R. H., and Jäger, E., 1977, Subcomission of geochronology: convention on the use of decay constants in geo- and cosmochemistry: Earth and Planetary Sciences Letters, v. 36, p. 359-362.

Stose, G. W., and Stose, A. J., 1944, The Chilhowee Group and Ocoee Series of the southern Appalachians: American Journal of Science, v. 242, p. 367-390.

Teichmüller, M., Teichmüller, R., and Weber, K., 1979, Inkohlung und Illit-Kristallinitüt-Vergleichende Untersuchungen im Mesozoikum und Paläozoikum von Westfalen: Fortschritte Geologie Rheinland und Westfalen, v. 27, p. 201-276.

Thompson, T. W., and Tull, J. F., 1991, Stratigraphy of the Mineral Bluff Group, southwestern North Carolina, *in* Kish, S. A., ed., Studies of Precambrian and Paleozoic stratigraphy in the western Blue Ridge: Carolina Geological Society Field Trip Guidebook, p. 97-110.

Thomas, W. A., and Hatcher, R. D., 1988, Deep-water off-shelf passive-margin setting of deposition of the rocks in the Murphy belt: Another outrageous hypothesis, *in* Fritz, W. J., and La Tour, T. E., eds., Geology of the Murphy belt and related rocks-Georgia and North Carolina: Georgia Geological Society Guidebook, v. 8, p. 103-109.

Trümpy, R., 1973, The timing of orogenic events in the central Alps, *in* DeJong, K. A., and Scholten, R., eds., Gravity and tectonics, New York, Wiley-Interscience, p. 229-251.

Tull, J. F., Ausich, W. I., Groszos, M. S., and Thompson, T. W., in press, Pelmatozoan echinoderm fragment constrains age units within the Murphy belt, southern Appalachian Blue Ridge: Geology.

Tull, J. F., and Groszos, M. S., 1988, Murphy belt: Stratigraphic complexities and regional correlations, *in* Fritz, W. J., and La Tour, T. E., eds., Geology of the Murphy belt and related rocks, Georgia and North Carolina: Georgia Geological Society Guidebook, v. 8, p. 35-74.

Tull, J. F., and Guthrie, G. M., 1985, Proposed stratigraphic linkages between the Talladega slate belt and the Appalachian miogeocline-tectonic implications, *in* Tull, J. F., Bearce, D. N., and Guthrie, G. M., eds., Early evolution of the Appalachian miogeocline: upper Precambrian-lower Paleozoic stratigraphy of the Talladega slate belt: Alabama Geological Society, 22nd. annual field trip, Guidebook, p. 1-10.

Tull, J. F., Harris, A. G., Repetski, J. E., McKinney, F. K., Garrett, C., and Bearce, D. N., 1988, New paleontologic evidence constraining the age and paleotectonic setting of the Talladega slate belt, southern Appalachians: Geological Society of America Bulletin, v. 100, p. 1291-1299.

Tull, J. F., and Telle, W. R., 1989, Tectonic setting of olistostromal units and associated rocks in the Talladega slate belt, Alabama Appalachians, *in* Horton, J. W., Jr., and Rast, N., eds., Mélanges and Olistostromes of the U.S. Appalachians, Boulder, Colorado, Geological Society of America Special Paper 228, p. 247-269.

Unrug, R., and Unrug, S., 1990, Paleontological evidence of Paleozoic age for the Walden Creek Group, Ocoee Supergroup, Tennessee: Geology, v. 18, p. 1041-1045.

Unrug, R., Unrug, S., and Palmes, S. L., 1991, Carbonate rocks of the Walden Creek Group in the Little Tennessee River valley: modes of occurrence, age, and significance for the basin evolution of the Ocoee Supergroup, *in* Kish, S. A., ed., Studies of Precambrian and Paleozoic stratigraphy in the western Blue Ridge: Carolina Geological Society Field Trip Guidebook, p. 27-37.

Unrug, R., Unrug, S., and Palmes, S. L., 1992, The position of the Walden Creek Group and Ocoee Supergroup basins and the evolution of the Laurentian margin: Geological Society of America Abstracts with Programs, v. 24, no. 2, p. 71.

Walcott, C. D., 1890, The fauna of the Lower Cambrian or *Olenellus* zone: U.S. Geological Survey 10th Annual Report, pt.1, Geology, p. 507-573.

Walker, D., and Driese, S. G., 1991, Constraints on the position of the Precambrian-Cambrian boundary of the southern Appalachians: American Journal of Science, v. 291, p. 258-283.

Walker, D., and Simpson, E. L., 1991, Stratigraphy of the Upper Proterozoic and Lower Cambrian siliciclastic rocks, southwestern Virginia and northeastern Tennessee, *in* Schultz, A., and Compton-Gooding, E., eds., Geologic evolution of the eastern United States, field trip guidebook: Virginia Museum of Natural History Guidebook 2, p. 121-159.

Weber, K., 1972, Notes on determination of illite crystallinity: Neues Jahrbuch Mineralogie Monatshefte, v. 6, p. 267-276.

Witherspoon, W. D., 1981, Structure of the Blue Ridge thrust front, Tennessee, southern Appalachians [Ph.D. thesis]: Knoxville, Tennessee, University of Tennessee, 165 p.

Woodward, N. B., ed., 1985, Valley and Ridge thrust belt: balanced structural sections, Pennsylvania to Alabama: Appalachian Basin Industrial Assosiates, University of Tennessee Department of Geological Sciences Studies in Geology no. 12, 64 p.

Woodward, N. B., Connelly, J. B., Walters, R. R., and Lewis, J. C., 1991, Tectonic evolution of the Great Smoky Mountains, *in* Kish, S. A., ed., Studies of Precambrian and Paleozoic stratigraphy in the western Blue Ridge: Carolina Geological Society Field Trip Guidebook, p. 57-68.

Wyborn, D., Owen, N., Compston, W., and McDougall, I., 1982, The Laidlaw volcanics; a Late Silurian point on the geological time scale: Earth and Planetary Sciences Letters, v. 59, p. 99-100.

VITA

Jeffrey Brian Connelly was born in Pittsburgh, Pennsylvania on August 1, 1961. He attended elementary school at Saint Dennis school, junior high school at Elizabeth-Forward public schools, and high school at Kiskiminetas Springs School in Saltsburg, Pennsylvania, from which he graduated in May, 1979. He attended the College of Wooster in Wooster, Ohio and received a B.A. degree in Geology in June, 1983. In September 1984, he began work on his masters degree at Bowling Green State University in Bowling Green, Ohio. After completing a thesis on strain within Triassic limestones, he received his M.S. degree from Bowling Green in August of 1986. In September, 1986, he began work towards a Ph.D. degree in Geologcal Sciences at the University of Tennessee, which was completed in May, 1993. During this period, he also spent time as a graduate teaching assistant, taught geology at Cumberland College in Williamsburg, Kentucky, and worked at an environmental consulting firm in Oak Ridge, Tennessee. He is presently employed as an assistant professor of geology at the University of Arkansas in Little Rock, Arkansas.